

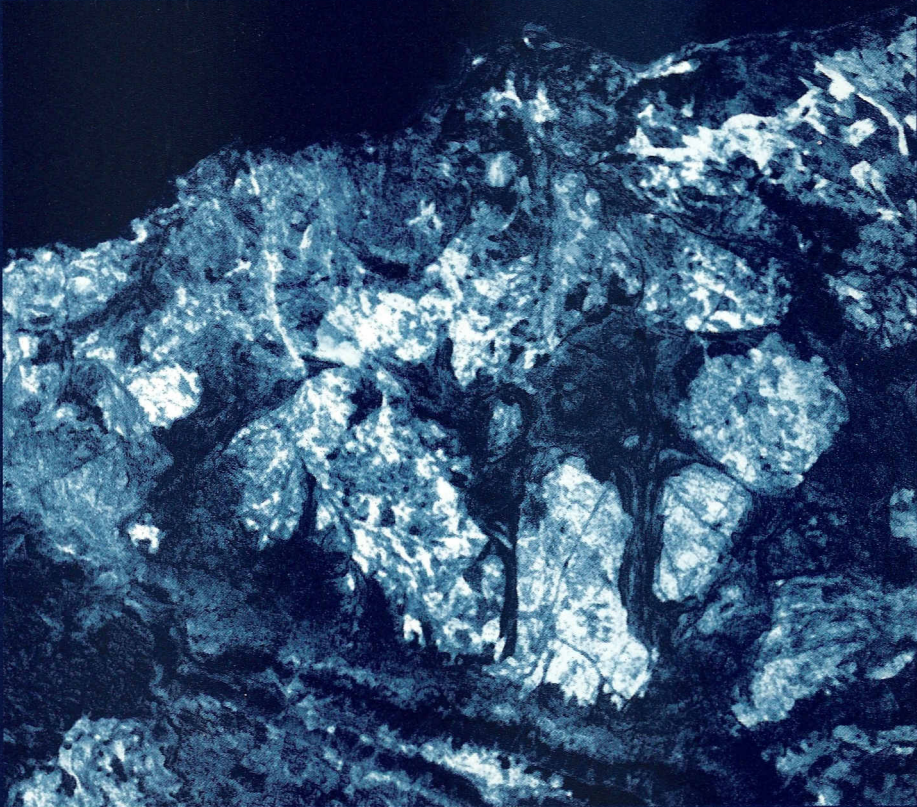
GEOLOGICA ULTRAIECTINA

Mededelingen van de
Faculteit Aardwetenschappen
Universiteit Utrecht

No. 146

**Structural, kinematic and
metallogenic evolution
of selected domains of the
Pilbara granitoid-greenstone terrain**

implications for mid Archean tectonic regimes



Tanja Elsa Zegers

GEOLOGICA ULTRAIECTINA

Mededelingen van de
Faculteit Aardwetenschappen
Universiteit Utrecht

No. 146

**Structural, kinematic and
metallogenic evolution
of selected domains of the
Pilbara granitoid-greenstone terrain**

implications for mid Archean tectonic regimes

Tanja Elsa Zegers

Cover illustration: Landsat image of the Pilbara Craton, Geological Survey of Western Australia

**Structural, kinematic and
metallogenic evolution
of selected domains of the
Pilbara granitoid-greenstone terrain**

implications for mid Archean tectonic regimes

**Structurele, kinematische en
metallogenetische evolutie
van delen van het
Pilbara graniet-groensteen terrein;**

implicaties voor midden Archaïsche tectonische processen
(met een samenvatting in het Nederlands)

Proefschrift

TER VERKRIJGING VAN DE GRAAD VAN DOCTOR AAN DE UNIVERSITEIT UTRECHT.

OP GEZAG VAN DE RECTOR MAGNIFICUS PROF. DR. J.A. VAN GINKEL,
INGEVOLGE HET BESLUIT VAN HET COLLEGE VAN DECANEN
IN HET OPENBAAR TE VERDEDIGEN OP

MAANDAG 9 DECEMBER 1996, DES NAMIDDAGS TE 12.45 UUR

door

Tanja Elsa Zegers

Geboren op 12 januari 1967 te Varese

PROMOTOR: Prof.Dr. S.H. White
CO-PROMOTOR: Dr. J.R. Wijbrans

Structural, kinematic and metallogenic evolution of selected domains of the Pilbara granitoid-greenstone terrain; implications for mid Archean tectonic regimes / Tanja E. Zegers: Faculteit Aardwetenschappen, Universiteit Utrecht - Proefschrift Universiteit Utrecht (Geologica Ultraiectina, No. 146) - met samenvatting in het Nederlands

ISBN 90-5744-004-0

Trefw.: Archean, Pilbara, deformation, dating, gold

Contents

Samenvatting	9
Abstract	11
I Introduction	13
1.1 Preamble	13
1.2 Aims and organization of this thesis	14
1.2.1 Aims	14
1.2.2 Organization of the thesis	14
1.2.3 Nomenclature and method	15
2 Archean geology: what is different ?	17
2.1 Introduction	18
2.2 The Archean rock record	18
2.2.1 Oldest relics pre-4.0 Ga	18
2.2.2 Archean terrains 4.0-2.5 Ga	18
2.2.2.1 High grade gneiss terrains	18
2.2.2.2 Granitoid-greenstone terrains	19
2.2.2.3 Deformation and metamorphism	22
2.2.2.4 Cratonic Basins	23
2.2.3 Mineralization in Archean terrains	23
2.2.4 Other constraints to early Earth evolution	24
2.2.4.1 Geochemical constraints	24
2.2.4.2 Geochronological constraints	24
2.2.4.3 Geophysical constraints	25
2.3 Thermal evolution, Archean dynamics and crustal growth models.	25
2.4 Synthesis.	29
3 Introduction to the geology of the Pilbara	31
3.1 Introduction	31
3.2 Lithologies and geochronology	31
3.2.1 Lithostratigraphy and geochronology of greenstones	31
3.2.2 Petrogenesis and geochronology of granitoids	35
3.2.3 Synthesis of geochronology	36
3.3 Structural and metamorphic events	36
3.4 Mineralization in the Pilbara granitoid-greenstone terrain	37
3.5 Tectonic interpretations.	38

4	Extensional structures during deposition of the 3460 Ma Warrawoona Group	41
4.1	Introduction	41
4.2	Geological setting of the Shaw Batholith and Coongan Belt	42
4.2.1	The Coongan Belt	44
4.2.2	The Shaw Batholith	44
4.3	Structural observations	45
4.3.1	The Shaw Batholith	45
4.3.2	The Coongan Belt	49
4.4	Discussion	52
4.5	Conclusions	56
5	Structural development and kinematics of compressional structures in greenstone belts, with emphasis on the Coongan Belt	57
5.1	Introduction	57
5.2	The Coongan Belt	58
5.2.1	Background	58
5.2.2	Lithology and stratigraphy	61
5.2.3	Alteration and metamorphism	61
5.2.4	Structural development	61
5.2.5	Geometrical/kinematic model for the Coongan Belt	68
5.3	Structures in other greenstone belts	70
5.3.1	The Tambourah Belt	70
5.3.2	Kelly Belt	72
5.3.3	The Warrawoona Belt	72
5.3.4	The Marble Bar Belt	72
5.3.5	Coppin Gap Greenstone Belt	73
5.3.6	The North Pole Dome area	73
5.4	Discussion	74
5.5	Conclusions	77
6	Craton scale shear zones in the Pilbara; a detailed study of the Mulgandinnah Shear Zone Complex	79
6.1	Introduction	79
6.2	Regional Setting	79
6.3	Lithologies of the Shaw Batholith	81
6.3.1	Migmatic gneiss & enclaves.	81
6.3.2	North Shaw Suite	83
6.3.3	Younger granitoids	83
6.4	Mulgandinnah Shear Zone Complex	83
6.4.1	Lithologies in the MSZC	85
6.4.2	MSZC mylonites	85
6.4.3	MSZC ultramylonites	87

6.4.4	Contact zone with greenstones	89
6.4.5	Relationship between MSZC and the Split Rock Shear Zone (SRSZ)	89
6.4.6	Northward continuation of the MSZC	89
6.5	Other major lineaments in the Pilbara	90
6.6	Discussion	90
6.7	Conclusions	94
7	Deformation and hydrothermal alteration in the Bamboo Creek Deposit, a komatiite-hosted lode-gold deposit	95
7.1	Introduction	95
7.2	Regional setting	96
7.3	Structural analysis	97
7.3.1	Introduction	97
7.3.2	Setting and lithologies of the BCSZ	99
7.3.3	Foliations and lineation in the BCSZ	100
7.3.4	Kinematics	100
7.3.5	Structure and kinematics of the Kitchener deposit	103
7.4	Alteration in the BCSZ	103
7.4.1	Alteration zones	103
7.4.2	Mineralogy of the alteration	106
7.4.3	Indications of environment of deposition	108
7.4.4	Enrichment/depletion	109
7.4.5	Light stable isotopes of dolomite	112
7.5	Lead-lead dating of galena	112
7.6	Discussion	113
7.7	Conclusions	117
8	Constraints on the timing of deformation and metamorphism in the Shaw Batholith area: U-Pb and $^{40}\text{Ar}/^{39}\text{Ar}$ dating	119
8.1	Introduction	119
8.2	$^{40}\text{Ar}/^{39}\text{Ar}$ dating	120
8.2.1	Background	120
8.2.2	Structural context and description of samples	121
8.2.2.1	Eastern Coongan Belt and adjacent Corunna Downs Batholith	121
8.2.2.2	The Split Rock Shear Zone, North Shaw Suite and the western Coongan Belt	121
8.2.2.3	The Mulgandinnah Shear Zone Complex	126
8.2.2.4	Black Range Dolerite Dyke	126
8.2.3	Sample preparation and analytical method	126
8.2.4	Results of $^{40}\text{Ar}/^{39}\text{Ar}$ dating	127
8.2.5	Synthesis and structural/metamorphic implications	132
8.3	U-Pb zircon dating	136
8.3.1	Structural context and description of samples for U-Pb dating	137

8.3.2	Sample preparation and analytical method	139
8.3.3	Results of U-Pb zircon dating	141
8.3.3.1	Zircon morphology	141
8.3.3.2	Results of SHRIMP analyses	144
8.3.4	Synthesis and structural implications of U-Pb zircon dating	154
8.4	Discussion and conclusions	157
9	Discussion and Conclusions	161
9.1	Introduction	161
9.2	Tectonothermal evolution of the Pilbara granitoid-greenstone terrain	162
9.2.1	The basement to the Duffer Formation	162
9.2.2	Upper Warrawoona Group evolution	164
9.2.3	Gold mineralization	168
9.2.4	Syn- to post Gorge Creek Group evolution	169
9.2.5	Craton Scale Strike Slip Faults and final doming	171
9.2.6	Dolerite dykes	173
9.2.7	The role of solid state diapirism	174
9.3	Comparison to other Archean terrains	175
9.4	Plate tectonics in the Pilbara	176
9.5	Conclusions	178
9.6	Future work	179
	References	181
	Appendix 1 Data set of $^{40}\text{Ar}/^{39}\text{Ar}$ step heating experiments	193
	Appendix 2 Whole rock XRF analyses of SHRIMP samples	205
	Curriculum Vitae	206
	Acknowledgements (dankbetuiging)	207

Samenvatting (Summary in Dutch)

Het ontrafelen van de vroegste geschiedenis van de Aarde, die een ouderdom heeft van 4600 miljoen jaar, wordt bemoeilijkt door het ontbreken van gesteenten die bewaard zijn gebleven uit de allervroegste periode. De oudst bekende gesteenten (4000 miljoen jaar) op Aarde, uit de Archaïsche periode (4000 tot 2500 miljoen jaar), zijn bovendien verstoord door latere tectonische gebeurtenissen. Er zijn echter twee plaatsen op aarde waar ongestoorde gesteenten uit de jeugd van de Aarde, zijn te bestuderen, namelijk het Kaapvaal Craton in Zuid Afrika en het Pilbara Craton in West Australië, waarvan het laatstgenoemde het onderwerp van deze promotie is. Deze cratons bestaan voornamelijk uit granieten en vulkanische gesteenten, ook wel groenstenen genoemd, met ouderdommen tussen de 3600 en 2800 miljoen jaar. Hiervan zijn de groenstenen in het algemeen bijzonder rijk aan een verscheidenheid van ertsen. Zo wordt een groot deel van de gouderts voorkomens op Aarde in Archaïsche groenstenen gevonden.

Een van de belangrijkste geologische problemen in het Archaïcum is het gebrek aan kennis omtrent de tectonische (deformatie) processen die zich in deze tijd in de Aarde afspeelden. Zo moet de temperatuur in de mantel van de Aarde in het Archaïcum hoger zijn geweest dan tegenwoordig. Dit maakt het onzeker of plaattectonische processen, zoals die nu plaatsvinden, waarbij platen lithosfeer langs elkaar bewegen, plaatselijk naar beneden worden gedrukt (subductie) en elders worden aangeemaakt (mid-oceanische ruggen), ook al actief waren in dit vroege stadium van de ontwikkeling van de Aarde. Geologisch onderzoek van deze mid Archaïsche gebieden kan belangrijke randvoorwaarden verschaffen voor geodynamische modellen van tectonische processen in het midden Archaïcum. Tijdens deze promotie is de vroegste geologische geschiedenis van het Pilbara Craton onderzocht. Hierbij is vooral gekeken naar de deformatie en de goudmineralisatie in het oostelijk deel van het Craton, met name in de Shaw Batholiet en de Coongan Groensteen Gordel. Er is bovendien veel aandacht besteed aan de datering van deze gebeurtenissen met behulp van verschillende isotopische daterings methoden, die gebaseerd zijn op het radioactief verval van verschillende elementen in mineralen van het gesteente. Met deze methoden kunnen bepaalde gebeurtenissen met grote nauwkeurigheid (beter dan 10 miljoen jaar) gedateerd worden.

Uit het onderzoek blijkt dat er in de 800 Ma durende Archaïsche evolutie van de oostelijke Pilbara een drietal belangrijke deformatie fasen onderscheiden kunnen worden die als volgt samen te vatten zijn:

- 1 Een WSW-ENE gerichte extensie fase, tijdens uitvloeiing van de oudste groep vulkanische gesteenten, de Warrawoona Groep, en intrusie van granodiorieten, 3470-3450 Ma geleden. Tijdens deze extensie fase onstonden koepelvormige structuren, vergelijkbaar met recente core-complexen, met graniet in de kern omgeven door vulkanische gesteenten.
- 2 Een E-W gerichte verkortings fase, gelijktijdig met de eerste klastische sedimenten tussen 3300 en 3200 Ma geleden. Hierbij zijn de oudere vulkanische gesteenten geplooid en over elkaar geschoven, waardoor de stratigrafische opeenvolging verstoord en in bepaalde gevallen tectonisch verdubbeld is.
- 3 Tijdens een van de laatste fasen van magmatische activiteit, ca. 2930 Ma, ontstond het grootschalige (>100 km lengte), noord strekkende sinistrale Mulgandinnah Shear Zone Complex.

In de west Pilbara onstond rond diezelfde tijd de even grootschalige E-W strekkende dextrale Sholl Shear Zone. Deze grootschalige schuifzones en een aantal kleinschalige structuren zijn te verklaren in een NE-SW gericht compressie veld

De goud mineralisatie van een van de belangrijkste goudmijnen in het Pilbara Craton, de Bamboo Creek Mijn, is gesitueerd in ultramafisch gesteente, in een groenschist facies schuifzone en heeft een ouderdom tussen 3400 en 3300 miljard jaar. Dit betekent dat dit het ouste beschreven goudvoorkomen op Aarde is. De mineralisatie en daaraan gerelateerde hydrothermale alteratie waren waarschijnlijk gerelateerd aan de extensie fase, of vonden kort na de extensie fase plaats. De temperatuur en druk omstandigheden en de chemie van de alteratie zijn vergelijkbaar met die van de zeer grote, laat Archaïsche, goud voorkomens in het Yilgarn Craton (zuidwest Australië).

De bovengenoemde ouderdommen van de deformatie fasen zijn verkregen door middel van een combinatie van U-Pb SHRIMP dateringen van zirkoon en $^{40}\text{Ar}/^{39}\text{Ar}$ dateringen van voornamelijk hoorblende. Deze geochronologische studie gaf bovendien nog een aantal andere resultaten:

- 1 De grijze gneissen in het centrale deel van de Shaw Batholiet vormen niet het basement van de Warrawoona Groep, maar hebben kristallisatie ouderdommen die vergelijkbaar zijn met het het bovenste deel van de Warrawoona Groep.
- 2 De thermische evolutie van de oostelijke Pilbara is voor een groot deel bepaald door contact metamorfose, mogelijk tijdens deformatie, als gevolg van graniet intrusie. Er is echter een groep Argon afkoelingsouderdommen, tussen 3300 en 3200 miljoen jaar, die gerelateerd zijn aan een regionale groenschist- tot amfibolietfacies metamorfe fase, die optrad tijdens de E-W compressie.

De structurele ontwikkeling, waarbij de extensie en compressie richtingen over een groot gebied constant waren, is een indicatie dat de deformatie gerelateerd was aan processen die te maken hebben met bewegingen in of langs plaatgrenzen. Deze structurele ontwikkeling is echter niet in overeenstemming met eerder voorgestelde modellen, waarin er van uit werd gegaan dat de deformatie veroorzaakt werd door puur gravitatieve processen, waarbij granitisch gesteente in vaste of vloeibare vorm, ten gevolge van het verschil in dichtheid tussen granieten en vulkanisch gesteente, opstijgt in de aardkorst.

Hoewel de structurele ontwikkeling van de oostelijke Pilbara, met extensie, compressie en strike-slip deformatie, vergelijkbaar is met de structurele ontwikkeling van grote laat Archaïsche provincies (Yilgarn, Superior), is de tijdsduur waarbinnen de structurele en magmatische fasen voorkomen langer in de Pilbara: 500 miljoen jaar vergeleken met 100-150 miljoen jaar in de Yilgarn Province.

De structurele en magmatische ontwikkeling van het Kaapvaal Craton in Zuid Afrika, die grotendeels gelijktijdig plaatsvindt met het Pilbara Craton, verschilt in de details van timing en opeenvolging van de vroegste structurele fasen. Hierdoor is het onzeker of deze twee mid Archaïsche cratons eens deel uit hebben gemaakt van één mid Archaïsch continent.

Delen van de structurele, magmatische, metamorfe en sedimentologische ontwikkeling van het Pilbara Craton zijn vergelijkbaar met moderne plaat tectonische settings. Hoewel de gegevens niet in tegenspraak zijn met interactie van lithosferische platen, is er geen direct bewijs gevonden voor een van de meest cruciale onderdelen van de huidige vorm van plaat tectoniek, namelijk subductie van oceanische lithosfeer. Hierdoor kan de geologie van deze gebieden nog steeds niet zonder meer geïnterpreteerd worden in termen van huidige plaat tectonische processen.

Abstract

The Pilbara Craton is one of only two well preserved mid Archean granitoid-greenstone terrains on Earth. Its geology offers important constraints to geodynamic models of tectonic environments in the Mid Archean.

This mainly structural study concentrates on the Coongan Greenstone Belt and Shaw Batholith in the well exposed and oldest rocks of the eastern Pilbara. It shows that the 800 Ma Archean evolution (from 3.6 to 2.8 Ga) of the Pilbara granitoid-greenstone terrains consists of a number of structural and magmatic events.

The main structural events are:

- 1 An ENE-WSW directed extensional event, during deposition of the mainly volcanic Warrawoona Group at ca. 3.46 Ga, in which a core-complex type geometry of granitoid domes developed.
- 2 An E-W directed compressional event, constrained between 3.3 and 3.2 Ga, during deposition of the volcano-clastic Gorge Creek Group. Thrusts and folds in the greenstones disrupted the stratigraphy and cause repetition of stratigraphic units.
- 3 During the final stages of magmatic activity (ca.2.93 Ga) a craton scale north trending sinistral strike-slip system, the Mulgandinnah Shear Zone Complex, developed in the eastern Pilbara, as a response to NE-SW directed compression. The E-W trending dextral Sholl Shear Zone in the western Pilbara developed at approximately the same time (2.96 Ga, Smith et al., in press) and is interpreted as a conjugate to the Mulgandinnah Shear Zone Complex.

One of the major gold deposit in the eastern Pilbara, the komatiite hosted Bamboo Creek Deposit is situated in a greenschist facies shear zone. The minimum age of the gold mineralization, as deduced from cross cutting relations with the northern Mt. Edgar Batholith, is ca. 3300 Ma. The mineralization is thought to be related to the late stages of the extensional event at ca. 3.4 Ga (Pb-Pb model age). The geochemistry of the alteration associated with the gold mineralization in the Bamboo Creek Deposit is similar to late Archean gold deposits in ultramafic hostrocks in the Yilgarn Craton. The above ages were constrained by a combination of U-Pb SHRIMP and $^{40}\text{Ar}/^{39}\text{Ar}$ dating. The geochronological study also revealed that:

- 1 The grey gneisses and diorites in the central Shaw Batholith are not the basement to the Warrawoona Group, but have crystallization ages similar to those found for the Warrawoona Group (3.47-3.45 Ga).
- 2 Much of the thermal evolution of the eastern Pilbara can be understood in terms of contact metamorphism, possibly during deformation, due to granitoid intrusion. However, a group of cooling ages between 3300 and 3200 Ma are inferred to be related to a regional greenschist-amphibolite facies metamorphic event, associated with the E-W compressional phase of deformation.

The structural development of the eastern Pilbara is inconsistent with purely gravitational tectonics, such as solid state diapirism, as the main cause of deformation.

Although the structural development (extension, compression, strike-slip) can be compared to the structural development of major late Archean provinces (Yilgarn, Superior), the time span over which this sequence of structural and magmatic events occur is much larger in the Pilbara, i.e. ca.

Abstract

500 Ma as compared to 100–150 Ma in the Yilgarn Craton.

The structural and magmatic evolution of the Barberton Mountain Land, which developed broadly during the same time as the Pilbara, differs in details of the timing and sequence of structural events, making it less likely that they were once part of one single terrain.

Parts of the structural, magmatic, metamorphic and sedimentological development of the Pilbara are similar to present day tectonic settings. However, there is no direct evidence that subduction of oceanic crust, which is one of the most critical aspects of present day plate tectonics, did occur in the eastern Pilbara between 3.5 and 2.8 Ga.

Introduction

1.1 Preamble

The Archean period (4000–2500 Ma) is one of the more enigmatic periods of the Earth's evolution. The oldest preserved rocks on Earth stem from this period, as does the oldest evidence of life and water on Earth. Much about the Archean is, however, still unknown. One of the main questions that has dominated studies in Archean terrains is when plate tectonic processes, as we know them in the present Earth, started to operate and whether or not they were active in the Archean (Condie, 1981; Kröner, 1981; Windley, 1984; Nisbet, 1987; Condie, 1994).

In geological studies of the Phanerozoic, the uniformitarian approach is usually adopted when interpreting geological data. The plate tectonic setting is commonly used as a key to understand geological processes that occurred in the past in a particular terrain. For example, an ophiolite complex is a reliable indication for oceanization, thick turbidite sequences usually form in trenches associated with subduction and at continental margins and calc-alkaline volcanism is a good indication for a volcanic-arc setting with subduction of oceanic crust.

This uniformitarian approach can not be used as rigorously in Archean terrains because there still is no consensus on whether the current style of plate tectonics was actually active. The reason for this uncertainty is not only based on theoretical considerations such as an expected higher heat production in the Archean, but also on differences observed in the Archean rock record. In many respects, including rock types, geochemistry of rocks, degree of alteration, intensity of deformation and large-scale geometry, Archean terrains are different from modern terrains (see Chapter 2).

The question of whether or not present day style plate tectonic processes operated in the (mid) Archean is one of the central themes of modern Archean geology. As a consequence it is the topic that underlies much of the research presented in this thesis.

Major mineral deposits are known to occur in late Archean (3.0–2.5 Ga) terrains such as the Yilgarn Block in Western Australia and the Superior Province in Canada (Figure 2.1). This has prompted an increased research effort in those terrains leading to a multi disciplinary data set (structural, geochemical, geochronological and geophysical) that is consistent with a slightly adapted present day plate tectonic model (Myers, 1995; Card, 1990; Calvert et al., 1995).

For the earlier mid Archean (3.5–3.0 Ga), of which the Kaapvaal Craton in South Africa and the Pilbara Craton in Western Australia (Figure 2.1) are the only two well exposed and undisturbed examples, this is not yet clear. The Kaapvaal Craton contains significant high grade gold deposits and has recently been studied in detail using a variety of techniques, c.f. de Ronde & de Wit (1994) for a summary. The present study is concerned with the Pilbara Craton. It is aimed at providing better constraints on the geodynamic processes active in the mid Archean using a combination of detailed structural field studies and isotopic dating. It is part of a research project involving structural, sedimentological, mineralization and geochronological studies of the Pilbara Craton that began at Utrecht University in 1992.

1.2 Aims and organization of this thesis

1.2.1 Aims

This study concentrated on the eastern Pilbara granite-greenstone terrain, because that is the part of the Pilbara with best outcrop conditions and where most of the previous geochronological work was concentrated. This provided the basis of a temporal framework for the initial structural studies undertaken in the course of this research.

The principal, underlying aim of this study is to answer fundamental questions regarding mid Archean tectonic regimes by studying the tectonothermal evolution of the Pilbara Craton. Were the lithospheric plates rigid enough to allow plate tectonic processes to take place, and is there direct geological evidence for present day style plate tectonic processes in the Pilbara Craton? To answer these questions the following objectives were formulated:

- 1 To provide a structural and kinematic framework for the mid Archean evolution of the eastern Pilbara.
- 2 To determine whether the structures can be explained by (solid state) diapirism, as previously proposed for the ovoid batholiths of the eastern Pilbara (Hickman, 1983).
- 3 To determine the relation between structural and magmatic events.
- 4 To determine the relation between gold mineralization and the structural evolution of the eastern Pilbara.
- 5 To analyze the kinematics of craton scale shear zones
- 6 To provide isotopic age constraints for the structural and thermal evolution of the early continental crust as exposed in the eastern Pilbara
- 7 To determine how the tectonothermal evolution of the Pilbara compares to the contemporaneous Kaapvaal Craton and the late Archean cratons (Yilgarn and Superior).

1.2.2 Organization of the thesis

This thesis is organized in three introductory Chapters, five Chapters presenting the data and conclusions based on these data, and a final Chapter with a general discussion on the geological implications arising from this study.

In Chapter 2, an overview of the principal observations and models concerning the specific problems in Archean geology is given. Much of the discussion on Archean processes hinges on a relatively small number of key observations. The interpretation and significance of the evidence used in different models is continuously changing as more data becomes available.

Chapter 3 provides an introduction to the geology of the Pilbara. The data that are available from different sources are discussed, emphasizing the eastern Pilbara.

In Chapter 4, the structural evidence for an early (ca. 3.46 Ma) extensional phase in the eastern Pilbara is presented. This deformation phase was not previously recognized and has major implications for the interpretation of the evolution of the Pilbara granite-greenstone terrain.

In Chapter 5, the details of the geometry of the compressional structures in the Coongan Greenstone Belt are presented. In the second part of the Chapter, evidence for similar compressional structures from other greenstone belts is presented.

Chapter 6 contains the results of a detailed analysis of the Mulgandinnah Shear Zone Complex, a cra-

ton scale late Archean strike-slip zone. Kinematic data from other crustal scale lineaments in the Pilbara Craton are integrated in a model for these late Archean structures.

Chapter 7 documents the geochemical and structural data collected from the Bamboo Creek Deposit, a greenschist facies shear zone hosted gold deposit.

In Chapter 8, the geochronological data (U-Pb SHRIMP and $^{40}\text{Ar}/^{39}\text{Ar}$) are presented that were used to constrain the main structural events recorded in this study.

In Chapter 9, the data and inferences from this study are combined and compared with data and interpretations of other workers in the Pilbara Craton. The tectonothermal evolution of the Pilbara Craton is compared to other Archean cratons and the implications of this study for mid Archean tectonic regimes are discussed.

1.2.3 Nomenclature and method

For the greenstone belt stratigraphy in the Pilbara the major subdivisions as defined by Horwitz (1990) are used, i.e. The Pilbara Supergroup which consists of the Warrawoona Group, Gorge Creek Group and Whim Creek Group, and the Mt Bruce Supergroup with the basal Fortescue Group. This is equivalent to the stratigraphic divisions in megasequences by Krapez (1993), except for the Whim Creek Group, which Krapez (1993) subdivided in the Roebourne Megasequence and the Mt. Negri Megasequence.

The names of the greenstone belts and granitoids are those defined by Hickman (1983), except for the Coppin Gap Belt, which is the northern part of their Marble Bar Belt (see Figure 3.1 for names). The term gneiss is used for felsic igneous rocks which show compositional banding. A foliated granite is not considered to be a gneiss under this definition. The term migmatitic gneiss is used for compositionally banded felsic igneous rocks that show macroscopic evidence for partial melting. The term granitoid is used as a general term for all felsic and intermediate igneous rocks, whereas the term granite is restricted to the composition as defined by Streckeisen (1974, 1976), in the Pilbara only the late to post-tectonic granites. The abbreviation BIF is used for Banded Iron Formation.

For fault and shear zones the classification of Sibson (1977) is used (protomylonite, mylonite and ultramylonite). Kinematic indicators are named after White et al. (1986) for shear band cleavages (shear-bands = R-shears = C'-type shear-bands = Extensional Crenulation Cleavages) and after Passchier & Trouw (1996) for porphyroclasts (∂ and σ clasts). SL fabric is used as an abbreviation for a foliated and lineated fabric. The term terrain is used for the geographic area, the Pilbara granitoid-greenstone terrain, the term terrane is used in the sense of a tectonostratigraphic terrane.

Mapping was done on various scales. The Shaw Batholith was mapped on 1:100,000 scale, using available (Royal Australian Survey Corps) topographic maps and satellite images produced at the University of Utrecht. The greenstone belts were mapped using 1:40,000 black and white aerial photographs, and in some cases more detailed, 1:25,000 and 1:5000, colour aerial photographs (Coongan belt and Bamboo Creek Mine). Grid references in the text and figures for sample locations refer to the Australian map grid with 1 km intervals.

Stereoplots of structural data are always lower hemisphere equal area plots. Contours are determined by counts on a sphere. Plots were made using the Stereoplot program by N. Mancktelow.

With relation to ages, Ma is used when the age can be estimated to better than 10 Ma, Ga for ages that are more loosely constrained or to indicate a time span of more than 100 Ma.

Archean geology: what is different?

2.1 Introduction

The Archean period, from 4.0 to 2.5 Ga, is defined as the period containing the earliest rock record on Earth. It has been the subject of a long-standing debate regarding the processes active in this early period of Earth history. Two major issues in this debate have been the growth of continental crust and when modern style plate tectonics started. In this Chapter a short review will be given of the data available in the Archean rock record and proposed models for early Earth evolution, to serve as a background to this study of the Pilbara granitoid-greenstone terrain. The emphasis will be on the data available in the rock record on mid Archean granitoid-greenstone belts, and the differences with modern terrains. In various extensive reviews (Condie, 1981, 1994; Kröner, 1981, 1982, 1984, 1991; Windley, 1984; Nisbet, 1987; de Wit & Ashwal, 1996), the broader subject of Archean geology, its implications and controversies have been documented. The evolution of the atmosphere and hydrosphere is an important issue in Archean geology, but is beyond the scope of this Chapter. It has been discussed by Nisbet (1987, 1995) and Des Marais (1994).

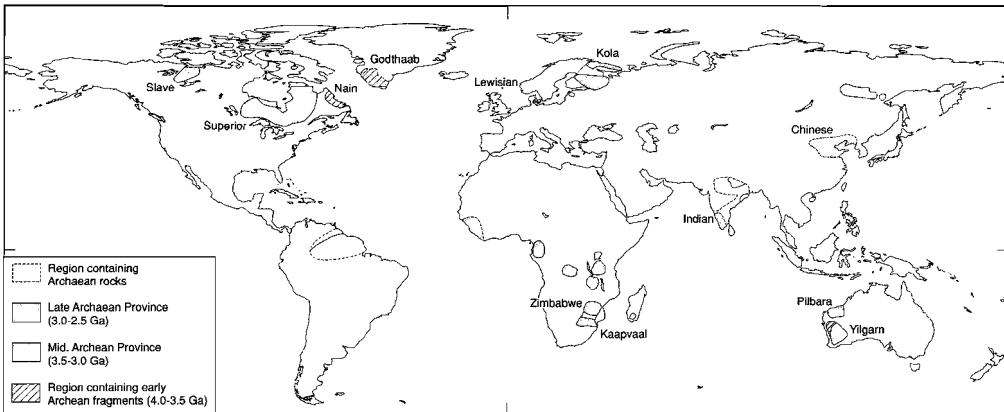


Figure 2.1 Schematic map, showing the main mid- and late Archean provinces, and regions that contain early Archean fragments.

Only a small part of the continents consist of Archean rocks and those Archean fragments consist mainly of late Archean terrains (Nisbet, 1987, see Figure 2.1). This causes a serious sampling problem, as discussed in detail by Condie (1981) and Nisbet (1987). The Archean rocks that have been preserved may have formed in a particular tectonic setting, resulting in their preservation, and therefore may not be representative of general processes active on Earth in the Archean. The data set from the oceanic crust, that has provided the key to our current understanding of plate tectonic process-

es, is completely lacking in Archean terrains. Within the Archean data set, there is strong bias toward late Archean terrains, which are aerially more extensive and contain a significant part of the Earth's mineral resources.

A number of models on the cooling of the Earth and its effects on the mantle and lithosphere geodynamics have been proposed in the past. With better understanding of current mantle and lithosphere geodynamics, the interaction between plate tectonics, plumes and convection, and improved numerical modeling techniques, these early Earth models have become more and more refined. Ultimately these models should agree with the limited data available on the Archean.

2.2 The Archean rock record

2.2.1 Oldest relics pre-4.0 Ga

The oldest rock record, summarized in Figure 2.2, starts with four zircons from the Mt. Narryer Sandstone in the Yilgarn (Australia), which have been dated between 4.1 Ma and 4.2 Ma (U-Pb, Froude et al., 1983; Kinny et al., 1990). The Mt. Narryer Sandstone itself is ca. 1000 Ma younger than the 4.2 Ga zircons. Assuming that the zircons are of terrestrial origin, they indicate that there was sialic crust present at 4.2 Ga. Although more >4.0 Ga zircons have been found recently (i.e. Nelson, 1996), no rocks of this age have been found.

There is general agreement that the earliest crust must have been oceanic, whereas continental rocks are 'second-hand' rocks (c.f. Taylor, 1989), formed during remelting of oceanic crust

By analogy with the moon, the Earth is likely to have been subject to intense meteorite bombardment until 3.8 Ga (Grieve, 1990). The lack of preserved rocks older than 4.0 Ga may indicate that older continental crust was recycled back into the mantle, possibly as a response to this bombardment (Taylor, 1989), or that continental rocks were extremely rare prior to 4.0 Ga (de Wit & Hynes, 1995).

2.2.2 Archean terrains 4.0-2.5 Ga

Archean terrains can be divided in three types: 1) gneiss terrains, 2) granitoid-greenstone terrains and 3) cratonic basins.

2.2.2.1 High grade gneiss terrains

The oldest rocks, ca. 4.0-3.9 Ga, are granitoid-gneisses and occur in Greenland (Itsaq Gneiss) and in

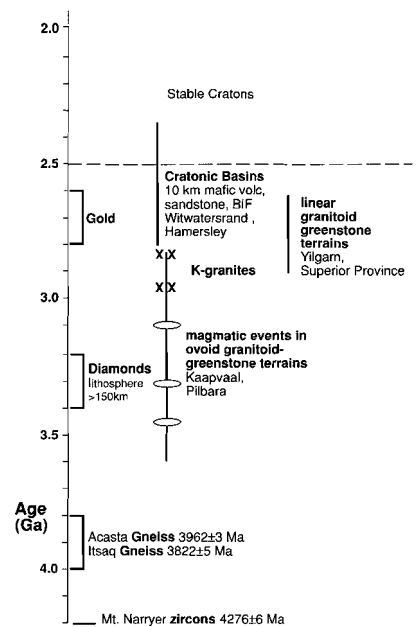


Figure 2.2 Summary of the Archean rock record, see text for discussion.

Canada (Acasta Gneiss & Nain Province). The overview of the oldest rocks by Nutman et al. (1996) shows that they are invariably overprinted by later (3.3. to 2.6 Ga) amphibolite to granulite facies metamorphism and are usually strongly deformed, making recognition of the earliest characteristics difficult. Lithologies are predominantly tonalitic and granodioritic (i.e. high Na-granitoids) with minor granites, supracrustal rocks, gabbros and ultramafics. Slightly younger, but otherwise similar gneisses occur in China (Anshan Complex, 3810 Ma, Song et al., 1996) and in Western Australia (Narryer Gneiss Complex, 3730 Ma, Nutman et al., 1991) and as enclaves in the Ancient Gneiss Complex in South Africa (3640 Ma, Compston & Kröner, 1988).

2.2.2.2 *Granitoid-greenstone terrains*

The second type of Archean terrain, granitoid-greenstone terrains, do not occur before, or are not preserved, until the mid Archean at ca. 3.5 Ga. They typically consist of granitoid-gneiss domes bordered by keels of volcano-sedimentary sequences (greenstones). The large-scale outcrop pattern of the granitoid-greenstone terrains is generally linear for late Archean terrains (e.g. Yilgarn Craton, Superior Province) but is ovoid for mid Archean terrains such as the Pilbara Craton (Figure 2.2).

Granitoids

The granitoid domes generally consist of early, variably deformed, tonalite-trondhjemite-granodiorite (TTG) suites, with enclaves of gabbro-diorite complexes, metavolcanics and metasediments. The TTG suites are intruded by late to post-tectonic higher K-granitoids (monzogranite, adamellite). This pattern of evolution toward higher K-granitoids in the final stages of cratonization is found in all granitoid-greenstone terrains (Condie, 1981), but the volume of late K-granitoids is more abundant in cratons which stabilized at ca. 2.7 Ga than in the older cratons (Ridley, 1992).

The TTG suites have been proposed to have formed by a variety of processes (Martin, 1994) including fractional crystallization of basaltic melts, alkali metasomatism and partial melting of a variety of sources (mantle, amphibolites, eclogites and tonalites). Most recent research favors an origin by partial melting of garnet-bearing amphibolite or hornblende eclogite, a model that is supported by both geochemical and experimental data (Martin, 1994; Rapp & Watson, 1995; Winther, 1996).

The origin of late monzogranites is less problematic as they can be modeled as partial melts of pre-existing TTG suites (Condie, 1981; Sylvester, 1994).

Greenstones

Greenstone belts typically consist of three to four volcano-sedimentary sequences, each a few km thick, divided by (angular) unconformities (Condie, 1994). The lower sequences are dominated by volcanic rocks, but the upper sequences commonly have a large component of clastic sediments (Hunter & Stowe, 1996). The volcanic rocks in greenstones are predominantly basalts (<18% MgO), estimated by Condie (1993) to constitute 55% of greenstone belt volcanics. Felsic volcanic rocks (dacites and rhyolites) and ultramafic volcanic rocks, komatiites (> 18% MgO, Arndt & Nisbet, 1982) are the two other main components of the volcanic sequences of greenstones. Andesitic volcanic rocks occur in some late Archean greenstone belts (Superior Province, e.g. Cousineau & Dimroth, 1982), but are rare in mid Archean greenstone belts. Due to the lack of intermediate volcanic rocks, the volcanic sequence in greenstones is frequently called a bi-modal sequence.

Before going into the chemical characteristics of volcanic rocks in greenstone belts, it has to be noted that they are often intensely altered (carbonate alteration and silicification) and generally metamorphosed under greenschist facies conditions. The alteration makes geochemical studies of volcanic rocks difficult, especially causing misinterpretation of discrimination diagrams relating bulk geochemistry to tectonic setting (Kröner, 1982).

Various groups of basalts have been recognized in greenstones, which are classified on the basis of MgO concentration and chondrite normalized La/Sm ratio, which is a measure of LREE enrichment. Low-Mg (< 9wt% MgO) basalts are referred to as tholeiites, Fe-rich tholeiites (Arndt et al., 1977) and calc-alkaline basalts if they are strongly LREE enriched (Sylvester et al., 1996). Various groups can be distinguished in high-Mg basalts, also called komatiitic basalts (9–18wt% MgO), including siliceous high Mg-basalts (Sylvester & Attoh, 1992), with more than 51% SiO₂. The abundance of subgroups show that greenstone basalts are a diverse group. The high-Mg basalts may have been derived directly from the mantle, with no differentiation on the way. In contrast, the low-Mg basalts must have been contaminated by crustal components or originated from an enriched mantle source (Arndt & Jenner, 1986; Barley, 1986; Sylvester et al., 1996). The REE patterns of Archean tholeiites show similarities to those of basalts occurring in oceanic ridges, oceanic plateaus and back-arc basins, depending on the LREE enrichment (Ludden, 1989; Thurston, 1994), but are enriched in Ni, Fe and Cr, and show subtle differences when compared to modern basalts (Cattell & Taylor, 1990). This means that they can not easily be assigned to a specific tectonic setting on the basis of trace element chemistry. The higher Ni, Fe and Cr was interpreted by Arndt (1989) as a result of deeper decompression melting due to a hotter mantle.

Basalts are commonly pillowed, indicating subaqueous extrusion, and high-Mg basalts contain spinifex textures much like komatiites, but with clinopyroxene and amphibole as the spinifex phase instead of olivine as in komatiites (Sylvester et al., 1996). Another unusual texture that is very common in Archean basalts are mm- to cm-sized felsic bodies, called ocelli. Their origin is not yet understood (Sylvester et al., 1996).

Komatiites, although a subordinate component of the typical greenstone belt sequence, take a prominent place in the discussion on Archean geology. They exhibit the very unusual spinifex texture of large (up to 0.5 m) bladed crystals of olivine or pyroxene. These spectacular rocks were first described by Viljoen & Viljoen (1969). Originally komatiites were all thought to be extrusive rocks, with the spinifex texture forming during rapid cooling. However, in recent re-examinations firm evidence was found for spinifex textured komatiitic sills (Arndt, 1994). Komatiites occur throughout the greenstone sequence and are not restricted to a basal position (McCall, 1981).

Komatiite melts are generally accepted to be the result of a relatively high degree of partial melting of a deep mantle source (Arndt, 1994). The high degree of partial melting is generally taken as evidence of a higher average mantle temperature. The estimates of the Archean mantle temperature based on the komatiite composition vary from 400–500°C hotter than at present, if komatiites are assumed to represent the overall mantle (Sleep, 1979; Nisbet & Fowler, 1983; Vlaar, 1986), to 100–300°C hotter than present if komatiites are assumed to represent hotspots (Sleep & Windley, 1982; McKenzie, 1984; Campbell & Griffiths, 1992). Campbell et al. (1989) suggested that the tholeiites result from melting in the cool head of a starting plume, whereas komatiites are produced by melt-

ing the hot conduit.

Grove & de Wit (1995) propose an alternative interpretation of the origin of komatiites, and regard komatiites as the result of melting of hydrous mantle at temperatures similar to present. The typical spinifex textures of komatiites in this view are regarded as ultramafic pegmatites and therefore as intrusive rather than volcanic rocks.

Komatiites are not restricted to the Archean, but are much more abundant than in later periods, with a few minor occurrences in the Proterozoic and Phanerozoic (McCall, 1981). Only one Phanerozoic komatiite (maximum MgO 19%) has been described, at Gorgona island (Echeverría, 1980).

Felsic volcanic rocks (dacites and rhyolites) consist of thick, often short flows, due to the high viscosity of Si-rich melts, and pyroclastic deposits. The felsic volcanos were generally partly submerged, unlike modern continental counterparts (Sylvester et al., 1996; Barley, 1993), producing mass-flow deposits around the volcano. The felsic volcanic rocks are commonly similar in age and composition to granitoids (TTG-suites) making up the batholiths in the granitoid-greenstone terrains (Halberg & Giles, 1986; de Wit et al., 1987; Bickle et al., 1993), and occur episodically, with intervals of 10-80 Ma.

Felsic volcanics can be subdivided in two groups (Condie, 1976). One has low concentrations of HREE and moderate to strongly fractionated chondrite-normalized REE patterns (La/Yb 10-100x chondrite), and the other has higher concentrations of HREE and moderately fractionated chondrite-normalized REE patterns. The first group formed by partial melting of basaltic rocks at lower- to sub crustal depth in the garnet-stability field and the second group formed by a similar process at shallower depth or by fractional crystallization of andesitic melt (Wyllie et al., 1996; Rapp, 1996). Intermediate to felsic assemblages of greenstone belts have been compared by many authors to island and continental magmatic arcs on the basis of their geochemical similarity to present day calc-alkaline suites (Glikson, 1972; Bickle et al., 1983; Nisbet, 1987; Barley et al., 1984). However this interpretation is regarded as unreliable by other authors because alteration and contamination of basaltic rocks can produce secondary calc-alkaline trends (Kröner, 1982; MacGeehan & McLean, 1980).

Sediments in lower greenstone sequences are thin, usually chert units, capping mafic to ultramafic volcanic succession. These are interpreted by Lowe (1994) as oceanic intraplate depositional systems. More mature clastic sediments in the upper greenstone sequences are thought to be related to orogenic/accretionary processes (Lowe, 1994; Eriksson et al., 1994).

One of the most crucial problems in granitoid-greenstone terrains concerns the basement to the greenstone sequences. Are the greenstones deposited on an underlying sialic basement or are greenstones the ophiolites of the Archean? Contacts between granite-gneisses and greenstones are almost always sheared or are intruded by younger granitoids (Nisbet, 1987; Bickle et al., 1994).

De Wit et al. (1987b) describe a ca. 3.5 Ga greenstone sequence as an ophiolite complex (The Jamestown Ophiolite Complex), which was subsequently obducted onto another terrane. However, Bickle et al. (1994) conclude that there is no good evidence for an ophiolitic origin of greenstones and does not accept the ophiolitic interpretation by de Wit et al. (1987b). Their conclusion is based on the lack of the lower part of the typical ophiolite complex, which consists of a sheeted dike com-

plex, gabbro and ultramafic cumulates, in greenstone sequences.

In some greenstone belts there is very reliable evidence that greenstones were deposited on continental crust from older xenocrystic zircons in the volcanics. These include ca. 3.4 Ga zircons in the 2.7 Ga Kambalda sequence in the Yilgarn (Compston et al., 1986) and a 3.7 Ga zircon in the 3.45 Ga felsic volcanic of the Warrawoona Group in the Pilbara (Thorpe et al., 1992).

Primitive ocean basin like greenstone sequences that lack evidence for a sialic basement, are alternatively interpreted as juvenile island arcs or as oceanic plateaus and hot spot islands due to plumes (Abbot & Mooney, 1995).

2.2.2.3 Deformation and metamorphism

Structural and metamorphic studies were carried out on high grade gneisses and granitoid-greenstone terrains. However, the general lack of pelitic rocks in Archean terrains make metamorphic studies difficult. A third source of metamorphic information comes from xenoliths of the lower crust in Southern Africa that are brought up in younger kimberlites.

High grade gneisses are intensely deformed and the original rock types have been transposed to a foliation parallel layering. TTG granitoids tend to intruded parallel to the layering and are also deformed. Several authors (Myers, 1980; Park, 1980) have stressed the original subhorizontal orientation of the gneissic foliation and some describe nappe-like large recumbent folds. The horizontal foliations have been variably explained by thrusting, extension and gravity spreading. Choukroune et al. (1995) describe domal structures in the gneisses of the Dharwar Craton (India) which they attribute to diapiric deformation.

Metamorphism of gneiss terrains is usually of the high temperature, low pressure type with anti-clockwise P-T-t paths (Percival, 1994). High pressure, low temperature metamorphism is extremely rare in Archean rocks. Eclogites were found in boudins in the late Archean (2.6 Ga) Snowbird tectonic zone in the Superior Province (Percival, 1994). Other Archean examples of blueschists or eclogites from surface rocks have not been described.

The above is in contrast to data available from Archean eclogitic xenoliths in kimberlites from South Africa and Siberia. Some of these xenoliths contain diamonds with inclusions of garnet which have been dated at 3.2–3.3 Ga (Sm-Nd, Boyd & Gurney, 1986; Richardson et al., 1984), indicating a relatively cool (900–1200°C) lithosphere at 150–200 km depth. Recently, oxygen isotope evidence was found for an Archean oceanic (Jacob et al., 1994) or continental crustal (Daniels et al., 1996) origin of these diamondiferous eclogites, indicating Archean subduction-type processes. The major uncertainties in interpretations from the xenoliths arise from the age constraints. A Sm-Nd age of 3.2–3.4 Ga of garnet inclusions in diamonds does not necessarily mean that either the diamond or the xenolith is that age.

Structures in granitoid-greenstone terrains were originally explained by (solid state) diapirism (MacGregor, 1951; Gee et al., 1981; Hickman, 1984; Anhaeusser, 1984). This is an especially appealing model to explain the circular outcrop pattern of the Pilbara and Zimbabwe Cratons. However, more detailed structural studies of granitoid-greenstone terrains showed a more complex structural evolution. Thrust structures are now widely recognized to be an important structural component in

greenstone belts (de Wit, 1982; Boulter et al., 1987; Kusky, 1989, 1990; Swager et al., 1990; Chown et al., 1992). Hammond and Nisbet (1992) and Williams and Whitaker (1993) related major shear-zones in the Kalgoorlie terrain to core-complex type extension controlling greenstone deposition and granitoid intrusion. Late stage extensional structures, post-dating thrusting, have recently been described for various terrains (James & Mortensen, 1992; Kusky, 1993; de Ronde & de Wit, 1994). Metamorphic studies of granitoid-greenstone terrains are few and biased toward higher grade domains. In general the metamorphic isograds are zonal around, and increasing toward, granitoid-gneiss terrains rather than toward individual plutons. This pattern is interpreted by Ridley (1992) as an indication of vertical movement rather than contact metamorphism. Most P-T estimates of peak metamorphic assemblages in greenstones are close to the aluminium silicate tripple point (600°C, 4 KBar, Grambling, 1981; Ridley, 1992). P-T-t paths are difficult to determine, but examples indicate prograde metamorphism at constant pressure (Bickle & Archibald, 1994; Wong, 1986).

The complex contact geometries of granitoids and greenstones and overprinting relations have led to a variety of genetic models for the overall development of granite-greenstone terrains ranging from solid-state diapirism to subduction related accretionary models (e.g. Nisbet, 1987). A group of models propose deposition of greenstones on a pre-existing continental crust with subsequent deformation through solid-state diapirism (e.g. Gee et al., 1981; Hickman, 1984; Collins, 1989; Delor et al., 1991; Jelsma et al., 1993; Boulhallier et al., 1993) or regional compression (e.g. Nisbet, 1987; Snowden, 1984).

Choukroune et al. (1995) propose an entirely diapiric origin of the structures in mid Archean terrains with regional compressional structures becoming more important toward the end of the Archean. Other models portray greenstone belts as allochthonous remnants of accreted oceanic crust, marginal basins and island arc material, with supracrustals forming contemporaneously with regional compressional deformation (de Wit, 1982; Barley et al., 1984; de Wit et al., 1987, 1992; Kusky, 1989, 1990; Hoffman, 1991). Extensional models for greenstone generation include early extension along continental rifts (Henderson 1981, 1985; Easton, 1985; Park, 1982; Williams & Whitaker, 1993), back-arc basin extension (Windley, 1984; Fyson and Helmstaedt, 1988), and late-orogenic extension due to the collapse of thickened crust (James and Mortensen, 1992; Kusky 1993).

2.2.2.4 Cratonic Basins

Mid Archean gneiss terrains and granitoid-greenstone terrains of the Pilbara and Kaapvaal Cratons are covered by relatively undeformed late Archean sedimentary/volcanic successions that developed in a syn-rift and stable shelf setting (Eriksson and Fedo, 1994). Examples of such sequences are the Pongola and Witwatersrand Supergroups in South Africa and the Mt. Bruce Supergroup in the Pilbara Craton. These have cumulative thicknesses up to 11 km, possibly indicating the Earth's first major phase of basin development following the Mid Archean.

2.2.3 Mineralization in Archean terrains

Archean terrains are some of the most richly mineralized areas on Earth. A recent overview of Archean mineralization is given by Groves & Barley (1994). The most highly mineralized Archean terrains are the granitoid-greenstone terrains, with large VMS Cu-Zn deposits, komatiite Ni deposits, lode-gold deposits and the 'cover' successions with large iron-ore provinces and the highly mineralized (Au-U) Witwatersrand Basin. High grade gneiss terrains are poorly mineralized, apart from rare-

metal pegmatites.

Most classes of mineral deposits are non-uniformly distributed in time (Woodall, 1988; Barley & Groves, 1992). This is especially apparent for lode-gold deposits, which show a large peak in the late Archean (ca. 2750) which is only rivaled by modern Pacific Rim gold deposits (Groves and Barley, 1994). Mid Archean greenstone belts generally host smaller gold deposits.

2.2.4 Other constraints to early Earth evolution

2.2.4.1 Geochemical constraints

Nd model ages (TDM) of crustal igneous rocks are assumed to reflect the age of first extraction of melt from the mantle. On the basis of Nd model ages it can be concluded that at least 50-60% of the continental crust was in place at ca. 2.6 Ga. (Taylor & McLennan, 1995).

The Sm/Nd isotopic composition of early Archean rocks has been used to constrain the geochemical characteristics of the Archean mantle (Bowring & Housh, 1995). The results indicate that the earliest mafic to ultramafic rocks (3.9 Ga) on Earth were derived from a mantle source that was already depleted (with a high Sm/Nd ratio) by extraction of an earlier (oceanic) crust. This is taken as evidence for the existence of an extensive earlier crust. However, this earlier crust or relicts of it have not been found yet on the Earth's surface. This is explained by assuming that it was recycled back into the mantle by subduction related processes (Bowring & Housh, 1995; Jacobson & Dymek, 1988). A recent independent evaluation of the Nd isotopic composition by investigation of Hf systematics of zircons from the same rocks, failed to verify the scale and variability of the Archean mantle depletion (Vervoort et al., 1996). The implication is that the Nd systematics of the 3.9 Ga gneisses are affected by later metamorphic events and are not a reliable record of early crust and mantle processes.

REE patterns in fine-grained sediments, and especially the presence or absence of the Eu anomaly, record an averaged signature of igneous events in the upper continental crust. Compared to the very consistent post-Archean REE pattern in fine-grained sediments the Archean record shows some abrupt changes from 3.2 to 2.5 Ga (Taylor & McLennan, 1995). The Eu anomaly is lacking in most Archean sediments and they show little enrichment in LREE, in contrast to post-Archean sediments, indicating an episodic change in the upper crustal composition at the end of the Archean. The lack of negative Eu anomalies in Archean sediments is strong evidence that intracrustal melting, whereby Eu is left in residual plagioclase in the lower crust, has only taken place to a limited extent in the Archean. The change in Eu and LREE signatures in the late Archean sediments may be related to emplacement of K-rich granitic rocks (Taylor & McLennan, 1995).

2.2.4.2 Geochronological constraints

The available geochronological data from crustal rocks show time periods when large areas of continental crust were formed, alternating with periods when no or little crust was formed. This was first noted by Moorbath (1978) and it is confirmed as more precise dates became available for Archean rocks. Peaks of dates in crustal rocks appear to occur at ca. 3.9 Ga, 3.5 Ga, a major peak at 2.7 Ga, 1.8 Ga, 1.3 Ga and 0.7 Ga (Stein and Hofmann, 1994). The dating record is still incomplete and may

change as more precise dates become available.

2.2.4.3 Geophysical constraints

Seismic reflection data are available from the Yilgarn Craton and the Superior Province (Drummond et al., 1993; Calvert et al., 1995). General characteristics are a ca 35 km thick, dominantly felsic crust with greenstones that are relatively shallow (not deeper than 6–9 km) and have a flat, probably structurally defined, base. This confirms earlier geophysical data on the Transvaal Craton (Stettler et al., 1988; de Beer & Stettler, 1988). Granites have a flat, sheetlike geometry, with a limited depth extent. In the Superior Province, a dipping seismic reflection that extends 30 km into the mantle was interpreted as a relic 2.69 Ga subduction zone (Calvert et al., 1995).

A worldwide review of seismological data for Precambrian provinces (Durrheim & Mooney, 1991, 1994) has shown that Archean crust is thinner (27–40 km) than Proterozoic crust (40–55 km) and lacks a basal high velocity (>7 km/s) layer. This trend was previously noted for the Precambrian crust of Australia (Drummond & Collins, 1986; Drummond, 1988). Seismological data also indicate (Beghoul & Meren, 1992) that the lithosphere is appreciably thicker under Archean provinces (260–300 km) than underneath Proterozoic provinces (240–280 km).

Durrheim & Mooney (1994) explain these features in a model in which the higher temperature of the mantle results in high partial melting of the mantle at the MOR, producing komatiitic melts and leaving an ultradepleted mantle lithosphere which is less dense than the surrounding lithosphere. The lower density of the Archean mantle lithosphere makes it stable and not prone to delamination and recycling in the asthenosphere, thereby preventing underplating of a high velocity basaltic layer at the base of the crust.

Heat flow measurements from Archean and Proterozoic terrains indicate that Archean cratons are characterized by low heat flow (ca. 40 MW/m²). The heatflow increases away from Archean cratons in Proterozoic provinces to ca. 80 MW/m² (Morgan, 1984; Nyblade & Pollack, 1993). This appears to be a consistent pattern worldwide. Nyblade and Pollack (1993) show that this pattern can be explained mainly by deflection of the heat flow by the thicker Archean lithosphere with possible additional effects of a high crustal heat production in Proterozoic crust.

2.3 Thermal evolution, Archean dynamics and crustal growth models.

The Earth has two primary sources of heat: continuous radioactive decay, principally from ⁴⁰K, ²³⁸U, ²³⁵U and ²³²Th, and primeval heat sources, such as secular cooling of the Earth and heat produced by core segregation during accretion of the Earth at 4.56 Ga (Taylor & McLennan, 1995). The relative importance of the two remains an outstanding question. Estimates vary from contributions of 20% to 50% of the primeval heat sources. The heat produced by radioactive decay has decreased markedly since the Archean (Figure 2.3): at 3.5 Ga the heat produced was approximately three times higher than it is today (O'Nions et al., 1978).

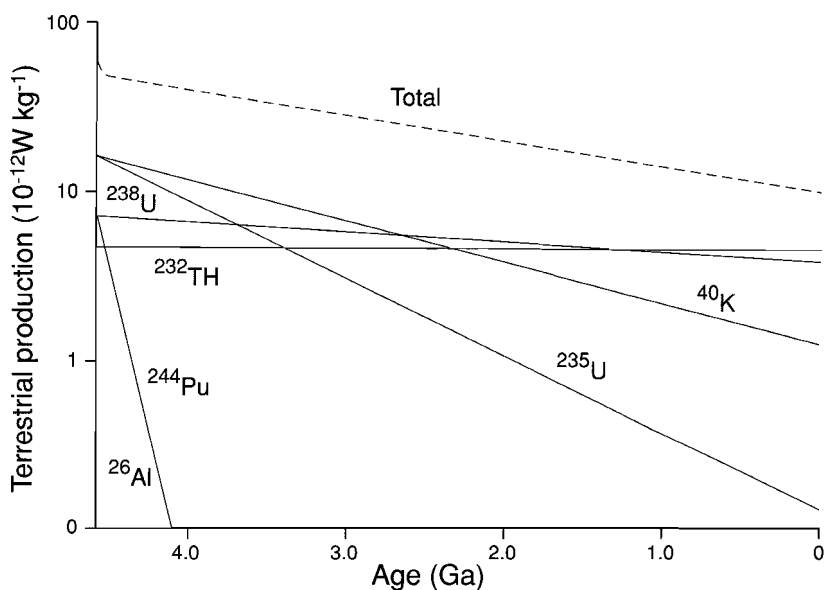


Figure 2.3 Heat production from the significant radioactive nuclides available in the Earth. K, Th and U values are extrapolated from present crust and mantle abundances. Al and Pu values are estimated from nucleosynthesis theory, using stable isotopes in the Allende meteorite (after O’Nions et al., 1978; Hall & Hughes, 1990)

The subsequent cooling of the Earth, geodynamic processes and the separation of the continental crust from the primitive mantle are intimately related subjects that have been discussed and modeled intensively over the last 15 years (for an overview see Nisbet, 1987 and Taylor and McLennan, 1995). In the seventies an intense discussion started on the subject of plate tectonics in the Archean (McCall, 1981). The discussion was largely based on a limited field data base and models on the thermal evolution of the Earth were not yet available.

In the eighties, when plate tectonic models for the Archean gained acceptance, especially among geochemists (Nisbet, 1987), there was a larger input of quantitative models on the evolution of the early Earth. Komatiitic lavas, at that time interpreted as whole mantle witnesses, indicated a substantially higher mantle temperature (Bickle, 1986). This led to the idea that the extra heat was dissipated by increased spreading activity, defined as total ridge length \times average spreading rate (Bickle, 1978; Nisbet & Fowler, 1983; Hargraves, 1986).

Nisbet & Walker (1982) raised the possibility that a buried magma ocean existed in the Archean mantle, based on the possibility that komatiitic melts could be denser than olivine. There is general agreement that a magma ocean existed in the moon at ca. 4.4 Ga (Shirley, 1983, Walker, 1983; Warren, 1985). This magma ocean led to the formation of lunar anorthosites and caused a strong fractionation of Eu, with enrichment in the plagioclase rich anorthosites and depletion in other lithologies. There is no evidence for massive volume of Archean anorthosites, or an early fractionation of Eu in the Earth. Therefore the existence of a shallow terrestrial magma ocean is unlikely (Simon, 1990).

In a hotter mantle, pressure release melting starts at a deeper level, producing a larger volume of melt, resulting in a thicker oceanic crust and a strongly depleted harzburgite zone in the mantle lithosphere

(Sleep & Windley, 1982; Vlaar, 1986; McKenzie & Bickle, 1988). Some calculations indicate that the Archean oceanic lithosphere remains stably stratified and subduction of the oceanic crust did not occur (Hoffman & Ranalli, 1988; Davies, 1992; Vlaar et al., 1994). Hoffman & Ranalli (1988) propose a delamination model, with obduction of the upper part of the oceanic crust. According to Davies (1992) this is only possible for an oceanic crust that is not too thick. A second model that has been proposed is the 'drip' model in which the lower part of the oceanic lithosphere, which is too soft to be plate like, becomes unstable due to density increase during conversion to garnet-granulite and eclogite (Campbell & Griffiths, 1992; Davies, 1992; Vlaar et al., 1994).

de Wit & Hart (1993) propose a model in which the hydration of the oceanic crust at the MOR plays a major role. In this model the pre-4.0 Ga MOR stood out above the sealevel, preventing hydration. The earliest dry crust is assumed to have been completely recycled back into the mantle. Between 4.0 and 3.0 Ga, after drowning of the MOR, an obduction dominated tectonic process was active. TTG suites are considered to be the melting product of the stacked hydrated oceanic crust. After ca. 3.0 Ga a modern style plate tectonic process with subduction took over, characterized by shallow subduction of oceanic crust.

Stein & Hofmann (1994) propose a model in which the crust grew episodically. Their model assumes that the Earth alternated between two modes of convection and dynamic evolution. In the first mode, called the Wilsonian period, plate tectonics operate in the present day manner. The upper mantle is isolated from the lower mantle. In the second mode, called MOMO period, there is significant exchange between lower and upper mantle (mantle overturn), with plumes originating from the core-mantle boundary causing major crustal growth as oceanic plateaus and continental flood basalts and/or underplating. The MOMO mode is regarded as the main crustal growth period (Figure 2.4).

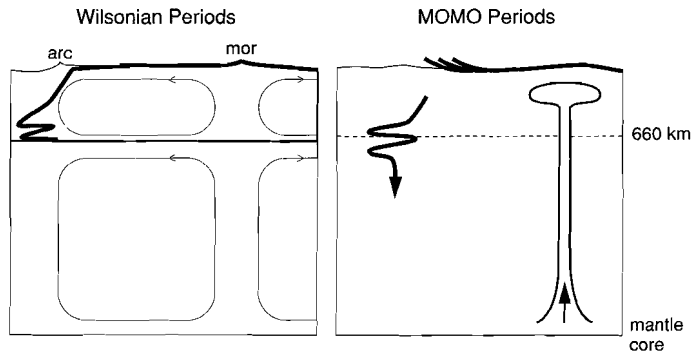


Figure 2.4 Schematic representation of the MOMO (Stein & Hofmann, 1994) and Wilsonian (Wilson, 1966) convection modes. Left, during Wilsonian periods, with plate tectonic operating much like at present, with opening and closing of oceans, subduction of oceanic crust, and mantle convection with isolated upper and lower mantle. Plumes originate from the base of the upper mantle. Right, during the mantle overturn (MOMO) episodes, accumulated cold material descends from the 660 km boundary layer into the lower mantle, and multiple plumes rise from the core-mantle boundary. This is the period during which massive crustal growth occurs. Subduction cannot occur because the oceanic crust is too thick and does not become unstable. (adapted after Stein & Hofmann, 1994; Davies, 1995)

Davies (1995) explores this idea using a thermal evolution model incorporating parametrized convection and two criteria for breakdown of layering causing mantle overturn. This model results in episodic behaviour of the mantle with long (>100 Ma) intervals of layering (plate tectonics) and short periods (>10 Ma) of mantle overturn (plumes and cold drips). Due to the rapidly cooled upper mantle in this model, plate tectonics could have developed at an early stage, but would have ceased during the hot mantle overturn periods. During the overturn periods large volumes of unobductable mafic crust is produced in a short time and accumulates into thick piles with both oceanic plateau and island arc characteristics.

Continental crustal growth models, that have been proposed over the last 25 years, describing the differentiation of the crust from the primitive mantle, reflect the discussion on the processes active in the early Earth (Figure 2.5).

Two basic groups of models can be distinguished. The first group of models (Hurley & Rand, 1968; Veizer & Jansen, 1979; McLennan & Taylor, 1982) are largely based on the preserved geologic record, with very little or no crustal growth prior to 4.0 Ga and a steadily increasing rate of crustal growth or episodic crustal growth, with a peak in the late Archean.

The second group of models (Fyfe, 1978; Armstrong, 1981; Reymer & Schubert, 1985) advocate rapid crustal growth prior to 4.0 Ga and a more or less steady state since. This can only be achieved if the crust is continuously being recycled by plate tectonic processes. This type of model is largely based on the Sm/Nd isotopic record and freeboard constraints, which are both considered to be less stringent than previously thought (Taylor & McLennan, 1995; Vervoort et al., 1996). General agreement has not yet been reached on the most likely continental crustal growth model.

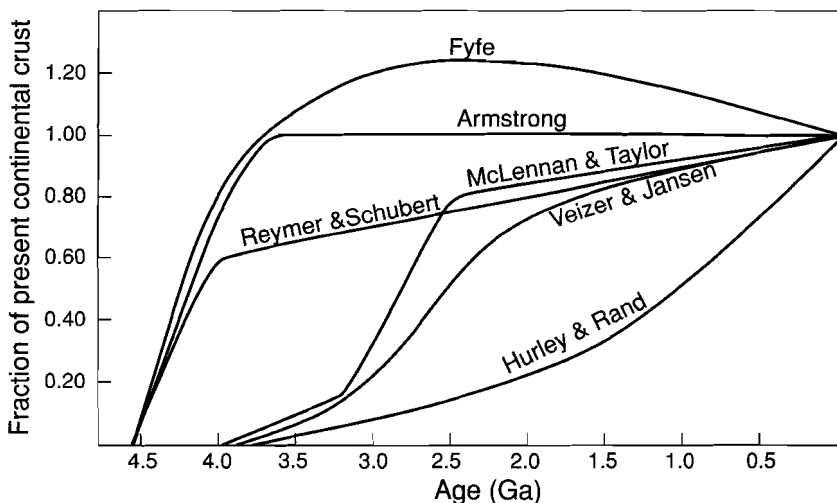


Figure 2.5 Various crustal growth models (from Taylor & McLennan, 1985). Models include those of Hurley and Rand (1969), Fyfe (1978), Veizer and Jansen (1979), Armstrong (1981), McLennan and Taylor (1982), Reymer and Schubert (1984).

2.4 Synthesis.

In the last years studies of Archean terrains have increasingly been interpreted in modern style plate tectonic settings. This is especially well documented for late Archean terrains such as the Yilgarn Craton and the Superior Province. In these cratons there is good evidence, based on geochronological data, for terrane accretion (Myers, 1995; Jackson & Cruden, 1995). However, apart from the inferred late Archean subduction zone in the Superior Province (Calvert et al., 1995), there is little direct evidence for subduction zones, such as found in most modern type accretionary zones in the form of high pressure mineral assemblages. Although modern day plate tectonic processes, such as subduction, seem to be supported by data in the late Archean this is not so clear for mid Archean terrains.

This is important because models for Archean geodynamics invariably indicate that subduction of oceanic crust in an Earth with a hotter mantle is not possible (Hoffman & Ranalli, 1988; Davies, 1992; Vlaar et al., 1994).

The rock record does show some important differences between Archean terrains and Proterozoic terrains, the most important being the abundance of komatiites, the bimodal character of greenstone sequences, the extensive alteration of greenstone sequences, general low pressure metamorphic assemblages, thickness and structure of the Archean lithosphere, large volume of mineral deposits in the late Archean, especially lode gold and the lacking Eu anomaly in Archean fine-grained sediments. In contrast, the early Proterozoic is characterized by crustal stability and intracratonic basins (Kröner, 1982), mafic dyke swarms, layered mafic to ultramafic intrusions (Hall & Hughes, 1993) and large anorthosite complexes (Ashwal, 1993)

For most greenstone sequences it is still uncertain in what type of setting they formed. Interpretations vary from ophiolite complexes, island arcs, oceanic plateaus, hotspot islands to continental flood basalts. There may not be one characteristic type of setting for all greenstone belt sequences (de Wit & Ashwal, 1996).

The interpretation of structures in granitoid-greenstone terrains is still a major point of discussion and is generally polarized in an interpretation involving only gravity induced structures versus an interpretation involving regional stress fields (extension and compression).

In order to resolve the many outstanding problems in interpreting Archean terrains and especially mid Archean terrains, integration of detailed field data (structural, stratigraphic and metamorphic), geochronological and geochemical data is needed as well as quantitative models on early Earth dynamics and thermal evolution.

If the episodic models by Stein & Hoffman (1994) and Davies (1995) are a realistic description of the evolution of the mantle and lithosphere dynamics, the main question governing Archean geology should be rephrased. Instead of: 'Were modern day tectonic processes active in the Archean and if not, when did they start?', it should be: 'Were there alternating periods in Earth history with and without modern day plate tectonic processes, and when did they occur?'

Introduction to the geology of the Pilbara

3.1 Introduction

The Pilbara Craton consists of a granitoid-greenstone terrain unconformably overlain by the relatively undeformed Fortescue Group, the basal sequence of the Hamersley Basin (Figure 3.1). The granitoid-greenstone terrain, which contains ovoid outcrops of granitoids surrounded by greenstone belts, formed between 3.5 and 2.8 Ga, whereas the base of the Fortescue Group was dated at 2.77 Ga (Arndt et al., 1991). This thesis is concerned with the granitoid-greenstone terrain; the Fortescue Group is therefore regarded as late cover.

This Chapter is aimed at providing an overview of the geological data available for the Pilbara thus far. It is not an exhaustive review of all data available on the Pilbara but provides a base for the following Chapters. Detailed data in relation to the studied areas are given in the introduction of each Chapter where necessary.

Although the Pilbara Craton is generally seen as one of the best exposed Archean Cratons, large parts in the western Pilbara are covered by Mesozoic and Cenozoic sediments (Hickman, 1983, Figure 3.1). The eastern Pilbara is well exposed although deeply weathered in places, and consequently most workers have concentrated on this part of the granitoid-greenstone terrain.

Much of the initial mapping in the 1970's and 1980's was done by the Geological Survey of Western Australia, producing 1:250,000 scale lithological maps covering the whole Pilbara granitoid-greenstone terrain. The results of this mapping work are described in an overview by Hickman (1983). Other workers in the Pilbara have concentrated on the geochronology, stratigraphy and geochemistry of the volcanics and granitoids (e.g. Thorpe et al., 1992; Bickle et al., 1989, 1993; Barley, 1993). On the contrary, metamorphism, structural relations and kinematics have received little attention (e.g. Bickle et al., 1985; Wijbrans & McDougall, 1987).

3.2 Lithologies and geochronology

3.2.1 Lithostratigraphy and geochronology of greenstones

Three established stratigraphic subdivisions are recognised for the supracrustal in the Pilbara: the Warrawoona Group, the Gorge Creek Group and the Whim Creek Group (Hickman, 1983; Horwitz, 1990). Recently, Buick et al. (1995) showed that locally a separate, older succession underlies the upper Warrawoona Group, called the Coonterunah Succession. See Figure 3.1 for the distribution of stratigraphic groups and locations of dated samples, and Figure 3.2 for an overview of isotopic dates and important stratigraphic subdivisions. The Warrawoona Group is the most widely

Figure 3.1

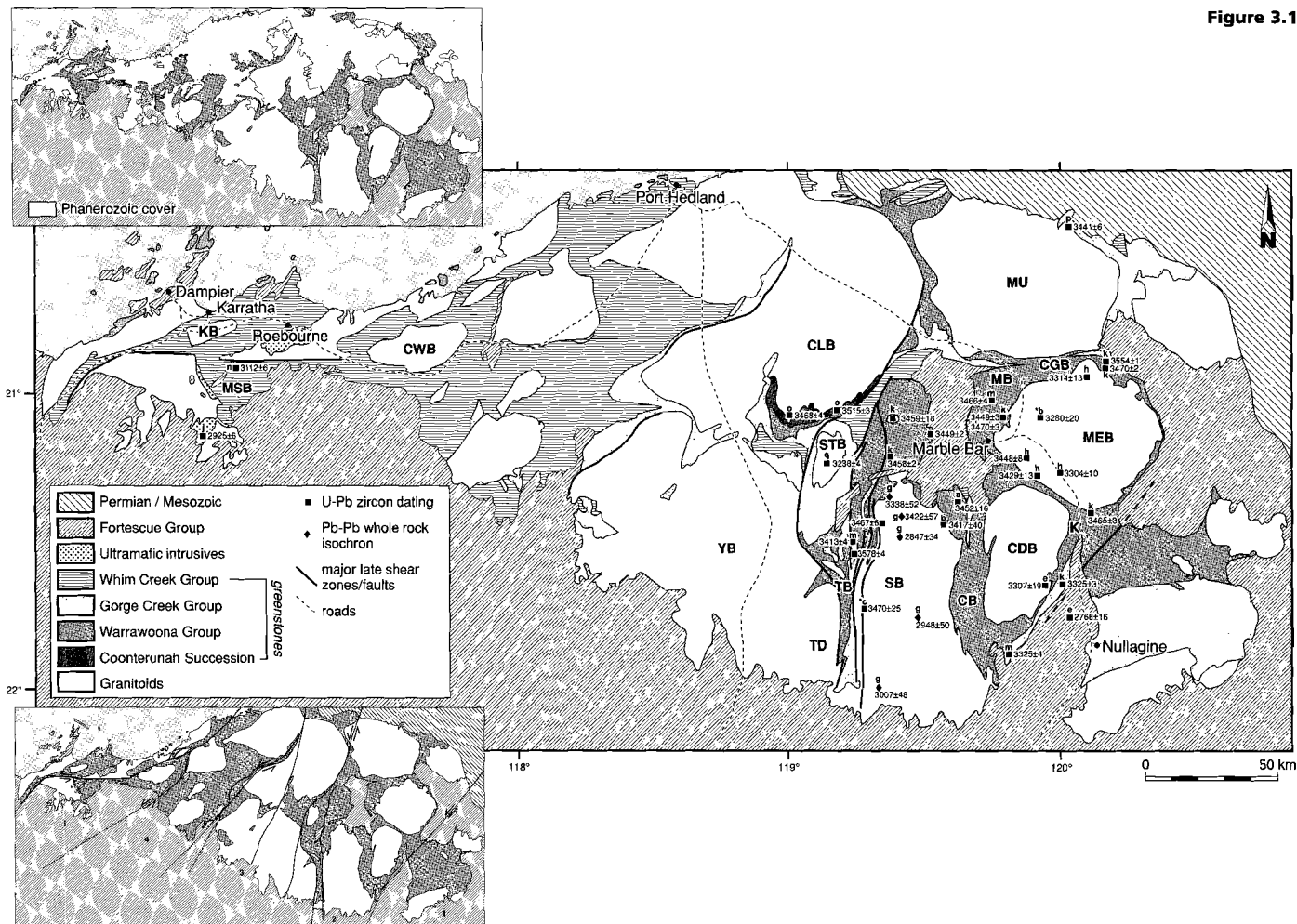


Figure 3.1 Interpretative geological map of the Pilbara granitoid-greenstone terrain based on Hickman (1983) and Krapez (1993), showing the distribution of granitoids and the four main stratigraphic divisions in the supracrustals. U-Pb and important Pb-Pb dating (indicated with references below) sample locations are shown. Letters refer to the following authors: a=Pidgeon (1978a), b=Pidgeon (1978b), c=Williams et al.(1983), e=Pidgeon (1984), f=McNaughton et al.(1988), g=Bickle et al. (1989) Pb-Pb whole rock, h=Williams & Collins (1990), i=Thorpe et al.(1990), j=Arndt et al. (1991), k=Thorpe et.al. (1992), l=Bickle et al. (1993), m=McNaughton et al. (1993), n=Horwitz & Pidgeon (1993), o=Buick et al. (1995), p=Nelson (1996), q=Smith et al. (in press).

CDB= Corunna Downs Batholith, CLB= Carlindi Batholith, CWB= Caines Well Batholith, KB=Karratha Batholith, MEB= Mt. Edgar batholith, MU= Muccan Batholith, SB= Shaw Batholith, YB= Yule Batholith, CB= Coongan Belt, CGB= Coppin Gap Belt, K= Kelly Belt, MB= Marble Bar Belt, MSB= Mt. Sholl Belt.

Inset above shows generalized geological map of the Pilbara showing the distribution of the granitoid-greenstone terrain, the Hamersley Basin (Fortescue Group) and the area covered by younger (Mesozoic and Cenozoic) sediments.

Inset below shows tectonostratigraphic division in domains (1-5) of the Pilbara granitoid-greenstone terrain according to Krapez (1993)

recognised part of the succession in the eastern Pilbara. It comprises of high Mg pillow basalts and massive tholeiites, subordinate peridotitic komatiites, minor chert units, BIF's and clastic sediments. Felsic volcanics of the Duffer Formation divide the Warrawoona Group into a lower Talga Talga Subgroup and an upper Salgash Subgroup (Figure 3.2). Geochronological data suggest deposition of the Warrawoona Group between 3475 and 3435 Ma (Thorpe et al. 1992). The felsic volcanics of the Duffer Formation give U-Pb single zircon ages consistent within error of the conventional U-Pb zircon age of 3452 ± 16 Ma (Pidgeon, 1978a; Thorpe et al. 1992; McNaughton et al., 1992). However, Hamilton et al. (1981) dated a suite of samples from the North Star Basalt Formation with the Sm-Nd whole rock method at 3560 ± 32 Ma. This may be an indication that the base of the Warrawoona Group is older than 3.5 Ga. Recent ion microprobe data by McNaughton et al.(1993) show that there are still inconsistencies in the dates for the individual members of the lower Warrawoona Group, but all are in the above range.

The upper Warrawoona Group unconformably overlies the Coonterunah succession, which contains mainly mafic volcanics and minor felsic volcanic rocks, of which a rhyolite was dated at 3515 ± 3 Ma (U-Pb, SHRIMP, Buick et al., 1995). The Gorge Creek Group, which consists mainly of clastic and BIF units, pillow tholeiites, and minor peridotitic komatiites, unconformably overlies the Warrawoona Group. The lowermost unit of the Gorge Creek Group, the felsic volcanic rocks of the Wyman Formation, has been dated at 3325 ± 4 Ma by conventional and ion-microprobe U-Pb methods (Thorpe et al., 1992; McNaughton et al., 1993). The upper age of the Gorge Creek Group is not well constrained, but is indirectly dated at ca. 3260 Ma (Vearnecombe et al., 1995). In the Shay Gap area, in the north eastern Pilbara, an unconformity was described (Dawes et al., 1995) between the foliated Muccan granitoid, dated at 3443 ± 6 Ma (U-Pb, SHRIMP, Nelson, 1996), and the BIF unit in the lower Gorge Creek Group.

The youngest of the four major stratigraphic subdivisions is the Whim Creek Group, constrained between ca. 3100 Ma and 2900 Ma (Horwitz and Pidgeon, 1993) and which is best developed in the western Pilbara. The precise date of this unit from felsic volcanics in the Whim Creek area, at 3112 ± 6 Ma (Horwitz & Pidgeon, 1993), is now confirmed by more recent dates in the Mt. Sholl area of felsic volcanics (3118 ± 3 Ma rhyolite, 3115 ± 5 Ma felsic tuff and 3125 ± 4 Ma dacite, U-Pb single zircon, Nelson, 1996). The clastic sediments in Lalla Rookh Basin are thought to belong to this group (Krapez and Barley, 1987).

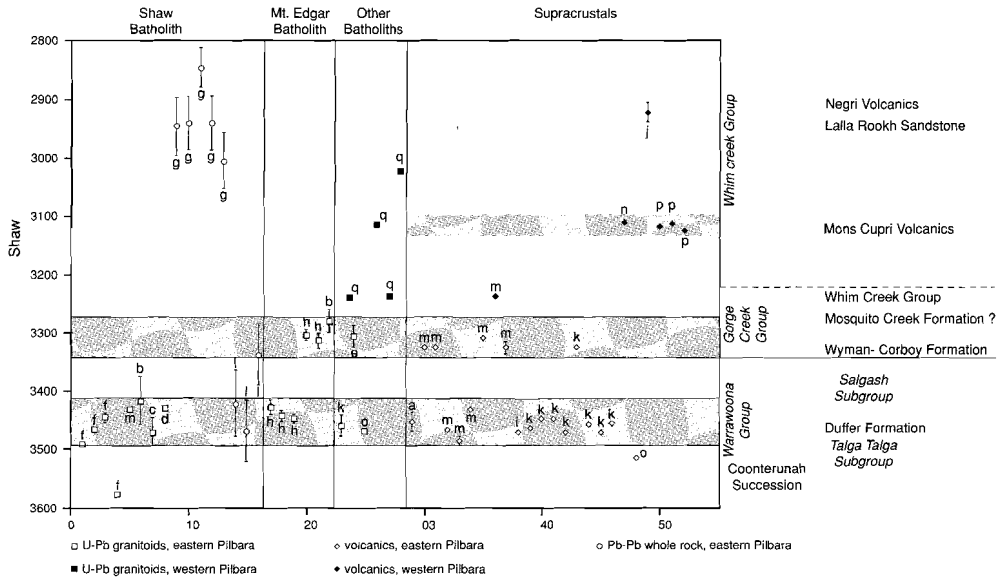


Figure 3.2 Stratigraphic column showing the main stratigraphic subdivisions and isotopic dates. a=Pidgion (1978a), b=Pidgion (1978b), c=Williams et al.(1983), d=Froude et al.(1984), e=Pidgion (1984), f=McNaughton et al.(1988), g=Bickle et al. (1989), h=Williams & Collins (1990), i=Thorpe et al.(1990), j=Arndt et al. (1991), k=Thorpe et al. (1992), l=Bickle et al. (1993), m=McNaughton et al. (1993), n=Horwitz & Pidgion (1993), o=Buick et al. (1995), p=Nelson (1996), q=Smith et al. (in press).

The originally proposed layer-cake stratigraphy (Hickman, 1983) in the Pilbara is no longer thought to be an accurate description of the supracrustal sequence. More detailed local studies showed major lateral facies variations in volcanic and sedimentary units (Lowe, 1983; Buick, 1985; DiMarco & Lowe, 1989; Horwitz, 1986, 1990). Facies variations and distribution of stratigraphic units may be related to major N-S trending lineaments that, according to Krapez & Barley (1987) and Krapez (1993), divide the Pilbara Craton in 5 tectonostratigraphic domains, with stratigraphic sequences becoming younger toward the west over these lineaments (Figure 3.1).

Geochemical studies of volcanic rocks in the Pilbara suffer from the general problem in greenstone belts: hydrothermal alteration and low grade metamorphism (Hickman, 1981; Barley, 1993). Barley (1993) interpreted the geochemical pattern of the Duffer Formation and sediments in the Warrawoona Group as part of a shallow water supra subduction volcanic arc setting. This is mainly based on the calc-alkaline type geochemistry of the Duffer formation. Mafic and ultramafic volcanics of the Warrawoona Group show a more oceanic type geochemistry (Glikson & Hickman, 1981) but are not unequivocal (Barley, 1993). The often large stratigraphic thickness of low grade hydrothermal metamorphism was interpreted by Barley (1993) as indicative of an island arc type environment. The Warrawoona Group sediments contain stromatolite-like structures that, if they are biogenetic, are among the oldest evidence for life on Earth (Lowe, 1980, 1983, 1994; Buick et al., 1981). The only felsic volcanic of the Gorge Creek Group, the Wyman Formation, is a rhyolite, and is best explained by melting of sialic crust (Hickman, 1983), whereas the mafic volcanics of the Gorge Creek Group have island arc or continental affinities (low TiO_2 and high K_2O , Hickman, 1983).

3.2.2 Petrogenesis and geochronology of granitoids

The granitoid batholiths in the eastern Pilbara cannot be described as simple dome structures. They comprise several plutons intruded during different episodes of the evolution from about 3500 Ma to 2850 Ma, and in turn contain enclaves of a variety of rock types. Two well studied granitoid complexes in the eastern Pilbara are the Shaw Batholith (Bettenay et al., 1981; Bickle et al., 1985, 1989, 1993, see also Figure 4.2) and the Mount Edgar Batholith (Collins, 1989, 1993; Williams and Collins, 1990). The two batholiths have much in common in geochemical and geochronological terms.

Evidence for a basement pre-dating the Warrawoona Group is presented by McNaughton et al. (1988) who identified relics of an anorthositic-gabbro suite dated at 3578 ± 4 Ma with the U-Pb zircon method in the western Shaw Batholith.

Highly deformed granodiorite gneisses with numerous greenstone enclaves occur in the western part of the Shaw Batholith. Their less deformed equivalents occur along the northern margin of the batholith and are considered to represent the oldest intrusive rocks in the Shaw Batholith (Bickle et al., 1993). The latter consist of granodiorites to tonalites that have been referred to as the North Shaw Suite (Bettenay et al., 1981, Bickle et al., 1993). The granodiorite gneisses have been dated at 3470 ± 25 Ma (U-Pb, Williams et al., 1983), whilst the North Shaw Suite yielded similar emplacement ages around 3470 Ma (Pb-Pb WR: 3468 ± 53 , 3422 ± 57 , Bickle et al., 1993; Pb-Pb WR: 3499 ± 22 , Bickle et al., 1983, U-Pb conventional: 3417 ± 40 , Pidgeon, 1978b; U-Pb single zircon: 3467 ± 6 , 3493 ± 4 , McNaughton et al., 1988). These coincide with an age of 3459 ± 18 Ma (U-Pb, Thorpe et al., 1992) for the North Pole Batholith 20 km to the north and the 3468 ± 4 Ma age of the Carlindi Batholith (U-Pb, single zircon, Buick et al., 1995). Sm-Nd isotopic systematics of this ca. 3460 Ma group of rocks imply derivation from a heterogeneous source that includes crustal and depleted mantle components (Bickle et al., 1993). A somewhat younger intrusive age of 3431 ± 4 Ma has been reported for the South Daltons Pluton in the western Shaw Batholith (U-Pb single zircon, McNaughton et al., 1993). This age is similar to emplacement ages from trondhjemitic and tonalitic gneisses in the Mt Edgar Batholith (3448 ± 8 Ma, 3443 ± 10 Ma, 3429 ± 13 Ma, U-Pb single zircon, Williams & Collins, 1990) and the 3443 ± 6 Ma age of the Muccan granitoid (U-Pb, single zircon, Nelson, 1996).

Widespread variably foliated tonalite/granodiorites in the Mt Edgar Batholith, yield U-Pb single zircon ages of 3304 ± 10 Ma and 3314 ± 13 Ma respectively (Williams & Collins, 1990). A similar age was obtained from the Boobina Porphyry in the Corunna Downs Batholith (3307 ± 19 Ma, U-Pb, multi zircon, Pidgeon, 1984). Slightly younger ages are recorded in the Moolyella granodiorite in the Mt. Edgar Batholith (3280 ± 20 Ma U-Pb, Pidgeon, 1978b) and in the Strelley Batholith (3238 ± 4 Ma, U-Pb, single zircon, Smith et al., in press).

Most batholiths in the eastern Pilbara were subsequently intruded by late- to post-tectonic granodiorite-adamellite plutons. In the Shaw Batholith these have been dated with the Pb-Pb whole rock isochron method. These include the weakly foliated porphyritic granite, leuco-adamellites at 2943 ± 46 Ma, the Garden Creek Adamellite at 3007 ± 48 Ma and the Cooglegong Adamellite at 2847 ± 34 Ma (Bickle et al., 1989). Sm-Nd isotopic compositions of the late plutons suggest that they were largely derived from the 3.5 to 3.3 Ga crust (Bickle et al., 1989).

Granitoids in the west Pilbara Mt. Sholl area have been dated recently by Smith et al. (in press) at 3261 ± 4 Ma, 3114 ± 5 Ma and 3024 ± 4 Ma.

The granitoids in the western Pilbara are intruded by the layered ultramafic Munni Munni Complex, which has been dated at 2925 ± 16 Ma (U-Pb, single zircon, Arndt et al., 1991)

3.2.3 *Synthesis of geochronology*

The U-Pb geochronological data (Figure 3.2) show that there were two major rock-forming events in the supracrustals during the mid-Archean of the eastern Pilbara: at ca. 3460 Ma and ca. 3300 Ma. They, in turn, can be related to plutonic events through coeval episodes of volcanism: the ca. 3460 Ma granodioritic-tonalitic plutonism is coeval with deposition of the upper Warrawoona Group and the ca. 3300 Ma tonalitic plutonic event is coeval with felsic volcanics of the Wyman Formation. During these two events, but especially the 3460 Ma event, a large portion of granitoids as well as supracrustal rocks in the eastern Pilbara were formed. These events are separated by more than 60 Ma of apparent quietude in which no new crustal rocks were formed. In the eastern Pilbara these early events are followed by a major thermal event between 3.0 and 2.85 Ga, related to late- to post-tectonic granitoids. In the west Pilbara the oldest ages are 3260 Ma granitoids, followed by 3100 Ma granitoids and volcanics and 3000 Ma granitoids (Smith et al., in press). Clearly the timing of major magmatic events is not synchronous in the east and west Pilbara.

Although these observations are based on a relatively small number of precise dates it does indicate that the Pilbara granitoid-greenstone terrain evolved during magmatic, and possibly related structural, events whose time span was short in comparison with the total period of evolution of the granitoid-greenstone terrain between 3.5 and 2.8 Ga.

The geochronology in the western Pilbara is likely to show a different pattern. Although data are insufficient, the main magmatic event appears to have taken place around 3.1 Ga.

After cratonization the Pilbara granitoid-greenstone terrain is intruded by a NNE trending dolerite dike system, the Black Range dike swarm. The dikes have not been directly dated but their age is constrained between 2.85 Ga, the age of the Cooglegong Adamellite which is intruded by the Black Range, and the Mt. Roe Basalt at the base of the Fortescue Group at 2.77 Ga (Arndt et al., 1991). The dolerite dikes may have been the feeder dikes to the Mt. Roe Basalt, but field relations are unclear.

3.3 Structural and metamorphic events

Workers in the western Shaw area (Bickle et al., 1980, 1985; Boulter et al., 1987) recognised two early structural events. The first event resulted in the high strain fabric in the gneisses and greenstone intercalations, thought to be caused by deformation in an overthrust belt. The second event resulting in recumbent folding and thrusting in greenstone sequences up to the Gorge Creek Group. Bickle et al. (1985) described the earliest deformation features as post-dating the emplacement of the South Daltons Pluton (3431 ± 4 Ma) and the lower Gorge Creek Group, which was thought to have been deposited around 3325 Ma. From $^{40}\text{Ar}/^{39}\text{Ar}$ dating of metamorphic hornblendes, Wijbrans and McDougall (1987) inferred a timing of deformation and regional metamorphism prior to 3200 Ma for the Western Shaw area. All sediments and structures were then folded around N-S trending upright folds during a third deformation phase (Bickle et al., 1980, 1985), which has been related to diapiric rise of the batholith as a direct result of earlier thickening of the crust.

Hickman (1983, 1984) proposes a structural evolution in which the earliest event, pre-dating deposition of the Warrawoona Group, produces the gneissic basement. This is followed by a solid state diapiric phase during and after deposition of the Warrawoona Group and Gorge Creek Group. Post Gorge Creek Group structures are thought to be related to E-W compression. A similar emphasis on diapirism is given to the evolution of the Mount Edgar Batholith by Collins (1989, 1983). Amphibolite metamorphism which encircles the above two batholiths is considered to be directly related to intrusion and solid state diapirism.

Of structures observed and described in these models all, except Hickman's pre-doming event, post-date deposition of the Warrawoona Group. In all models, the domal shape of the granitoids is assumed to be the result of (solid state) diapirism either lasting a long period (Hickman, 1983, 1984; Collins, 1989) or occurring in a late stage of the evolution (Bickle et al., 1985) post-dating a thrusting event.

The Pilbara granitoid-greenstone terrain has been subdivided into a number of tectonostratigraphic domains on the basis of lithostratigraphic studies (Krapez & Barley, 1987; Krapez, 1989, 1993). However, the boundaries between those domains, formed by north to north east trending sinistral lineaments (Figure 3.1) in the view of Krapez (1993), have not been studied in detail.

3.4 Mineralization in the Pilbara granitoid-greenstone terrain

As in all Archean granitoid-greenstone terrains (Figure 3.3), the Pilbara contains a variety of mineral deposits including gold and base metal deposits. However, it is notable for an abundance of small, low- to high grade deposits and a paucity of large deposits (Marston & Groves, 1981). The base metal association includes an unusual suite of barite deposits and un-economic Cu-Zn base metal deposits with high concentrations of Ba, Pb and Ag and low Fe-sulfide concentrations (e.g. Big Stubby, Barley, 1992). In a recent paper a black smoker VMS deposit (Sulphur Springs) is described (Vearncombe et al., 1995), which has been isotopically dated at 3.26 Ga. In the eastern Pilbara there are several examples of stockwork Cu-Mo and porphyry-style Mo-Cu deposits associated with sub-volcanic granitoid intrusives (Barley, 1992). Tin deposits in the eastern Pilbara are associated with the last phase of granite intrusion at 2.85 Ga (Hickman, 1983). In the west Pilbara a number of small Ni deposits occur (Marston & Groves, 1981; Horwitz, 1990).

Gold was first discovered in 1877 in the Pilbara, but large deposits were not found. The Pilbara has a low gold production when compared to the late Archean Yilgarn Block and the contemporaneous Barberton Greenstone Belt. The total gold produced in the Pilbara is 137.5 t (Geological Survey of Western Australia, 1995). Of this, a small part is situated in veins in relatively young (Gorge Creek and Whim Creek Group) sedimentary basins such as the Nullagine Block (see Figure 3.3). The majority of the gold deposits occur in the metasomatised ultramafics, in shear zones in the Warrawoona Group (Hickman & Keats, 1990). Of these, the major deposits are the Bamboo Creek Deposit, Marble Bar Deposit and the deposits in the Warrawoona Belt. There is little modern documentation of gold deposits in the Pilbara Craton. The deposits in the shear zones in the Warrawoona Group typically show low grade carbonate and fuchsite alteration zones (Hickman, 1983), but Neumayr et al. (1993a) describe an amphibolite grade deposit in the Mt. York district in a detailed study of the alteration associated with the deposit.

The timing of the gold in the Pilbara is uncertain. Barley & McNaughton (1988) assume that gold is related to the ca. 2950 Ma sinistral lineaments. Neumayr et al.(1993b) confirmed this for the Mt. York district.

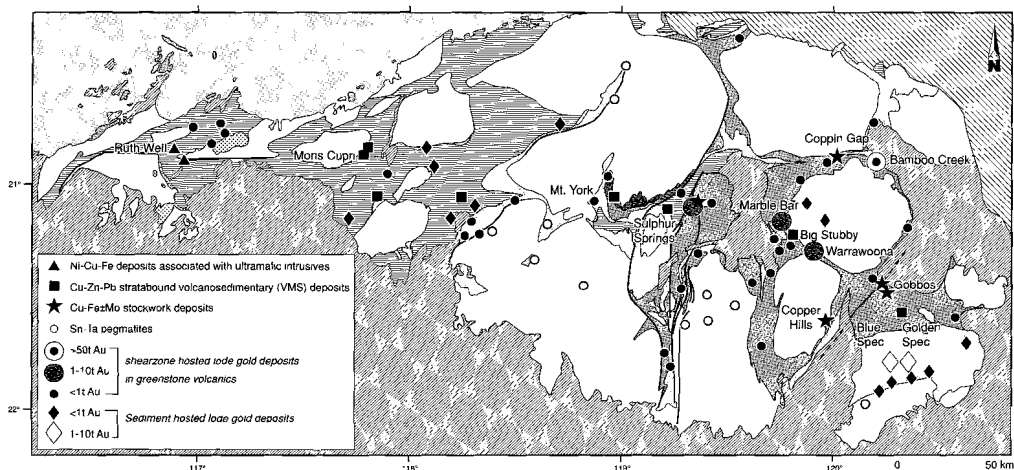


Figure 3.3 Simplified geological map of the Pilbara granitoid-greenstone terrain showing the main mineral deposits. See Figure 3.1 for legend of geological units.

3.5 Tectonic interpretations.

In the Pilbara, as in many Archean terrains, tectonic interpretations can be divided in two broad categories. In the first group, workers see no evidence for plate tectonic processes and solid state diapirism is thought to be the main process causing deformation. Hickman (1981, 1983) first proposed such a model for the Pilbara. In this model, the Warrawoona Group was deposited on a pre-existing and deformed gneissic basement. Diapirism was then initiated as a result of the density inversion between gneisses and mafic volcanics. It is thought to have continued throughout deposition of the Gorge Creek and Whim Creek Groups. Variations on this model were proposed by Collins (1989) for the Mt. Edgar Batholith and by Delor et al.(1991) for the Warrawoona and Coongan Belts. Choukroune et al.(1995) mention the Pilbara Craton as the prime example of pre-plate tectonic diapiric structural development. However, most workers in the Pilbara interpret the data within the context of plate tectonic settings. From their work the following tectonic interpretation of the evolution of the Pilbara can be described.

There is now ample evidence for a basement that pre-dated the upper Warrawoona Group, represented by the supracrustals of the Coonterunah Succession (Buick et al.1995), the anorthositic fragments in the western Shaw Batholith (McNaughton et al.1988) and a 3.7 Ga xenocrystic zircon in the Salgash Subgroup (Thorpe et al. 1992) There is no evidence that the granodioritic gneisses, found in many batholiths, were basement to the Warrawoona Group, but geochronological data are insuf-

ficient to ascertain this. The Warrawoona Group volcanics and contemporaneous granitoids are generally interpreted as melt or melting due to dehydration of a basaltic crust (Barley, 1993; Buick et al. 1993, Collins 1993, Bickle et al., 1993) with eruption of calc-alkaline volcanic centres in shallow water in basins with little topography (Barley et al. 1979). The tectonic setting is likened to marginal basins of volcanic arcs, back arc basins and oceanic arcs (Barley 1993; Collins 1993; Bickle et al., 1993), but DiMarco and Lowe (1989) note that there are important differences with modern arc settings because most Phanerozoic arc- and marginal basins contain thick deposits of deep water facies and large-scale deformation is an important feature. No mention is made of structures formed during deposition of the Warrawoona Group.

A compressional structural event is described after deposition of the Warrawoona Group in the Shaw area by Bettenay et al. (1981), Bickle et al. (1985) and Boulter et al. (1987) with an early phase causing interleaving of granites and greenstones producing gneissic rocks and a post Gorge Creek Group thrusting phase in the greenstones. Relatively high pressure (kyanite/sillimanite) assemblages are thought to belong to this compressional event and led to an interpretation of this event an Alpine style orogenic belt (Bickle et al. 1985). Clastic sediments in the Gorge Creek Group contain granitic fragments and were found unconformably overlying foliated granites (Dawes et al., 1995). These clastic sequences are interpreted as foreland basin deposits by Krapez (1993). Collins (1993) interpreted the geochemistry of the ca. 3.3 Ga granitoids as the product of partial melting of a dacite/tonalite precursor (3.45 Ga crust) in the presence of water, possibly during delamination of the lower mafic crust. $^{40}\text{Ar}/^{39}\text{Ar}$ data from Wijbrans & McDougall (1987) indicate a regional metamorphic event at ca. 3200 Ma and more localized contact metamorphism at 2.95 and 2.85 Ga. These interpretations all point toward an important compressional event during deposition of the Gorge Creek Group in eastern Pilbara, although no further evidence was found for an Alpine type orogeny. In the western Pilbara the tectonic setting during and after deposition of the Gorge Creek Group may have been different. Ohta et al. (1996) describe an accretionary complex of mid-oceanic ridge basalts of Gorge Creek Group age (3.1 to 3.3 Ga).

The Whim Creek Group occurs as a thick sequence in the west Pilbara, but only occurs locally in the rest of the Pilbara. Eriksson (1981) and Horwitz (1990) interpreted these deposits as syn-rift deposits whereas Krapez and Barley (1987) interpreted the Whim Creek Group deposits in the Lalla Rookh Basin and in the Whim Creek Belt as sinistral pull apart basin infills.

The eastern Pilbara was subsequently intruded by voluminous granites (3 - 2.85 Ga), cratonized, intruded by the Black Range dike swarm and unconformably covered by the Fortescue Group.

Many of the large-scale tectonic interpretations in the Pilbara are based on data from a small area or from a limited data set (Trendall 1995) rendering the importance of the interpretation uncertain. Accretionary complex and volcanic arc interpretations are favored by geochemical data but are hard to reconcile with the circular outcrop pattern in the eastern Pilbara. Calc-alkaline trends do not necessarily mean that there was a subduction zone in all respects similar to present day subduction zones. The geochemical calc-alkaline pattern is caused by melt processes related to dehydration of previously hydrated basaltic crust and could equally well be caused by partial melting of a stacked obducted oceanic crust as proposed by de Wit and Hart (1992) for the Barberton Belt, or in a worse case may be the result of secondary alteration processes, such as silicification (Barley, 1984). If solid state diapirism, as indicated by many interpretations, was not the main process in the evolution of the Pilbara, there should be another explanation for the circular domal outcrop pattern and the general

lack of large-scale linear belts in the eastern Pilbara.

One of the problems in comparing the evolution of the Pilbara Craton to modern tectonic settings is the lack of structural and metamorphic data and especially the lack of good timing constraints on structures.

Extensional structures during deposition of the 3460 Ma Warrawoona Group¹

4.1 Introduction

Archean granite-greenstone terrains have a long history of development, in which supra-crustals and intrusive granitoids occur episodically over what may be short time spans (Condie, 1994). The net result is a common basic geometry of granitoid-gneiss domes bordered by keels of mafic volcanic-dominated supra-crustals that locally include komatiites. The large-scale outcrop pattern of the granitoid-gneiss domains is generally linear (e.g. Yilgarn Craton, Abitibi Belt) for late Archean terrains but is typically circular and reminiscent of batholiths (Macgregor, 1951) for mid Archean terrains (Pilbara Craton, Kaapvaal Craton).

The complex contact geometries, lithostratigraphy of the supra-crustals and overprinting relations have led to a variety of genetic models for the overall development of granite-greenstone terrains ranging from solid-state diapirism to subduction related accretionary models (e.g. Nisbet, 1987). Depending on the point of view (structural, metamorphic or geochemical), elements supporting each of these models exist in most mid-Archean granite-greenstone terrains. However, this could be a function of their extended, multi-stage histories, especially those affected by the late Archean tectonism (e.g. Yilgarn Craton and Abitibi Belt). The question of the primary structural control of greenstone belt development can be addressed in the eastern Pilbara, because it is little affected by late Archean or Proterozoic deformation.

The evolution of the eastern Pilbara granite-greenstone terrain is marked by a number of distinct magmatic events that occurred between 3.6 Ga and 2.8 Ga (Bickle et al., 1989). Boundaries between the greenstone belts and granitoid domains are governed by a complex interplay of multiphase shear zones and intrusive contacts, which formed during separate events. Structural models for the eastern Pilbara such as solid-state diapiric rise of granitoid-gneisses into the overlying greenstones (Hickman, 1984; Collins, 1989) and horizontal compression resulting in thrusts and recumbent folds (Bettenay et al., 1981; Bickle et al., 1985; Boulter et al., 1987), have concentrated on the post-depositional events.

In this Chapter a group of syn-depositional structures that were preserved in a relatively unaffected state by later structures are discussed. The early (ca. 3460 Ma) structural evolution of the Shaw Batholith and its relation to the coeval deposition of the Warrawoona Group in the adjacent Coongan Belt (Figure 4.1) was studied. It will be shown that there are early extensional structures, which are coeval with the extrusion of volcanics of the Duffer Formation and emplacement of a

¹ Published as: Zegers, T.E.; White, S.H.; de Keijzer, M. and Dirks, P. (1996). Extensional structures during deposition of the 3460 Ma Warrawoona Group in the eastern Pilbara, Western Australia. *Precambrian Research* No. (in press)

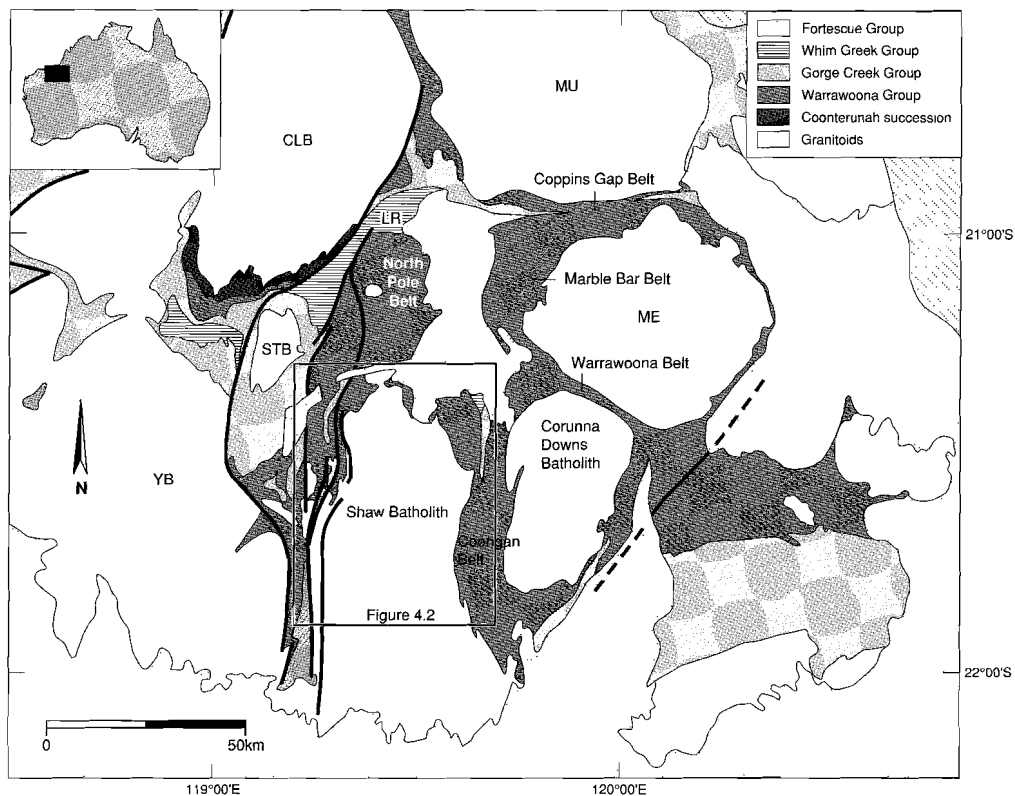


Figure 4.1 The eastern Pilbara granitoid-greenstone terrain, the frame represents the area discussed in this Chapter. CLB= Carlindi Batholith, ME= Mt. Edgar batholith, MU= Muccan Batholith, STB=Strelley batholith, YB= Yule Batholith, LR= Lalla Rookh Basin.

major granitoid suite. These structures are most conspicuous around the eastern margin of the Shaw Batholith, and combine both horizontal extension and vertical doming. The structural data imply that some kind of extensional tectonic regime was responsible for this early deformation event.

4.2 Geological setting of the Shaw Batholith and Coongan Belt

Although many details of the 800 Ma evolution of the granitoid-greenstone terrain remain elusive, published data are sufficient to temporally constrain structures found in this study. Geochronological sample locations from the Shaw Batholith area are shown in Figure 4.2, and dates from the literature are summarised in Figure 4.3.

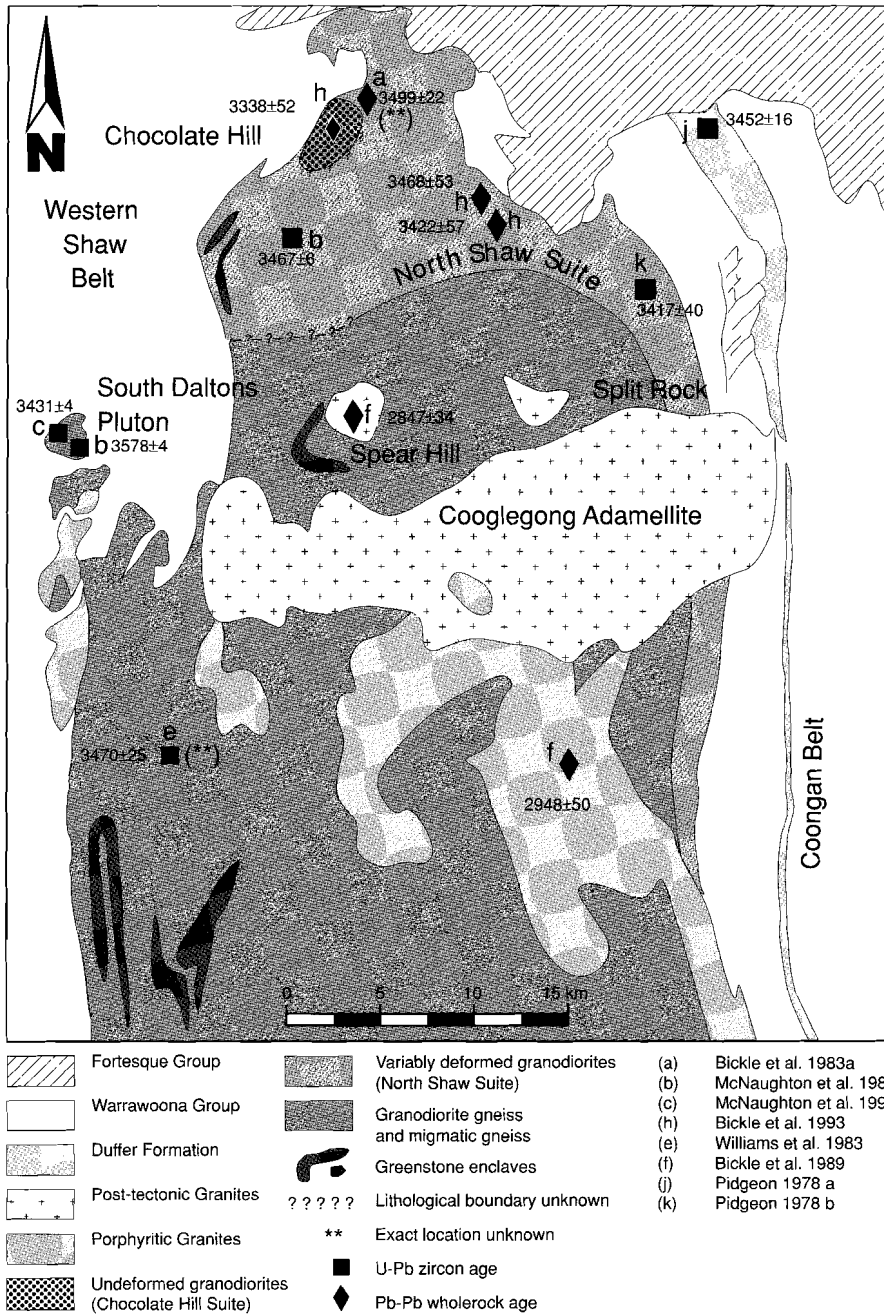


Figure 4.2 Lithology and dates of the Shaw Batholith and surrounding greenstones.

4.2.1 *The Coongan Belt*

The Coongan Belt consists of mainly mafic volcanics with minor komatiitic and felsic volcanic units. Apart from some small zones in the north and the south of the Coongan Belt, which may represent the lower units of the Gorge Creek Group, these volcanics are part of the Warrawoona Group (Barley, 1993). Few geochronological data are available. A U-Pb 3452 ± 16 date was obtained by Pidgeon (1978a) in the Duffer Formation in the northern Coongan Belt (Figure 4.2), and Rb-Sr data (Cooper et al, 1982) exist for granitoids adjacent to the eastern side of the belt, constraining the upper Warrawoona Group to older than 3270 Ma. The Duffer Formation felsic volcanics and volcanoclastics are well developed and their characteristics have been discussed by DiMarco & Lowe (1989), who show that there is a general coarsening upward sequence in the Duffer formation.

The lower Warrawoona Group (Talga Talga Subgroup), underlying the Duffer Formation, has not been isotopically dated. In the Coongan Belt it consists of mafic pillow basalts, komatiites and thin (2–3 m.) BIF units. A large volume of the Talga Talga Subgroup (up to 40%) consists of gabbroic and doleritic sills, a feature also seen in the type area of the Talga Talga Subgroup (Barley, 1993).

4.2.2 *The Shaw Batholith*

Evidence for a rocks pre-dating the Warrawoona Group is presented by McNaughton et al. (1988) who identified relicts of an anorthositic-gabbro suite dated at 3578 ± 4 Ma with the U-Pb zircon method in the western Shaw region in enclaves in the South Daltons Pluton.

Highly deformed granodiorite gneisses with numerous greenstone enclaves occur in the western part of the Shaw Batholith. Their less deformed equivalents occur along the northern margin of the batholith and are considered to represent the oldest intrusive rocks in the Shaw Batholith (Bickle et al., 1993). The latter consist of granodiorites to tonalites that have been referred to as the North Shaw Suite (Betténay et al., 1981, Bickle et al., 1993). The granodiorite gneisses have been dated at 3470 ± 25 Ma (U-Pb, Williams et al., 1983), whilst the North Shaw Suite yielded emplacement ages around 3470 Ma (Pb-Pb WR: 3468 ± 53 , 3422 ± 57 , Bickle et al., 1993; Pb-Pb WR: 3499 ± 22 , Bickle et al., 1983, U-Pb conventional: 3417 ± 40 , Pidgeon, 1978b; U-Pb single zircon: 3467 ± 6 , 3493 ± 4 , McNaughton et al., 1988). Sm-Nd isotopic systematics of this ca. 3460 Ma group of rocks imply derivation from a heterogeneous source that includes crustal and depleted mantle components (Bickle et al., 1993). A somewhat younger intrusive age of 3431 ± 4 Ma has been reported for the South Daltons Pluton in the western Shaw Batholith (U-Pb single zircon McNaughton et al., 1993). This age is similar to emplacement ages from trondhjemitic and tonalitic gneisses in the Mt Edgar Batholith (3448 ± 8 Ma, 3443 ± 10 Ma, 3429 ± 13 Ma, U-Pb single zircon (Williams & Collins, 1990). The significance of the 3338 ± 52 Ma Pb-Pb whole rock isochron age (Bickle et al., 1993) is uncertain, because the field and chemical data do not show evidence for a new intrusive events. The data may represent the age of a hydrothermal event in the Shaw Batholith which corresponds to the age of the variably foliated tonalite/granodiorite in the Mt Edgar Batholith, yielding U-Pb single zircon ages of 3304 ± 10 Ma and 3314 ± 13 Ma respectively (Williams & Collins, 1990) and 3307 ± 19 Ma in the eastern Corunna Downs Batholith (Pidgeon, 1984).

The Shaw Batholith was subsequently intruded post-tectonically by granodiorite-adamellite plutons. These include the weakly foliated porphyritic granite, leuco-adamellites, Garden Creek Adamellite and Cooglegong Adamellite dated between 3000 Ma and 2830 Ma (Bickle et al., 1989). Sm-Nd isotopic compositions of the late plutons suggest that they were largely derived from the 3.5 to 3.3 Ga

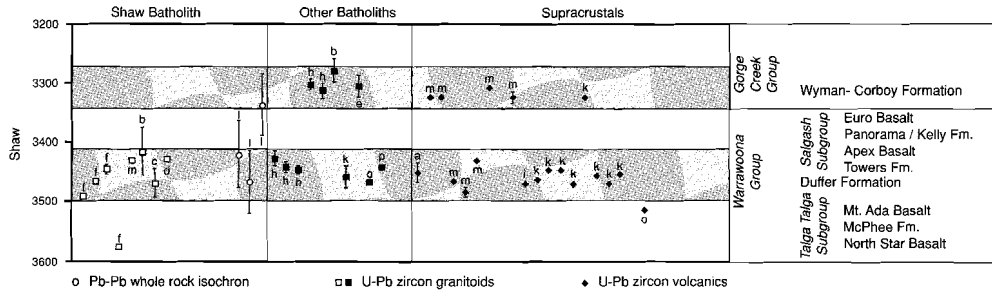


Figure 4.3 Table of U-Pb and Pb-Pb dates in the eastern Pilbara, showing two major events in the mid Archean at approximately 3460 Ma and 3300 Ma. a=Pidgeon (1978a), b=Pidgeon (1978b), c=Williams et al.(1983), d=Froude et.al.(1984), e=Pidgeon (1984), f=McNaughton et al.(1988), h=Williams & Collins (1990), i=Thorpe et al.(1990), l=Bickle et al. (1993), m=McNaughton et al. (1993).

crust (Bickle et al., 1989).

The U-Pb geochronological data (Figure 4.3) show that there were two major rock-forming events in the supracrustals during the mid-Archean of the eastern Pilbara at ca. 3460 Ma and ca. 3300 Ma. They in turn can be related to plutonic events through coeval episodes of volcanism: the ca. 3460 Ma granodioritic-tonalitic plutonism is coeval with deposition of the Warrawoona Group and the ca. 3300 Ma tonalitic plutonic event is coeval with felsic volcanics of the Wyman Formation. Especially during the first of these two events a large portion of granitoids as well as supracrustal rocks in the eastern Pilbara were formed (Carlindi, Muccan, North Pole). These events, which last ca. 50 Ma, are separated by more than 100 Ma of quietude in which no new crustal rocks were formed. They indicate that the Pilbara granitoid-greenstone terrain evolved during magmatic, and possibly related structural, events whose time span was short in comparison with the total period of evolution of the granitoid-greenstone terrain between 3.5 and 2.8 Ga.

4.3 Structural observations

The principal observations in the field were the orientations and superposition of planar and linear structures, and, where ductile or brittle shear zones occur, their kinematics. Where possible, relations between structures and previously dated rocks were studied in order to determine the temporal relationships.

Structures in the batholith generally formed under amphibolite facies conditions whereas in the adjacent greenstone belts structures formed under lower amphibolite to lower greenschist facies conditions

4.3.1 The Shaw Batholith.

Two major ductile shear zone systems have been mapped in the Shaw Batholith (Figure 4.4); the Mulgandinnah Shear Zone Complex (MSZC, see Chapter 6) in the western Shaw and the Split Rock Shear Zone (SRSZ) in the east. The SRSZ forms the central part of the contact of the Shaw

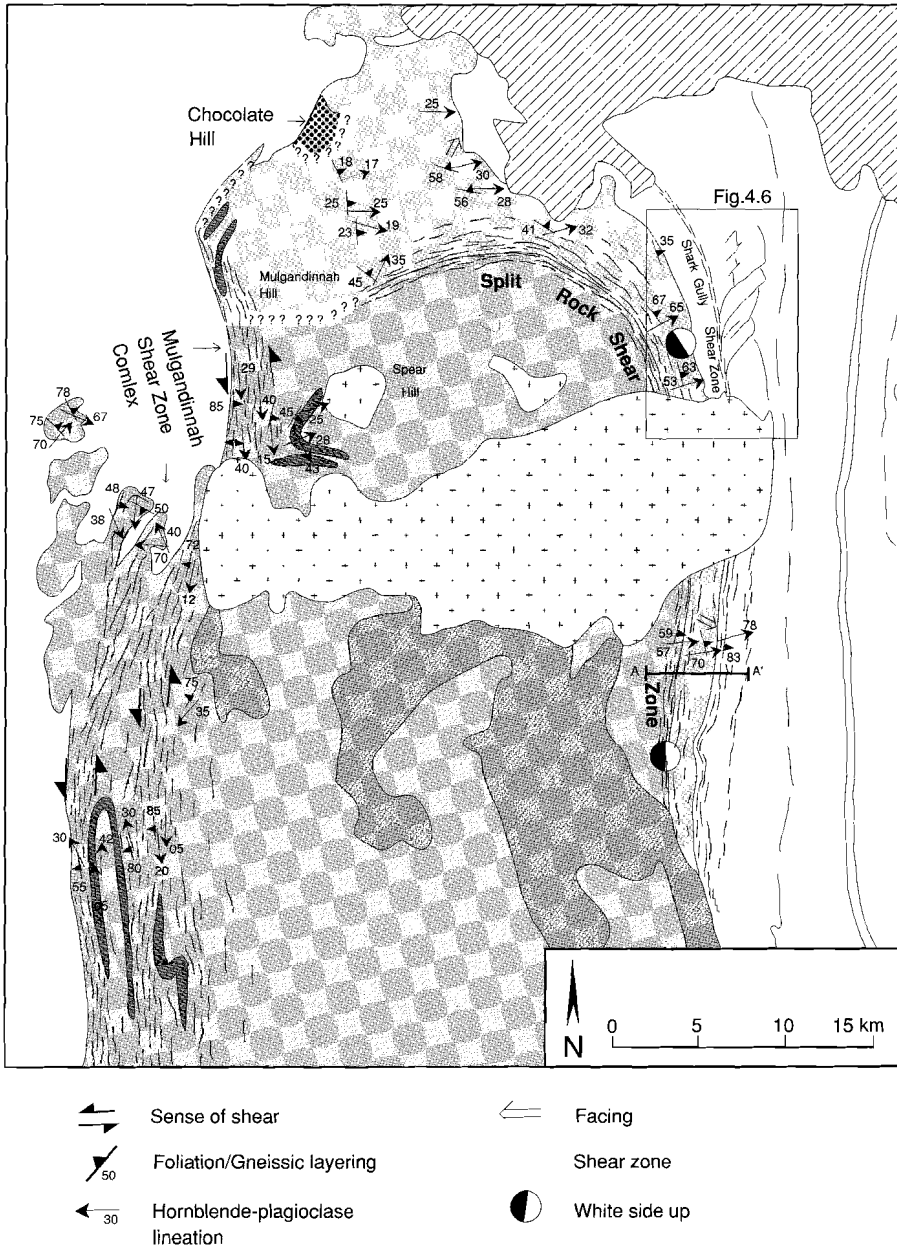


Figure 4.4 Structural relations in the Shaw Batholith showing the Split Rock Shear Zone and the Mulgandinnah Shear Zone Complex, lithologies are indicated in Figure 4.2. A detailed map of the framed area is shown in Figure 4.6, the structural section AA' is shown in Figure 4.5a. For a detailed description of structural, metamorphic and intrusive relations see text.

Batholith with the Coongan Belt. Towards the N, the shear zone bends into a E-W orientation, delineating the contact between the North Shaw Suite to the north and east and migmatic gneisses to the south and west. To the south, the SRSZ is truncated by a porphyritic granite dated at 2948 ± 50 Ma by Bickle et al. (1989). Along the contact with the Coongan Belt, south of the Cooglegong Adamellite, a wedge-shaped granodiorite body, which is thought to be the southward extension of the North Shaw Suite tonalite/granodiorite, occurs adjacent to the shear zone. This granitoid wedge has all the characteristics of the North Shaw Suite, including the typical magmatic layering as described by Bickle et al. (1993) and has been dated in this study (Chapter 8) at 3468 ± 2 Ma (U-Pb single zircon).

An E-W traverse through the SRSZ in its N-S trending part, which includes the detailed section AA' (Figures 4.4 and 4.5) across the contact, shows the following features. The greenstone sequence about 2 kilometers east of the contact consists of weakly deformed volcano-sedimentary sequences that are the right way up and which dip steeply to the east. Contained micaceous units have preserved a weak fine-grained, layer-parallel muscovite-chlorite foliation with, locally, fine needles of randomly orientated actinolite. Upon approaching the contact (eastern side of section AA', Figure 4.5) the layer-parallel foliation related to the SRSZ (SSRSZ), gradually becomes pervasive in both the micaceous units and the more massive metabasites. Along a 100-150 m wide zone directly on the contact with the Shaw Batholith, the foliation is strong and defined by oriented blue-green hornblendes which are also aligned in an east plunging, down-dip mineral elongation lineation LSRSZ. In a number of outcrops amphibolites contain rounded green-brown hornblendes of several mm diameter, with recrystallized tails of finer-grained blue-green hornblende that define clear S-C fabrics indicative of an east-up sense of movement (Figure 4.5b). These mylonitic amphibolites are overprinted by local greenschist facies shear zones with foliations parallel to the amphibolite foliations. The SRSZ is defined as the amphibolite grade mylonite zone in both the Shaw batholith and the western Coongan Belt, that shows a consistent E to ENE plunging stretching lineation and east up sense of shear indicators. The contact between the Coongan Belt and the North Shaw Suite, which largely parallels SSRSZ, is originally intrusive because enclaves of schist occur in the granodiorite (Figure 4.5c) and weakly deformed dike-like protrusions of granodiorite truncate and or cross cut the SSRSZ. The granodiorite immediately along the contact is only weakly foliated and locally preserves magmatic layering defined by ferromagnesian minerals concentrated along a sharp basal plane, grading into more leucocratic granodiorite. This layering dips east, parallel to So in the greenstones and SSRSZ. Going west through the granodiorite the intensity of SSRSZ and LSRSZ increases to a one kilometer wide mylonite zone, the basal and most intensely deformed Split Rock Shear Zone. This amphibolite facies mylonite forms the contact between the granodiorite and composite layered grey gneiss to the west. It is very strongly sheared, masking any intrusive relationships. The gneiss in the mylonite zone preserves a mm-scale, planar foliation defined by oriented biotites and feldspar segregations, in part consisting of strung-out augen with asymmetrically recrystallized tails (Figure 4.5d). The foliation dips moderately east and contains a down-dip stretching lineation. These orientations are identical to SSRSZ and LSRSZ in the greenstone belt. Locally, aligned amphibolite lenses occur with fine-grained syn-tectonically recrystallized blue hornblende defining S-C fabrics. These, and cm-scale shear-bands give a consistent E-up sense of shear. The mylonitic gneisses extend west for about 1 km, before strain intensities drop to expose a more coarsely-banded migmatic grey gneiss. The observed timing relations (both intrusive and foliated granodiorite) indicate that the wedge

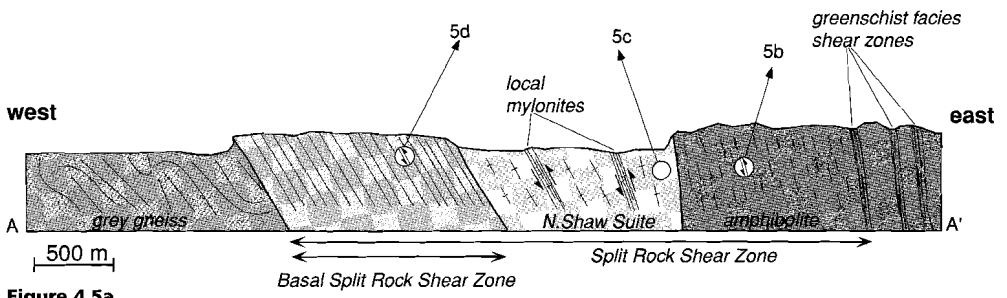


Figure 4.5a

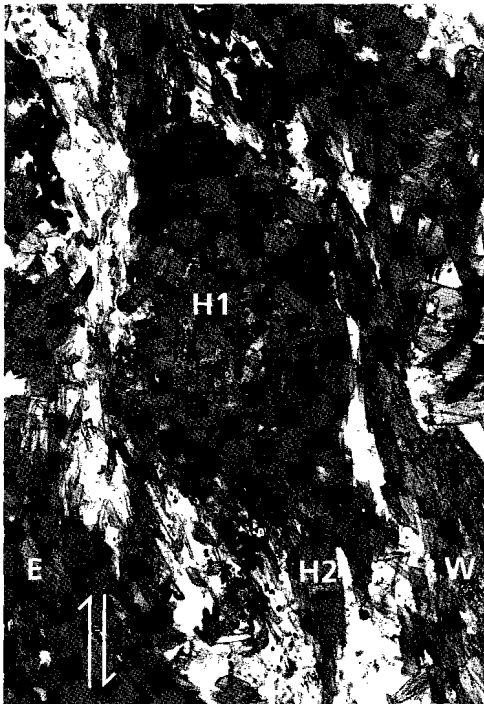


Figure 4.5b

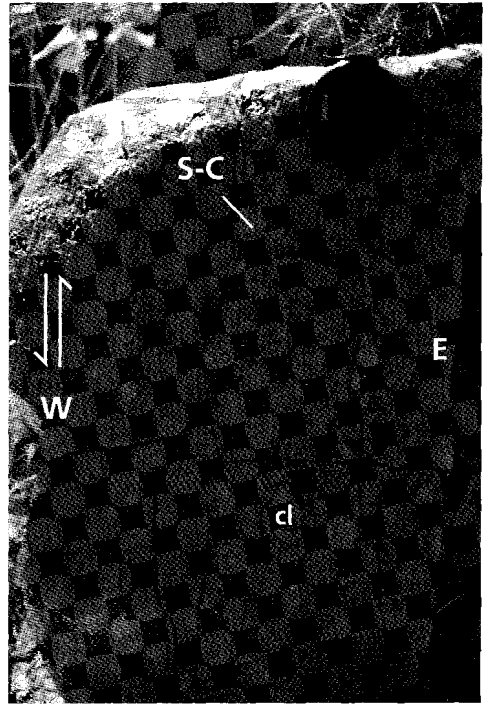


Figure 4.5d

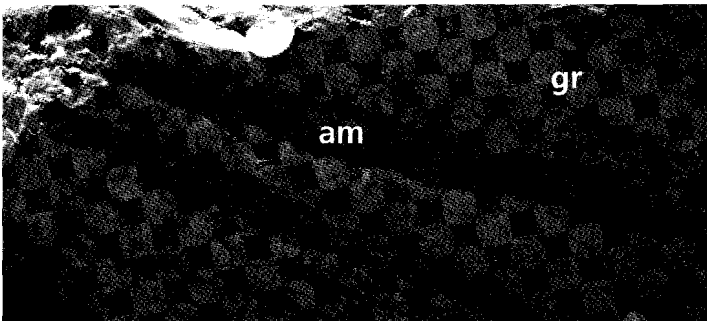


Figure 4.5c

Figure 4.5 a. Structural section through the contact between the Shaw Batholith and the Coongan Belt, for the location of line AA' see Figure 4.4. Points 5b, 5c and 5d refer to the photographs below, showing key structural and kinematic relations.

b. Photomicrograph showing a σ -clast, formed by hornblende, indicating a hanging wall up, i.e. E, up sense of shear. In the photograph h1 is a brown-green hornblende σ -clast and h2 is fine grained blue-green hornblende. The width of the photomicrograph is 1 mm.

c. Field photograph showing the intrusive relation of the North Shaw Suite granitoid with amphibolitic greenstones as indicated by the foliated amphibolite enclaves (am) in the weakly deformed granodiorite (gr). Diameter of the coin is 2 cm.

d. Field photograph of Plagioclase σ -clasts (cl) and a S-C (s-c) fabric which indicate an E up sense of shear in the Split Rock Shear Zone. The lens cap has a diameter of 5 cm.

shaped granodiorite body, which is regarded to be part of the North Shaw Suite (Bickle et al., 1983), intruded syn-kinematically into the SRSZ. As part of the North Shaw Suite has been dated at around 3460 Ma, the SRSZ is inferred to have been active at this time.

Foliation-lineation development within the North Shaw Suite rocks in the northern part of the Shaw Batholith is generally weak. These rocks are mostly homogeneous biotite-rich (\pm hornblende) granodiorites to tonalites, in which the lineation-foliation is defined by oriented hornblendes and patches of, now recrystallized, biotite. The foliation dips mostly shallowly to moderately N to NE, but steepens along the eastern margin of the Shaw Batholith. Likewise, the lineation plunges shallowly east but steepens considerably to the east. This lineation follows the orientation of LSRSZ. Most of the contact between the North Shaw Suite and the greenstones is clearly intrusive (Bickle et al. 1993), but more or less follows the lower Warrawoona Group stratigraphy, suggesting a wedge or sheet like geometry.

The SRSZ pre-dates the N-S trending MSZC located parallel to the western margin of the Shaw Batholith. This is inferred from a greenstone enclave 2 km SW of Spear Hill (Fig. 4.4). Here a well developed lineation made up of coarse-grained grunerite (amphibolite facies) with the orientation 070/25 parallels the constant E-plunging lineation observed in the North Shaw Suite and is overgrown by a second lineation (150/40) made of cm-scale aligned spots which have been completely recrystallized and are now made up of fine-grained white mica and chlorite. The second SE-S plunging lineation parallels the very consistent and well developed lineations in the MSZC.

The MSZC is formed by a series of N-S trending shear zones at the western margin of the Shaw Batholith. Apart from sheared gneisses and granitoids, this complex also contains a relatively large number of meta-volcanic and occasionally metapelite lenses.

South of Mulgandinnah Hill the structure basically consists of a 2-3 km wide shear zone in which the strain increases from E to W, towards the granite-greenstone contact, with a sinistral sense of shear. The MSZC is described in detail in Chapter 6. The timing of the late stages of movement on the MSZC are constrained to 2934 ± 2 Ma (Chapter 8).

4.3.2 The Coongan Belt

Structurally, the Coongan Belt is highly asymmetric, with a relatively undeformed eastern part, a 300 to 1500 m. wide ductile/brittle shear zone in the centre and a more variably deformed western half (see Chapter 5 for details on the Coongan Belt). Where bedding planes can be distinguished in the eastern part they are steeply dipping with a N-S trend. Younging is to the west, as indicated by

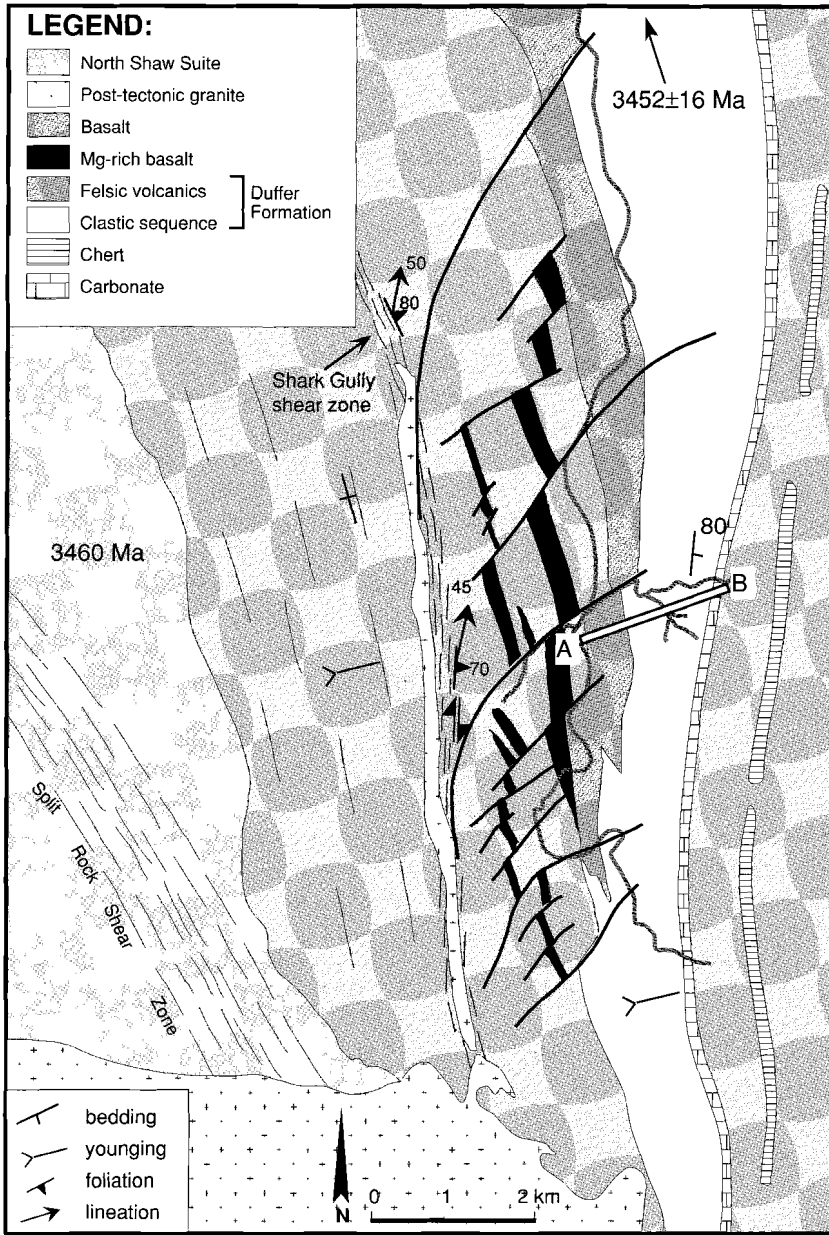


Figure 4.6. Brittle extensional fault array in the Coongan Belt. The faults were active during deposition of the Duffer Formation dated at 3452 ± 16 (Pidgeon, 1987). Section AB refers to the stratigraphic sequence described in the text. The mafic sequence underlying (west of) the Duffer Formation is the Talga Talga Subgroup.

komatiite sequences and flow top breccias in Mg-basalts. In the western part bedding has a similar strike and dip. In the less deformed parts younging is observed to be to the east, as indicated by cross-bedding in clastic sequences. Asymmetry is also apparent in the metamorphic grade developed within the belt: very low grade in the eastern half, apart from a narrow amphibolite grade contact metamorphic aureole from the intrusive Corunna Downs Batholith, variable metamorphic grade in the central part and an amphibolite facies zone near the contact with the Shaw Batholith parallel to the Split Rock Shear Zone. At the north-western contact of the Coongan Belt with the Shaw Batholith, a narrow amphibolite facies contact metamorphic aureole is developed.

The earliest structures were found in the north-western part of the Coongan Belt (Figures 4.6). Here, north-east trending brittle faults offset stratigraphic units in a dextral sense. These faults terminate within felsic volcanics and clastic sediments of the Duffer Formation. Variations in stratigraphic thickness associated with these (Figure 4.6), indicate that these faults were active during extrusion and sedimentation of the Duffer Formation.

The faults are clearly visible on the aerial photographs, but in the field it is extremely difficult to record kinematic data. The faults themselves are not exposed, but their position can be located from outcrop patterns. In the vicinity of fault traces the host rocks are brecciated and extensively quartz veined. The footwall rocks are frequently gossaneous. Occasionally intrusive mafic dykes were found parallel to the fault trace. Both the volcanic and sedimentary sequences vary across the faults, and their thicknesses are clearly controlled by them (Figure 4.6). The stratigraphic sequence (see line A-B in Figure 4.6) in the fault blocks from west to east can be summarised as follows. A fine-grained basalt is overlain by coarse felsic volcano-clastic sediments. These are overlain by a clastic sequence with a coarsening up character, starting with a BIF followed by a carbonaceous sandstone sequence with well developed cross-bedding, giving a younging direction towards the east. The sandstone grades into a conglomerate with pebbles up to 40 cm in size of sandstone, BIF and volcanics. The thickness of the sandstone/conglomerate varies laterally from 200 to 700 m., generally thickening towards the north. This clastic sequence alternates with fault controlled wedges of felsic volcanics of the Duffer Formation, dated in this area at 3452 ± 16 Ma by U-Pb zircon dating (Pidgeon, 1978a). It is concluded that the faults form an extensional fault array whose activity is well constrained in time to about 3450 Ma. The faults and the fault controlled wedges of Duffer Formation are blanketed by a 20 m thick dolomite unit, containing stromatoloid structures that can be traced for a distance of 20 km along strike. It is emphasized that all of the faults that affected sedimentation of the Duffer Formation terminate before or upon reaching this dolomite unit. The dolomite is commonly completely silicified along strike and was mapped as a chert unit by DiMarco & Lowe (1989), who correlated it with the Strelley Pool Chert in the North Pole area. It is in turn overlain by basalts with interflow cherts of the Salgash Subgroup (Figure 4.6).

Deformation within the greenstone sequence enclosed within the above mentioned fault blocks increases towards the west. The felsic and mafic volcanics just show a bedding parallel foliation which is inhomogeneously distributed. Lincations are not developed. The deformation then increases to a maximum in an ultramafic unit in which a ductile greenschist facies shear zone, the Shark Gully Shear Zone, is developed (Figure 4.6). This shear zone is intruded and truncated by the post-tectonic Coongong Adamellite. The extension of the Shark Gully Shear Zone can be traced to the southern part of the Coongan Belt, where it joins the amphibolite grade foliation of the SRSZ (see also Figure 5.4 for a more detailed map of the Coongan Belt structures). The mylonitic foliation in the

shear zone is steeply dipping to the ENE. Stretching lineations and related shear-bands and crenulations indicate a dextral/east up sense of shear with a transport direction dipping 40–50° to the N-NE. The brittle NE trending extensional faults sole into this shear zone and are therefore assumed to be part of the same kinematic framework. The original transport direction, obtained by rotating the top of the sequence back to a horizontal position, is NE-SW with a top to the SW displacement. That is similar to the transport direction in the SRSZ.

4.4 Discussion

The nature and geometry of the Warrawoona Group depositional basin is largely unknown mainly because of the absence of undeformed basement–cover contacts and the extensive post-depositional deformation. Stratigraphic mismatches and recent geochronological work (Horwitz, 1986, 1990; Krapez and Barley, 1987; Horwitz and Pidgeon, 1993; Barley, 1993; McNaughton et al., 1993; Krapez, 1993) indicate that the tabular stratigraphy as initially proposed by Hickman (1983) is inappropriate. Evidence that there was a deformed and metamorphosed basement prior to deposition of the Warrawoona Group is given by McNaughton et al. (1988) who dated zircons from a gabbroic anorthosite from one of the greenstone enclaves in the South Daltons pluton at 3578 ± 4 Ma. This is supported by the evidence by Buick et al. (1995) that there is another greenstone sequence which was deformed and metamorphosed prior to deposition of the upper Warrawoona Group. This is further evidence for an event prior to deposition of part of the Warrawoona Group. Morant (1984) reported relatively high pressure metamorphic assemblages (kyanite–sillimanite) from the enclaves in the South Daltons Pluton. However, the timing of these relatively high pressure assemblages is uncertain, and they may represent an old event, predating and not post-dating, deposition of the Warrawoona Group as inferred by Bickle et al. (1985).

This study shows that a group of extensional structures, which influence sedimentation in the Duffer Formation, is related to the ca.3460 event. They include low temperature brittle faults in the greenstones and a ductile shear zone in the Shaw Batholith (Figure 4.7a). The timing of the brittle extensional faults in the Coongan Belt is constrained by the age of the syn-tectonic Duffer Formation (3452 ± 16 Ma, Pidgeon, 1978), whereas the Split Rock Shear Zone (SRSZ) is inferred to have been active during intrusion of a wedge shaped granodiorite body, which has been dated at 3468 ± 2 Ma (U-Pb, SHRIMP this study, Chapter 8). This is consistent with the 3467 ± 6 Ma date of the North Shaw Suite (McNaughton et al., 1988, U-Pb zircon), which is within error of most other dates of the North Shaw Suite (Figure 4.3). The crystallization age of the granitoid sample in the intensely sheared part of the SRSZ in the Shaw batholith is 3469 ± 3 Ma (U-Pb, SHRIMP, this study, Chapter 8), constraining the age of the SRSZ to between 3469 and 3468 Ma. The basal shear zone truncated grey gneisses dated at 3451 ± 1 ma (U-Pb, SHRIMP, this study), indicating that the basal part of the SRSZ must have been active at least until 3450 Ma. This means that the SRSZ and the extensional fault array in the Coongan Belt are broadly contemporaneous structures at different levels in the crust.

The SRSZ can, on geometrical grounds, be interpreted in two ways: 1) the shear zone was originally a low angle thrust, 2) the shear zone was originally a low angle extensional contact.

Both models are consistent with the following characteristics of the SRSZ:

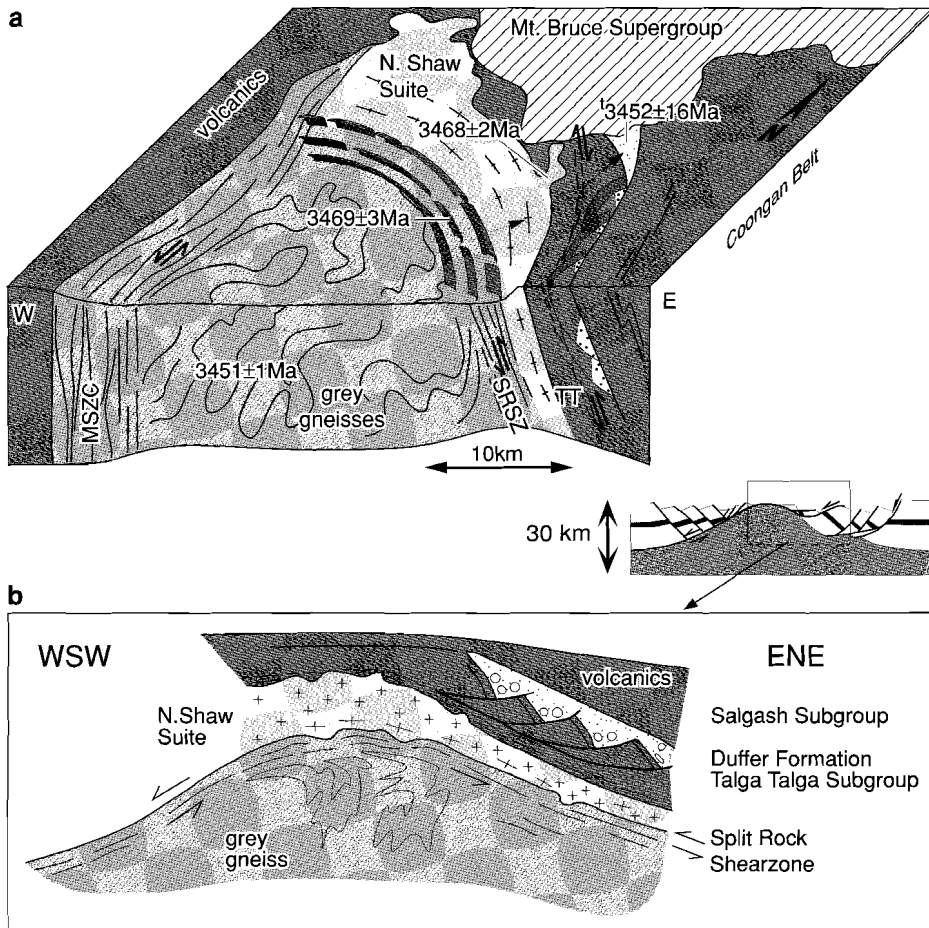


Figure 4.7
a Schematic block diagram of the Shaw Batholith showing the present geometry. The three dates shown are U-Pb single zircon dates (see Chapter 8), the exact location of the samples are shown in Figure 8.1. The date indicated with † is a conventional U-Pb zircon age of the Duffer Formation by Pidgeon (1978a), TT= Talga Talga Subgroup.
b Conceptual model for the evolution of the Split Rock Shear Zone, the North Shaw Suite granitoid intrusion and the extensional structures in the Coongan Belt greenstones.

- Parallelism between the SRSZ shear zone, bedding in the supracrustals and magmatic layering in the syn-kinematic North Shaw Suite.
 - The younging direction in greenstones is eastward, i.e. away from the contact.
 - The dome shaped foliation pattern combined with the unidirectional stretching lineation.
 - The consistent transport direction of eastern block to the WSW on the shear zones .
- In both models the initial dome shape of the granitoid must have originated during this deformation phase, i.e. early in the evolution, in order to produce the characteristic foliation/lineation pattern.

This foliation/lineation pattern combined with a consistent transport direction to the WSW is in distinct disagreement with a solid state diapiric model for granitoid emplacement.

Additional geochronologic and metamorphic data are needed to conclusively distinguish between the extensional or compressional models (Wheeler & Butler, 1994). In its present orientation, combined with the east up sense of shear, the SRSZ has a thrust geometry. However, there is no evidence for metamorphic or large-scale stratigraphic repetition associated with the SRSZ. The steep metamorphic gradient over the shear zone, juxtaposing low grade greenstones of the hanging wall against high grade gneisses in the foot wall block, and an accompanying rapid transition from brittle to ductile conditions is more characteristic of an extensional structure than an compressional structure. Melting at deeper crustal level, producing granitoid intrusions at a higher crustal level can be the result of both crustal thickening and crustal thinning. The timing of intrusion however, is different relative to the main deformation event. Intrusion mainly post-dates deformation in the case of crustal thickening (England & Thompson, 1984) whereas it is synkinematic in crustal thinning (Buck et al., 1988; Kuznir, 1987). The North Shaw Suite has intruded during deformation and is therefore more consistent with crustal thinning in an extensional regime. In a model on the effects of sheetlike intrusions during deformation in extensional and compressional settings, Pavlis (1996) has shown that in an extensional setting the main shear zone develops in the basal part of the granitoid sheet, similar to the SRSZ, whereas in a thrust regime the main shear zone develops at the top of the granitoid sheet. However, the most important argument for an extensional setting of the SRSZ is that it is contemporaneous with the recorded brittle extensional structures in the Coongan Belt.

An important early structural/metamorphic event is supported by $^{40}\text{Ar}/^{39}\text{Ar}$ dating of hornblende in the SRSZ by Davids et. al. (1996). In that study the amphibolite facies metamorphic event in the western Coongan Belt and eastern Shaw area was constrained by a cooling age of 3240 Ma, providing a minimum age of metamorphism, and spot fusion data of hornblende clasts indicating that the earliest metamorphic event may have been as old as 3520 Ma. It is however possible that part of the deformation recorded close to the contact between the Shaw and the Coongan Belt is the result of a later deformation event at ca. 3300 Ma (Chapter 5). Some of the locally developed low grade shear zones, cross-cutting the SRSZ, may be related to this younger event. It is therefore considered likely that some activity of the SRSZ system occurred at or after 3300 Ma.

The combined data imply regional extension in the greenstones during deposition of the Warrawoona Group between 3470 and 3450 Ma, with a low-angle detachment zone at the top of the basement underlying the greenstones. This structure is identical to that seen in core-complexes (Crittenden et al., 1980) in which forward migration of the active detachments has occurred (model 2, Gautier & Brun, 1994). Doming is a characteristic of modern core-complexes and has been ascribed to unloading and isostatic rebound (Spencer, 1984; Buck et al., 1988; Wernicke and Axen, 1988; Brun & van den Driessche, 1994) and more recently to intrusion of sill like magma bodies during deformation (Lister & Baldwin, 1993). In this last model, magmas are thought to intrude along the detachment fault in a wedge shaped geometry, thereby effectively lifting the supracrustal rocks, enhancing the dome geometry. The thermal effect of intrusions is to maintain ductile deformation even at a relatively high crustal level, thereby impeding the development of brittle detachment faults. The geometrical and temporal relations in the eastern Shaw Batholith are in agreement with such a model.

The doming has caused a back rotation of the former low-angle extensional shears along the eastern

margin into their present position, which now indicates a hanging wall up sense of shear (Figure 4.7b). This is a feature common to core-complexes (Wernicke & Axen, 1988 ; Lister & Davis, 1989). The amphibolite grade of greenstone rocks directly adjacent to the Shaw Batholith is the likely result of a combination of the emplacement of mid-crustal rocks against greenstones during extensional shearing, and simultaneous intrusion of the North Shaw Suite in the SRSZ and into the overlying supracrustal rocks. To the north, where the SRSZ bends away from the contact, extensive low-grade greenstones adjacent to the less deformed North Shaw Suite support the view that metamorphism in the greenstones is not only the effect of intrusion of the North Shaw Suite but also the effect of the emplacement of mid-crustal rocks against the greenstones.

The part with the normal sense of displacement in the metamorphic core-complex geometry would be expected on the western side of the Shaw Batholith. Unfortunately this side is cut and overprinted by the younger N-S trending MSZC and structures related to the earlier evolution can no longer be recognised.

Similar syn-sedimentary brittle extensional structures have been found in other greenstone belts (Figure 5.9) in the North Pole area and the Marble Bar Belt (Nijman et al., in press; this study Chapter 7). In the North Pole Belt the extensional faults pre-date the Strelley Pool Chert (Nijman et al., in press), the felsic volcanics of the Duffer Formation are not developed in this area, but the Strelley Pool Chert is correlated to the dolomite unit in the Coongan Belt (DiMarco & Lowe, 1989). In the Marble Bar area, the extensional faults were active during deposition of the Duffer Formation (Nijman et al., in press). Although the transport directions are not precisely established, they are consistent with a general westward transport direction of the hanging wall.

The end product of the extensional phase would result in granitoid domes within the greenstone belts (Figure 4.7b). Therefore we suggest that the characteristic domal geometry of the eastern Pilbara is not solely the result of late doming, but was initiated during the early extensional phase. As extension occurred during intrusion and extrusion of large volumes of magma, the distribution and thickness of granitoids and volcanics are largely determined by the extensional geometry. It remains unclear whether the ca. 3460 Ma extensional event represents the final stages of an earlier thickening event (extensional collapse) or is related to rifting. This is further discussed in Chapter 9.

The eastern Pilbara has a long history post-dating the 3460 Ma extensional event. The main post-extensional thermal event was at ca. 3300 Ma, which is marked by granitoid intrusion. This magmatic event was associated with a tectonic phase of recumbent folding and thrusting in the Warrawoona and lower Gorge Creek Group as described by Bickle et al. (1985) and Boulter et al. (1987) in the Western Shaw area and in the Coongan Belt (Chapter 5). It is likely that steepening of previously formed structures, such as the eastern margin of the Shaw Batholith and part of the Split Rock shear zone, occurred during this event.

4.5 Conclusions

The data indicate that a complex of structures in both the Shaw Batholith and the Coongan Belt formed during deposition of the Duffer Formation, i.e. between 3470 and 3450 Ma. These structures and kinematic relations are consistent with initial doming during deposition of the Warrawoona Group in an extensional tectonic regime. This resulted in a ductile detachment zone (the SRSZ) at the contact between gneisses in the Shaw Batholith and greenstones in the Coongan Belt, and brittle syndepositional listric extensional faults in the Coongan Belt. During this event the North Shaw granodiorite intruded at the contact between gneisses and greenstones and doming of the underlying basement occurred. The tectonic scenario resembles that associated with modern 'core-complexes'. The initial dome shape of the granitoids may have been further enhanced during post Warrawoona deformation. However, structures described here are inconsistent with the solid state diapiric rise of granitoids into overlying greenstones.

Structural development and kinematics of compressional structures in greenstone belts, with emphasis on the Coongan Belt

5.1 Introduction

The overall geometry of greenstone belts appears at first glance to be relatively simple: A layered volcano-sedimentary sequence surrounds ovoid granitoids (Mid-Archean) or forms linear belts between granitoid terrains (Late-Archean).

Detailed structural analysis of most Archean greenstone belts is seriously hampered by poor outcrop conditions and low relief in greenstone belts (Yilgarn, Abitibi). Structural work that was done shows that the geometry of greenstone belts can be described in terms of relatively undeformed, but isoclinally folded 'panels', separated by narrow ductile to brittle shear zones (Boulter et al., 1987; Kusky, 1990; Chown et al., 1992; de Ronde & de Wit, 1994; Myers, 1995). These structures are generally interpreted in terms of fold and thrust belts, but have also been interpreted as second order structures related to solid state diapirism (Anhaeusser et al., 1969; Hickman, 1984; Collins, 1989; Jelsma & van der Beek, 1993).

The greenstone belt stratigraphy typically consists of a number of volcano-sedimentary sequences, separated by unconformities. In many cases, the nature of contacts (unconformity or shear zone) are difficult to determine due to poor outcrop conditions. This can give rise to opposing interpretations of field data in terms of tectonic setting (Bickle et al., 1994). Although outcrop conditions in the eastern Pilbara greenstones are generally good, these problems must be kept in mind while analysing structural/kinematic data.

In the Pilbara greenstone belts, Hickman (1983) described folds and cross-cutting brittle faults, which he related to solid state diapirism. In a small area to the north west of the Shaw batholith, Bickle et al. (1985) described recumbent folding and thrusting, intercalating gneisses and greenstones. They interpreted these structures as part of an Alpine style orogenic belt. The direction of transport as well as the extent of this belt remain unclear. Boulter et al. (1987) described thrust structures post-dating the Warrawoona Group and Gorge Creek Group, but pre-dating deposition of the Lalla Rookh Sandstone. In a study of the greenstones to the west of the Mt. Edgar Batholith, van Haften & White (in press) described layer parallel shears which were interpreted as thrusts with an initial ESE transport direction, reactivated with a NE transport direction.

In this Chapter, the results will be presented of a detailed structural and kinematic study of the Coongan Belt, with emphasis on the compressional structures (early extensional structures are discussed in Chapter 4). The results of this detailed study will be compared with structural and kinematic data collected from surrounding greenstone belts (see Figure 5.1), in order to assess the uniformity of the structural evolution. The timing and significance of compressional structures in the overall evolution of the Pilbara will be discussed.

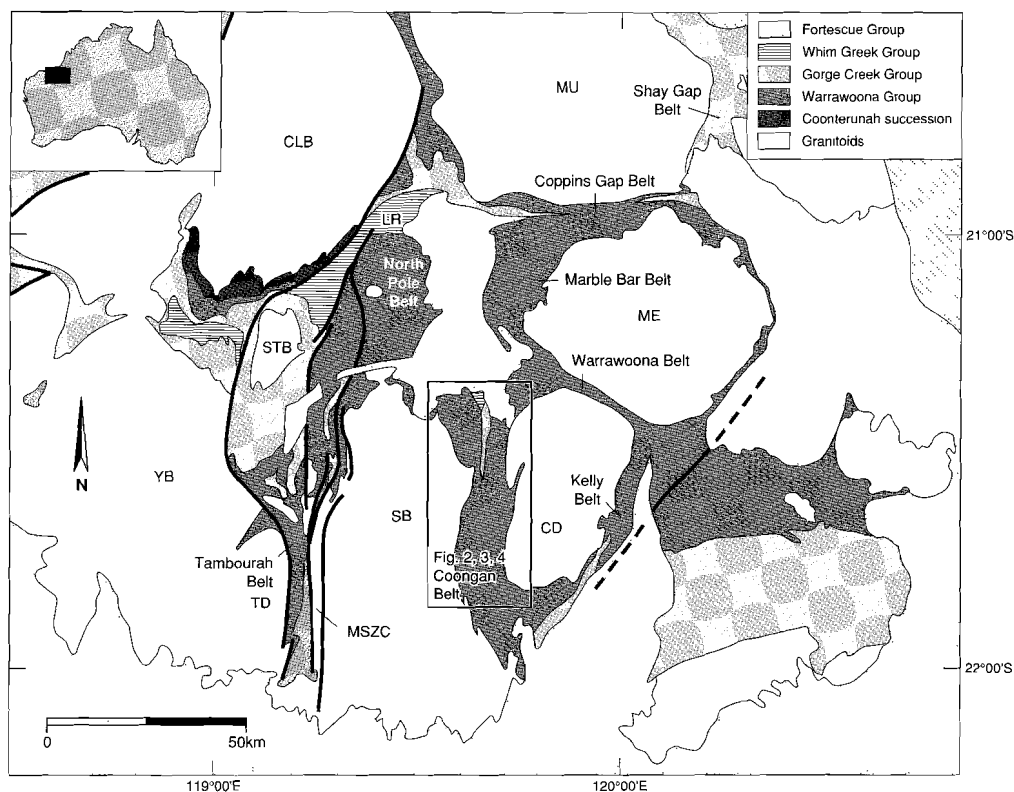


Figure 5.1 Schematic overview map of the eastern Pilbara showing the greenstone belts discussed in this chapter. CD= Corunna Downs Batholith, CLB= Carlindi Batholith, ME= Mt. Edgar batholith, MU= Muccan Batholith, SB= Shaw batholith, STB= Strelley batholith, TB= Tambourah Dome, YB= Yule Batholith, MSZC= Mulgandinnah Shear Zone Complex.

5.2 The Coongan Belt

5.2.1 Background

The Coongan Belt is a 70 km long and 14 km wide greenstone belt situated between the Shaw Batholith and the Corunna Downs Batholith. (Figure 5.2). It consists mainly of Warrawoona Group volcanics and minor sediments. In the north-west, a thick felsic volcanic sequence was dated at

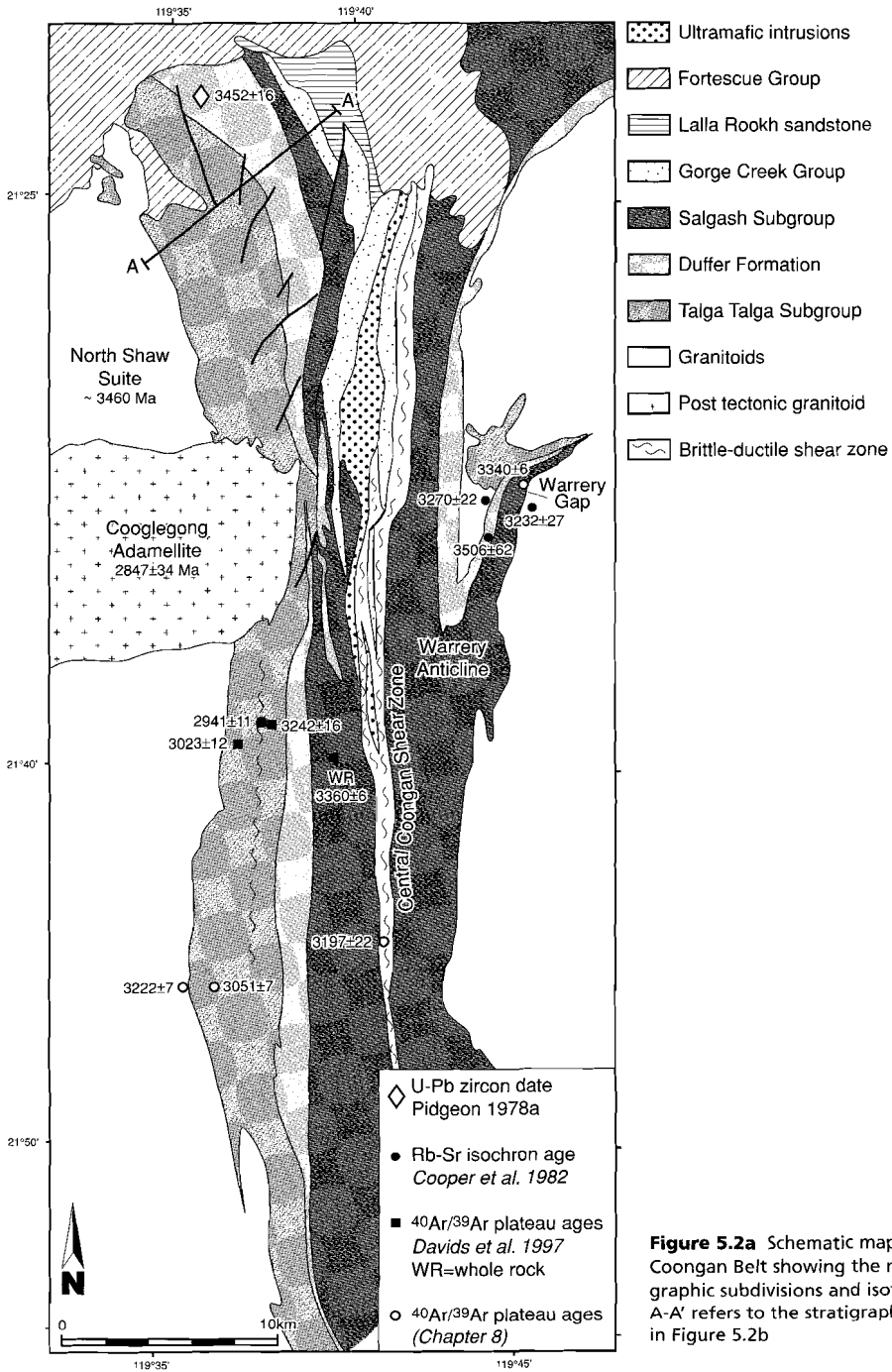


Figure 5.2a Schematic map of the Coongan Belt showing the major stratigraphic subdivisions and isotopic dating. A-A' refers to the stratigraphic sequence in Figure 5.2b

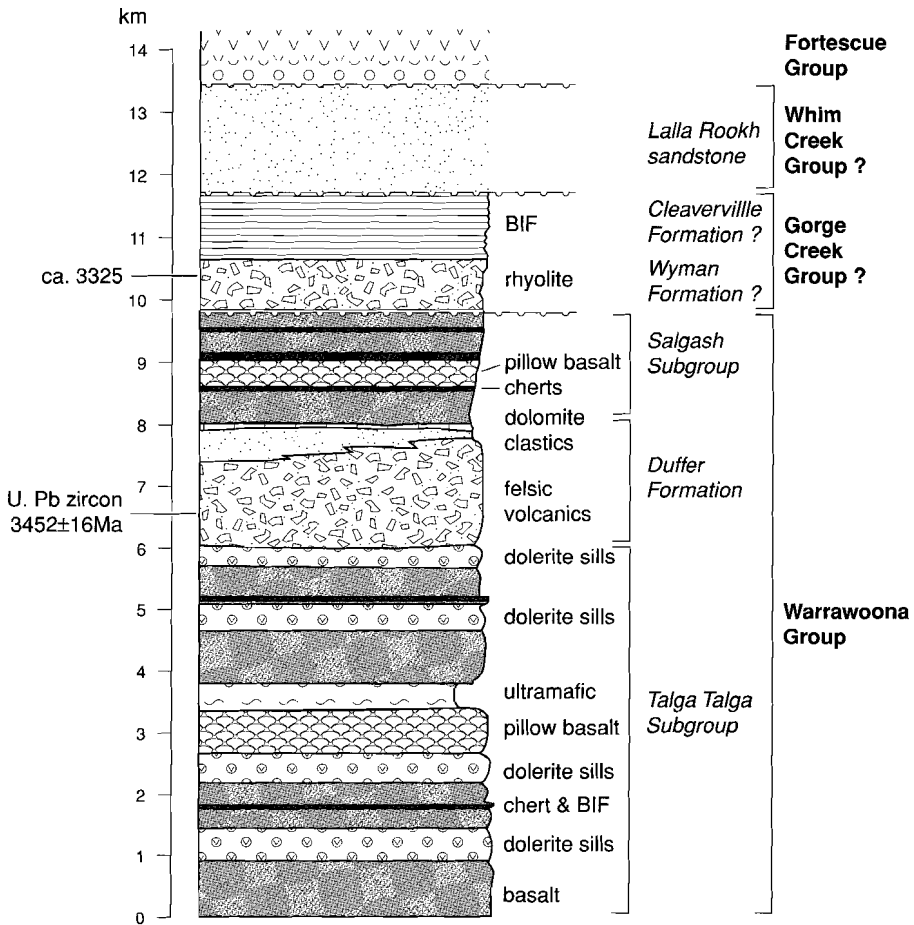
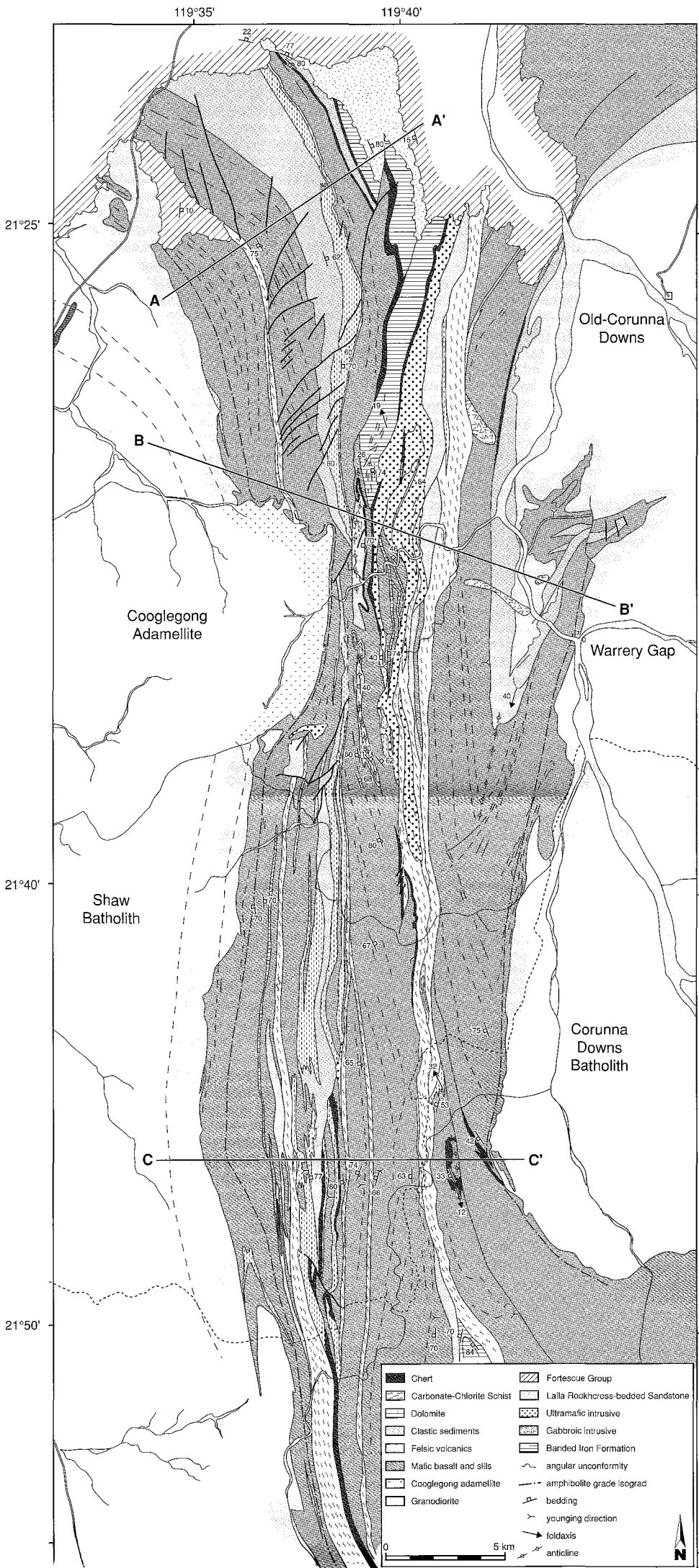


Figure 5.2b Stratigraphic sequence as found in the least deformed part (section A-A') of the Coongan Belt. Cross section A-A', on which the stratigraphic sequence is based, is shown in Figure 5.7, the trace of A-A' is shown in Figure 5.2a.

3452±16 Ma (Pidgeon, 1978a), which is the age of the well constrained Duffer Formation. The central part of the Coongan Belt is usually interpreted as belonging to the Gorge Creek Group (Thorpe et al., 1992; Barley, 1993; Krapez, 1993). However, there are no isotopic data to confirm this. Cooper et al. (1982) report Rb-Sr isochron ages for the contact between the Coongan Belt and the Corunna Downs Batholith. The felsic volcanics gave an isochron age of 3506±62 Ma, consistent with the age of the Duffer Formation. The Corunna Downs granite gave isochron ages of 3270±22 Ma and 3232±27 Ma. The Rb-Sr systematics of the granites may have been reset (Williams and Collins, 1989), therefore these ages should be taken as minimum ages of granite emplacement. The eastern side of the Shaw batholith consists of the 3470 Ma North Shaw Suite (Bickle et al., 1983; McNaughton et al., 1988) and the post-tectonic Cooglegong Adamellite dated at 2847±34 Ma (Pb-Pb whole-rock, Bickle et al., 1989, see also Chapter 4). ⁴⁰Ar/³⁹Ar cooling ages for hornblendes were

Figure 5.3 General lithological map of the Coongan Belt, cross sections are shown in Figure 5.7.



obtained for parts of the Coongan Belt by Davids et al. (1997) and this study (Chapter 8). Their locations are shown in Figure 5.2.

Structural studies in the Coongan Belt prior to this study are limited to a small area around Warrery Gap (Figure 5.2) by Cooper et al. (1982). They described the Warrery Anticline and its strongly foliated eastern limb. The syn-Duffer Formation extensional listric faults in the northwest Coongan Belt have been described in Chapter 5 (Zegers et al., 1996). In this section, the emphasis will be on structures post-dating the early extensional phase.

5.2.2 Lithology and stratigraphy

Due to the general structural disruption of the rocks in the Coongan Belt and obvious lateral stratigraphic variations, it is not possible to define and use a single stratigraphic sequence. However an outline can be obtained from the little deformed northeastern most part of the Coongan Belt. This stratigraphy will be compared to published stratigraphic and geochronological studies (Hickman, 1983; Thorpe et al., 1992; Krapez, 1993).

From old to young (west to east) the lithologies in this traverse (A-A') are as follows (Figure 5.2a,b and 5.7a): An approximately 6 km thick mafic volcanic sequence, consisting of massive and pillow basalts and a large proportion (up to 40%) of dolerite and gabbro sills, contains a ca. 0.5 km thick deformed ultramafic unit and minor thin chert and BIF units. This sequence can reliably be assigned to the lower Warrawoona Group, the Talga Talga Subgroup because it is overlain by the Duffer Formation. The Duffer Formation consists of mainly felsic volcanics (rhyolites, dacites and agglomerates; DiMarco & Lowe, 1989) and sediments (BIF, sandstone and conglomerates), capped by a 20 m thick dolomite unit, which contains stromatoloids. The thickness of the Duffer Formation varies between 1 and 3 km

The dolomite is overlain by a massive to pillowed basalt to komatiitic basalt, which contains chert units at regular intervals. This unit is thought to be part of the upper Warrawoona Group, the Salgash Subgroup. In turn the basalt is overlain by a rhyolite and chert unit. The bedding of the pillow basalt makes a 22° angle with the bedding of the chert/rhyolite, indicating an unconformable contact. Although undated, the rhyolite unit is assumed to represent the ca. 3325 Ma (Thorpe et al., 1992) Wyman Formation, the base of the Gorge Creek Group. Barley (1980) and Hickman (1983) previously described local unconformities between the Salgash Subgroup and the Wyman Formation. The thick BIF which overlies the rhyolite can be correlated to the Cleaverville Formation. The rhyolite and BIF are unconformably covered by a thick cross-bedded sandstone unit with an angular unconformity angle of 28°. This sandstone should be interpreted as the equivalent of the Lalla Rookh sandstone, if the overall stratigraphy for the eastern Pilbara holds for the Coongan belt.

The major divisions of the Warrawoona Group (i.e. Talga Talga Subgroup, Duffer Formation and Salgash Subgroup) can be traced further south in the Coongan belt, although extensively disrupted, partly repeated and with large lateral variations (Figure 5.2 and 5.3).

In the eastern Coongan Belt, the thick agglomerate unit next to the Corunna Down Batholith can reliably be correlated to the Duffer Formation because of its lithology and the Rb-Sr age. This implies that the basalt unit (2-3 km), forming the western limb of the Warrery Anticline, is part of the Salgash Subgroup.

The central part of the Coongan Belt is not easily assigned to any particular part of the stratigraphy. It is intensely deformed, with a major ductile shear zone (Central Coongan Shear Zone, CCSZ), in

originally ultramafic rocks, forming the eastern part of the central Coongan Belt. In the northern part of the central Coongan Belt extensive intrusive ultramafic bodies occur, consisting of serpentinized dunite and pyroxenites. The strongly deformed rhyolite unit in the central Coongan Belt could possibly be assigned to the Wyman Formation.

5.2.3 *Alteration and metamorphism*

Most of the Coongan Belt rocks show greenschist facies metamorphic assemblages (albite, actinolite-tremolite, epidote, chlorite, sericite, chloritoid) and, in places, where they are not intensely deformed, they preserve primary textures. Amphibolite facies grade rocks occur only in a zone ± 1 km wide, adjacent to the two granitoids. These contact zones consist mainly of amphibolites, but in one location in the southwestern Coongan Belt a thin schist unit containing large (5 cm) garnets+muscovite+chlorite was found, constraining their metamorphic grade to upper greenschist-lower amphibolite facies.

Alteration is widespread in the Coongan Belt. Extensive alteration in the Pilbara greenstones was already recognized in a regional geochemical survey by Hallberg (1974), who reported unacceptable amounts of CO_2 (>4 wt%) in most of the samples collected. Carbonate alteration is most conspicuous in the vicinity of shear zones, typically developed in ultramafic units, where Mg-bearing carbonates are often the main mineral phase.

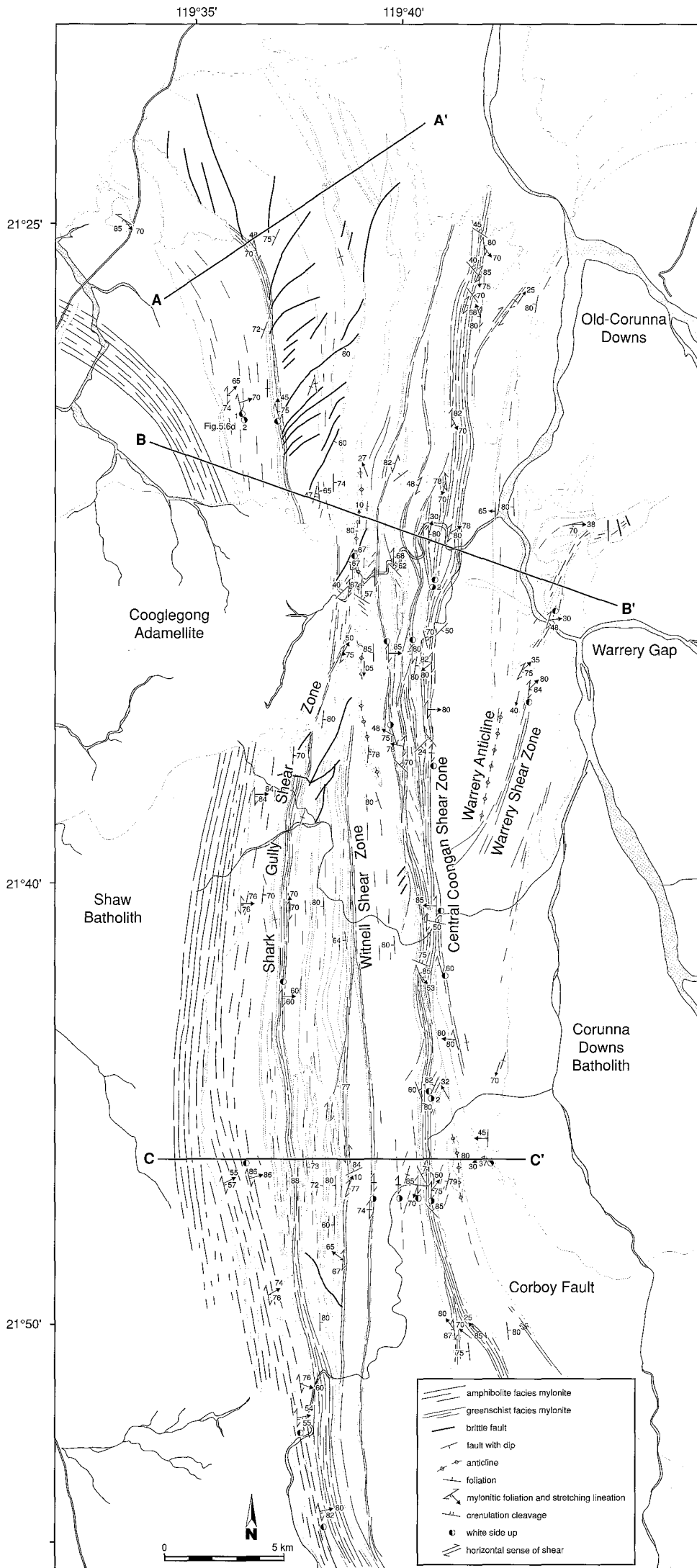
Undeformed basalts typically show alteration of plagioclase and are more or less carbonate altered. Silicification is another very common alteration process. In some cases pillow basalts were found to be completely silicified. However, silicification is most commonly related to deformation and typically occurs throughout the greenstone belt as metre wide green cherts with an extremely strongly developed SL fabric, indicating a tectonic connection to the silica alteration.

5.2.4 *Structural development*

Deformation is inhomogeneously distributed in the Coongan Belt and is concentrated in N-S trending shear zones (Figure 5.4). Between these shear zones are sheets, or panels of rocks, with a much lower deformation intensity. In some cases these panels preserve very early structures such as the extensional faults in the northwestern Coongan Belt (see Chapter 4). Usually the bedding and primary volcanic or sedimentary textures are preserved within these panels. Bedding is N-S trending and is folded on a regional scale within the panels. Large-scale examples of these folds are the Warrery anticline, and the Triberton Anticline (Figure 5.4). This folding is not easily recognised in homogeneous mafic volcanics, but can be traced by reversal of the younging direction as deduced from pillow basalts. Fold hinges are tight with interlimb angles between 20° and 40° and are characterized by abundant folding and faulting. Where cherts, or especially, banded iron sequences are present (central Coongan Belt), the folding is much more obvious and parasitic folds are well developed on outcrop scale (Figure 5.6a). A contour plot of poles to the bedding in the Coongan Belt is shown in Figure 5.5a. The poles to the bedding form an E-W trending, steeply dipping great circle. The contour plot of the fold axis (Figure 5.5b) shows shallowly to moderately north and south plunging fold axis, with a maximum for the shallowly north plunging axis. This fold axis orientation is consistent with the contour plot of the poles to the bedding.

Within the fault bounded panels an axial planar foliation is developed that is steeply dipping, N-S trending and has an associated down-dip stretching lineation. This fabric is especially clear in agglom-

Figure 5.4 General structural map of the Coongan Belt, cross sections are shown in Figure 5.7.



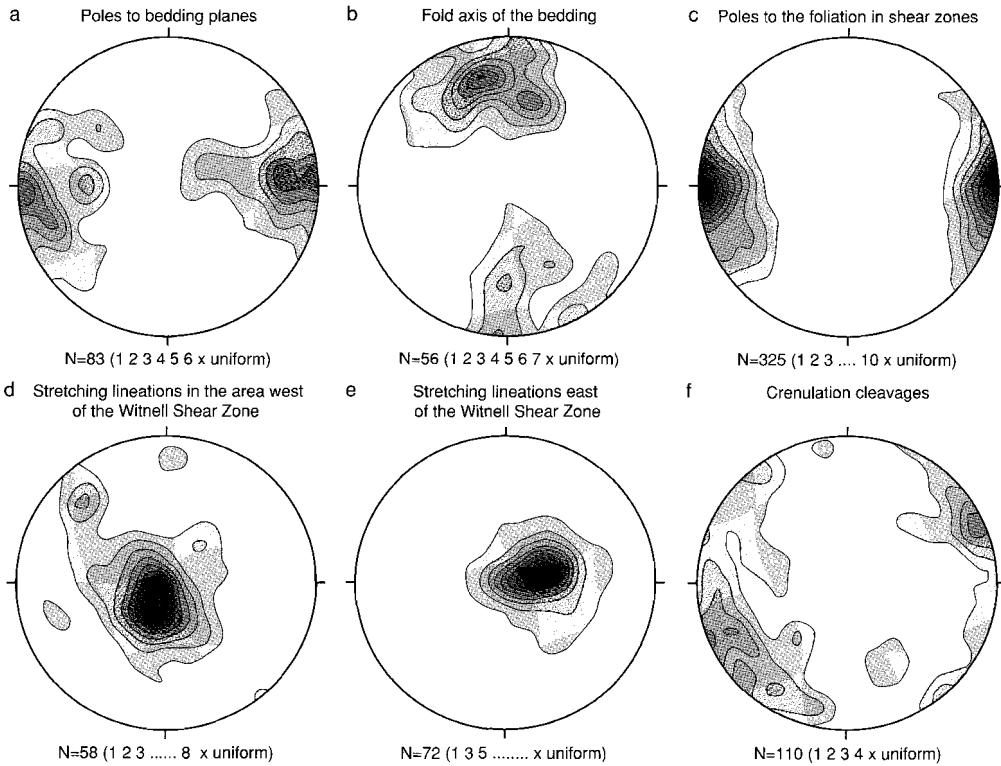


Figure 5.5 Equal area stereographic plots of structural data in the Coongan belt

erates and spherulitic basalts, where flattened clasts and spherulites define a foliation and 3-d strain markers are visible (Figure 5.6b).

Shear zones

The main shear zones in the Coongan Belt are the Shark Gully, Witnell, Warrery and, the largest, Central Coongan Shear Zone (Figure 5.4). These shear zones vary in width between 20 m and 1 km. Thin shear zones (1–10 m) have not been mapped, but are widespread in the panels between the major shear zones. Where the shear zones cut through incompetent rocks, such as sandstones, the shear zones narrow to a 1–5 m wide fault zone. An example of this occurs in the northward continuation of the Witnell Shear Zone.

In the shear zones, an intense mylonitic foliation is developed, formed by various greenschist facies minerals (chlorite, talc, serpentine and carbonates). The mylonitic foliation is usually planar when developed in a homogeneous rock type, but forms an anastomosing pattern on a cm–km scale where boudins of more competent rocks occur. These boudins may consist of boudinaged quartz veins, cherts, or massive spinifex textured komatiites or coarse-grained pyroxenites. Other than in these boudins, the original textures have been completely transposed by the strong foliation.

Figure 5.5c shows a contour plot of the poles to the mylonitic foliation measured in the Coongan

Belt. Although there is a significant spread in foliation orientation, there is a clear point maximum for N-S trending, subvertical foliations.

A stretching lineation is usually present in the shear zones. It is marked by elongate carbonates, chlorite and occasional actinolites, and is particularly well developed on quartz veins or cherts that have been caught up in the shear zones, but less so in chlorite rich rocks. Close to the Shaw Batholith, in the amphibolite zone, lineations are formed by oriented hornblende grains (see also Chapter 4). The stretching lineations have been plotted in two separate contour plots (Figure 5.5d,e), one for the part of the Coongan Belt west of the Witnell Shear Zone and one for the rest of the Coongan Belt. This was done to test whether lineations in the western subarea, probably related to the early extensional deformation phase (see Chapter 4), show a different pattern than lineations in the rest of the Coongan Belt, which are thought to be related to a later deformation event. The stretching lineations in the western subarea (Figure 5.5e) show a well defined maximum plunging 70° to 070° , entirely consistent with the orientation of stretching lineations in the Split Rock Shear Zone (Chapter 4). In the eastern subarea lineations are more variable (Figure 5.5d), but show a maximum of lineations plunging steeply to the south. A number of shallowly plunging lineations were recorded on the Corboy Fault, a NW trending section of the southern Central Coongan Shear Zone and on parts of the Witnell Shear Zone (Figure 5.4).

Whereas most shear zones in the Coongan Belt are developed in the greenschist facies, the Warrery Shear Zone is an exception. This shear zone forms the eastern limb of the Warrery Anticline (Figure 5.4) and dies out towards the south. A strong mylonitic foliation and lineation are developed in a tuffaceous layer over a width of 500 m. The SL fabric is formed by quartz, hornblende and plagioclase. Biotite granodiorite veins, similar in appearance to the Corunna Downs granodiorite, intrude the mylonitic foliation at a small angle and are boudinaged with the boudin axis perpendicular to the stretching lineation, which is steeply to moderately north plunging, in contrast to the mainly south plunging lineation in other shear zones (Figure 5.6c). This structural/ intrusive relation shows that the Warrery Shear Zone was active during intrusion of the granodiorite, i.e. at 3340 Ma, see Chapter 8.

Kinematics

In the western subarea the sense of shear is consistently ENE up. Kinematic indicators include hornblende and garnet porphyroclasts close to the Shaw Batholith, and S-C fabrics and shear-bands (Chapter 4). In one location, a later east-down reactivation could be deduced (Figure 5.6d). At this location (Figure 5.4), a subvertical anastomosing mylonitic foliation and down-dip stretching lineation is developed in a pillow basalt. The pillows act as more rigid objects and show an internal S foliation, indicating an initial east-up sense of shear. The S foliation subsequently formed drag folds

Figure 5.6 Photographs of:

- a) BIF of the Gorge Creek Group showing asymmetric parasitic fold in the central Coongan Belt
- b) Co-axial foliation and lineation developed in the Duffer Formation agglomerate in the eastern Coongan Belt.
- c) Granitic boudins intruded during activity on the Warrery Shear Zone in the eastern Coongan belt. The coin has a diameter of 2 cm.
- d) Shear sense reversal in pillow basalt in the western subarea, in the Talga Talga Subgroup. The S foliation is formed during the east up sense of shear and subsequently dragged into folds on the rim of the pillow during shear sense reversal.



Figure 5.6a



Figure 5.6b

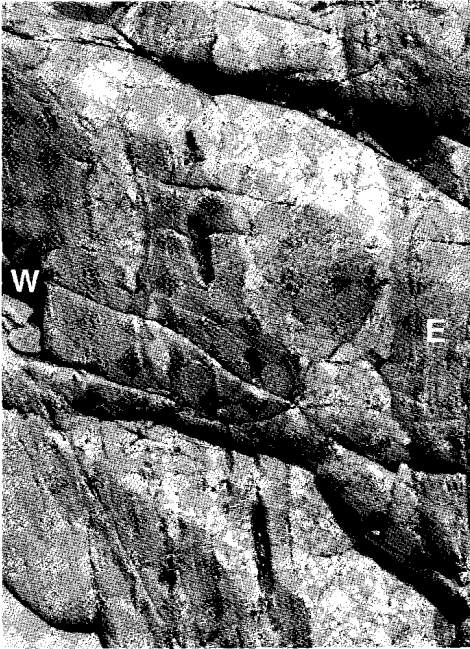


Figure 5.6c

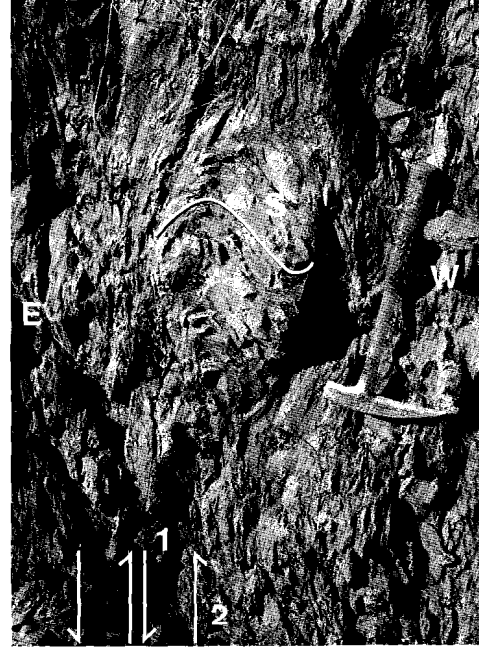


Figure 5.6d

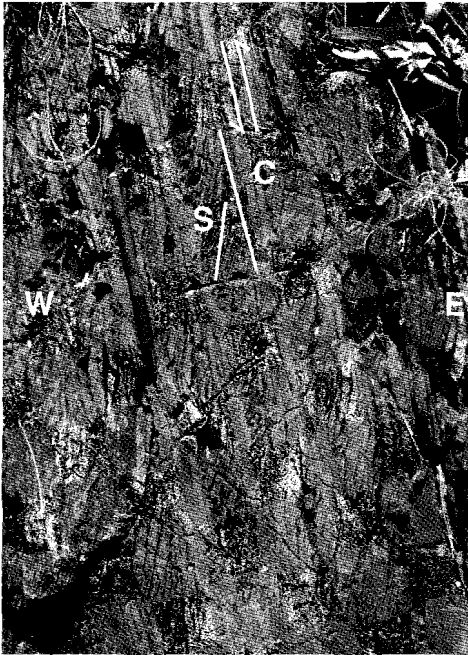


Figure 5.6e

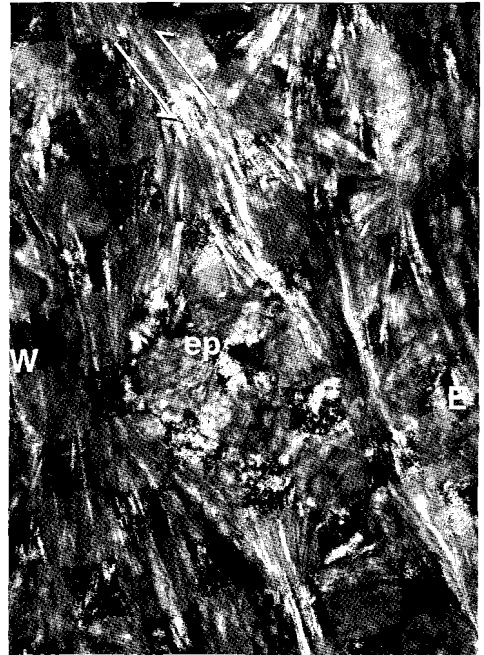


Figure 5.6f

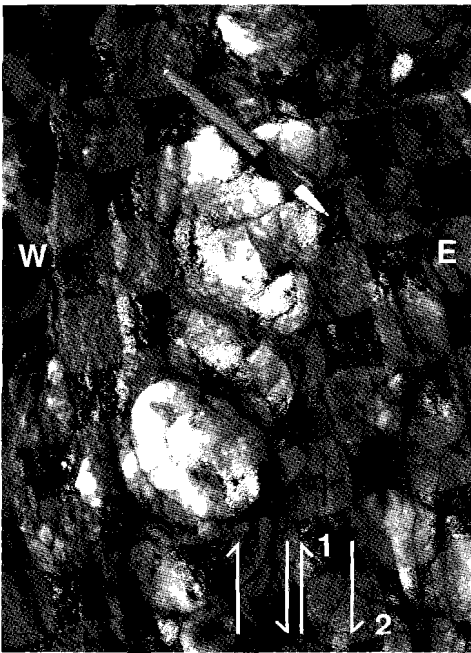


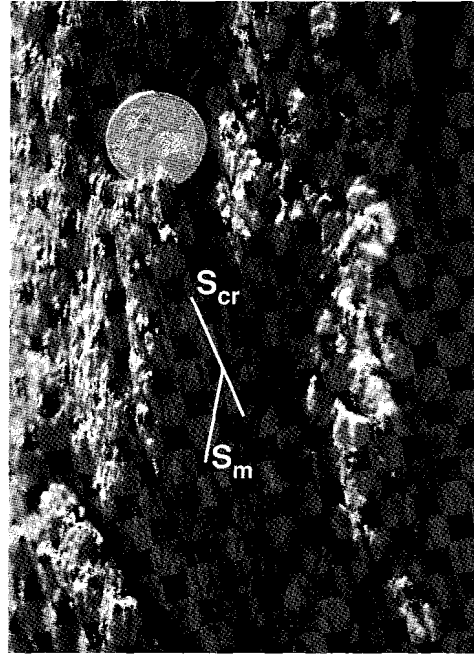
Figure 5.6g



Figure 5.6h

Figure 5.6 Photographs of:

- e) Dm-scale S-C fabric in a chert unit in eastern sub-area, showing an east-up sense of shear
 f) Photomicrograph of the Central Coongan Shear Zone mylonite with epidote (ep) grains as clasts, indicating an east-up sense of shear. Width of the photomicrograph is 0.2 mm.
 g) Boudinaged quartz vein in the Central Coongan Shear Zone formed during east-up sense of shear, but shortened during subsequent west-up sense of shear.
 h) Photomicrograph of randomly oriented actinolite grains growing over the mylonitic fabric (m) of the Central Coongan Shear Zone. Width of photomicrograph is 0.4 mm.
 i) NW-SE trending crenulation cleavage (S_{cr}) as seen in the Central Coongan Shear Zone overprinting the mylonitic foliation (S_m). The coin is 2 cm in diameter.

**Figure 5.6i**

in the rim of the pillows, indicating an east-down reactivation of the mylonite.

In the eastern subarea, the sense of shear recorded in the shear zones is usually E up (Figure 5.4).

This sense of shear prevails in most of the CCSZ and its splays, the northern part of the Witnell

Shear Zone and the Warrery Shear Zone. Kinematic indicators include S-C fabrics, shear-bands, and asymmetric clasts or boudins, found in outcrops or in thin sections. Figure 5.6e shows a dm-scale S-C fabric, indicating an E up sense of shear, found in a silicified splay of the CCSZ. Typical microstructures from the CCSZ mylonite are shown in Figure 5.6f, where epidote grains form asymmetric clasts.

Isoclinal asymmetric folding occurs frequently in the shear zones but is not considered to be a reliable kinematic indicator. The fold axis of these folds, typically developed in chert bands, are variable but mostly parallel the stretching lineation. The folds have sheath fold geometries on various scales (cm-km).

In two locations in the CCSZ, indications were found for later west up reactivation of the CCSZ (see Figure 5.4 for locations $119^{\circ}41'E21^{\circ}45'S$ and $119^{\circ}41'E21^{\circ}33'S$).

In the south CCSZ, in a riverbed outcrop, a subvertical mylonitic foliation is developed which contains a boudinaged quartz vein, with the boudin axis perpendicular to the stretching lineation (Figure 5.6g). The boudinage is interpreted to have formed during the initial E up event. The boudins have subsequently been flattened, forming a foliation with an S orientation in a west up kinematic framework.

In the central part of the Coongan Belt, a sample shows microstructural evidence of west up reactivation. Asymmetric folds related to an east up sense of shear are cut by west up shear-bands. The west up sense of shear is developed on a small number of strands of the CCSZ and the Witnell Shear Zone.

Deformation and metamorphism post-dating shear zones

In a number of samples, randomly orientated grains of tremolite or muscovite have overgrown both the east up and west up mylonitic foliation (Figure 5.6h).

The mylonitic foliation is overprinted by a regionally developed ESE trending crenulation cleavage (Figure 5.6i). This cleavage is usually not developed in the less foliated rocks away from the shear zones, but does occur throughout the Coongan Belt in previously foliated zones. The mineralogy of the crenulation cleavage is the same as the mylonitic foliation. A relation between the crenulation cleavage and the random muscovite and tremolite was not observed.

Limited parts of the shear zones have been reactivated by brittle faulting with a strike-slip sense of shear (Witnell Shear Zone), as indicated by sub-horizontal stretching lineations or slickensides. A sinistral sense of shear is associated with the sub-horizontal lineations. The Corboy Fault is another example of late strike-slip faulting, but the sense of shear could not be deduced.

5.2.5 Geometrical/kinematic model for the Coongan Belt

In order to construct a structural/kinematic model for the Coongan Belt, the structures need to be interpreted in 3 dimensions. This step is not straight forward since outcrops are flat and essentially provide a 2 dimensional view. There are no detailed geophysical data available on the Pilbara Craton that could provide the third dimension. Therefore, a number of assumptions need to be made for the deeper parts of the Coongan Belt.

Geophysical studies in the Kaapvaal and Yilgarn Craton and the Superior Province have consistently shown that greenstones do not extend to a depth greater than 5-7 km (de Beer & Stettler, 1988; Drummond et al., 1993; Jackson et al., 1995) and are underlain by a mainly felsic granitic crust to the Moho depth of ca. 30 km (Drummond & Collins, 1986). The base of the greenstone belts and the underlying rocks are dominated by subhorizontal structures in contrast to the subvertical structures in the greenstones (Goleby et al., 1993).

Although such detailed seismic profiles are not available for the Pilbara Craton, the above characteristics are assumed to hold for the Coongan Belt. The vertical sections, shown in Figure 5.7, were constructed assuming a maximum depth of the greenstones of 7 km and a flat base to the greenstones. Section A-A' was constructed in the least deformed part and shows the stratigraphic sequence. The Warrawoona and Gorge Creek Group are overturned and are unconformably covered by the Lalla Rookh Sandstone, which in turn is unconformably covered by the flat lying Fortescue Group. Note that the Lalla Rookh Sandstone is offset by a brittle strand of the Witnell Fault.

Section B-B' shows the more complex structures in the central Coongan Belt. Here, the Split Rock Shear Zone is thought to flatten towards the east, thereby providing the flat base to the greenstones. The relatively undeformed panel between the Witnell Shear Zone and the Shark Gully Shear Zone preserves the early (3460 Ma) extensional structures (Chapter 4). The Triberton Anticline forms the hanging wall anticline to the Witnell Shear Zone thereby causing the doubling of the stratigraphy (Duffer Formation) and is consequently interpreted as a thrust zone. The strongly folded Cleaverville BIF occupies a wedge between the Triberton Anticline and a strand of the CCSZ. The central intrusive ultramafic body contains localized shear zones that may have repeated it. Directly to the south of section B-B' a thrust culmination is present, where a 10 m thick BIF is repeated several times due to thrusting. The younging direction in these BIF units is to the east.

The CCSZ forms the boundary between the intrusive ultramafics and a felsic unit, equivalent to the

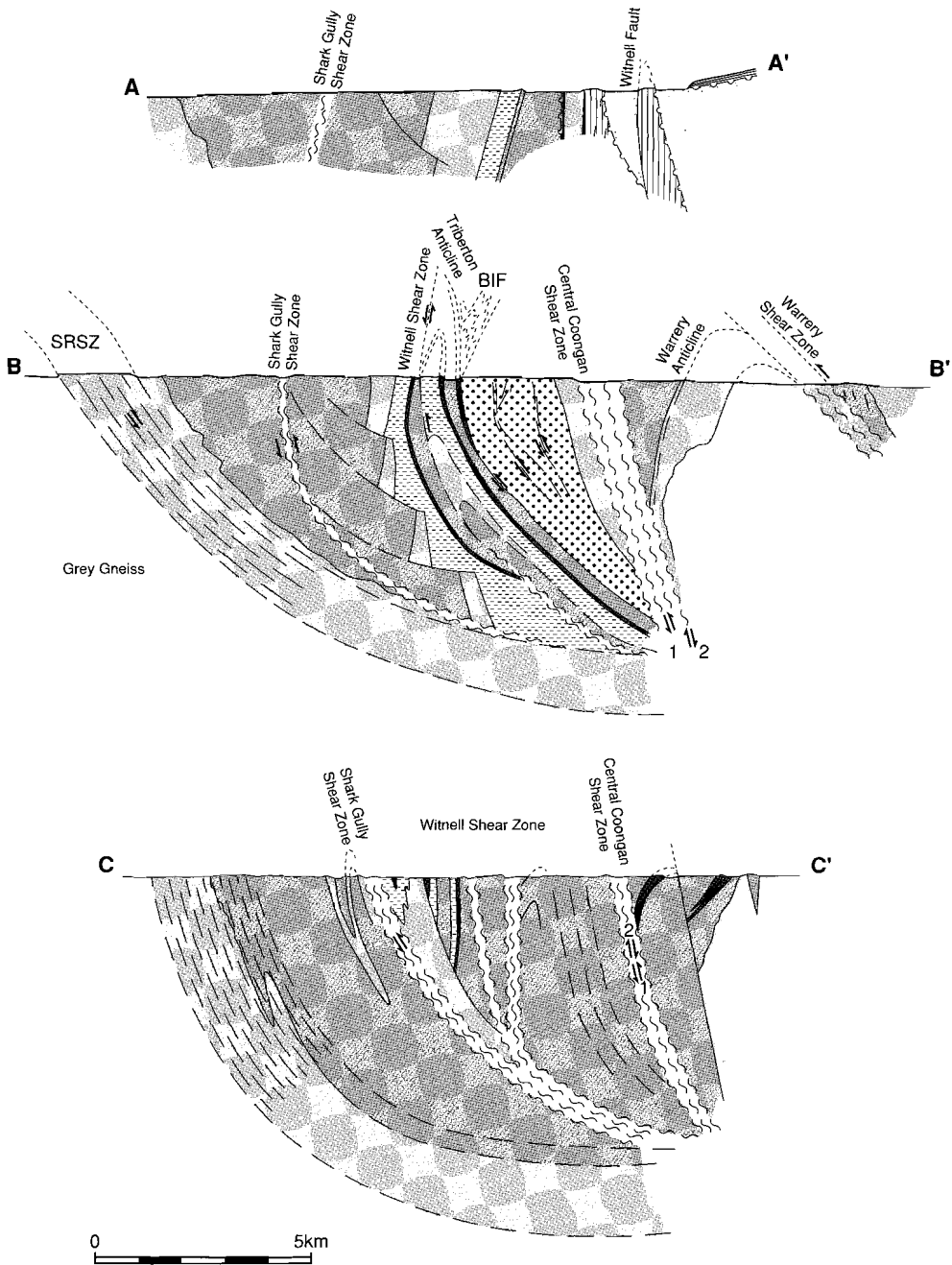


Figure 5.7 Vertical sections of three traverses in the Coongan Belt, see text for discussion For legend and transects see Figure 5.3 and 5.4.

Wyman Formation, on the western side and the western limb of the Warrery Anticline to the east. The eastern limb of the Warrery Anticline is truncated by the Warrery Shear Zone.

Section C-C' shows a similar geometry to B-B', with relatively undeformed but folded panels between shear zones, but simpler because it is not disturbed by the ultramafic intrusives.

5.3 Structures in other greenstone belts

In order to be able to judge to what extent the structural and kinematic characteristics of the Coongan belt (extension and compression) apply to other greenstone belts in the eastern Pilbara a number of other greenstone belts will be discussed briefly. The structural and kinematic data presented for these belts is usually based on a small number of traverses, on 1:50,000 scale, and not on detailed mapping.

The most important shear zones, and their kinematic data, are summarized in Figure 5.8

5.3.1 The Tambourah Belt

The Tambourah Belt (Figure 5.1) consists of mainly mafic volcanics with minor chert units and a number of pelitic units. No isotopic dates are available on the volcanics but they are thought to be part of the Warrawoona and Gorge Creek Group (Krapez, 1993). The metamorphic grade is greenschist facies in the centre of the belt but increases to amphibolite facies towards the granitoids.

The eastern half of the Tambourah Belt is weakly to moderately foliated with a steeply west dipping foliation. The foliation forms the axial plane to tightly folded bedding planes with a shallowly north plunging fold-axis. The eastern margin shows a strong mylonitic foliation with a down-dip stretching lineation and a west up sense of shear predating the sinistral sense of shear on the Mulgandinnah Shear Zone Complex (Chapter 6).

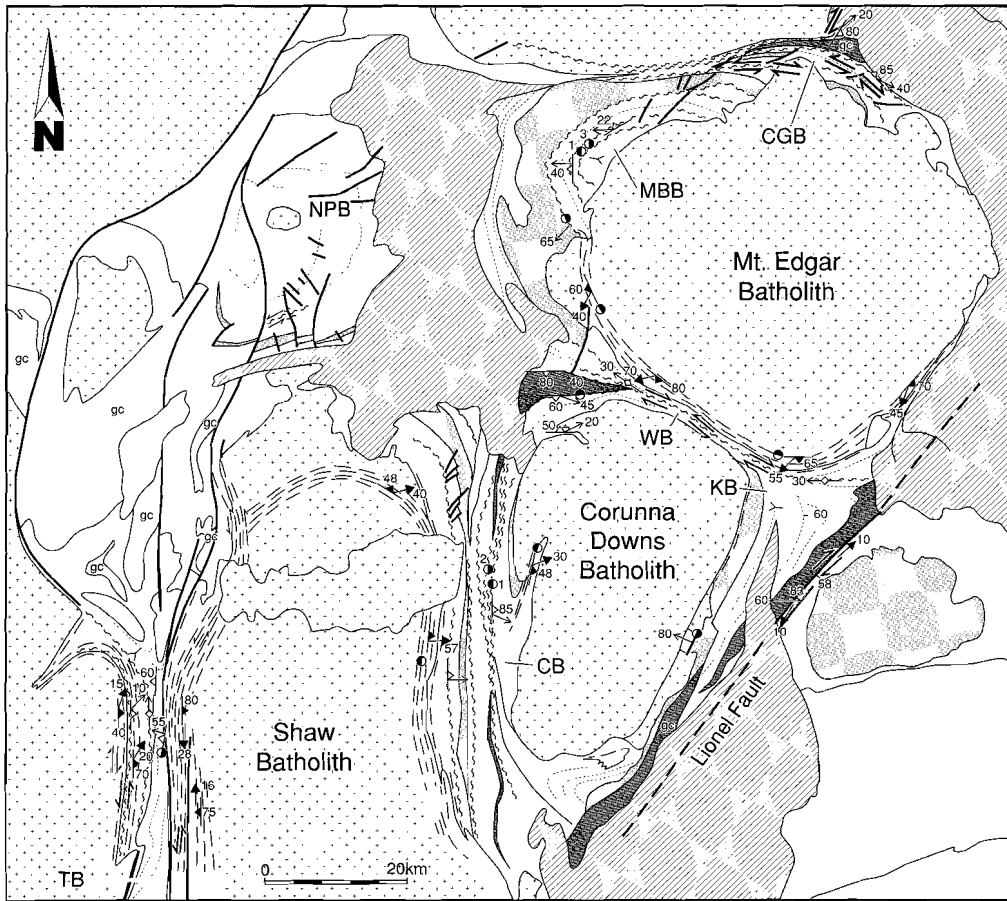
The western half of the Tambourah Belt consists of amphibolite with a N-S trending steeply dipping foliation and 15-30°N pitching stretching lineation formed by blue hornblende. In the Tambourah Dome, this foliation and lineation are associated with a dextral sense of shear. In the centre of the Tambourah Belt, a 100-200 m wide N-S trending chlorite-carbonate mylonite is developed. The mylonitic foliation is subvertical with a subhorizontal lineation; the sense of shear was not established. Randomly oriented green amphiboles grow over the fabric in the western part of the belt.

A chloritic mylonite with a sinistral sense of shear forms the western contact of the Tambourah Belt with the Yule Batholith. This mylonite overprints the randomly oriented amphiboles.

Both the amphibolite grade foliation and the greenschist facies shear zone at the contact are folded on a 10 km scale, forming the Tambourah Dome. The pitch of the lineations remains constant, indicating that folding occurred after the development of the SL fabrics.

An ⁴⁰Ar/³⁹Ar study by Wijbrans and McDougall (1987) showed a cooling age for the blue hornblende of ca. 3200 Ma, whereas the overprinting thermal event was dated by them at ca. 2950 Ma.

Some of the structures with down-dip lineations in the eastern Tambourah Belt may be preserved fold and thrust structures, but the strike-slip kinematics is dominant in both the amphibolite and greenschist grade shear zones.



- | | | | |
|--|---|--|----------------------------------|
| | amphibolite grade shearzone | | Fortescue Group |
| | greenschist facies shearzone in ultramafics | | Wyman formation formation 3325Ma |
| | Brittle fault | | Duffer formation 3450Ma |
| | Bedding trace & younging direction | | Granitoids |
| | white side up | | gc = Gorge Creek Group |
| | fold axis | | |

Figure 5.8 Summarized structural data in greenstone belts in the eastern Pilbara, see text for discussion. TB= Tambourah belt, CB= Coongan Belt, KB= Kelly Belt, MBB= Marble Bar belt, CGB= Coppins Gap Belt, NPB= North Pole Belt.

5.3.2 *Kelly Belt*

The Kelly Belt consists of the Duffer Formation, part of the Salgash Subgroup and Wyman Formation, dated at ca. 3325 Ma (Thorpe et al., 1992). These rocks are intruded by the Boobina Porphyry, dated at 3307 Ma (Pidgeon, 1984). Sills and dykes of pyroxenite and dunite intrude the volcano-sedimentary sequence.

The metamorphic grade of the Kelly belt is lower greenschist facies. Only a zone of 20 m next to the Corunna Downs Batholith attains amphibolite facies.

The most striking characteristic of the Kelly Belt is the very low intensity of deformation. A weak foliation is developed in the agglomerate next to the Corunna Downs Batholith, but otherwise rocks are unfoliated with steeply, east dipping bedding planes, younging to the east. An early NE trending fault, intruded by the Boobina porphyry, preserves a down-dip lineation. The major structure in the Kelly Belt is the Lionel Fault, which shows a dominant dextral sense of shear. In the vicinity of the Lionel Fault, a number of older NE trending faults occur with a down-dip lineation, as well as folds with subhorizontal foldaxes. The Lionel fault may have been a reactivated older structure, but has been active after deposition of the Wyman Formation, which it truncates.

5.3.3 *The Warrawoona Belt*

The Warrawoona Belt consists of Warrawoona Group volcanics with a wedge of felsic volcanics in the western part of the belt which are thought to be part of the Wyman Formation (Hickman, 1983). The Warrawoona Belt is probably the most intensely deformed belt in the Eastern Pilbara and consists of an amphibolite facies northern zone, a weakly deformed southern zone and the Central Warrawoona Shear Zone (CWSZ) which forms the contact between the latter two zones. The southern zone and the CWSZ both contain greenschist facies assemblages. Kloppenburg et al. (1997) give a detailed description of the structures in the Warrawoona belt.

The northern zone is characterized by steep foliations forming a semi-circle with consistently SSW plunging stretching lineations, the sense of shear is SSW up, with occasionally a late N up reactivation. The Southern Zone is weakly foliated with a number of E-W trending shear zones in the western part with east plunging lineations and an east up sense of shear. The CWSZ is situated in a carbonate altered ultramafic unit and consists of a chlorite-carbonate mylonite with a subvertical foliation. The kinematic history is complex and involves an early south up sense of shear, followed by an oblique dextral sense of shear, locally overprinted by a sinistral sense of shear.

The timing of deformation is uncertain but postdates the Warrawoona Group and the Wyman Formation. The CWSZ truncates all other structures.

5.3.4 *The Marble Bar Belt*

The Marble Bar Belt is the type area of the Warrawoona Group stratigraphy. The volcanics show greenschist facies assemblages but in general preserve primary textures. Van Haften & White (in press) describe a number of strike parallel greenschist facies shear zones in the type area of the lower Warrawoona Group. These occur as narrow shear zones in the North Star Basalt and the Mt. Ada Basalt, whereas the McPhee Formation, which was mapped as a schist, is in fact mainly a shear zone. They distinguish an early ESE directed extensional event followed by an east directed thrusting event. One of the main shears, that forms the contact between the Mt. Ada Basalt and the Duffer Formation, is reactivated with a transport direction to the northeast during intrusion of a Mt. Edgar

granodiorite (ca. 3300 Ma). They found evidence for an even later NW-SE compressional event. The result of the tectonic disturbance of the lower Warrawoona Group in the type section is that the type section can not be regarded as an undisturbed stratigraphic sequence, but is a lithotectonic sequence.

5.3.5 *Coppin Gap Greenstone Belt*

The Coppin Gap Greenstone Belt consists in part of the Duffer Formation and Salgash Subgroup mafic volcanics overlain by a felsic volcanic unit and a strongly folded BIF sequence, both thought to be part of the Gorge Creek Group (Hickman, 1983), which are in turn unconformably overlain by a thick sandstone sequence. Metamorphic assemblages do not exceed greenschist facies. Structures in the central-northern part are complex and include intense folding and shearing.

In the southern, less deformed part, a number of extensional faults occur, that influence the thickness of the Duffer Formation. They faults are consistent with an approximately E-W extensional setting (Nijman et al., in press). These are cut by bedding parallel shear zones situated in carbonate altered ultramafic units, one of which is the Bamboo Creek Shear Zone, described in detail in Chapter 7. In the Bamboo Creek area, the NW trending shear zone shows an early sinistral sense of shear with a stretching lineation pitching 45° SE, followed by a more horizontal dextral sense of shear. Nijman et al. (1995) described these shear zones as west-vergent thrust zones causing doubling of the stratigraphy in the Shay Gap Belt.

A similar shear zone was found in the northern part of the Coppin Gap Greenstone Belt (Figure 7.8 and 8.1). This 50 m wide, subvertical, 030 trending bedding parallel shear zone contains a 20° N pitching stretching lineation and shows a dextral sense of shear. It is truncated and unconformably covered by an E-W trending, steeply to moderately south dipping, sandstone unit, indicating that the shear zone must have been passively tilted after deposition of the sandstone unit.

After deposition of the clastic sediments, the greenstones were steepened, forming a synclinal structure with a well preserved southern limb. The northern limb is truncated and strongly sheared by a late E-W trending shear zone at the contact with the Muccan Batholith, the South Muccan Shear Zone. This shear zone shows an early sinistral sense of shear followed by dextral sense of shear.

5.3.6 *The North Pole Dome area*

The stratigraphy of the North Pole Dome area, famous for its stromatolites (Dunlop et al., 1978), has been studied extensively (e.g. Dunlop & Buick, 1981; Buick, 1985), and is generally interpreted as a shallow marine environment. Large barite deposits occur, which are thought to represent baritized gypsum evaporites (Barley, 1992; Lambert et al., 1978)

In a detailed structural and sedimentological study of the North Pole Dome area, Nijman et al. (In press) describe early syn-Warrawoona Group extensional faults. These are interpreted as north-block-down growth faults in a NE-SW extensional setting. The barite deposits are shown to be related to these extensional faults, similar to black smokers in modern oceanic settings (Nijman et al., in press). In the southern part of the North Pole Dome area a number of strike parallel E-W trending shear zones occur which are interpreted as east-vergent thrust zones active prior to tilting of the bedding around the North Pole Dome (Nijman et al., in press).

5.4 Discussion

The greenstone belts in the eastern Pilbara show varying deformation intensities, but are always inhomogeneously deformed on regional scales, with deformation sometimes concentrated in narrow shear zones. Since the most deformed rocks are most easily weathered and very difficult to sample, this can easily give the false impression that the greenstones are little deformed. Another consequence of the inhomogeneous deformation and weathering is skewed sampling for geochemical studies, since rocks collected for geochemical studies need to be fresh and thereby preferentially undeformed. One of the consequences is that ultramafic rocks, which predominantly form shear zones, are under sampled in the Pilbara.

In this section the results and implications of the structural study of the Coongan Belt will be discussed first. These will be placed in the larger framework of the eastern Pilbara with results of structural studies in different greenstone belts.

The structural studies in the Coongan Belt show that the belt consists of a steepened fold and thrust belt with a dominantly E up sense of shear. In the past, structures in greenstone belts in the Pilbara have been interpreted in terms of interdiapir synclines (Hickman, 1983; Collins, 1989; Delors et al., 1991). This detailed study shows that the structures in the Coongan Belts are at odds with such an interpretation. This is best seen when structures in the Coongan Belt are compared with the centrifuge model of Dixon & Summers (1983) for interdiapir synclines. A number of characteristics of the structures in the Coongan Belt are in agreement with this model. These include: a strong horizontal contraction and vertical extension, and folds with subhorizontal axes. However, no areas of vertical constrictional strain were found. The main characteristics that disagree with the solid state diapir model are the asymmetry of the belt and the kinematics. The Coongan Belt structures are strongly asymmetric with thrust vergences consistently towards the west throughout the belt. Deformation intensity and geometry are not symmetrical with respect to the central axis of the belt. The formation of the Warrery Anticline cannot be understood in the context of a diapiric interpretation.

If the density contrast between granites and greenstones is the driving force for solid state diapiric deformation, then shear localization would be expected to occur at the contact between greenstones and granitoids. The shear zone at the contact should in that case always indicate a granitoid up sense of shear. This is not the case in the Coongan Belt. Deformation is not always most intense at the contact between granites and greenstones, many of these contacts are intrusive and where shear zones occur at the contact (southern Shaw contact), the sense of shear can be convincingly shown to be greenstones up relative to the granites.

The 3-d structure of the Coongan Belt appears to consist of a west-vergent, steepened fold and thrust belt. These compressional structures overprint structures formed in an extensional regime at ca. 3460 Ma. Although the early structures are in a favorable orientation to be reactivated during thrusting, this appears to have happened only to a small extent as indicated by the different lineation trends for the extensional and compressional phase. At greater depth the SRSZ is interpreted to form the detachment to the thrust zones.

The timing of deformation in greenstone belts is not easily established, due to large uncertainties in

the age of stratigraphic units. The extensional structures in the Coongan Belt are constrained in time between 3470 and 3450 Ma, as discussed in Chapter 4. If the stratigraphic correlations as proposed in Figure 5.2 are correct, the compressional deformation in the Coongan Belt must at least partly post-date the lower Gorge Creek Group. The youngest unit that is clearly part of, and incorporated into the fold and thrust belt is the thick BIF unit which is probably part of the Gorge Creek Group (Figure 5.7). The Lalla Rookh sandstone unit is partly cut by a strand of the Witnell Shear Zone; this may, however, be due to late brittle reactivation of the strand.

Another source of information on the timing of deformation are the $^{40}\text{Ar}/^{39}\text{Ar}$ cooling ages of amphiboles from the Coongan Belt (Davids et al., 1997 and Chapter 8). A number of cooling ages in the Coongan Belt fall between 3309 and 3197 Ma. The 3340 ± 6 Ma age for hornblende from the contact aureole at Warrery Gap, providing the best estimate of the age of the Warrery Shear Zone, is not included because it is related to granitoid intrusion, and the Warrery Shear Zone may be related to granitoid intrusion and not to the E-W compressional phase. The 3197 ± 22 Ma age of post-tectonic actinolites in the Central Coongan Shear Zone provides an upper constraint to the thrusting event. Other cooling ages in the Coongan Belt (ca. 3030 Ma and ca. 2950 Ma) are thought to record the age of post-tectonic plutons in the Shaw Batholith and possibly strike-slip reactivation of shear zones.

Therefore, the best estimate for the age of the compressional deformation in the Coongan Belt from Argon data is between 3309 Ma and 3200 Ma. If the stratigraphic correlation is correct, and the felsic volcanic in the central part of the Coongan Belt is the equivalent of the Wyman Formation, this gives a similar constraint, to between 3325 and 3200 Ma.

The timing of these structures in the Coongan Belt agree well with the compressional structures described by Boulter et al. (1987), i.e. after deposition of the Gorge Creek Group and before deposition of the Lalla Rookh Sandstone, probably between 3300 and 3200 Ma (Wijbrans & McDougall, 1987). The structures in the western Shaw area are consistent with E-W compression.

In the Coongan Belt, all greenschist facies shear zones are situated in carbonate altered ultramafic units. This is not the case for amphibolite grade shear zones such as the Warrery Shear Zone, which is situated in a tuffaceous unit, or parts of the Split Rock shear zone which are situated in mafic volcanics. This shows that under greenschist facies conditions the particular composition of carbonate altered ultramafics, consisting mainly of Mg-rich carbonates and chlorite, is the weakest unit in the greenstone belt sequence. Because these units are invariably strongly deformed, it is not possible to distinguish originally intrusive ultramafic units (sills) from volcanic ultramafic units. The contacts with other units are too deformed to identify intrusive relations or flow top breccias. The carbonate alteration must have occurred at an early stage, prior to deformation. Unaltered ultramafics are extremely strong (Drury et al., 1991) and would not have been the preferential site for a shear zone to develop.

Although the geometry of the Coongan belt is dominated by the fold and thrust structures, there are a number of later structures and reactivations of older shear zones. These include a west up reactivation of shear zones in the CCSZ, and west of the CCSZ, steepening of the bedding and structures after deposition of the Lalla Rookh sandstone, as indicated by the steep dips of the Lalla Rookh Sandstone, minor strike-slip movements and the development of a NW-SE trending crenulation cleavage.

The steepening of the bedding and structures and the west up reactivation may be related to a late

doming event around the batholiths. This could be caused by the intrusion of late stage granitoids or by a weak solid state diapiric process. The sinistral strike-slip movements could be related to late (2930 Ma) large-scale strike-slip deformation in the MSZC (Chapter 6). The NW-SE trending crenulation cleavage indicates a NE-SW compressional event that was not recognized in other greenstone belts.

Structural studies in the greenstone belts in the area between the Mulgandinnah Lineament and the Lionel Lineament show that there are many similarities with the Coongan Belt. Typically, early syn-Duffer Formation brittle growth faults precede a compressional phase forming fold and thrust belts. Deformation is concentrated in carbonate altered ultramafic units, where greenschist facies bedding parallel shear zones occur. The southern Kelly Belt is unusual because it does not contain these shear zones. All deformation in the Kelly belt is taken up by brittle faults. The belt contains a number of bedding parallel intrusive ultramafic dikes. These may represent the undeformed equivalent of the strongly deformed ultramafics in other belts.

It is important to note that the compressive structures in some greenstones have been passively rotated after formation. This is best shown in the northern Coppin Gap Belt, where a bedding parallel shear zone in the Shay Gap Belt is truncated and unconformably covered by a now moderately south dipping sandstone unit.

The general pattern appears to be of doming of greenstones around granitoids after deposition of the (Lalla Rookh ?) sandstone unit, strengthening the pattern of initial doming that developed during the 3460 Ma extensional phase (Chapter 4). This causes folding of the bedding and earlier structures in broad synclines between the granitoids. This is least apparent in the North Pole area, where the bedding consistently dips shallowly away from the North Pole granitoid, but is strongly developed in the Coppin Gap Belt where structures and bedding are folded in an E-W trending synclinal structure. In the Coongan Belt this pattern is not as obvious because the structures were already N-S trending. However the steeply NE dipping upper sandstone unit indicates that the main tilting occurred at a late stage in the Coongan Belt as well, so that the steepening of the thrust structures must be a late feature.

To reconstruct the original transport direction during thrusting and, during the earlier extensional phase, the bedding and bedding parallel structures must be rotated back to a near horizontal position, eliminating the effect of the late stage doming. This was done for all major structures in the greenstone belts whose nature (extension or thrusting) are well established. The resulting transport directions are shown in Figure 5.9. Strike-slip zones such as the Central Warrawoona Shear Zone (CWSZ) and the South Muccan Shear Zone (SMSZ) have not been rotated because they truncate other structures and there is no indication that they have been rotated. The pattern that emerges shows a general E-W compressional event throughout the study area, but with reversal of the transport direction across the CWSZ and SMSZ strike-slip shear zones. The west ward continuation of the CWSZ is uncertain because the area is covered by Fortescue Group rocks, but is tentatively drawn in Figure 5.9. These E-W trending strike-slip-faults can be regarded as transfer faults in the thrust system. West of the Mulgandinnah Shear Zone, in the Tambourah Belt, structures are dominated by late strike-slip deformation, obscuring older structures.

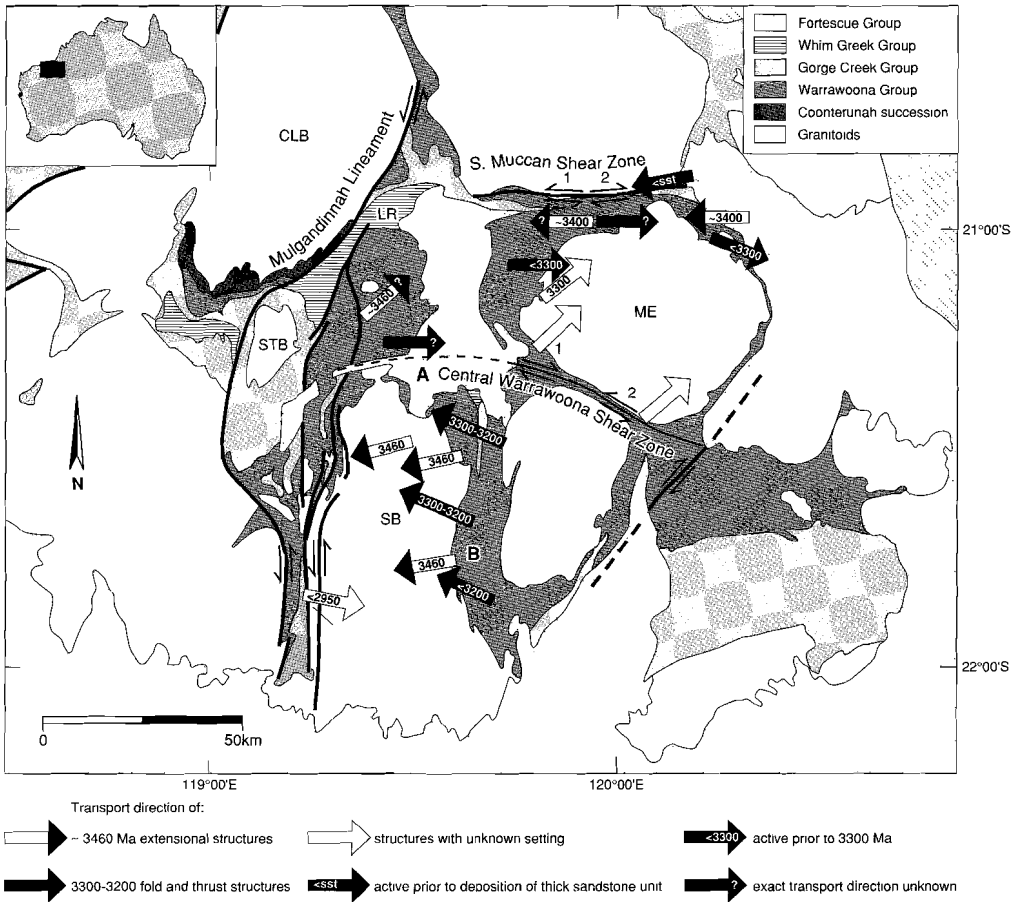


Figure 5.9 Transport directions in different greenstone belts in the eastern Pilbara for the ± 3460 Ma extensional event and the 3300-3200 Ma compressional event. The transport directions were obtained by undoing the late rotation due to doming around granitoids. See text for discussion.

5.5 Conclusions

1. Structures and kinematics in the Coongan Belt are consistent with a west-vergent steepened fold and thrust belt.
2. Greenschist facies thrust zones are invariably situated in carbonate altered ultramafic units. These units have undergone carbonate alteration prior to the development of the shear zones, mechanically softening the ultramafic rocks.
3. The compressional structures in the Coongan Belt formed between 3360 Ma and 3200 Ma, prior to deposition of the Lalla Rookh Sandstone.

4. The fold and thrust belt structures and the Lalla Rookh sandstone in the Coongan Belt were steepened during a late stage doming event postdating deposition of the Lalla Rookh Sandstone unit.
5. Similar fold and thrust structures were found in other greenstone belts. An exception is the Kelly Belt, which is very little deformed.
6. If the late stage doming effect is undone, the compressional structures show a consistent E-W compressional direction in a large part of the eastern Pilbara, between the MSZC and the Lionel Fault.

However, the transport direction is partitioned into east- and west-vergent areas, separated by E-W trending transfer zones such as the Central Warrawoona Shear Zone and the South Muccan Shear Zone.

Craton scale shear zones in the Pilbara; a detailed study of the Mulgandinnah Shear Zone Complex²

6.1 Introduction

Major shear zones are important structural features in crustal blocks of all ages. In orogenic belts they often form the boundary between different tectonostratigraphic terranes³. In recent years, terrane analysis has been applied successfully to Archean cratons (Myers, 1995; de Ronde & de Wit, 1994; Jackson & Cruden, 1995). The recognition and structural/kinematic study of possible terrane boundaries is an important step towards unraveling the often complex tectonic evolution of such areas. In addition, major shear zones in Archean terrains also have an important economic significance, because large lode gold deposits, late in the history of the belts, tend to be spatially associated with them (Bursnall 1989; Eisenlohr et al., 1989; Groves et al., 1992).

The Pilbara granitoid-greenstone terrain has been subdivided into a number of tectonostratigraphic domains on the basis of lithostratigraphic studies (Krapez & Barley 1987, Krapez 1993). However, the boundaries between these domains, formed by north- to northeast-trending lineaments (Figure 3.1) have not been studied in detail. Here, we report on a detailed structural study of part of one of these boundary structures, the Mulgandinnah Shear Zone Complex (MSZC). This is a major ductile shear zone in the eastern Pilbara and forms the western part of the Shaw Batholith, where it truncates the Split Rock Shear Zone (SRSZ, Figures 6.1 and 6.2). The MSZC is part of the north-trending Mulgandinnah Lineament, which consists of two major strands and extends from the Shaw and Yule Batholiths to the Lalla Rookh Basin in the north. The MSZC forms the eastern strand of the Mulgandinnah Lineament.

This study covers geometry and kinematics, conditions of deformation and time constraints of the MSZC. The position and kinematics of the other major lineaments in the Pilbara will be briefly discussed and compared to the MSZC.

6.2 Regional Setting

In order to facilitate the discussion of the major lineaments in the Pilbara Craton they have been named (Figure 6.1). The names used here are, where possible, in keeping with the names used by Hickman (1983) and Krapez (1993). From east to west the lineaments are: the Lionel Lineament, the Mulgandinnah Lineament, the Mallina Lineament and the Sholl Lineament.

Although previous workers (Krapez & Barley, 1978, Krapez, 1993 and Eriksson et al., 1994) consid-

² Parts of this Chapter will be published as: Zegers, T.E.; de Keijzer, M.; Passchier, C.W. and White, S.H.L. The Mulgandinnah Shear Zone Complex: an Archean crustal-scale shear zone, eastern Pilbara, Western Australia. *Precambrian Research*, in press.

³ The term terrane is used in the sense of tectonostratigraphic terrane (Jones et al., 1983), whereas the term terrain is used for a geographic area, i.e. Yilgarn terrain. Domain is a general term for a geological terrain that is thought, but not proven to be a tectonostratigraphic terrane.

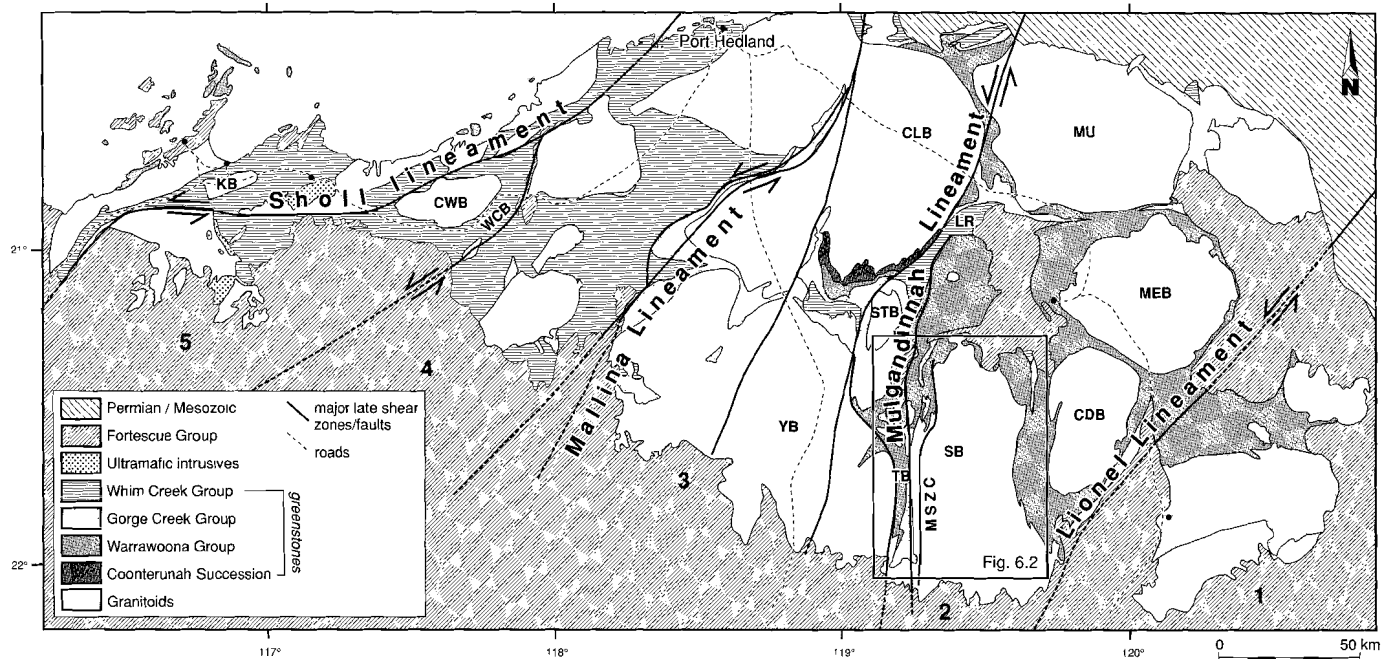


Figure 6.1 Schematic representation of the Pilbara granitoid-greenstone terrain, based on previously published geological maps (Krapez, 1993), showing major lineaments and their names.

CDB= Corunna Downs Batholith, CLB = Carlindi Batholith, CWB= Caines Well Batholith, KB= Karratha Batholith, MEB = Mount Edgar Batholith, MU= Muccan Batholith, SB = Shaw Batholith, STB= Strelley Batholith, TB = Tambourah Greenstone Belt, LR = Lalla Rookh Basin, WCB= Whim Creek Basin, MSZC = Mulgandinnah Shear Zone Complex.

Framed area represents Figure 6.2.

1= Nullagine Domain, 2= Marble Bar Domain, 3= Pilgangoora Domain, 4= Mallina Domain, 5= Whim Creek Domain

er the lineaments important features dividing the Pilbara into domains and believe they influenced the sedimentary patterns, there have been no structural studies of the lineaments themselves, or of their precise positions. In the above mentioned papers, the lineaments are thought to be sinistral strike-slip faults. This general inference follows the interpretation by Hickman (1983), which was based on the outcrop pattern of a felsic volcanic unit, that sinistral displacement occurred along the Sholl Shear Zone. Krapez and Barley (1987) considered the Whim Creek Basin and the Lalla Rookh Basin (Figure 6.1) to be related to this sinistral strike-slip movement and loosely constrained the age of the lineaments and sediments in these basins to 2950 Ma.

The Mulgandinnah Lineament, part of which was analysed in detail in this study, consists of a number of shear zones that follow a northerly trend. They enclose an area of Warrawoona, Gorge Creek and Whim Creek Group deposits (Figure 6.1) and the Strelley Batholith, which was dated at 3238 ± 4 Ma (Smith et al., 1997). Both to the east (Shaw Batholith and Muccan Batholith) and to the west (Carlindi and Yule Batholith) the granitoids contain an important 3460 Ma component.

In a study of the thermal evolution of the area around the Tambourah Belt (TB, Figure 6.1), a $^{40}\text{Ar}/^{39}\text{Ar}$ study (Wijbrans & McDougall, 1987) indicates an age of at least 3200 Ma for a regional metamorphic event, and a younger, 2950 Ma, cooling age for the area adjacent to the Yule Batholith and in the western Shaw Batholith.

Previous structural work in the area includes a study by Bickle et al. (1985) and Boulter et al. (1987) who recognised a fold and thrust event in the western Shaw Batholith and in the adjacent greenstones, that was constrained between 3325 and 3200 Ma. These structures were found to be overprinted by 'steep structures' that were proposed to be related to diapirism (Bickle et al., 1985). Zegers et al. (1996) describe core-complex type extensional structures in the Shaw area that developed during deposition of the Warrawoona Group, resulting in the initial weak domal geometry of the granitoids. Two shear zones were mapped in the Shaw Batholith: the Split Rock Shear Zone, at ca. 3460 Ma, which appears to be the remnant of an early detachment, and the Mulgandinnah Shear Zone Complex, which is the main subject of this Chapter.

6.3 Lithologies of the Shaw Batholith

The MSZC forms the western margin of the Shaw batholith. It reworks the adjacent rocks of the batholith. Lithologies have been described to a large extent by Bettenay et al. (1981), but the lithologies and structures that make up the rest of the Shaw Batholith will be briefly discussed here (Figure 6.2) as they form the precursor rocks of the MSZC.

6.3.1 *Migmatic gneiss & enclaves.*

The central part of the Shaw Batholith contains extensive areas of migmatic gneiss with a variety of enclaves. The migmatic gneiss paleosome is mainly of biotite granodiorite composition. The foliation in the fine-grained, light grey gneisses is formed by variations in biotite content and layer parallel pegmatite-aplite veins. These are interlayered with complex, medium-grained clinopyroxene-bearing dioritic gneisses, which show a strong compositional banding. Both grey and dioritic gneisses show a completely statically recrystallized microstructure. The gneisses are complexly deformed. Gneissic layering is frequently folded in dm-scale folds with an associated crenulation cleavage (see

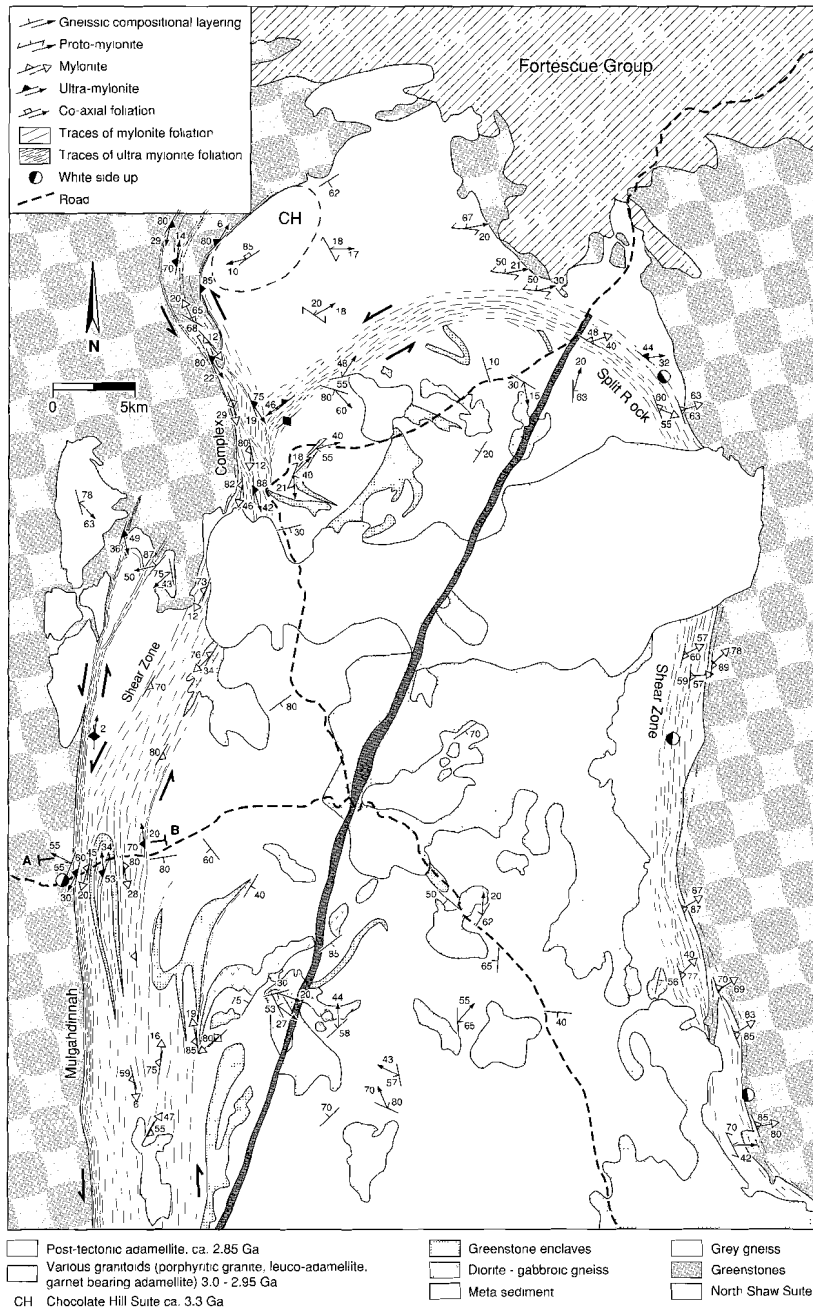


Figure 6.2 Structural map of the Shaw Batholith, showing the Split Rock Shear Zone, the Mulgardinnah Shear Zone Complex and the various granitic lithologies in the Batholith. A-B is the Tambourah traverse, on which Figure 6.4 is largely based.

Figure 6.5a). Leucosomes are typically formed as axial planar structures, but occasionally melting has been so extensive that a nebulitic schlieren textured gneiss has developed. The gneissic layering (see Figure 6.2) does not show consistent orientations.

Enclaves that occur in the migmatic gneisses include amphibolitic metabasalts, metasediments, mostly pelites and calcisilicates (Bickle et al., 1985), and coarse to very coarse-grained dioritic to gabbroic anorthosites, which are the oldest rocks in the Pilbara at 3577 ± 4 Ma (U-Pb single zircon, McNaughton et al., 1988).

6.3.2 North Shaw Suite

The North Shaw Suite of granodiorite-tonalites, which have been extensively studied by Bickle et al. (1993), are separated from the migmatic gneisses in the centre of the Shaw Batholith by the Split Rock Shear Zone (SRSZ, Figure 6.2). The North Shaw Suite, which has been dated at ca. 3460 Ma (Bickle et al., 1983, 1993; Pidgeon 1978; McNaughton et al. 1988), was inferred to be a syn-kinematic intrusion into the Split Rock Shear Zone (Zegers et al., 1996).

Structures in the SRSZ and at the contact with the adjacent Coongan Belt have been described in detail in Chapter 4. The main characteristic of the SRSZ is a mylonitic foliation, forming part of a domal shaped shear (see Figure 6.2) with a stretching lineation consistently trending ENE. The sense of shear is E-up with subsidiary sinistral movement on the E-W trending part and a subsidiary dextral movement on the N-S trending part at the contact with the Coongan Belt

6.3.3 Younger granitoids

The gneisses and North Shaw Suite rocks are intruded by a number of younger, late- to post-tectonic granitoids. The oldest of these, the Garden Creek Adamellite, dated at 3007 ± 48 Ma (Pb-Pb, Bickle et al., 1989), is a garnet-bearing muscovite-biotite adamellite that occurs in the southern part of the Shaw Batholith. A second group of granitoids, dated at ca. 2950 Ma (Pb-Pb, Bickle et al., 1989), intruded large parts of the gneiss in the central Shaw Batholith. They consist of K-feldspar porphyritic adamellites and fine-grained leuco-adamellites. These two groups of granitoids are undeformed in the eastern Shaw Batholith, but are locally deformed in the western Shaw Batholith.

A late, post-tectonic muscovite-adamellite intruded the Shaw Batholith at ca. 2850 Ma (Pb-Pb, Bickle et al., 1989).

6.4 Mulgandinnah Shear Zone Complex

The Mulgandinnah Shear Zone Complex (MSZC) is a high strain zone along the western margin of the Shaw Batholith. It can be traced over a strike distance of at least 70 km and is up to 6 km wide in the SW of the Shaw Batholith, but narrows to a width of ca. 2.5 km in the northern part of the Shaw Batholith.

Typical structures and their relations are shown in Figure 6.4 and are discussed further in the text below.

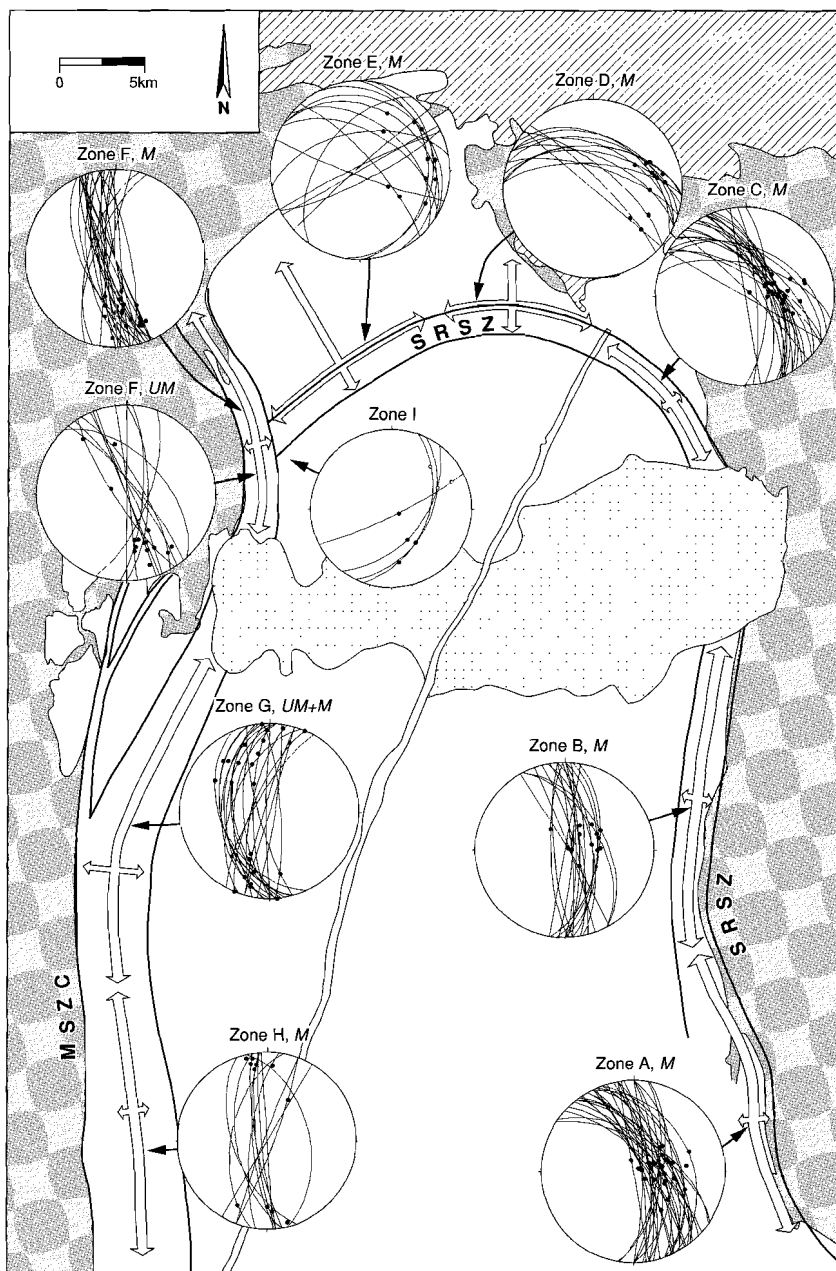


Figure 6.3 Structural data from the SRSZ (zone A to E) and MSZC (zone F to H) in lower hemisphere equal area projections. Great circles represent mylonitic (M) or ultra mylonitic (UM) foliation planes, dots represent mineral stretching lineations. In the plot for zone I foliations with two stretching lineations are shown. The filled dots represent lineations belonging to the MSZC, the unfilled dots represent lineations belonging to the SRSZ.

6.4.1 Lithologies in the MSZC

Rocks are so strongly deformed in the MSZC that it is usually not possible to convincingly identify the protolith granitoid/gneiss. Where the deformation intensity decreases towards the east, the transition to gneisses can be seen. The variably folded gneisses become progressively more deformed as the MSZC is approached, with the development of a N-S to NE-SW trending foliation. In the MSZC, the gneissic layering is transposed to the mylonitic foliation ($S_{M,MSZC}$). This produces a heterogeneous mylonitic rock with varying proportions of mafic minerals, thought to reflect the initial variations in the precursor gneisses. Other parts of the MSZC consist of a more homogeneous augen gneiss. Here, the protolith could well have been part of the North Shaw granodiorite suite. In the western part of the MSZC there are abundant enclaves of amphibolite and minor metasediments. These enclaves occur as m-scale lenses but also as layers that can be traced in a km-scale rootless fold (see Figure 6.2). Several generations of pegmatites are present in the MSZC, which show a complex spatial distribution. These pegmatites make up a volume up to 30% of the total rock.

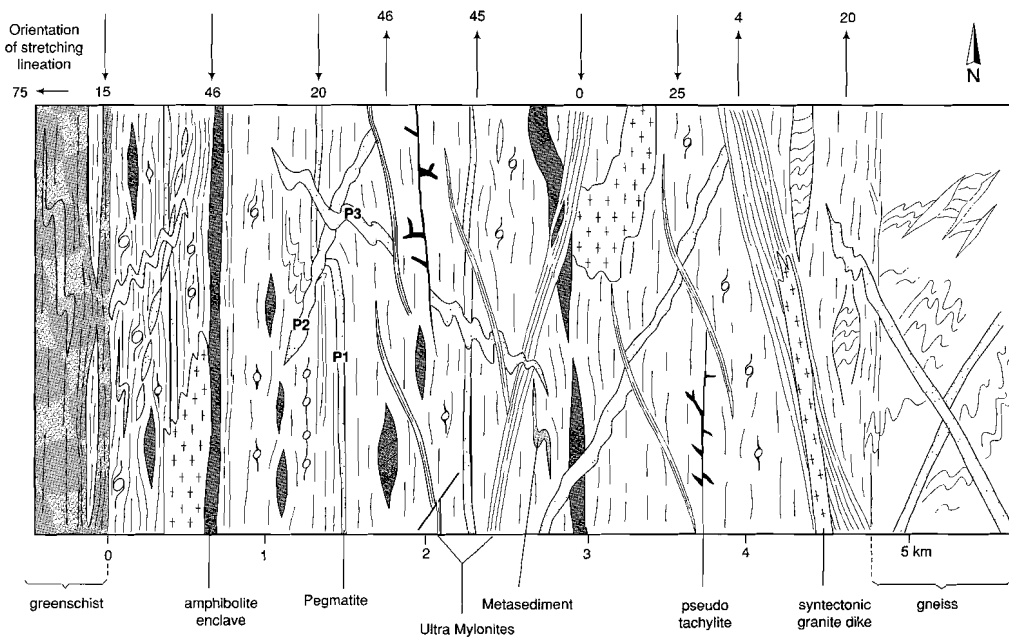


Figure 6.4 Diagram showing the structures and their relations as found in the MSZC on the horizontal plane, based on the Tambourah traverse (see Figure 6.2). For the description of these structures see the text. P1, P2 and P3 are three generations of pegmatites.

6.4.2 MSZC mylonites

The mylonitic foliation in the MSZC (see Figures 6.2,3 & 4) is subvertical to steeply W dipping over the total length of the MSZC. The stretching mineral lineation on the mylonitic foliation ($L_{M,MSZC}$) is defined by quartz-feldspar and biotite in granitic rocks and by oriented dark hornblende crystals



Figure 6.5a Folded grey gneiss with leucosomes (L) following the crenulation foliation planes.



Figure 6.5b δ -type porphyroclast with a non-stairstepping geometry, showing a sinistral sense of shear in the mylonitic foliation of the MSZC. The coin is 2 cm in diameter.

and plagioclase rods in mafic layers. The orientation of the mineral stretching lineations is variable. In the northern zone (F in Figure 6.3), $L_{M,MSZC}$ is shallowly to moderately S plunging, in the central zone (G in Figure 6.3) they vary strongly from 50° N to 50° S plunging, whereas in the southern zone (H in Figure 6.3) the mylonitic stretching lineations are subhorizontal. Numerous σ and δ -type porphyroclasts of K-feldspar occur on surfaces normal to the foliation and parallel to the lineation, whereas other mineral phases, such as quartz and plagioclase, have recrystallized to a finer grain size. There are some especially good examples of δ -type porphyroclasts. The recrystallized tails of these clasts show a non stair-stepping geometry (Figure 6.5b) in which the tails of the δ -clast and the centre of the clast lie in one plane (Passchier et al., 1993). The porphyroclasts consistently indicate a sinistral sense of shear.

A particular structure occurs in amphibolite layers and boudins. Amphibolites with a strong internal layering are extended and pulled apart along planes at a high angle (60 – 70°) to the amphibolite layering (Figure 6.5c). The separate blocks are subsequently rotated with a sinistral sense.

The $S_{M,MSZC}$ is truncated by at least 3 sets of pegmatites with one set (P1, Figure 6.4) typically parallel to $S_{M,MSZC}$, a second set (P2, Figure 6.4) often boudinaged at a small angle to $S_{M,MSZC}$, and a third set (P3, Figure 6.4), generally folded, of pegmatites at a high angle to $S_{M,MSZC}$. The $S_{M,MSZC}$ shows a very consistent folding pattern, adjacent to the P2 pegmatites (Figure 6.5d). A single isoclinal fold occurs on the SE side of the pegmatite and a fold train on the NW side. This pattern is consistent with progressive sinistral rotation and deformation of the pegmatites after intrusion into the mylonite.

Pseudotachylites are present in a number of mylonite outcrops. The planar generation surface is parallel to $S_{M,MSZC}$ with injection veins extending into the host rock, often infilling ten-

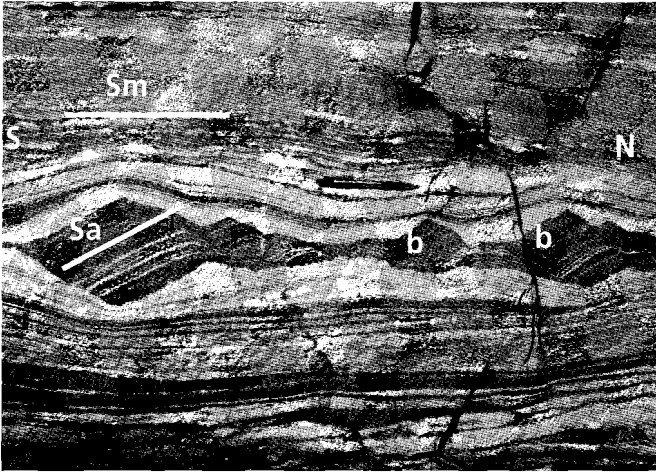


Figure 6.5c Broken and boudinaged amphibolite layer in the mylonitic foliation of the MSZC. The amphibolitic layering (S_a) in the boudins (b) is rotated sinistrally with respect to the mylonitic foliation (S_m).

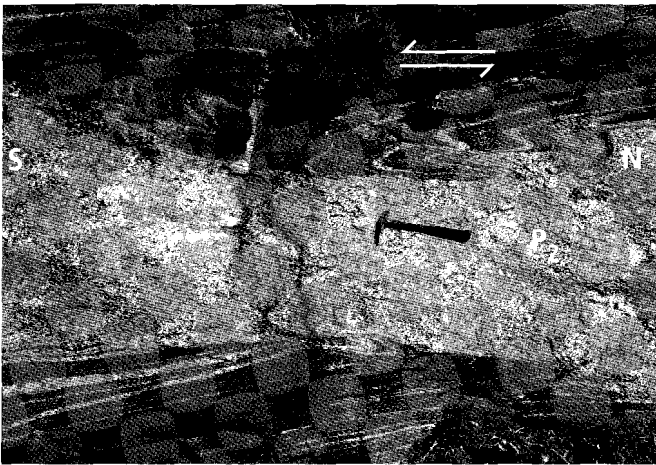


Figure 6.5d Pegmatite (P_2) with adjacent folds. The folding pattern is thought to be the result of sinistral rotation of the pegmatite in the MSZC.

sion fractures formed during the sinistral movement. The pseudotachylites contain a dark glassy matrix with minor rock fragments floating in the matrix.

6.4.3 MSZC ultramylonites

Towards the western side of the MSZC, the deformation intensifies to a ca. 500 m wide ultramylonite zone. The foliation, $S_{UM,MSZC}$, is defined by fine-grained biotite flakes and by extremely strung out quartz and feldspar in a fine-grained matrix. The latter also define a stretching lineation $L_{UM,MSZC}$. The grain size of the matrix is markedly decreased relative to the mylonite. Individually grains in the matrix are indistinguishable in the hand specimens. Microscopically, the matrix consists of equigranular, rounded, quartz grains (20–30 μm), with aligned biotite grains of similar dimensions. Mineral assemblages (quartz, plagioclase, biotite and hornblende) indicate amphibolite facies grade conditions during deformation. The stretching lineation is variable between 50° N and 50° S plunging. K-feldspar σ and δ porphyroclasts are well rounded and generally small (2–4 mm) compared to

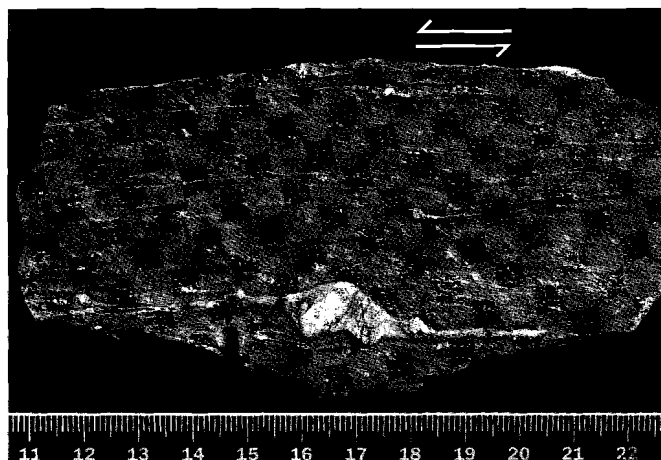


Figure 6.5e Ultramylonite foliation (plane parallel to lineation) with mm-size σ -type porphyroclasts and one larger porphyroclast (scale is in cm), indicating a sinistral sense of shear.



Figure 6.5f Granitic dike (D) intruding the ultramylonite foliation at a small angle. The granite dike shows the same foliation/lineation as the ultramylonite, indicating intrusion during deformation.

the cm-dm size objects in the mylonitic foliation. Sense of shear markers such as porphyroclasts and S-C fabrics indicate a consistent sinistral sense of shear (Figure 6.5e). Similar sets of pegmatites occur as in the mylonitic foliation, but the angle between the pegmatites is smaller and they are more commonly boudinaged.

In the main part of the mylonitic MSZC, ultramylonites occur in an anastomosing pattern of 20 cm to 5 m wide zones that cut across the mylonitic foliation. In the few cases where these thin ultramylonitic bands could be traced, they end by bending into the mylonitic foliation (Figure 6.4).

In the ultramylonite zones fine-grained biotite-granite dikes intruded parallel to $S_{UM,MSZC}$ and locally cut across the ultramylonite foliation at a small angle (Figure 6.5f). The granitic dikes themselves show the same foliation and lineation as the ultramylonitic host rock. The granitic dikes are therefore inferred to have intruded during activity in the ultramylonite zones.

6.4.4 Contact zone with greenstones

The contact between the granitoids in the MSZC and the Tambourah Greenstones is sharp. The greenstones contain chlorite schists and metasediments with a steeply west dipping foliation and a down-dip stretching lineation. Occasional shear-bands indicate a west up sense of shear. Upon approaching the contact from the west, the metamorphic grade increases over a distance of tens of metres to amphibolite grade. The metabasalts and metasediments are isoclinally folded with steeply plunging fold axes. In a 40 m wide zone, supracrustal rocks alternate with granitic dikes, which show an ultramylonitic foliation and shallowly S plunging lineation. Sense of shear markers in this mixed zone are all consistently sinistral (σ and δ clasts and S-C fabrics). The mixed zone grades into the granitic ultramylonite zone of the MSZC.

6.4.5 Relationship between MSZC and the Split Rock Shear Zone (SRSZ)

Shear activity on the MSZC postdates the SRSZ. This can be seen from the foliation pattern in Figure 6.2. The typical MSZC mylonitic and ultramylonitic foliation can be traced further north than the intersection area between the SRSZ and the MSZC, implying that the MSZC truncates the SRSZ. Additional evidence was found in a greenstone enclave to the SE of the MSZC/SRSZ intersection area. In a number of outcrops in this area, two stretching lineations were found on the foliation plane (see plot I in Figure 6.3). The NE plunging lineation formed by pale green amphiboles (grunerite) is overprinted by a south plunging lineation of mm-cm scale aligned spots with randomly oriented fine-grained chlorite and mica. The first lineation is thought to be related to the SRSZ, the second to the MSZC.

6.4.6 Northward continuation of the MSZC

It is difficult to trace the northward continuation of the MSZC beyond the northern margin of the Shaw Batholith. The foliation bends to a more north-westerly trend, thereby crossing the contact between the granite and greenstones. In the greenstones, the deformation is localized into shear zones which are tens of metres wide with shallowly plunging lineations, leaving relatively undeformed areas in between. However, the intensity of deformation and the width of the shear zones do not appear to match the MSZC as found in the Shaw Batholith a few km to the south. No trace of a mylonitic foliation was found in the NW area of the Shaw Batholith, where Bickle et al. (1993) sampled a range of granitoids, called the Chocolate Hill Suite, giving a Pb-Pb isochron age of 3338 ± 52 Ma. The hornblende rich granodiorite is weakly subvertically foliated (see Figure 6.2) This foliation follows the contact with the greenstone belt. A weak, gently plunging mineral lineation is locally present. All structures found in this area are symmetric, indicating that deformation was non-rotational in this granitoid. This observation, and the locally almost E-W trend of the foliation in the granitoid, make it unlikely that this fabric is of the same age and tectonic significance as the MSZC.

The zone between the two strands of the Mulgandinnah Lineament further north shows complex structures that have been described in part by Boulter et al. (1987) next to the Shaw Batholith, and Krapez (1984) for the Lalla Rookh Basin. Both studies show post Gorge Creek, syn- Lalla Rookh Sandstone open folds with 020 to 060 trends. Some of these have also been mapped on the Geological Survey of Western Australia 1:250,000 geological map. The time constraints on these folds show that they formed during activity on the Mulgandinnah Lineament. The sinistral sense of shear on the Mulgandinnah Lineament and the NE trending folds are both consistent with a NW-SE com-

pressional regime.

Van Kranendonk & Collins (1997) show that the structures between the main shear zones of the Mulgandinnah Lineament are consistent with sinistral movement over the whole length of the lineament.

6.5 Other major lineaments in the Pilbara

The three other lineaments in the Pilbara have not been studied in as much detail as the MSZC. However, their position has been analysed using TM satellite images and aerial magnetic contour maps (Geological Survey of Western Australia 1: 250.000) and the kinematics have been analysed in a number of locations along each lineament (Figure 6.6).

The results are generally consistent with previous work (Krapez, 1993) for the eastern Pilbara (Figure 6.6a), the Lionel, Mulgandinnah and Mallina Lineaments, but are considerably different for the trace of the Sholl Lineament. This is best seen on the aerial magnetic contour map (Figure 6.6b) of the western Pilbara. The Sholl Shear Zone is exposed south of Karratha over a distance of only ca. 20 km. The rest of the trace is covered by recent sediments (see also Figure 3.1), but is clearly visible on the aerial magnetics map. It can be traced to the west where it bends to the SW, and to the east, where it remains E-W trending and follows a trace south of the Caines Well Batholith. This contrasts with previously published traces for the main lineament, where it was thought to bend to a NE trend and pass to the north of the Caines Well Batholith. This NE trending structure is not very clear on the aerial magnetic map, but may be a shear zone, although it is almost completely covered by recent sediments, making kinematic studies difficult.

The shape of the granitoids and greenstone belts to the north of the E-W trending lineament are consistent with dextral movement on the lineament and bend into parallelism with the shear zone upon approaching it. Spot checks on the kinematics of the Sholl Shear Zone show that it is a dextral strike-slip shear zone, with lineations pitching 10–40° both east and west on steeply dipping foliation planes. The Sholl Lineament can not be traced any further to the east than just past the Caines Well Batholith. This is where the sedimentary sequences of the Mallina Basin occur, which may indicate that the shear zone is covered by these sediments.

The Mallina Lineament consists of intensely sheared volcanics, gabbros and granites. The foliation is steeply NW dipping. Stretching lineations are usually down-dip to steeply NE pitching. Kinematic indicators show a NW up sense of shear. The Lionel Lineament consists of a brittle fault with a main dextral displacement component (see, Kelly Belt, Chapter 5).

6.6 Discussion

The MSZC forms a high strain shear zone that can be traced over a distance of at least 70 km with a width of up to 6 km in the south, decreasing to 2.5 km in the north. It truncates the Split Rock Shear Zone and the complex structures in the migmatitic gneisses towards the east.

The MSZC forms part of an anastomosing group of shear zones that form a major N-S trending lineament, the Mulgandinnah Lineament, (Figure 6.6) that runs along the Tambourah Belt, the Lalla

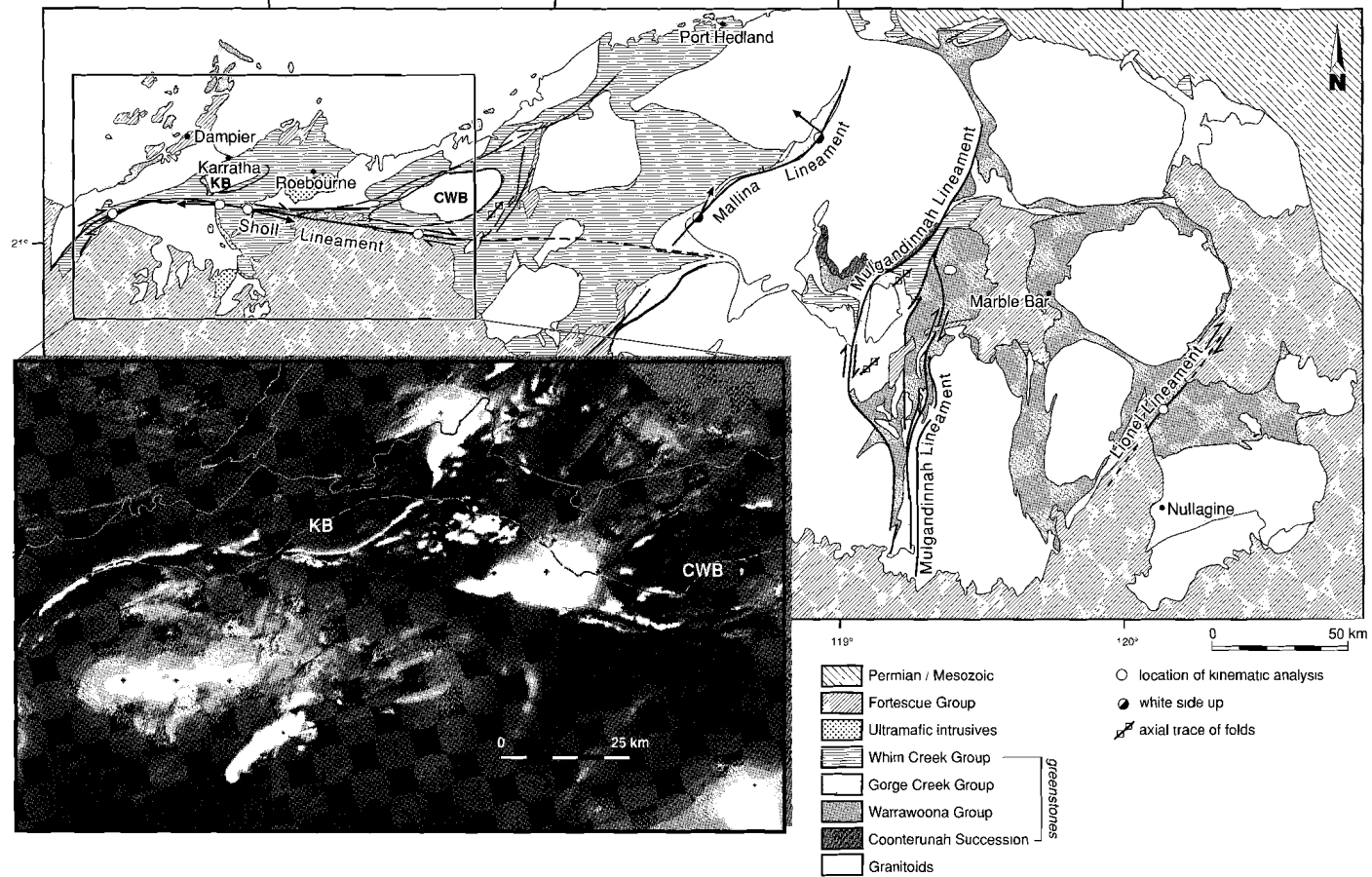


Figure 6.6 Lineaments and their kinematics in the Pilbara as proposed in this study. The inset shows a total magnetic intensity raster image (processed by A.Y.Glikson, AGSO). See text for discussion of the lineaments.

Rookh Basin and the Strelley Granitoid. Krapez and Barley (1987) relate these faults to the deposition of the Lalla Rookh Basin, with an inferred age of 2950 Ma. The U-Pb zircon age of the synkinematic dike (Chapter 8) is 2934 ± 2 Ma, providing a precise age constraint to the last movement on the MSZC.

The $^{40}\text{Ar}/^{39}\text{Ar}$ cooling ages from hornblendes (Chapter 8) in amphibolite enclaves in the MSZC are 2944 ± 9 Ma, for a sample hundreds of metres away from the SHRIMP sample of the granitic dyke, and 2909 ± 12 Ma for a sample from an amphibolite layer next to extensive pegmatite veins. The first cooling age indicates that the MSZC had cooled below the closure temperature of hornblende (ca. 550°C) before intrusion of the granitic dyke. The younger cooling age is regarded as the cooling age after intrusion of the syn-tectonic granite, which locally heated the MSZC above the hornblende closure temperature.

The decrease in width towards the north is partly explained by strands of the MSZC splitting off the main shear zone on the eastern side. Another marked decrease in width occurs north of the junction between the SRSZ and the MSZC, where the MSZC bends into the greenstone belt. A possible explanation for the decrease in width is that the MSZC followed reactivated older structures such as the continuation of the SRSZ. In the previous two Chapters (4 and 5), it was shown that at least two important structural phases pre-dated the 2.93 Ga sinistral movement on the MSZC in the Shaw Batholith area. During the 3.46 Ga extensional event (Chapter 4), the initial Shaw Dome developed in an extensional core-complex. On geometrical grounds (see Figure 9.2), a major extensional west-down shear zone would be expected at the western side of the Shaw Dome, with steeply south plunging ($70\text{--}80^\circ$) stretching lineation. During the following E-W compressional phase (Chapter 5), this shear zone on the western margin of the Shaw Dome would have been steepened and it is likely to be the predecessor to the present MSZC. However, in the MSZC itself there is no trace of these older deformation events.

The internal structure of the MSZC is complex. The relation between the mylonitic and ultramylonitic foliation is uncertain. Do they record two separate events, or did they form during one progressive deformation event with strain becoming more localized over time? The ultramylonites consistently overprint the mylonitic foliation, but form an anastomosing pattern, with strands of ultramylonite merging with the mylonitic foliation. This pattern can be interpreted as a 100 m scale shear band pattern (Figure 6.4), with ultramylonites forming as secondary shears within the main shear zone in the R- and P-shear orientations (Rutter et al., 1986) during the sinistral movement. Mineral assemblages in the mylonitic and ultramylonitic foliation are the same, chiefly quartz, plagioclase, biotite and hornblende, indicating lower amphibolite facies conditions during deformation in both mylonites and ultramylonites. $L_{\text{M,MSZC}}$ and $L_{\text{UM,MSZC}}$ do not show markedly different groups of orientations. Both lineations are dominantly south plunging but can vary between 50°N and 50°S , with rapid changes in strike and traverse direction of the MSZC. In the southern part, lineations are sub-horizontal, in the mid part both S and N dipping and in the northern part they are mainly S dipping. This pattern can partly be explained by the variations in strike of the shear foliation, with a releasing bend in the north, causing south dipping lineations. However, in the Tambourah Creek traverse, which formed the basis for Figure 6.4, the foliations are N-S trending but lineations still show variable plunges. Here, the ultramylonite lineation appears to have a shallower plunge than the mylonitic lineation.

This may indicate that there were different phases of movement on the MSZC, in which the shallow plunging lineations represent the last activity, and the more steeply plunging lineations an earlier phase. However, steeply south dipping lineations ($70-80^\circ$), which would be expected if relicts of the extensional (3.46 Ga) or compressional phase were present, do not occur in the MSZC. This indicates that if the MSZC formed as a reactivation of a previous major structure, the 2.93 Ga phase caused a complete overprint of older structures in the MSZC. The sense of shear, as indicated by widely distributed kinematic indicators, is always sinistral, in both mylonites and ultramylonites, independent of the plunge of the lineation.

Most of the above points are consistent with the mylonite and ultramylonite developing during one progressive deformation event. It is, however, likely that the MSZC is partly a reactivated older structure, which has been completely overprinted.

The pseudotachylite veins are probably genetically related to the mylonitic and ultramylonitic foliation in the MSZC and may represent seismic pulses during deformation. They post-date the mylonitic foliation, but have been observed to be deformed by the ultramylonites.

At the contact between the MSZC granitoids and Tambourah Greenstones there is a sudden change from amphibolite facies in the MSZC to greenschist facies metamorphic assemblages in the Tambourah Greenstone Belt. The MSZC ultramylonite truncates the east dipping greenschist facies foliation with down dip lineations in the greenstone belt. Kinematic indicators in the greenschist facies foliation indicate uplift of the greenstones relative to the granitoids in this early phase of deformation. These structures can be correlated with recumbent fold and thrust structures in the greenstones described by Bickle et al. (1985) and Boulter et al. (1987) further to the north, which formed between 3325 and 3200 Ma. This indicates that the MSZC ultramylonite at the contact formed later than ca. 3200 and locally exploited the earlier thrust structure.

The generally south plunging lineation and west dipping foliation of the MSZC ultramylonite, combined with the sinistral sense of shear, resulted in the relative uplift of the eastern block and produced the final juxtaposition of the amphibolite facies Shaw Batholith and the greenschist facies Tambourah Greenstone Belt.

Based on lithostratigraphy, the lineament of which the MSZC forms part, does not directly classify as a terrane boundary, i.e. dividing rock masses which have a unique history before the event that brought them together (Jones et al., 1983). No dramatic changes in stratigraphy on either side have been described. The Warrawoona Group is much more extensive in the domain east of the MSZC lineament, but it does also occur on the western side. The stratigraphy of the Gorge Creek Group and Whim Creek Group have not been sufficiently dated in this area to allow their distribution to be mapped in detail. The general impression is that the extent of these younger groups increases towards the west of the Pilbara (Krapez, 1993). Batholiths on either side of the Mulgandinnah Lineament show major 3.46 Ga components. The structural and metamorphic evolution on either side of the MSZC is not sufficiently well known to determine whether the MSZC lineament is a terrane boundary on those grounds.

However, the internal high shear strain structures, the extent of the MSZC, the metamorphic break across it, and the fact that it truncates all other structures in the area do indicate that it accommodated a considerable displacement and must have played an important role during the final stages of the crustal development of the Pilbara granitoid-greenstone terrain.

Analysis of the three other major lineaments in the Pilbara shows that they are not all NNE trending sinistral shear zones as previously proposed (Krapez, 1993). The Lionel Fault is a brittle dextral fault and the Mallina Lineament shows a reverse NW-up movement. The Sholl Lineament is not NNE-trending but mostly E- trending and not sinistral, but dextral.

The pattern of the Sholl, Mallina and Mulgandinnah Lineaments is more consistent with a conjugate set of shear zones in a NE-SW compressive setting, with north-trending sinistral shear zones, east trending dextral shear zones and NE trending compressional shear zones. This is consistent with the development of NE-trending folds in the Whim Creek Belt as described by Barley (1987) and NE-trending folds in the Soansville area and the margin of the Lalla Rookh Basin, as described in detail by van Kranendonk & Collins (in press) (see Figure 6.6). The Lionel Fault, of unknown age, is not consistent with the NW-SE compression. Its importance as a terrane boundary remains uncertain until more dates are available from the area east of the Lionel Fault. If this is an appropriate model, the age of all these major shear zones in the Pilbara, except the Lionel Fault, should be approximately the same. Smith et al. (1997) estimated a ca. 2960 Ma age for the Sholl Shear Zone, whereas the MSZC is constrained to ca. 2930 Ma, placing both shear zones within the same broad time range. However, more precise dating is needed to establish the age of movements on the other structures.

6.7 Conclusions

1. The MSZC is a major ductile shear zone in the western Shaw area with a consistently sinistral sense of shear, and locally a vertical component, causing uplift of the Shaw Batholith relative to the Tambourah Greenstone Belt
2. The mylonitic and ultramylonitic foliations formed during one progressive deformation event. The MSZC locally exploits an earlier thrust shear in the Tambourah Greenstone Belt and it is likely to have formed as a reactivation of an earlier extensional shear zone.
3. The MSZC forms part of a group of north-trending shears that form the Mulgandinnah Lineament that can be traced further north where it runs along, and influences the Lalla Rookh Basin.
4. Large scale open 020 to 060 trending folds between the two main strands of the Mulgandinnah Lineament are consistent in timing and orientation with the sinistral movement on the Mulgandinnah Lineament.
5. The final stages of activity on the MSZC have been constrained to 2934 ± 2 Ma.
6. The MSZC must have caused a considerable displacement, but data on the stratigraphy and structures from the adjacent crustal blocks are not consistent with an interpretation of the Mulgandinnah Lineament as a terrane boundary.
7. The MSZC is responsible for the final juxtaposition of the Shaw Batholith and the Tambourah Greenstone Belt.
8. The other main shears in the Pilbara granitoid-greenstone terrain display the following late movement: Sholl Lineament is an E-W trending dextral shear zone, the Mallina Lineament shows reverse movement and the Lionel Lineament is a dextral brittle fault.
9. The pattern of craton-scale shear zones is consistent with a conjugate set of shear zones formed in a NE-SW compressional setting.

Deformation and hydrothermal alteration in the Bamboo Creek Deposit, a komatiite-hosted lode-gold deposit

7.1 Introduction

Globally, the most abundant lode gold deposits occur either in the Late-Archean (± 2700 Ma) in granitoid-greenstone terrains or in modern convergent plate margins (Woodall, 1988; Barley & Groves, 1992; Kerrich & Cassidy, 1994). In recent years, lode gold deposits in Archean cratons have been intensively studied. Systematic chemical, structural and geochronological studies of lode gold deposits have been carried out mainly in the richest Late-Archean greenstone belts which occur extensively in the Superior Province of Canada (Robert, 1990; Kerrich and Kyser, 1994) and the Yilgarn Craton of Western Australia (Groves et al., 1992). This has led to the development of various genetic models for lode gold deposits, including the metamorphic devolatilization model of Phillips & Powell (1993) and the crustal continuum model of Groves et al. (1992). Various workers have emphasized the similarities between Archean lode gold deposits and Phanerozoic gold deposits (Barley et al., 1989; Kerrich & Wyman, 1990), which are both thought to be related to the final stages of terrane accretion in a subduction setting.

The 3.5 to 2.8 Ma Pilbara granitoid-greenstone terrain contains only minor amounts of known gold deposits compared to the Kaapvaal terrain of similar age in Southern Africa, and especially compared to the Late-Archean terrains mentioned above. The reason for this discrepancy in gold mineralization in terrains of otherwise broadly similar geology is not clear. Possible explanations have been offered by Groves & Batt (1984) who considered the greenstones in the Pilbara to be of the 'platform' type, whereas the Yilgarn greenstone belts represent the 'rift-type'. Barley & McNaughton (1988) postulated that gold mineralization in the Pilbara is associated with late strike-slip faulting, with an age of approximately 2950 Ma. This age was confirmed by Neumayr et al. (1993b) for the Mt. York district, who dated gold-associated minerals with the Pb-Pb isochron method at 2888 ± 6 Ma. The low abundance of gold in the Pilbara is possibly the result of the low abundance of major terrain boundaries or craton wide shear zones. However, the necessary systematic studies on gold deposits in the Pilbara are limited. Hence, it is not possible to assess whether there are systematic differences in gold mineralization style or structural setting in the Pilbara compared to Late-Archean occurrences or deposits in the Barberton Mountain Land (Kaapvaal Craton).

The Bamboo Creek Mine is the most prominent gold producer in the Pilbara. Production up to 1987 was 3.4 tons of gold with an average grade of 14.4 g/ton. The gold mineralization is hosted by a

strongly deformed komatiitic sequence, which is part of the Warrawoona Group dated between 3475 and 3435 Ma (McNaughton et al., 1993). Ultramafic hosted gold deposits are common in the eastern Pilbara. This is in contrast to the Yilgarn Craton to the south, where komatiite-hosted gold deposits are relatively rare. Yilgarn examples include Paddys Flat, Gabanintha and Reedys deposits in the Murchison Province and the Harbour Lights Mine (Skwarnecki, 1988) in the Norseman–Wiluna Belt. A comprehensive study of Late-Archean ultramafics-hosted gold was published by Kishida & Kerrich (1987) on the Kerr–Addison deposit in Ontario, Canada.

Ultramafic-hosted gold deposits are more common in the Mid-Archean Barberton and Murchison belts in South Africa and several aspects have been studied by de Ronde et al. (1992), Vearncombe et al. (1988) and Houston (1988).

The aim of this study is to characterize the Bamboo Creek Deposit in terms of its structural setting, host rock, alteration assemblages, metamorphic grade, fluid composition and relative and isotopic timing of gold mineralization. Possible conceptual models for mineralization are discussed and the results are compared with other typical Archean gold deposits.

The petrological/chemical study is based on sampling in the Kitchener and Prophecy Perseverance ore bodies in the underground mine of the Bamboo Creek Deposit.

7.2 Regional setting

The Bamboo Creek Deposit is situated in the Coppin Gap Greenstone Belt northeast of the Mt. Edgar Batholith (Figure 7.1). The gold deposits, which are collectively called the Bamboo Creek Deposit, all occur in the Bamboo Creek Shear Zone (BCSZ), within the Warrawoona Group. The BCSZ is parallel to the bedding in this area and is situated in an ultramafic unit, now consisting mainly of a talc-chlorite mylonite schist. Similar shear zones occur at a stratigraphically lower position, a few kilometres to the south of Bamboo Creek, and in an area to the north in the Shay Gap Belt (see Figure 7.1).

A number of isotopic dates are available in the area of the Bamboo Creek Deposit (see Figure 7.1). The Duffer Formation, adjacent to the Mt. Edgar Batholith, is dated at 3471 ± 5 Ma (U-Pb zircon, Thorpe et al., 1992). A felsic volcanic sample from the overall mafic Salgash Subgroup gives two age populations at 3454 ± 1 and 3470 ± 2 Ma (U-Pb zircon, Thorpe et al., 1992). The significance of the two ages is uncertain, but if the older age is interpreted as a xenocrystic age, the younger age reflects the extrusion age of the Salgash Subgroup. The Bamboo Creek Deposit is situated stratigraphically above the sample from the Salgash Subgroup, still within the Salgash Subgroup. Thorpe et al. (1990) reported a Pb-Pb model age of a galena from the Bamboo Creek Deposit to be between 3470 and 3415 Ma.

In the early 1980's a structural mapping program was carried out in the Bamboo Creek area by students of the University of Utrecht (Marcelis, 1986 and references therein). Other than this, and some internal reports of the mining company, no data are available on the Bamboo Creek Deposit.

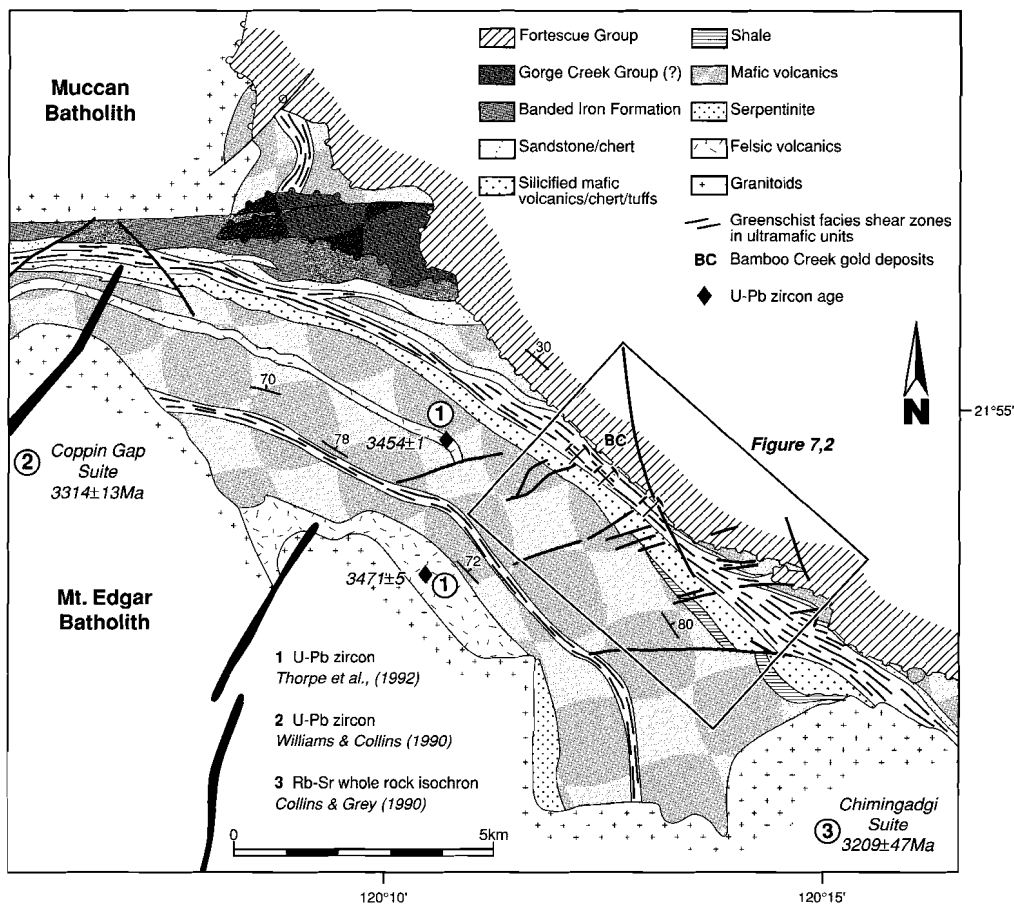


Figure 7.1 Schematic geological map of the Coppin Gap greenstone belt showing the location of the study area. Locations of samples that have been previously dated are shown.

7.3 Structural analysis

7.3.1 Introduction

During the study of the BCSZ and Bamboo Creek gold deposits, structural data were collected from the surface as well as from open pits and underground mines. Because the BCSZ itself is not well exposed, most of the data come from mining sites (Mt. Prophecy, Bamboo Queen, Kitchener, Bonnie Doon and Bulletin, see Figure 7.2). A more detailed study was done underground in the Kitchener Mine.

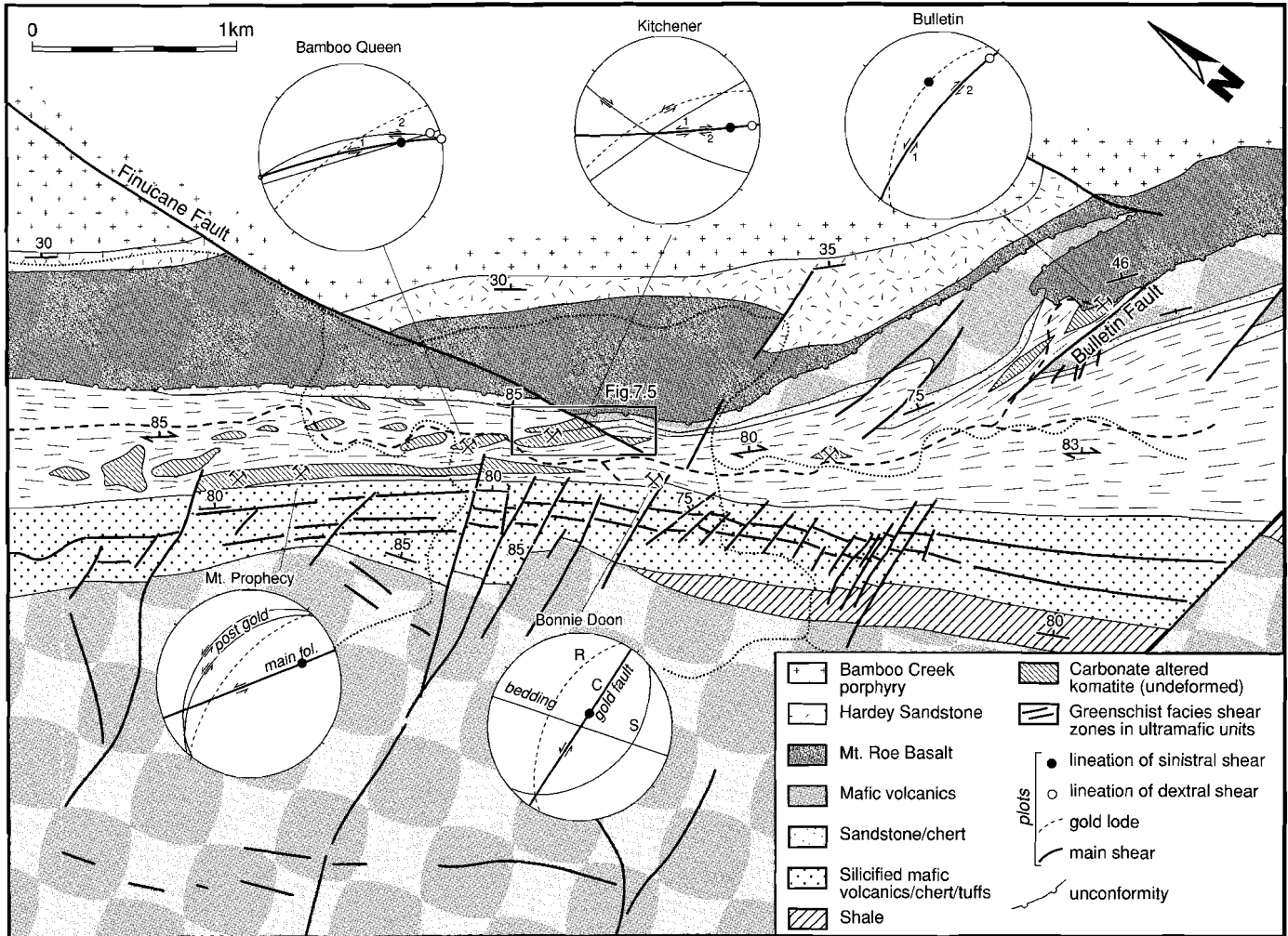


Figure 7.2 Structural map of the Bamboo Creek mining area, showing the location and structural/kinematic data collected from the various gold deposits in the Bamboo Creek Shear Zone. The frame indicates the detailed map of the Kitchener Mine in Figure 7.5

7.3.2 Setting and lithologies of the BCSZ

The BCSZ is a bedding parallel mylonite zone up to 1 km wide, striking 140° and steeply north dipping (Figure 7.2) with an anastomosing foliation. The footwall of the BCSZ to the south consists of a silicified and carbonate-altered volcano-sedimentary unit, comprising shales, tuffs, altered pillow basalts and grey and black and white banded cherts. This unit is underlain by a massive mafic to ultramafic basalt unit. The hanging wall of the BCSZ consists of a felsic volcanic to clastic unit overlain by massive basalts. All of these units have bedding orientations similar to the shear zone orientation, i.e. steeply dipping to the NE. This steeply dipping sequence is unconformably overlain by the moderately north dipping Mt. Roe Basalt and the Hardey Sandstone, both part of the Late Archean Fortescue Group.

Two lithologies can be distinguished within the BCSZ. The bulk of the BCSZ consists of a talc-chlorite mylonitic schist. Primary textures have been largely obliterated by intense deformation, but the Mg and Cr rich mineralogy and rare relict spinifex textures indicate that this was originally an ultramafic unit. The second rock type occurs in boudins, surrounded by the talc-chlorite schist. The boudins consist of carbonate and silica altered komatiites, in which the original textures have been preserved (Figure 7.3a). These boudins are deformed, but deformation is generally localized in faults and narrow shear zones, leaving low strain areas in between. Gold mineralization occurs within these boudins (Figure 7.2), and occurs in 1–3 m wide quartz-carbonate gold lodes.

To the south of the BCSZ, a number of approximately E-W trending, steeply north dipping faults offset the volcano-sedimentary unit with a consistent sinistral/N up displacement and steeply north-east plunging lineations.

The northern part of the BCSZ and overlying units are cut by E-W (Bulletin Fault) and N-S (Finucane Fault) trending faults with dextral displacements and subhorizontal lineations. The E-W trending dextral faults are covered by the Mt. Roe Basalt, whereas the Finucane Fault shows some



Figure 7.3a Photograph of the altered spinifex-textured komatiite in the Kitchener Mine.

offset of the Hardey Sandstone, and must therefore have been active after deposition of the basal units of the Fortescue Group.

7.3.3 *Foliations and lineation in the BCSZ*

Figure 7.4a is a contour plot of the poles to the foliations measured in the BCSZ in the mine area. The foliations are subvertical and the strike varies 45° around the orientation of the shear zone boundary (050/85). This variation in foliation orientations reflects the anastomosing pattern of the foliations, formed by a combination of shear zone boundary parallel foliations (C foliations) and secondary foliations, such as R-, P- and S-shears.

Figure 7.4b is a contour plot of all lineations measured in the BCSZ in the mine area. In the field and especially in underground mines, the difference between mineral stretching lineations and intersection lineations is not evident. The plot shows a number of point maxima which have been labeled. Maximum A (subvertical plunges) is consistent with the intersection between C-foliations and secondary foliations. In most cases, these subvertical lineations could be identified as intersection lineations in samples and thin-sections.

The maxima B and B' define a girdle of lineations pitching 40 to 25° SE on the foliations. These lineations are, in all cases, mineral stretching lineations formed by quartz, carbonates, chlorite, fuchsite and talc. These orientations are most abundant in the boudins.

The last group of lineations are subhorizontal and define maxima C and C'. These lineations consist of mineral stretching lineations and more brittle striations. The subhorizontal lineation orientation is most abundant in the talc-chlorite mylonite outside of the boudins.

The variety and spread of mineral stretching lineations and striations indicate a complex deformation history for the BCSZ.

7.3.4 *Kinematics*

Kinematic indicators, related to the subhorizontal lineations in the talc-chlorite mylonite normally indicate a dextral sense of shear (C in Figure 7.4b). These include shear-bands, asymmetric clasts, boudins and asymmetric folds. The E-W trending dextral faults to the north of the BCSZ show similar subhorizontal striations and are thought to belong to the same dextral kinematic framework.

Within the carbonate-quartz boudins the rocks are less intensely deformed. Normally a weak foliation, formed by carbonate, chlorite \pm fuchsite, is present, parallel to the main foliation in the surrounding mylonite. Kinematic analysis within the boudins, based on shear-bands and S-C fabrics,

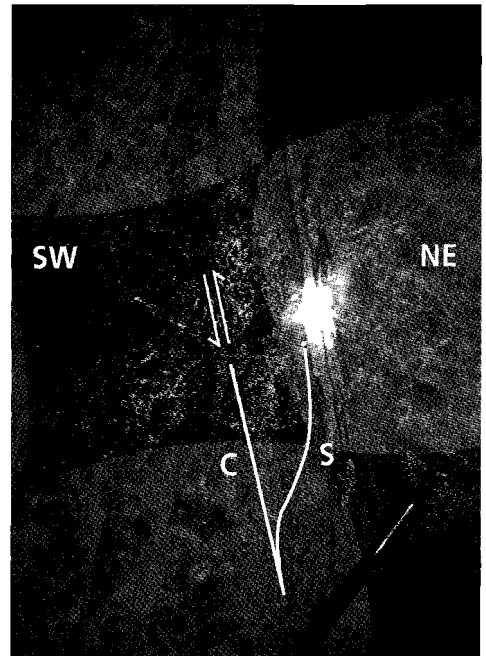


Figure 7.3b Photograph of S-C fabric indicating a sinistral/NE up sense of shear in the Kitchener mine.

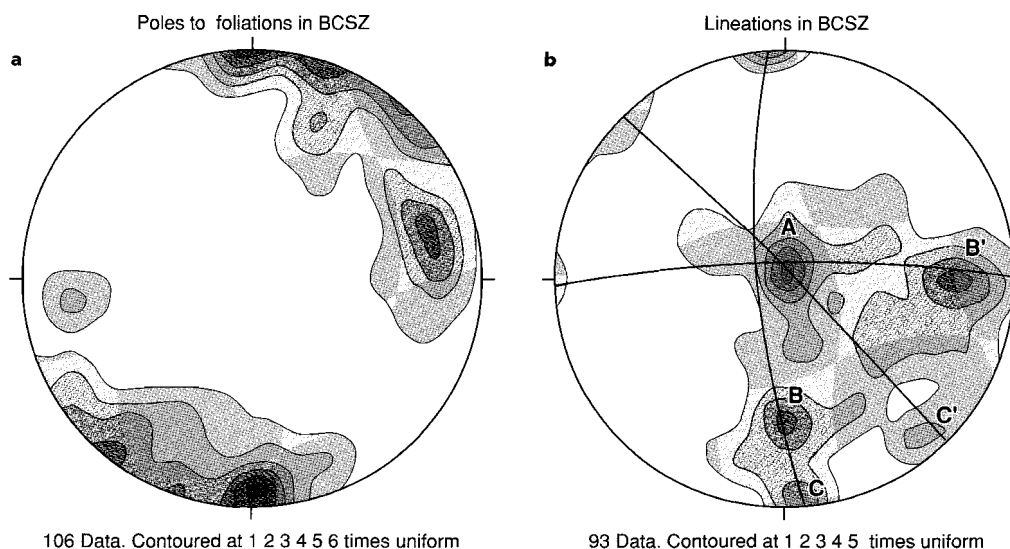


Figure 7.4

- a. Lower-hemisphere equal-area contour plot of all poles to foliations measured in the Bamboo Creek Shear Zone in the mining area. See text for discussion.
- b. Lower-hemisphere equal-area contour plot of all mineral lineations measured in the Bamboo Creek Shear Zone in the mining area.
 maximum A - intersection lineations,
 maximum B-B' - mineral lineations related to sinistral/northeast up sense of shear, mainly in boudins,
 maximum C-C' - mineral lineations related to dextral reactivation of the BCSZ.

shows structures consistent with an early sinistral/NE-up sense of shear, related to the gold mineralization. On the scale of the boudin, the gold bearing lodes have an orientation that is consistent with sinistral R-shears with respect to the main shear orientation (Figure 7.2, plots), but gold also occurs in shears that occupy the C orientation of sinistral S-C fabrics. This is confirmed by outcrop scale structures where gold-bearing R-shears and S-C fabrics consistently indicate a sinistral/NE up sense of shear in the Mt. Prophecy, Bamboo Queen and Kitchener mines (Figure 7.2 and 7.3b), which all lie within the main BCSZ. Stretching lineations (B in Figure 7.4b), formed by quartz, carbonates and fuchsite, pitch approximately 40° east. In a number of cases, dextral shears cross cut or reactivate sinistral structures, with a more horizontal lineation. This is clearly seen in Bulletin Mine, where the dextral E-W trending Bulletin Fault, with a subhorizontal lineation, post-dates the sinistral, gold related system, with a steeply E dipping lineation (Figure 7.2).

Bonnie Doon is a special case, since the gold bearing lode is not developed within the main BCSZ, but on one of the E-W trending sinistral faults south of the BCSZ. The gold lodes are situated along the fault and on north dipping R-shears, indicating a sinistral/north up sense of shear, with steeply east plunging stretching lineations.

In general, the gold lodes occur in ductile shears in the boudins related to the sinistral/NE up kinematic framework.

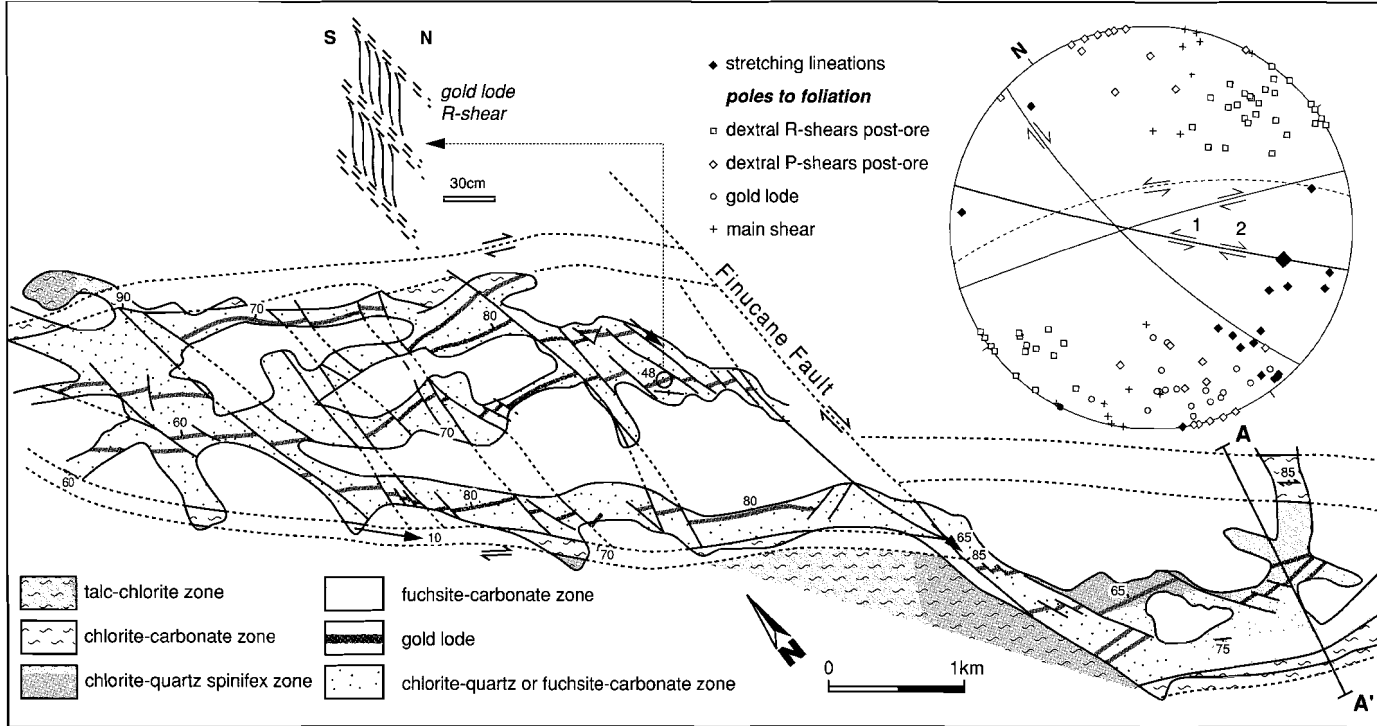


Figure 7.5 Geological map, largely based on the mine map produced by J.Peters, of the carbonate altered boudin in the underground Kitchener mine, showing gold lodes, alteration zones where they have been distinguished and a lower hemisphere equal area plot of structural data collected in the Kitchener deposit. A-A' indicates the traverse where samples for geochemical analysis were collected.

7.3.5 Structure and kinematics of the Kitchener deposit

Figure 7.5 is a detailed map of the Kitchener boudin in the underground mine. The boudin contains three gold lodes, which make a small angle with the boudin boundary and the main BCSZ foliation. The gold lodes are related to sinistral/NE up displacement with lineations pitching ca. 40° SE. The three gold lodes are offset by N-S trending faults with dextral displacements and shallow south plunging lineations. Most of these faults end at the boudin boundary, and are thought to be part of the dextral system that is prevalent in the BCSZ talc-chlorite mylonite. However, the Finucane Fault displaces the whole boudin with a dextral sense and is an even later (post-lower Fortescue Group) dextral reactivation of one of the faults in the boudin.

In some parts of the boudin primary textures have been so well preserved that the original layering, defined by textural zones, can be estimated, which is subparallel to the boundary of the boudin. The gold lodes cut across the bedding at a small angle.

7.4 Alteration in the BCSZ

7.4.1 Alteration zones

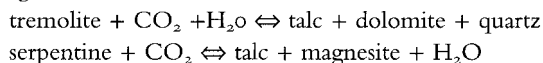
Relic volcanic textures and relict chromite grains throughout the BCSZ and carbonate altered boudins indicate that the BCSZ is situated in what was originally a komatiite, but igneous minerals have not been preserved. All rocks in the mining area show signs of metasomatic alteration. In the wider area of the greenstone belt, the mineralogy is consistent with greenschist facies metamorphism. This includes albite/chlorite/quartz \pm epidote assemblages in mafic rocks and serpentine/tremolite assemblages in ultramafic rocks.

The metasomatic rocks in the BCSZ are divided into alteration zones, according to co-existing diagnostic minerals (Figure 7.6), from the least-altered distal alteration zone in the mylonitic schist to the most proximal alteration in the mineralized zone. This division is based on the transect A-A' in the Kitchener Mine (Figure 7.5). A description of these zones follows.

Talc-chlorite alteration zone

The BCSZ mylonitic schist shows an anastomosing foliation pattern on a centimetre scale, leaving areas between with relic spinifex blades. The mineralogy consists of talc, chlorite, dolomite, magnesite and albite. The groundmass is formed by talc/chlorite intergrowth, whereas carbonates and albite occur as equidimensional, relatively undeformed grains. Carbonates commonly have a core of dolomite and a rim of Fe-rich magnesite.

Talc and magnesite are alteration products of serpentine and tremolite in the original ultramafic schist following the reactions:



The following alteration zones are limited to the boudins in the BCSZ.

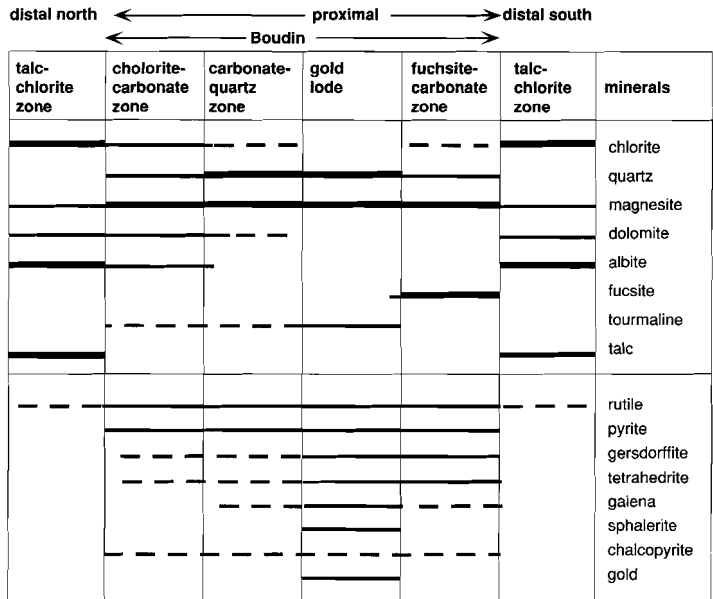
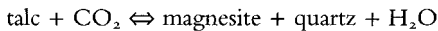


Figure 7.6 Alteration zoning profiles for the Kitchener transect, shown in the order in which they occur. Minerals constituting major, common or minor phases are represented by double, solid and dashed lines, respectively.

Chlorite-carbonate alteration zone

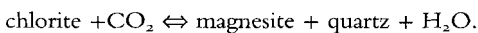
The most distal alteration zone in the boudin is the chlorite-carbonate alteration zone. This zone consists of a mylonitic schist with abundant chlorite and magnesite and minor dolomite. Magnesite occurs as euhedral grains and quartz and albite occur in minor amounts. Rare grains of light coloured tourmaline grow over the foliated fabric. Accessory minerals include rutile, pyrite, gersdorffite and tetrahedrite. The main difference between this zone and the talc-chlorite zone is the absence of talc. This is the result of the reaction:



The chlorite-quartz zone

The chlorite-quartz zone consists of well preserved spinifex textured rocks. The original mineralogy is now completely altered to quartz, magnesite, plagioclase and chlorite. The quartz is normally fine-grained with no preferred orientation and sutured grain boundaries. The quartz grains commonly define the spinifex blades. Magnesite grains are larger and irregularly shaped. Albite fills the interstitial spaces and chlorite is a minor constituent. Tourmaline-quartz-veins of several millimetres width cut across these rocks. The veins contain fine-grained sulfides, including pyrite, gersdorffite, tetrahedrite and galena. Rutile and pyrite both occur in the spinifex textured hostrock and in the tourmaline veins.

The main mineralogical difference between this zone and the chlorite-carbonate zone is the small amount of chlorite and the increased amount of quartz and magnesite. This is probably due to the reaction:



Gold lode

The mineralized zone is 1–3 m wide and consists of quartz, carbonate and sulfides. The quartz is normally laminated, alternating with thin screens of host rock (Figure 7.7a), and does not show a distinct texture. Quartz grains are recrystallized to fine to coarse grains with no undulose extinction. As described in §7.3.4, the mineralized zone is situated in ductile shears associated with a sinistral sense of shear.

Fuchsite occurs in small quantities within the screens of host rock. Gold is closely associated with tourmaline, galena and tetrahedrite. It occurs as millimetre-size grains of free gold with these minerals, as infill of brecciated zones of quartz and carbonate, commonly at the interface of quartz and carbonate (Figure 7.7b). Other sulfides that occur disseminated in the gold lode are pyrite and gersdorffite.

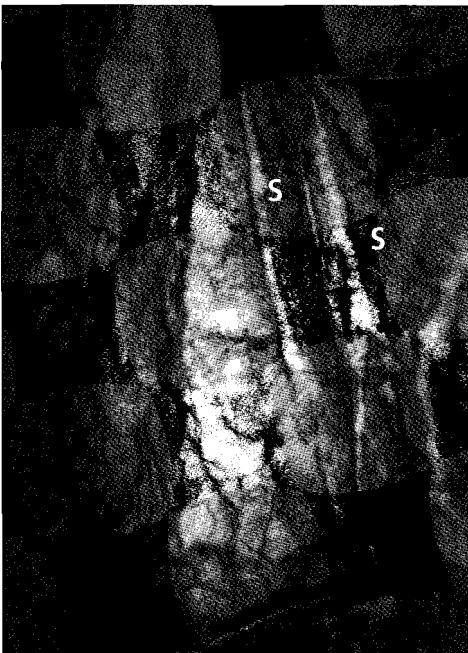


Figure 7.7a Photograph of the gold lode in the Kitchener Mine showing laminated quartz-carbonate and screens (s) of hostrock.

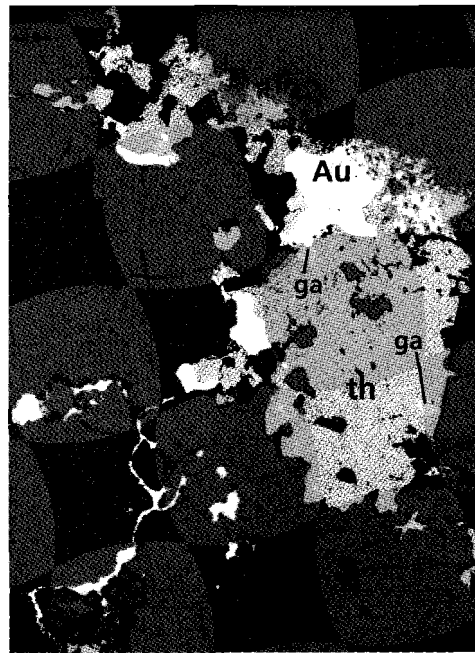


Figure 7.7b Photomicrograph of gold (Au) and associated galena (ga) and tetrahedrite (th) as infill of brecciated quartz and carbonate in the Kitchener gold lode. The width of the photomicrograph is 0.8 mm.

Fuchsite-carbonate zone

The fuchsite-carbonate zone consists of a granular rock type consisting of mainly carbonate and fuchsite. Equidimensional millimetre-size magnesite grains cause the granular characteristic of this zone. This texture is probably the result of the cumulate texture of the parent rock texture. Fuchsite and quartz occur as fine grains aggregates between the carbonate grains. A special type of quartz texture that occurs in this zone is the plumose texture (Gebre-Mariam et al., 1993). In this texture, quartz

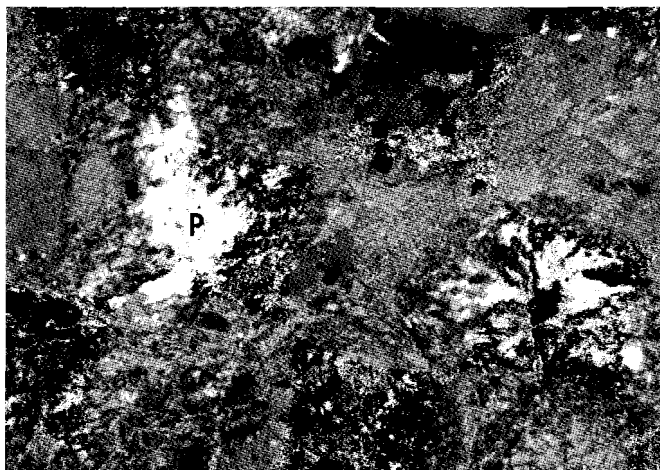


Figure 7.7c Photomicrograph of plumose quartz textures (p) in the fuchsite-carbonate alteration zone. The height of the photomicrograph is 0.2 mm.

fibers grow in a radial fashion from a central point (Figure 7.7c). Aggregates of sulfides occur in the fuchsite/quartz domains, and include gersdorffite and tetrahedrite, rimmed by galena.

Distribution of alteration zones.

The talc-chlorite zone occupies the area of the main BCSZ surrounding the boudins. The other alteration zones occur within the boudins. The chlorite-carbonate zone is restricted to the outer parts of the boudin (Figure 7.5), where the rocks are intensely deformed to a mylonitic schist forming the boundary between the boudin and the main mylonite zone. In the section that was mapped on a 1:100 scale (A-A' in Figure 7.5), the chlorite-quartz zone is restricted to the hanging wall (northern side) of the ore lode, and the fuchsite-carbonate alteration zone to the footwall (southern side) of the ore lode. In the rest of the Kitchener Mine, these alteration types have not been distinguished nor mapped in detail.

7.4.2 Mineralogy of the alteration

The mineral chemistry was determined using a JEOL JSM 6400 Scanning Electron Microscope (SEM) at the University of Western Australian Centre for Microscopy and Microanalysis. The quantitative analysis were done using a LINK-EDS X-ray analysis system (take off angle 40°, counting time 60s, accelerating voltage 15KV, beam current 3.0x10⁻⁹ nA). ZAF corrections follow Ware (1981) and all analysis were recalculated using the RECALC2 computer program (B. Griffin)

Two groups of carbonates occur in the alteration zones of the Kitchener Mine (Figure 7.8): magnesite and dolomite. Magnesite is the main carbonate throughout the alteration envelope. The Fe content can be as high as 40% in the most distal alteration

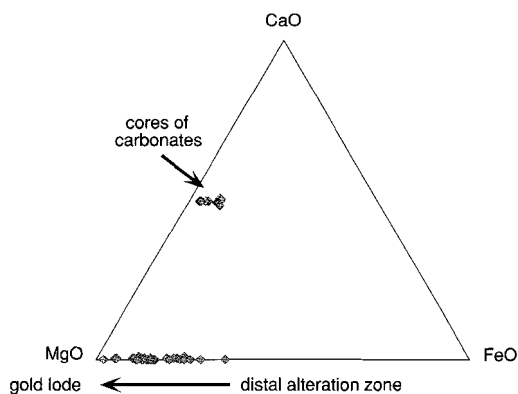


Figure 7.8 Plot showing composition of carbonates in the Kitchener deposit.

zone and decreases to 0% in the gold bearing zone. Dolomite is developed in the talc-chlorite zone and the chlorite-quartz zone, associated with plagioclase or in cores of magnesite grains. Chlorite is generally Mg and Si rich with Fe/Fe+Mg increasing toward the mineralized zone (Table 7.1).

Table 7.1 Composition of chlorite and geothermometry, following Kranidiotis and Maclean (1989). See text for discussion.

	chlorite-carbonate zone	carbonate-quartz zone		Fuchsite-carbonate zone			
	Wt %						
SiO₂	29.31	30.23	30.23	30.63	30.66	30.35	30.44
Al₂O₃	17.65	18.27	18.27	18.78	18.95	18.58	18.78
Cr₂O₃	0.6	2.08	2.08	1.17	1.03	1.06	0.92
FeO	10.84	8.69	8.69	6.2	6.4	6.29	6.33
NiO	0	0	0	0	0	0.23	0.26
MgO	26.8	28.56	28.56	29.98	29.88	30.08	29.96
Total	85.2	87.83	87.83	86.76	86.92	86.59	86.69
Number of ions on the basis of 28 oxygens							
Si	5.881	5.836	5.836	5.886	5.883	5.858	5.864
Al	4.174	4.156	4.156	4.252	4.287	4.225	4.264
Cr	0.096	0.316	0.318	0.178	0.157	0.162	0.140
Fe²⁺	1.818	1.404	1.402	0.997	1.028	1.016	1.020
Ni	0.000	0.000	0.000	0.000	0.000	0.036	0.040
Mg	8.016	8.216	8.216	8.585	8.546	8.655	8.604
Fe/Fe+Mg	0.185	0.146	0.146	0.104	0.107	0.105	0.106
Temperature calculated following Kranidiotis & Maclean (1989)							
T (°C)	256	258	258	250	250	253	252

Typical analysis of fuchsite are shown in Table 7.2. Fuchsite is a Mg-phengite which contains variable amounts of Cr, up to 3 wt%, which causes the bright green colour. Tourmaline analysis (Table 7.2) show that the tourmaline has a dravite composition, i.e. Mg rich, Fe poor.

The sulfides, pyrite, gersdorffite, tetrahedrite and very minor chalcopyrite, occur throughout the alteration zones in the boudin, but are concentrated in the most proximal alteration zones. Galena occurs mainly in the ore lode and to a small extent in the proximal alteration zones.

Microprobe analysis of pyrite shows that gold is not present in quantities above the detection limit (0.03 wt%).

Table 7.2 Typical composition of fuchsite and tourmaline, see text for discussion.

Tourmaline					Fuchsite		
zone	chlorite- carbonate	carbonate- quartz	ore	ore	zone	ore	fuchsite- carbonate
Wt %					Wt %		
SiO₂	37.68	36.72	37.84	36.96	SiO₂	50.76	50.09
TiO₂	0.40	0.97	0.00	0.00	Al₂O₃	29.63	32.62
Al₂O₃	31.13	30.46	32.84	31.14	Cr₂O₃	0.34	1.68
Cr₂O₃	0.91	1.68	0.00	0.00	Fe(total)	0.53	0.45
Fe(total)	6.11	2.76	2.47	2.64	MnO	0.00	0.00
MgO	8.77	9.11	9.85	10.25	MgO	2.29	0.95
Na₂O	2.96	2.61	2.63	2.69	CaO	0.00	0.00
Total	87.96	84.31	85.63	83.68	Na₂O	0.00	0.00
					K₂O	10.64	10.33
					total	94.19	96.12
Numbers of ions on the basis of 31 oxygens					Numbers of ions on the basis of 24 oxygens		
Si	5.906	5.908	5.993	5.952	Si	6.770	6.550
Ti	0.047	0.118	0.000	0.000	Al	4.658	5.027
Al	5.751	5.776	6.132	5.908	Cr	0.036	0.174
Cr	0.112	0.215	0.000	0.000	Fe(total)	0.060	0.049
Fe(total)	0.801	0.371	0.327	0.356	Mn	0.000	0.000
Mg	2.049	2.184	2.325	2.459	Mg	0.456	0.186
Na	0.900	0.813	0.801	0.839	Ca	0.000	0.000
					Na	0.000	0.000
					K	1.810	1.724

Comparison with other parts of the Bamboo Creek Deposit

A second underground traverse was made through the Prophecy-Perseverance line. The alteration zones and mineralogy are very similar to the Kitchener Mine, but rocks are generally more intensely deformed. The main difference is the larger abundance of sulfides in the ore lode (up to 20% of the ore lode). The sulfides and gold occur in a similar way to those in the Kitchener Mine, as the infill of brecciated quartz-carbonate veins. Sphalerite is rare in the Kitchener mine, but is abundant in the Prophecy-Perseverance samples.

7.4.3 Indications of environment of deposition

The Ag content of gold, the fineness ($1000 \times \text{wt\%Au}/(\text{wt\%Au}+\text{wt\%Ag})$), varies with geologic environment and deposit style (Fisher, 1945; Morrison et al., 1991). Samples from the Kitchener Mine were analysed for Au and Ag. The analysis were done on the JEOL JXA-8800M microprobe at the Free University in Amsterdam by W.M. Lustenhouwer. Analytical errors for gold and silver were less than 0.02 %. The fineness was determined in two samples from the Kitchener deposit, 957 ± 4 (10 grains) and 980 ± 3 (20 grains), respectively. This range of fineness is typical of Archean mesothermal lode-gold deposits (Morrison et al., 1991)

The Al^{IV} content of chlorite is used to estimate the temperature during the alteration process, following Cathelineau & Nieva (1985), who calibrated this thermometer from an active geothermal area. Chlorites from rocks that contain another Al phase (fuchsite or plagioclase) are used to ensure that the system is Al saturated. A correction is made for the Fe content, according to Kranidiotis & Maclean (1989). The equation used to calculate the temperature is: $T^{\circ}C = 106Al_{COR}^{IV} + 18$ with $Al_{COR}^{IV} = Al_{sample}^{IV} + 0.7 Fe/(Fe+Mg)$. The temperature during alteration within the boudin, as estimated using this procedure, is between 250 and 258°C (Table 7.1). Taking analytical errors and errors in the initial calibration into account the temperature is constrained to $253 \pm 50^{\circ}C$.

7.4.4 Enrichment/depletion

In the traverse A-A' in the Kitchener Mine (Figure 7.5) five samples were collected for major and trace element analyses. All analyses were done on powdered pills using the XRF at the University of Western Australia. The results are shown in Table 7.3. In Figure 7.9a, the variation of element abundance in the various parts of the boudin are shown. Most elements show strongly asymmetric pat-

Table 7.3 Major and trace elements of samples collected in the Kitchener deposit and reference samples from a relatively fresh komatiite flow from the Barberton Mountain Land (Smith et al., 1980).

texture	Bamboo Creek-Kitchener Mine					Barberton, Smith et al.(1980)			
	K-1 schist	K-2 spinifex	K-6 spinifex/ lode	K-8 cumulate	K-9 cumulate	HSS-531 spinifex	HSS-532 spinifex	HSS-533 spinifex	HSS-534 cumulate
	recalculated including volatiles								
SiO₂	38.55	36.83	34.34	32.07	32.91	41.46	41.29	42.33	39.53
TiO₂	0.49	0.53	0.25	0.19	0.26	0.33	0.33	0.35	0.29
Al₂O₃	10.43	7.83	5.78	4.43	5.65	3.70	3.68	3.81	3.18
Fe₂O₃	8.97	9.07	8.06	7.71	7.15	10.16	9.78	10.53	8.71
MnO	0.14	0.17	0.09	0.1	0.1	0.16	0.16	0.17	0.16
MgO	16.82	16.79	22.65	24.5	23.74	23.97	24.35	22.63	25.75
CaO	4.78	5.76	1.89	0.44	0.66	6.33	6.24	7.69	5.21
Na₂O	2.32	2.04	0.79	0.29	0.04	0.16	0.17	0.19	0.08
K₂O	0.02	0.01	0.03	1.06	1.25	0.02	0.02	0.03	0.03
P₂O₅	0.13	0.14	0.05	0.06	0.04	0.02	0.02	0.02	0.02
Cr₂O₃	0.18	0.2	0.34	0.32	0.43	0.30	0.29	0.33	0.27
NiO	0.04	0.04	0.12	0.1	0.12	0.16	0.16	0.13	0.18
LOI	16.95	20.74	25.68	28.73	27.51	13.21	13.47	11.77	16.57
total	99.82	100.15	100.07	100	99.86	99.98	99.97	99.98	99.97
Rb	1	0	1	32	32	2	1	1	1
Sr	64	71	26	8	16	28	25	29	21
Y	15	18	5	6	4	7	6	8	4
Zr	75	78	29	23	27	23	23	26	19
Ba	8	8	15	90	101	3	5	4	30
Pb	21	0	22	7	13				
Cu	35	19	11	8	25	80	54	109	61
Zn	97	75	55	45	53	80	70	68	62
As	10	9	758	802	921				
Sb	5	12	73	112	117				

terns relative to the ore lode. Na_2O , TiO_2 , CaO , P_2O_5 , Y, Zr and Sr are more abundant in the northern spinifex-textured part of the alteration envelope, whereas K_2O , Rb, As, Sb, Ni and Ba are more abundant in the southern base-of-flow cumulate part of the alteration envelope. A small number of elements show close to symmetrical abundance in Figure 7.9. These include Pb, with a peak

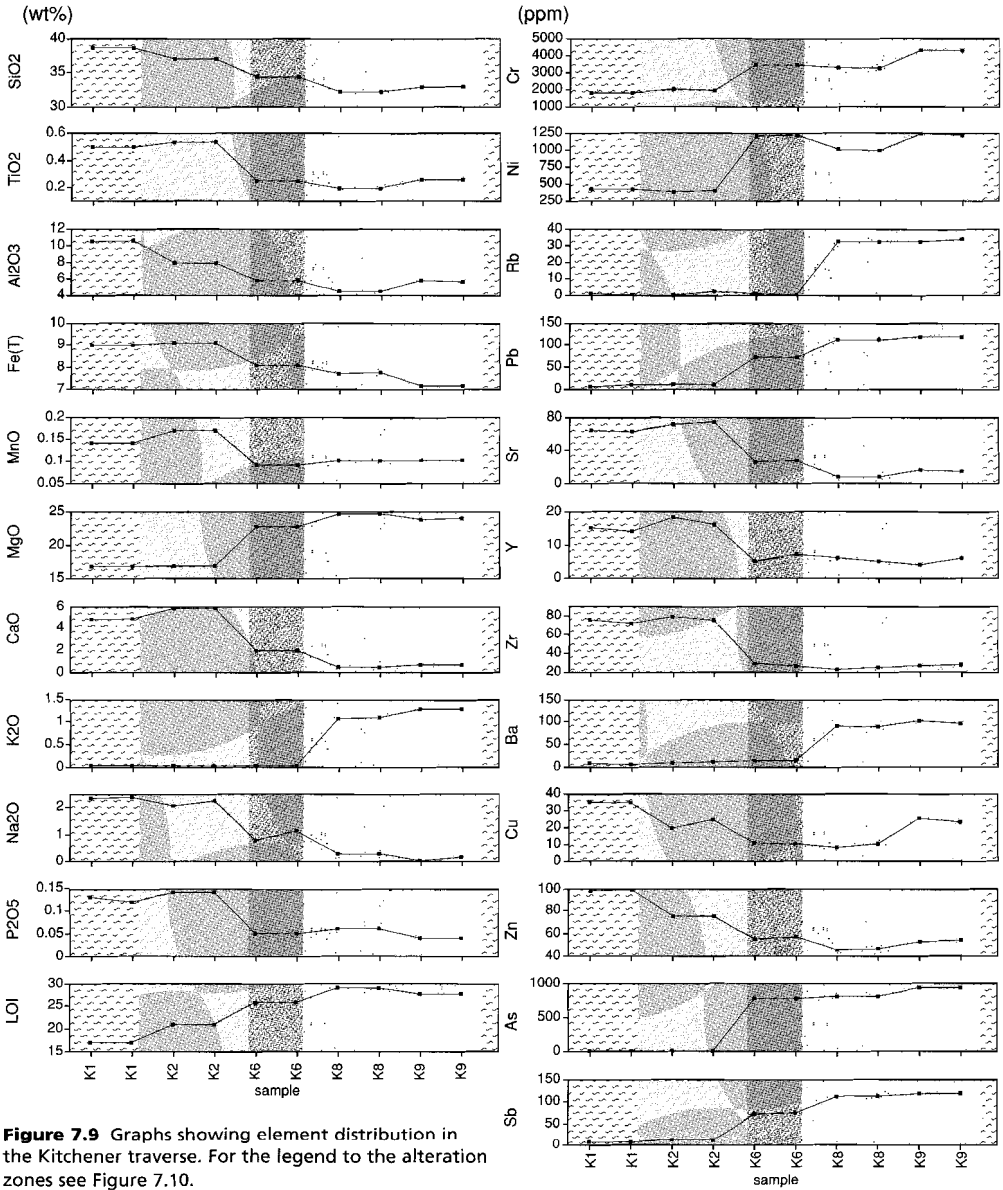


Figure 7.9 Graphs showing element distribution in the Kitchener traverse. For the legend to the alteration zones see Figure 7.10.

in the mineralized zone, and Cu, with a low abundance close to the mineralized zone. To distinguish the effects of alteration from the effects of primary composition, the analysis from the alteration envelope are compared to analysis from a relatively fresh komatiite flow. No detailed analysis are available from the one komatiite flow in the Pilbara Craton from the Warrawoona Group. Therefore, the data from the Bamboo Creek Deposit were compared to data from a komatiite flow in the Barberton

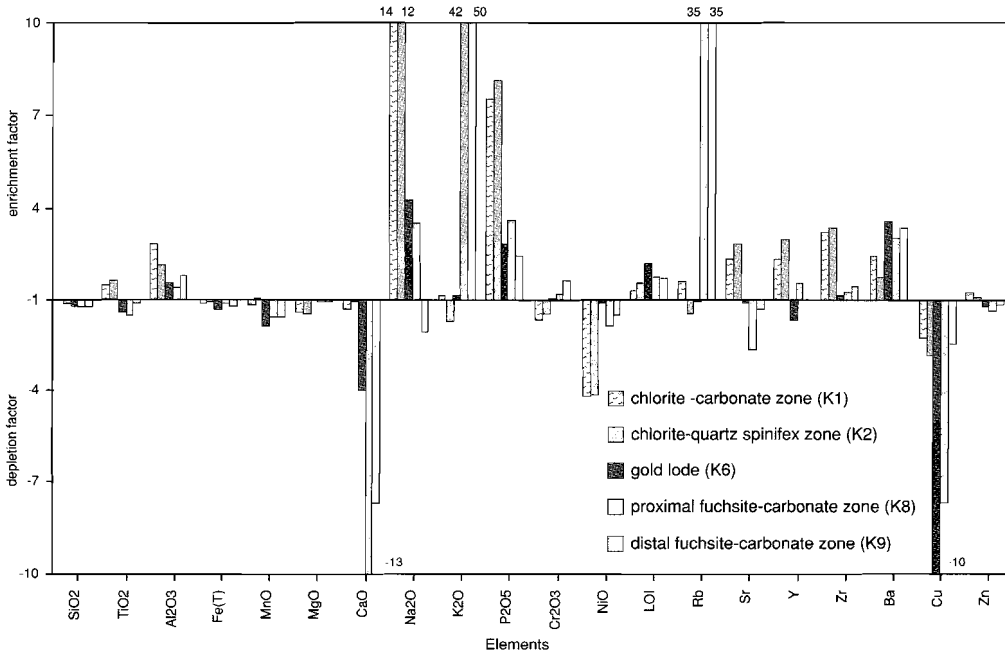


Figure 7.10 Enrichment and depletion diagram of the alteration zone in the Kitchener deposit. The enrichment factors are calculated by dividing the concentrations of elements in the altered zone by unaltered komatiites (Smith et al., 1980) with similar textures.

Greenstone Belt (Smith et al., 1980). The komatiites in the Warrawoona Group are Al-depleted and in most respects similar to the Barberton komatiites (Arndt, 1994). Table 7.3 shows the geochemical data of the komatiite from the Bamboo Creek Deposit and the data from the Barberton komatiite, that are used to calculate the depletion and enrichment factors. Sample K8 and K9, from the cumulate textured part, are compared to HSS-534, K6, K₂ and K₁ are compared with HSS-533, HSS-532 and HSS-531, respectively, which are samples from the spinifex zone. The resulting enrichment/depletion diagram is shown in Figure 7.10

TiO₂, Fe(total) and Cr₂O₃, which are considered to be relatively immobile elements (Böhlke, 1989; Skwarnecki, 1988) remain close to 1, consistent with the assumption that the Barberton komatiite analyses that were used, do represent rocks with chemical compositions close to the parent rocks in the Kitchener Mine. Of the major elements, enrichment of Al₂O₃ and P₂O₅ occurs in the whole alteration envelope, Na₂O mostly in the northern alteration zone, and K₂O in the southern alteration zone. Other major elements (SiO₂ and MgO) remain remarkably constant. LOI shows a gen-

eral enrichment, probably caused by CO₂ and H₂O in the alteration envelope.

Of the trace elements, Ni and Cu are depleted in all zones, whereas most other trace elements show relative enrichment (Rb, Zr, Ba), or were immobile (Zn). Three elements that are not shown in this diagram are Pb, As and Sb. These elements were not analysed by Smith et al. (1980) in the 'fresh' komatiite. They can be assumed to be very low (<3 ppm) in fresh komatiites, but are strongly enriched in the alteration envelope, especially in the southern part and particularly for As and Sb.

This diagram also shows that much of the asymmetry in the element abundance can be explained by variations in the original rock type, causing relatively symmetric enrichment/depletion profiles (Zn, Ba, Zr, Cr, MgO). Exceptions are CaO, NaO, K₂O and Rb, and probably also As and Sb, which appear to be asymmetrically enriched or depleted.

7.4.5 Light stable isotopes of dolomite

For nine samples in the Kitchener traverse A-A', the carbon and oxygen stable isotopic composition was determined. The method used is described in detail by McNaughton et al. (1988b). Reproducibility of dolomite standard δ values was better than 0.1 ‰. This was done to test whether the wallrock alteration, as described above, can be attributed to the same fluid that deposited the quartz-carbonate-gold veins. The $\delta^{13}\text{C}$ and $\delta^{18}\text{O}$ values for dolomite from all samples are remarkably constant at +0.24 and +14.6 respectively (Table 7.4) and similar to the range for gold deposits in other Archean terrains (de Ronde et al., 1992; Kishida & Kerrich, 1987, McNaughton et al., 1992), although $\delta^{13}\text{C}$ is distinctly more positive than in other Archean gold deposits.

Table 7.4 Comparison between carbon and oxygen isotopes in carbonates from the Bamboo Creek Deposit and other Archean lode-gold deposits.

Stable isotope	Bamboo Creek Deposit	Barberton Greenstone Belt ¹	Abitibi Greenstone Belt ²	Yilgarn Craton ³
$\delta^{13}\text{C}_{(\text{PDB})}(\text{‰})$	+0.24±0.6	-4.4 to -2.2	-8 to -2	-3.4 to -7
$\delta^{18}\text{O}_{(\text{SMOW})}(\text{‰})$	+14.6±0.6	+11 to +13	+8 to +15	+6 to +14

¹ Data from de Ronde et al.(1992), ² Data from Keshida & Kerrich (1987), ³ Data from McNaughton et al.(1992). Errors are 1 σ errors of the arithmetic mean.

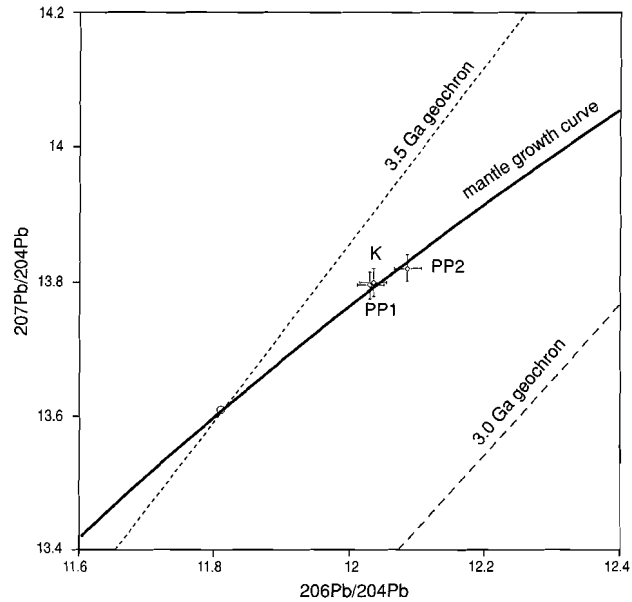
7.5 Lead-lead dating of galena

Galena from three samples of the ore lode, one from Kitchener and two from Prophecy-Perseverance, were used for Pb-Pb isotopic dating. Small amounts of galena were gouged from the

Table 7.5 Lead isotope composition of galena from three samples in the Kitchener (K) and Prophecy-Perseverance (PP1 and PP2) deposit. Errors on ratios are all < 0.15% (2 σ) and model ages are calculated following Cumming & Richards (1975, model III).

Sample	²⁰⁶ Pb/ ²⁰⁴ Pb	²⁰⁷ Pb/ ²⁰⁴ Pb	²⁰⁸ Pb/ ²⁰⁴ Pb	model age (Ma)
K1	12.036	13.798	31.921	3412±40
PP1	12.031	13.794	31.938	3414±40
PP2	12.086	13.819	31.990	3376±40

Figure 7.11 Uranogenic lead diagram showing the mantle growth curve (Cumming & Richard, 1975, model II), geochrons for 3.5 and 3.0 Ga and the data from Bamboo Creek. K is a sample from the Kitchener Mine, PP1 and PP2 are samples from the Prophecy-Perseverance Mine.



samples with a pre-cleaned scalpel point and processed directly to determine their Pb isotope composition. The Pb isotopic composition of the galenas was analysed with a VG[®]354 multi-collector mass spectrometer, at Curtin University of Technology, with Pb analysis corrected for mass discrimination using NBS-981 (McNaughton et al., 1988) as a standard. The mass discrimination factor on repeated measurements of the standard was 1.2 ‰ per mass unit. Pb isotopic compositions are determined to better than $\pm 0.15\%$. Isotopic and decay constants and other parameters follow Steiger & Jaeger (1977) and Tatsumoto et al. (1973), isotope ratios by Todt et al. (1984) were used. All errors quoted are 2σ errors. The results for the three analysis are shown in Table 7.5 and Figure 7.11. The data cluster tightly on the mantle growth curve, and give model ages all within error (2σ) of 3400 Ma (Cummins & Richards, 1975, model III).

7.6 Discussion

In summary, the Bamboo Creek Deposit is situated in a bedding-parallel ultramafic brittle/ductile shear zone in ultramafic rocks. At least two phases of movement can be distinguished on the sub-vertical NW-SE trending BCSZ: a relatively late dextral movement with shallowly southeast plunging stretching lineations, and an earlier sinistral/northeast up displacement, with ca. 45° southeast plunging stretching lineations. The late dextral movement is best represented in the main body of the shear zone, the mylonitic talc-chlorite schist. The earlier sinistral/northeast up movement has been preserved in the strongly carbonate-quartz altered boudins within the BCSZ. The gold lodes are associated with the sinistral/northeast up shears in the boudins (see Figure 7.12b). Dextral shears cut across the gold lodes, and therefore the dextral movement post-dates the gold mineralization event.

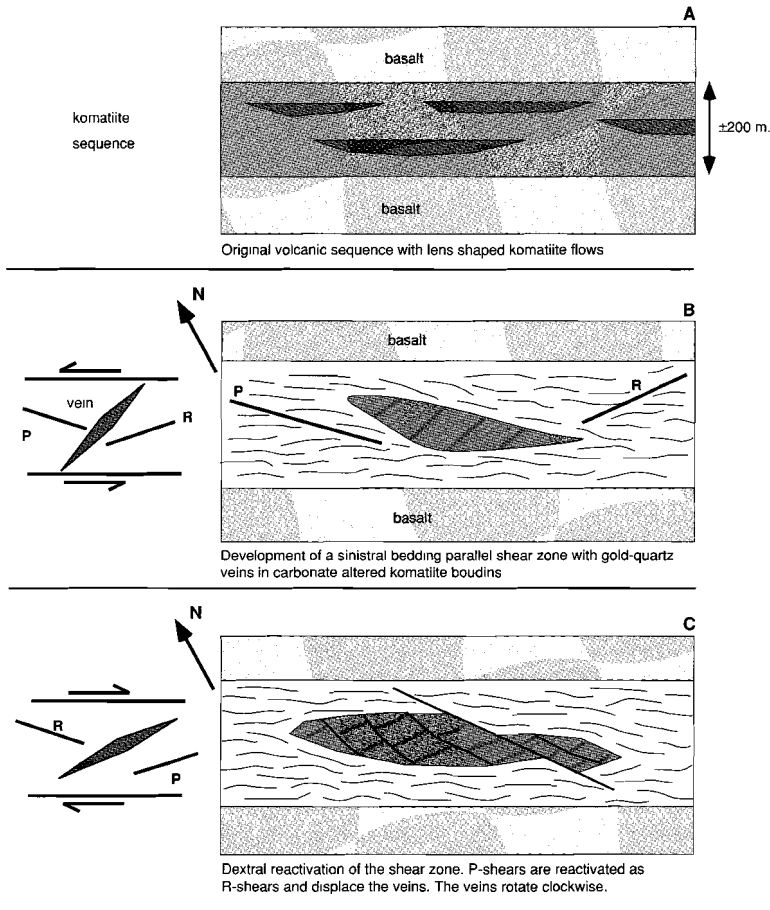


Figure 7.12 Conceptual model of structural and rheological controls on gold mineralization in the Bamboo Creek Deposit.

Apart from the localized sinistral and dextral shears, the rocks in the boudins are relatively undeformed and preserve primary textures such as spinifex blades and base-of-flow cumulates.

There is clearly a contrast in rheological properties between the boudins and the talc-chlorite mylonite. The boudins are intensely carbonate altered and silicified, resulting in the main mineral phases (>50%) magnesite and quartz, whereas the main mineral phases in the surrounding mylonite are talc and chlorite.

The initial alteration, causing the contrasts in rheological properties, must have occurred at an early stage, pre-dating or during the sinistral movement. During the sinistral movement, gold was deposited in extensional type shears (R-shears), within the more rigid altered boudins.

Carbon and oxygen stable isotopic compositions of dolomite throughout the Kitchener boudin and in the gold lode are constant, indicating that the fluid that caused the alteration envelope was the same as the fluid from which gold was precipitated. So far there is no evidence from the stable iso-

tope record for more than one alteration event. However, it would be interesting to study the light stable isotopes in the BCSZ further away from the gold deposits.

The $\delta^{13}\text{C}$ and $\delta^{18}\text{O}$ signatures for carbonates from the Bamboo Creek Deposit ($+0.24\pm 0.6$ and $+14.6\pm 0.6$, respectively) are similar to values recorded for other Archean mesothermal gold deposits, although the $\delta^{13}\text{C}$ values at Bamboo Creek are slightly more positive.

Although the light stable isotope signatures are very constant for Archean lode-gold deposits, the data are non-definitive (Golding et al., 1989; Groves et al., 1995) and are interpreted by most authors as the result of various fluid sources, including mantle derived fluids, various crustal reservoirs and seawater/meteoric water (de Ronde et al., 1996; Groves et al., 1995; McNaughton et al., 1992).

In the Kitchener boudin, three alteration zones, related to the gold-mineralization, can be distinguished: the carbonate-chlorite alteration zone forming the boundary zone between the boudin and the BCSZ mylonitic schist, the carbonate-quartz zone in spinifex textured rocks and the fuchsite-carbonate zone in the cumulate textured rocks, both adjacent to the mineralized zone.

Chlorite thermometry on the Kitchener traverse gives temperatures of alteration of ca. 250°C. This is consistent with mineral assemblages in the alteration zones (chlorite + muscovite + albite + quartz, no tremolite or biotite, (Mikucki et al., 1990) and can not be distinguished from greenschist facies conditions in the surrounding unaltered volcanics.

The alteration zones are very similar to those described for the Kerr-Addison deposit by Kishida and Kerrich (1987). Many mineral assemblages in the alteration zones can be explained by increased X_{CO_2} towards the mineralized zone. In the most distal part this causes the breakdown of tremolite + serpentine to form talc + chlorite + carbonate, and the breakdown of titanite to rutile. Subsequently talc breaks down to magnesite and quartz, and finally chlorite breaks down to magnesite and quartz. Where chlorite is absent, Al is taken up by muscovite, incorporating the high Cr of the ultramafic parent rock to form fuchsite, and /or albite. The high Ni content of the parent rock results in gersdorffite (NiAsS). Pyrite and minor chalcopyrite are present throughout the boudin, whereas tetrahedrite + galena \pm sphalerite are restricted to the inner alteration zones and are strongly associated with gold.

These mineral assemblages are similar to those described in other Archean sub-amphibolite facies mesothermal lode-gold deposits (Mikucki et al., 1990; Kishida and Kerrich, 1987), indicating that the nature (X_{CO_2} , pH, f_{O_2} and mS) of the Bamboo Creek ore fluids are in the same range.

Enrichment/depletion analysis shows that the gold alteration envelope is strongly enriched in Na_2O , K_2O , Rb, Pb, As and Sb. This is characteristic for Archean mesothermal lode-gold deposits, in contrast to epithermal deposits which are also enriched in Hg, Cu and Zn (Barley et al., 1989; Perring et al., 1991).

The low-temperature mineral assemblages, brittle fracturing during mineralization, and the plumose quartz textures indicate that the Bamboo Creek Deposit formed at a shallow crustal level.

Gold in the Bamboo Creek Deposit is coarse-grained and limited to the quartz-carbonate gold lode. This indicates that gold deposition occurred as a consequence of either fluid mixing or phase separation due to changes in P and T conditions of the ore fluids. Deposition as a result of chemical changes of the ore fluid due to interaction with the wall rock would normally produce gold disseminated in the wall rock (Skinner 1979).

The BCSZ that contains the gold mineralization is situated in the 3475 to 3435 Ma Warrawoona Group (Thorpe et al., 1992). A felsic unit, stratigraphically underlying the BCSZ, is dated at 3454 ± 1 Ma (U-Pb, zircon, Thorpe et al., 1992). This provides a minimum age for the BCSZ. An upper limit to the age of the BCSZ is provided by the Chimingadgi granitoid suite, which intrudes and truncates the BCSZ at the south eastern end. This granitoid suite has a Rb-Sr whole-rock age of 3209 ± 47 Ma (Collins & Gray, 1990). However this probably records a post-intrusion fluid-circulation event because similar granitoid suites in the Mount Edgar Batholith gave U-Pb zircon ages ca. 3300 Ma (Williams and Collins, 1990). Therefore the upper limit to the age of the final dextral movement along the BCSZ is taken to be 3300 Ma. The gold mineralization event is related to the sinistral event which pre-dates the dextral event and must have been even earlier. Therefore the timing of the gold mineralization is relatively early in the history of the Coppin Gap Belt.

The three Pb-Pb model ages from galena from the Kitchener and Prophecy-Perseverance deposits are all three within error of 3400 ± 40 Ma. Galena is strongly associated with gold mineralization, therefore the Pb-Pb model ages are an indication of the age of gold mineralization. Lead that is found in galena associated with the gold is likely to be a mixture of juvenile lead (i.e. lead coming from the mantle along the shear zones) and crustal lead (i.e. lead that came from the mantle along with the volcanic melt). The early component should have an isotopic composition reflecting mantle lead at the time of extrusion at ca. 3450 Ma. As a consequence, the juvenile contribution is likely to be somewhat younger than 3400 Ma found in the galena associated with the gold. McNaughton et al. (1990) showed that in the Norseman-Wiluna Belt in the Yilgarn, the Pb-Pb model ages are approximately 70 Ma older than the age of gold mineralization. If this applies to the Pilbara, the actual age of gold mineralization may be 3330 Ma. The three ages are within error of each other, indicating that gold mineralization occurred during one single event. The Pb-Pb model ages are in agreement with timing constraints for the BCSZ as discussed above (i.e. between 3454 and 3300 Ma).

The local structures in the mining area do not permit a direct interpretation in terms of extensional versus compressional deformation. The 45°N dipping bedding of the base of the Fortescue Group, which unconformably overlies the BCSZ, shows that the orientation of the BCSZ during deformation must have been shallower than its present day orientation and possibly formed in a near horizontal position parallel to the bedding (see Chapter 5).

Nijman et al. (1995) recognised two structural events in the Coppin Gap greenstone belt: an early extensional event at ca. 3445 Ma, succeeded by a compressional thrusting event during deposition of clastic sequences post-dating deposition of the Warrawoona Group (ca. 3300 Ma). In the Bamboo Creek area, these two structural events can be correlated with the early sinistral/northeast up movement on the BCSZ, together with sinistral faults in the footwall of the BCSZ, belonging to the extensional phase, post-dated by dextral movement on the BCSZ and dextral thrust faults in the hanging wall of the BCSZ belonging to the compressional phase. In this scenario, gold mineralization must have formed during a late (3400 Ma) stage of the extensional event.

Hence, although the chemical characteristics and alteration types are very similar to typical Archean lode gold deposits in the Yilgarn (Groves et al., 1992), Superior Province (Colvine, 1989) and southern Africa (Foster and Piper, 1993), the structural setting may be different.

The tectonic setting of Archean lode gold deposits has been the subject of a long-standing debate. In early studies, structures related to gold mineralization were not recognized and gold deposits were

thought to be syn-volcanic in nature (Fripp, 1976, Kerrich & Fryer, 1979). In more recent studies, the importance of structural controls on gold mineralization has been recognized. This led to models involving remobilization of syngenetic gold into structural sites (Hutchinson, 1993). However, most recent models on lode gold mineralization are epigenetic and involve the transport of gold in a fluid phase from a remote source to the structurally controlled deposit site at various crustal depths, during or after deformation (Groves et al., 1992, crustal continuum model; Foster & Piper, 1993). This implies that the tectonic setting of gold mineralization will have no relation to the host rock, but will be related to the hosting structure.

There are problems in interpreting the structural/tectonic setting of gold deposits. One of the problems is the lack of a good regional structural framework. Usually it is not possible to determine the tectonic setting (extensional/compressional) from mine scale structures alone. The mine scale structures need to be related to regional structures. The second problem is related to uncertainties in the timing of gold mineralization. Robust age determinations of the mineralizing event are not easily obtained.

Recent studies in the Superior Province and the Yilgarn Craton combine regional structural data with mine scale structures and robust ages of gold mineralization. These show that the gold mineralizing event is strongly related to accretion in the final stages of cratonization and is generally related to compressional and strike-slip structures (Kerrich & Cassidy, 1994; Groves et al., 1995). Age determinations of gold mineralization are 2635 ± 10 Ma and 2710–2670 Ma for the Yilgarn Craton and the Superior Province, respectively. One of the few models involving an extensional setting during gold mineralization in the Late-Archean was proposed by Williams & Whitaker (1993). They link part of the gold mineralization in the Leonora District in the Yilgarn Craton, with a core-complex type extensional setting. However the timing of gold mineralization remains uncertain.

In Mid-Archean terrains, such as the Pilbara and Kaapvaal Craton, few data exist. In a well documented study of lode gold deposits in the Barberton greenstone belt, the mineralization event was constrained to 3126–3084 Ma (de Ronde et al., 1992) and was found to be related to a change from a convergent tectonic regime to a transtensional regime (de Ronde & de Wit, 1994).

The Bamboo Creek Deposit is certainly older than 3209 Ma, possibly as old as 3400 Ma, making it the oldest recorded gold deposit world wide. This contrasts with the 2950 Ma age for gold mineralization recorded in the Mt. York district by Neumayr et al. (1993b), indicating that there were at least two gold mineralization events in the Pilbara Craton. The Bamboo Creek gold mineralization probably formed during an extensional event or during a change from an extensional to a compressional setting, whereas the Mt. York deposit formed in a strike-slip setting (Neumayr et al., 1993b).

7.7 Conclusions

1. The Bamboo Creek gold deposits are situated in relatively undeformed boudins of carbonate altered komatiite in an intensely deformed talc-chlorite mylonite zone (BCSZ).
2. The gold mineralization occurred during sinistral/northeast up movement on the steeply dipping northwest trending Bamboo Creek Shear Zone, with a stretching lineation pitching at about 45° southeast. The BCSZ was subsequently reactivated with a dextral sense of shear.

3. The gold occurs as free gold in microbrecciated zones in laminated quartz-carbonate lodes and is directly associated with galena, gersdorffite, tetrahedrite \pm sphalerite and tourmaline.
4. Four alteration zones are distinguished in the Kitchener deposit: a talc-chlorite zone in the BCSZ mylonite, a chlorite-carbonate zone at the boundary between the mylonite and boudin and a carbonate-quartz and fuchsite-carbonate zone in the boudin.
5. The temperature during gold deposition was ca. 250°C, as determined from chlorite thermometry. This temperature is consistent with the mineral assemblages in the alteration envelope.
6. Enrichment/depletion analysis indicates that the gold alteration envelope was enriched in Na₂O, K₂O, Rb, Pb, As and Sb.
7. Dolomite has a constant stable isotope composition throughout the alteration envelope, indicating one alteration event in the boudin.
8. All chemical characteristics of the alteration related to gold mineralization (mineralogy, assemblages, depletion/enrichment of elements and light stable isotope composition of dolomite) are consistent with results from other greenschist-facies Archean lode gold deposits.
9. Pb-Pb model ages of galena are ca. 3400 Ma, providing a maximum age of gold mineralization. This age for gold mineralization is in agreement with age constraints in the area for the BCSZ between 3454 and 3300 Ma.
10. The gold mineralization at Bamboo Creek is tentatively correlated to a regional extensional tectonic event. This is in contrast to the majority of Archean lode-gold deposits, which are generally thought to be related to compressional events.

Constraints on the timing of deformation and metamorphism in the Shaw Batholith area: U-Pb and $^{40}\text{Ar}/^{39}\text{Ar}$ dating

8.1 Introduction

In Archean terrains, isotopic dating is the only reliable source of information on the absolute age of rocks or geological events. Lithostratigraphic correlations in the greenstone belts have been shown to be incorrect on many occasions, because very similar sequences may have formed during different time intervals. Similarly, the age of granitoids can not be reliably distinguished on the basis of field characteristics or geochemical characteristics.

Large scale numerical models on the cooling history, crustal growth and geodynamics of the early Earth (e.g. Vlaar, 1986; Vlaar et al., 1994; Stein & Hofmann, 1994; Davies, 1995, see also Chapter 2) are difficult to compare and test with field observations in Archean terrains due to differences in scale and in depth of observations. However, many of the models predict episodic magmatic events and this can be compared to episodic tectonothermal events in various Archean terrains. Isotopic age constraints combined with regional structural studies are a prerequisite for such a comparison.

In the Pilbara, previous geochronological studies (see Chapter 3 and Figure 3.1 for an overview) were usually aimed at dating the age of the crystallization of granitoids or volcanics. Samples were not chosen to provide information on the structural evolution and often sample locations are not given in sufficient detail to allow later workers to use the dates in detailed structural interpretations. Furthermore, a number of dating methods (Sm-Nd, Rb-Sr and Pb-Pb) may have relatively large errors (>20 Ma) and are of limited use in reconstructing tectonothermal events.

The three main structural episodes in the eastern Pilbara, described in from Chapter 4, 5 and 6, are an early (3460 Ma) extensional phase with deformation occurring on the Split Rock Shear Zone, a compressional phase involving thrusting (e.g. Central Coongan Shear Zone) and folding, probably during deposition of the Gorge Creek Group (3300 Ma ?) and a late strike-slip phase with deformation occurring on the Mulgandinnah Shear Zone Complex, probably during deposition of the Lalla Rookh Basin (2950 Ma ?). Although broad estimates can be made of the age of these structures by using previously published data, but their precise age constraints are unknown and are the subject of this dating study.

The objectives of this geochronological study are:

- 1 To constrain the timing and nature of the three main structural episodes in the Shaw Batholith

and Coongan Belt, using relations between structures and intrusions and metamorphic mineral growth.

- 2 To date the thermal evolution of the Shaw Batholith area and to establish what caused the metamorphism in and around the Shaw Batholith. Was it caused by contact metamorphism during granitoid intrusion or is there evidence for a regional dynamothermal metamorphic phase?

Two different isotopic dating methods were used: U-Pb dating on zircons from the Shaw Batholith and $^{40}\text{Ar}/^{39}\text{Ar}$ of mainly amphiboles from the Shaw Batholith and Coongan Belt. These two methods provide different types of age information and have different limitations so that they complement each other.

The U-Pb zircon method is used for Si-saturated rocks such as granitoids and felsic volcanic rocks. Zircons usually form during magmatic crystallization and have very high closure temperatures. Therefore U-Pb zircon ages usually represent magmatic crystallization ages. Once formed, zircons are very resistant and preserve the original U-Pb systematics well. Later events can produce complex zircons with metamorphic or second stage magmatic rims (Vavra et al., 1996; Hancher & Rudnick, 1995), providing more age information if the rim is wide enough to be analysed.

The $^{40}\text{Ar}/^{39}\text{Ar}$ method, based on the decay of ^{40}K to ^{40}Ar , can be used on rocks or minerals that contain potassium (muscovite, biotite, amphiboles). Different minerals have different closure temperatures (T_c) for ^{40}Ar gas and therefore record different cooling ages. Most of the dates in this study come from amphiboles, which are assumed to have a closure temperature between 500 and 550°C (McDougall & Harrison, 1988). The $^{40}\text{Ar}/^{39}\text{Ar}$ age records the moment that the mineral cooled below the closure temperature for the last time. The closure temperature is generally well below the solidus temperature of the magma, so it will represent the cooling age of the magma body or alternatively the cooling age of a subsequent thermal event at a later stage.

The concept of a single closure temperature for minerals has been under discussion for a long time. The retention capability of minerals for Ar-gas is controlled by other factors than temperature alone, such as rate of cooling, chemical composition, exsolution (particularly in hornblende), fluid interaction and deformation (Hanes, 1991; Chopin & Maluski, 1980; Kerrich & Cassidy, 1994; Lister and Baldwin, 1996).

The combination of $^{40}\text{Ar}/^{39}\text{Ar}$ and U-Pb zircon dating in this study provides a range of age information on the rocks that have been dated, but also provides an independent check on the methods because of the necessary internal consistency of data on a single sample. An overview of previous dating in the Shaw Batholith and Coongan Belt area is shown in Figure 8.1.

8.2 $^{40}\text{Ar}/^{39}\text{Ar}$ dating

8.2.1 Background

Two previous $^{40}\text{Ar}/^{39}\text{Ar}$ dating studies were undertaken in the eastern Pilbara. Wijbrans & McDougall (1987) reported step heating experiments on samples from the Tambourah Greenstone Belt and western Shaw Batholith area (Figure 8.1). The main result from this study was a ca. 3200 Ma cooling age after regional amphibolite facies metamorphism as inferred from blue-green hornblendes, and ca. 2950 Ma cooling ages from olive green hornblendes and muscovites from the greenstones close to

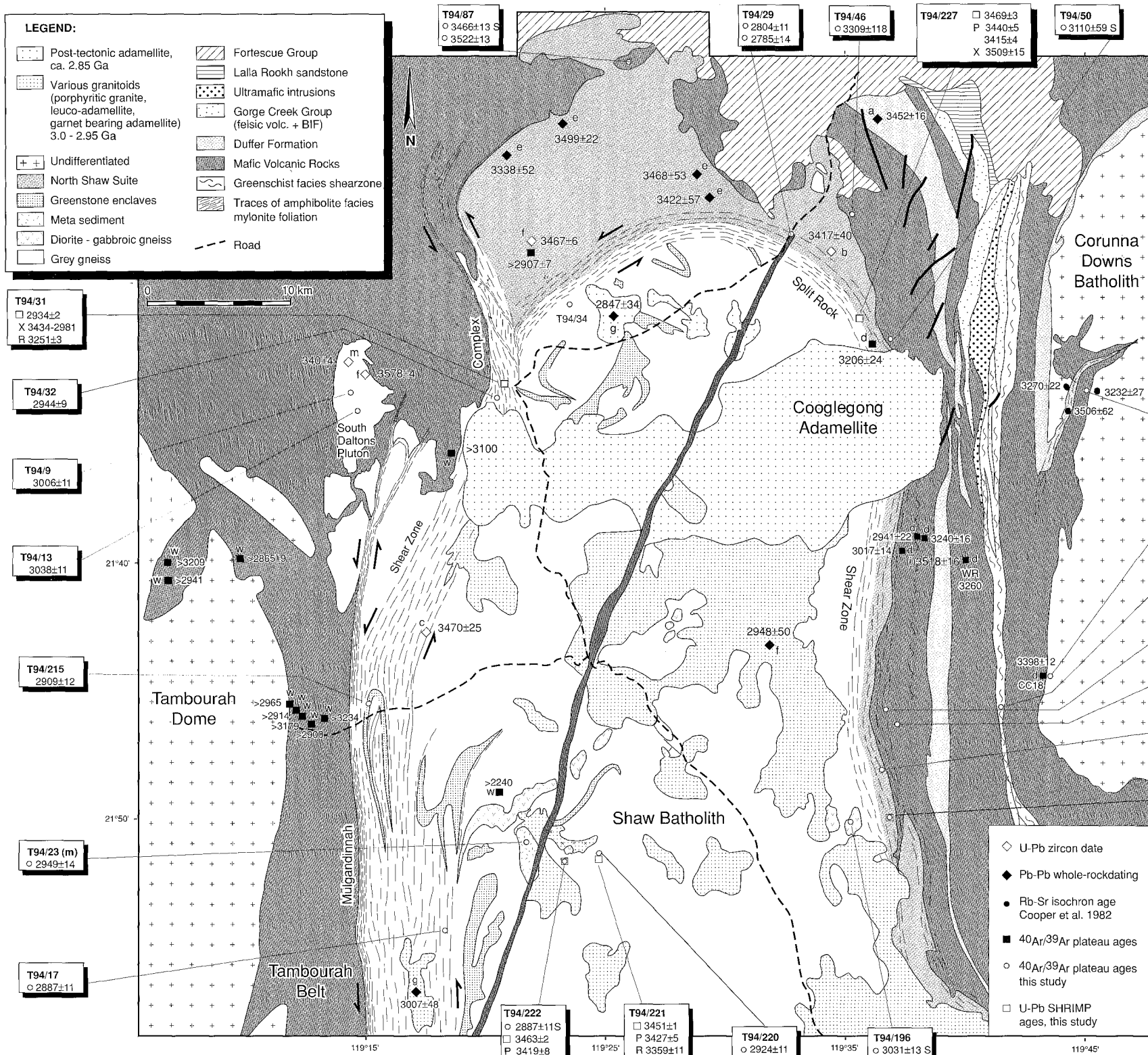


Figure 8.1 Map of the Tambourah Belt, Shaw Batholith and Coongan Belt, showing lithologies and major structures. Previous $^{40}\text{Ar}/^{39}\text{Ar}$, U-Pb and Pb-Pb dating sample locations are shown as well as sample locations in the present study. The letters next to the dates refer to the following references: a=Pidgeon (1978a), b=Pidgeon (1978b), c=Williams et al.(1983), e=Pidgeon (1984), f=McNaughton et al.(1988), g=Bickle et al. (1989), l=Bickle et al. (1993), m=McNaughton et al. (1993), w= Wijbrans et al. (1987), d= Davids et al. (in press), (i)= $^{40}\text{Ar}/^{39}\text{Ar}$ isochron age, Rb-Sr isochron data are by Cooper et al. (1982). $^{40}\text{Ar}/^{39}\text{Ar}$ plateau ages and U-Pb zircon ages from this study are shown in boxes. $^{40}\text{Ar}/^{39}\text{Ar}$ plateau ages were measured on hornblende, except T94/23 (muscovite) and T93/122 (biotite), all errors are 2σ -errors, X= xenocrystic zircon, R= recrystallized part of zircon, P= pooled age other than crystallization age.

- ◇ U-Pb zircon date
- ◆ Pb-Pb whole-rock dating
- Rb-Sr isochron age Cooper et al. 1982
- $^{40}\text{Ar}/^{39}\text{Ar}$ plateau ages
- $^{40}\text{Ar}/^{39}\text{Ar}$ plateau ages this study
- U-Pb SHRIMP ages, this study

the granitoids.

Davids et al. (1997) report a number of $^{40}\text{Ar}/^{39}\text{Ar}$ experiments on hornblendes from the Coongan Belt. The main results are cooling ages between 3260 Ma and 3200 Ma for hornblendes from amphibolites in the Coongan Belt, a cooling age of ca. 2950 for actinolites in a greenschist facies shear zone and a ca. 3400 Ma cooling age for contact metamorphic hornblendes next to the Corunna Downs Batholith.

Here, the results of 24 $^{40}\text{Ar}/^{39}\text{Ar}$ step heating experiments (22 hornblende, 1 biotite, 1 muscovite) of samples from the Shaw Batholith and Coongan Belt are reported. The samples were collected during a structural/kinematic field study in the Shaw Batholith and the Coongan Belt with the primary aim of placing temporal constraints on large-scale structures in the area: the Split Rock Shear Zone (Chapter 5), the Central Coongan Shear Zone (Chapter 6) and the Mulgandinnah Shear Zone (Chapter 7).

By combining the results of this study and those of the previous two studies, the thermal evolution can be interpreted over the larger area between the Corunna Downs Batholith and the Yule Batholith.

8.2.2 Structural context and description of samples.

A detailed description and analyses of the structures and kinematics is presented in previous Chapters. Figure 8.1 shows the major shear zones with their kinematics of the area where the samples were collected for dating. Table 8.1 gives the coordinates of the sample location, characteristics and setting of the samples. The groups of samples, and where necessary additional details of the samples will be discussed below.

8.2.2.1 Eastern Coongan Belt and adjacent Corunna Downs Batholith

Three samples were collected in the eastern Coongan Belt/ Corunna Downs area: T94/203 and T93/182 and T93/122.

T94/203 is a sample from an undeformed amphibolitic pillow basalt a few meters from the intrusive contact with the Corunna Downs Batholith. The granitoid intrudes syn-kinematically into the Warrery Shear Zone one km to the west (Chapter 6). The sample is expected to provide the cooling age of the Corunna Downs granitoid and thereby a minimum age of the Warrery Shear Zone.

T93/122 is a sample of the southern Corunna Downs Batholith next to the Coongan Belt contact. It was sampled next to the CC18 sample described by Davids et al. (1997), which gave a hornblende cooling age of ca. 3400 Ma. Since no hornblende was present in sample T93/122, biotite was used, although it has a lower closure temperature (300–350°C, McDougall & Harrison, 1988).

T93/182 was collected in the Central Coongan Shear Zone. It has a mylonitic foliation formed by talc, chlorite and opaques. Colorless clear amphiboles form rosette shaped porphyroblasts that grow across the mylonitic foliation (Figure 5.6h). The cooling age of the actinolites is expected to provide a minimum age for the CCSZ.

8.2.2.2 The Split Rock Shear Zone, North Shaw Suite and the western Coongan Belt.

A range of samples was collected to provide information on the cooling history of the Split Rock Shear Zone and its foot and hanging wall. From crosscutting, intrusive and structural relations (Chapter 4) the SRSZ was inferred to have been an extensional detachment zone active at ca. 3460

Table 8.1 $^{40}\text{Ar}/^{39}\text{Ar}$ sample co-ordinates, description, grainsize and summarized results.

Sample Lithology	grid ref. E/S	petrography, microstructure	Other comments	a _{size}	b _{fusion age}	T ₁ plateau	d% ³⁹ Ar	eT ₂ , exc.Ar	f ^{Significance}
Eastern Coongan Belt and Corunna Downs Batholith									
T94/203 amphibolite	783.9 7612.2	granoblastic texture plag, opa _q , ol.gr.hbl, relict br.hbl	undeformed metabasalt, few metres from intrusive Corunna Downs granitoid	hbl 150- 250	3338±9	3341±13	89.3	3200	Well defined T ₁ is cooling age after amphibolite facies contact metamorphism, the minimum age of granite intrusion and the minimum age of the Warrery Shear Zone. T ₂ is a minimum estimate of the age of overprinting.
T93/182 talc-chlorite mylonite	777.8 7592.8	foliation: tlc, chl, opa _q porphyroblast: act	actinolites grow randomly over the mylonitic foliation	act 150- 300	3177±9	3197±44	92.1	2800 excess argon	Well defined T ₁ is the cooling age of actinolite and provides a minimum cooling age after metamorphism and a minimum age for the Central Coongan Shear Zone. T ₂ is a minimum estimated age for overprinting.
T93/122 Corunna Downs granodiorite	781.0 7594.9	plag, Kfs, bt	undeformed, sampled next to metabasalt with hbl cooling age 3400 Ma (Davids et al., 1997)	Bt 250- 500	incomplete analysis	2987±10	50.5		T ₁ is well defined and is the biotite cooling age (T _c =300-350°C). For the Corunna Downs Batholith.
Southern Traverse Shaw Batholith/ Coongan Belt									
T94/220 diorite gneiss	747.9 7582.5	d.gr.hbl, l.gr.opx, plag (alt), qtz, sph granoblastic with weak shape preferred orientation of hbl	weakly foliated	hbl 500- 1000	2933±9	2924±11	98.2	excess argon	The well defined T ₁ is the cooling age for the diorite gneiss in the central part of the Shaw Batholith.
T94/222 diorite gneiss	747.9 7582.5	d.gr.hbl, l.gr.opx (alt), plag, qtz, sph granoblastic texture with weak shape preferred orientation of hbl	weakly foliated U-Pb SHRIMP age 3463±2 Ma (this study)	hbl 500- 1000	2864±9	2878±12 S	72.6	2750- 2930 excess argon	The well defined T ₁ is the cooling age for the diorite gneiss in the central part of the Shaw Batholith. T ₂ is a minimum estimated age for overprinting.
T94/196 diorite gneiss	767.1 7585.1	d.gr.hbl, l.gr.opx (alt), plag, qtz,sph granoblastic with weak shape preferred orientation of hbl	weakly foliated very coarse grained (hbl> 1cm) occurs as boudins in grey gneiss	hbl 250- 500	3052±9	3031±13 S	59.9	2800 excess argon	Disturbed age spectrum. T ₁ is semi-plateau cooling age of the eastern part of the Shaw Batholith. T ₂ is a minimum estimated age for overprinting.
T94/193 N. Shaw granodiorite	768.5 7583.6	plag, Kfs (alt), qtz, bt, gr.hbl, sph, ep weak undulose extinction of qtz	protomylonitic foliation/lineation U-Pb SHRIMP age 3462±3 Ma (this study)	hbl 250- 500	3034±9	3028±12	99.2	excess argon	Slightly disturbed age spectrum. T ₁ is cooling age of the North Shaw Suite close to the greenstone contact.
T94/181 N.Shaw granodiorite	768.5 7589.2	plag, Kfs (alt), gr.hbl, qtz, ep undulose extinction of hbl, qtz, recrystallized	mylonitic foliation/lineation, S-C fabric indicates E up sense of Shear	hbl 250- 1000	3230±9	3222±13	90.2	<3136 excess argon	The well defined plateau age T ₁ is the cooling age of the North Shaw Suite in the Split Rock Shear Zone, next to the greenstone contact.

Table 8.1 Continued.

Sample Lithology	grid ref E/S	petrography, microstructure	Other comments	^a size	^b fusion age	^c T1 plateau	^d % ³⁹ Aru	^e T2, exc.ar	^f Significance
Southern Traverse Shaw Batholith/ Coongan Belt									
T94/185i Amphibolite mylonite	769.0 7589.2	hbl, qtz, opa ^q mylonitic fabric with porphyroclasts of br.gr hbl, tails of blue hbl, aligned inclusions in br.gr.hbl	mylonite from hanging wall of SRSZ, E up sense of shear. Fine blue hbl is used here	hbl 150- 250	2994±9	2959±15	100.0		Accidental too large first step (see text). T ₁ is the age of cooling of hornblende porphyroclasts in the Split Rock Shear Zone
T94/185ii idem	769.0 7589.2	idem	idem coarse br.gr.hbl is used here	hbl 500- 1000	2969±9	2993±21	81.6	2000	The well defined plateau age T ₁ is the cooling age of blue-green hornblendes in the tails of porphyroclasts in the Split Rock Shear Zone. T ₂ is a minimum estimated age for overprinting.
T94/189 amphibolite	769.0 7589.2	coarse (1 cm) interlocking gr.hbl, qtz, bt, carb, opa ^q aligned inclusions in hbl	undeformed sample next to the SRSZ, sampled next to T94/185	hbl 250- 500	3043±9	3075±15	71.8	2800	The well defined plateau age T ₁ is the cooling age of the undeformed amphibolite next to the Split Rock Shear Zone. T ₂ is a minimum estimated age of overprinting.
North of the Cooglegong Adamellite									
T94/50 amphibolite	768.6 7620.0	mainly hbl, minor plag, chl, ep, opa ^q porphyroclasts of br.gr.hbl, tails of gr.hbl, random blue hbl	mylonite in SRSZ with static thermal overprint	hbl 250- 500	2374±36	3110±59 S	23.6	1200	Very disturbed age spectrum. The last three steps define an age plateau, T ₁ , but its geologic value is uncertain.
T94/46 amphibolite	767.2 7626.3	interlocking hbl and minor chl, plag, sph, opa ^q magmatic br.hbl cores rimmed by gr.hbl	undeformed metadolerite at contact between Shaw batholith and Coongan Belt	hbl 250- 500	3312±9	3309±118	100.0		The well defined plateau age T ₁ is the cooling age after amphibolite grade metamorphism of the undeformed dolerite dike.
T94/87 amphibolite	748.3 7637.6	hbl, plag, ep, opa ^q , qtz. Complex texture, see text	undeformed metabasalt, sampled next to N.Shaw Suite	hbl 500- 1000	3439±10	3466±13 S	88.4	2800	The plateau age T ₁ is the cooling age of metamorphism related to the intrusion of the North Shaw Suite (see text). T ₂ is a minimum estimated age of overprinting.
T94/87 dupl idem	748.3 7637.6	idem	idem	hbl 500- 1000	3599±11	3522±13	50.7	excess argon	The well defined plateau age T ₂ could be the cooling age after crystallization of the basalt/dolerite (see text).
T94/34a amphibolite	747.6 7622.7	gr.hbl, plag (alt), qtz, ep, opa ^q foliation formed by hbl	foliated amphibolite enclave in gneiss south of MSZC	hbl 250- 500	2797±11	2950±14 S 2877±18 S	31.6 24.3		Very disturbed age spectrum. Two semi plateau ages may have geologic significance (see text).

Table 8.1 Continued.

Sample Lithology	grid ref E/S	petrography, microstructure	Other comments	^a size	^b fusion age	^c T1 plateau	^d % ³⁹ Ar	^e T ₂ , exc.ar	^f Significance
Mulgandinnah Shear Zone Complex area									
T94/32 amphibolite	742.0 7616.0	d.gr.hbl porphyroclasts, tails of chl, ep, matrix qtz, plag, sph	mylonitic boudin in the MSZC	hbl 250 500	2950±9	2944±9	97.3	2800 excess argon	The well defined plateau age T ₁ is the cooling age of the amphibolite boudin in the Mulgandinnah Shear Zone Complex, and provides a minimum age for the central part of the MSZC. T ₂ is a minimum estimated age of overprinting.
T94/215 amphibolite	731.5 7592.3	d.gr.hbl, plag, qtz, ep, sph recrystallized to granoblastic texture	foliated enclave in the MSZC forming the km-scale sheath fold	hbl 150- 500	2978±9	2909±12	94.4	excess argon	The well defined plateau age T ₁ is the cooling age of the amphibolite enclave in the Mulgandinnah Shear Zone Complex and provides a minimum age for the central part of the MSZC.
T94/17 granodiorite	735.8 7575.6	gr.hbl, plag (alt), Kfs, ep, sph aligned hbl and qtz ribbons	mylonitic foliation, from outer MSZC	hbl 250- 500	2891±9	2887±11	98.1	excess argon	The well defined plateau age T ₁ is the cooling age of the outer part of the MSZC.
T94/23 sillimanite gneiss	743.0 7584.5	qtz, fibrolitic sillimanite, musc.	metapelitic enclave in the Shaw Batholith, east of the MSZC. Strong SL and folded	musc 250- 500	2974±14	2949±14	99.4		The well defined plateau age is the muscovite cooling age (T _c ~ 350°C) of the sillimanite gneiss enclave in the Shaw Batholith east of the MSZC.
T94/9 granodiorite	731.5 7615.3	Kfs (alt), plag, qtz, bl.gr. hbl, ep, sph, statically recrystallized mylonitic Texture	pre-MSZC mylonitic foliation (see text)	hbl 250- 500	2969±9	3006±11	72.0	2575	The well defined plateau age T ₁ is the cooling age of the pre-MSZC shear zone in the South Dalton Pluton area. T ₂ is a minimum estimated age of overprinting.
T94/13 amphibolite	731.5 7615.3	ol.gr.hbl, plag (alt), qtz, sph recrystallized to granoblastic texture	foliated sample from enclave in the South Dalton Pluton	hbl 250- 500	3161±10	3038±11	78.2	2630 excess argon	The well defined plateau age T ₁ is the cooling age of the amphibolite enclave in the South Dalton Pluton area. T ₂ is a minimum estimated age of overprinting.
Black Range Dolerite Dyke									
T94/29 dolerite	762.8 7626.0	plag, hbl, chl undeformed	Sample from the coarse grained core of the Black Range Dyke	hbl 250- 500	2832±9	2804±11	75.5	excess argon	The well defined plateau age T ₁ is the cooling age after crystallization of the Black Range dolerite dike.
T94/29 duplo idem	762.8 7626.0	idem	idem	hbl 250- 500	2783±6	2785±14	86.4	2700	The well defined plateau age T ₁ is the cooling age after crystallization of the Black Range dolerite dike. T ₂ is a minimum estimated age of overprinting.

^a Mineral used for step heating experiment and grainsize in μm . ^b Calculated age for summed intensities, should be equal to single fusion age. ^c Ages in this column are best estimates for the cooling age of the sample, following the convention for the definition of plateaus (McDougall & Harrison, 1988). Those indicated with S are semi-plateaus. ^d Percentage of total ³⁹Ar in the plateau. ^e Ages in this column are estimates for the time of overprinting, based on the low ages in the low temperature part of the age spectrum. ^f A brief statement on the structural and metamorphic significance of the each age spectrum is given. tlc= taic, chl= chlorite, act= actinolite, hbl= hornblende, plag= plagioclase, opa= opaques, Kfs= K-feldspar, bt= biotite, opx= orthopyroxene, sph= sphene, ep= epidote, qtz= quartz, (alt)= altered, gr= green, br= brown, bl= blue, ol= olive, l=light, d= dark

Ma. The collected samples were aimed at confirming the timing of tectonic activity on the SRSZ and to provide an insight in the nature (extensional vs. compressional) of the SRSZ. If the SRSZ was an extensional structure, the upper block would have remained relatively cool (at shallow depth), whereas the lower block was brought up and cooled during the uplift. Therefore, the cooling ages of the lower block would be younger than cooling ages of the same mineral in the upper block. In a compressive structure this pattern would be inverted, with younger ages in the upper block and older ages in the lower block. This is a simplified model and is complicated by syn-tectonic intrusions of granite. It can only give good results if the area is not heated after activity on the shear zone, thereby destroying the signals related to movement on the shear zone.

Southern traverse

Samples in this traverse through the lower and upper block of the SRSZ are T94/220, T94/222, T94/196, T94/193, T94/181, T94/185 and T94/189 (see Figure 8.1 for locations).

The footwall block samples (T94/220, T94/222, T94/196) were collected in grey gneisses and dioritic gneisses, assumed to be 3460 Ma or older, in the core of the Shaw Batholith, as far as possible away from younger granitoids. T94/222 is also used for SHRIMP dating (see §8.3)

T94/193 and T94/181 are samples of the North Shaw Suite granodiorite, collected close to the contact with the greenstones. They were collected to provide a cooling age for the North Shaw Suite in the SRSZ. Both samples are weakly foliated and lineated. T94/181 shows a well developed S-C fabric on a 2 cm scale, indicating an east up sense of shear. T94/193 was also used for U-Pb SHRIMP dating. T94/185 and T94/189 are samples of greenstone belt amphibolites from the hanging wall of the SRSZ. They were collected to provide a cooling age of the amphibolite grade metamorphism associated with deformation in the SRSZ.

T94/185 is an amphibolite mylonite and contains two generations of hornblende: brown-green rounded hornblende porphyroclasts and finer needle shaped blue green hornblendes in the tails of the porphyroclasts and in the matrix. The porphyroclast hornblendes contain abundant aligned inclusions of quartz and opaques (Figure 4.5b). Two grain size separates were made of this sample, to distinguish the porphyroclasts from the hornblende in the tails.

Sample T94/189 was taken close to T94/185 but does not show the mylonitic foliation. The interlocking hornblende grains do contain an aligned inclusion pattern, indicating a previous foliation, before growth of metamorphic hornblende.

North of the Cooglegong Adamellite

Three samples were collected in the greenstones north of the Cooglegong Adamellite, i.e. in the upper block of the SRSZ: T94/50, T94/46 and T94/87.

T94/50 is a coarse (>0.5cm)-grained foliated and lineated amphibolite. Three different generations of hornblende can be distinguished. Brown-green rounded hornblende grains occur as porphyroclasts, green hornblende occurs in the tails of porphyroclasts and forms the foliation and lineation. A third group of blue green hornblende grains grew randomly over the foliation.

T94/46 is a coarse-grained undeformed metadolerite at the contact between the Shaw Batholith and the Coongan Belt.

T94/87 is an undeformed metabasalt sampled next to the contact with the North Shaw Suite. The amphibolite is very coarse-grained close (<2cm) to irregular aplite dykes, but otherwise it is gener-

ally fine-grained. The fine-grained part consists of a network of brown-green hornblende rimmed by green hornblende, and a matrix of plagioclase, epidote, opaques and minor quartz. The coarse-grained part consists of large clean brown hornblende grains and large quartz grains in equal proportions. The hornblende grains usually have a thin rim of fine-grained epidote.

8.2.2.3 The Mulgandinnah Shear Zone Complex

A number of samples were collected from within, and close to, the high strain zones of the MSZC to determine the cooling age of the amphibolite grade metamorphism during deformation. Two samples were collected in the South Daltons Pluton to determine whether the thermal evolution of this area was distinctly different from that to the east of the MSZC.

T94/32 and T94/215 were sampled from a m-scale amphibolite boudin in the ultramylonite part and an amphibolite enclave in the mylonitic part of the MSZC, forming the km-scale fold of the MSZC (see Chapter 7). T94/32 was sampled close to the SHRIMP sample T94/31 (§8.3).

T94/17 is a sample from the outer part of the MSZC in a hornblende granodiorite.

T94/23 is a sample from a sillimanite gneiss enclave in the Shaw Batholith, to the east of the MSZC. The rocks in the enclave are strongly foliated, lineated and folded with the foldaxis parallel to the lineation. The muscovite (T_c ca. 350°C, McDougall & Harrison, 1988) was analysed to determine whether it would give consistent cooling ages with hornblende in the area.

T94/9 and T94/13 are samples from the South Daltons Pluton. T94/9 is a mylonitic granodiorite with a foliation and lineation (steeply plunging) which do not fit with the MSZC and probably represents an earlier deformation event. T94/13 is a foliated coarse-grained amphibolite sampled from an enclave in the South Daltons Pluton.

8.2.2.4 Black Range Dolerite Dyke

T94/29 is a sample from the core of the Black Range dolerite dyke at the northern end in the Shaw Batholith. The Black Range postdates all structures in the eastern Pilbara, except for occasional local brittle faults. No reliable age is available of the Black range, but it is constrained between 2.77 Ga (base of the Fortescue Group, U-Pb SHRIMP, Arndt et al., 1991) and 2.85 Ga (Cooglegong Adamellite, Bickle et al., 1989).

8.2.3 Sample preparation and analytical method

The samples were crushed and sieved, and based on the crystal size in the thin sections, an optimum sieve fraction between 150 and 500 μm was selected for further separation by hand. Clean separates of hornblende, muscovite and biotite were then selected by hand-picking under a microscope. For large grain sizes only a few grains (1–3) were selected, for finer grain sizes (150–250 μm) ca. 50 grains were selected (see table 1 for grain sizes per sample). During the hand-picking care was taken to select clean, pure mineral grains. Before and after hand-picking the grains were ultrasonically cleaned in H_2O to remove dust particles.

The mineral separates were loaded on a 2 cm diameter aluminium tray with 20, 2 mm wide, holes. On each tray 4 holes were loaded with flux monitors (ANU standard biotite GA1550, K/Ar age 97.9 Ma). The 16 remaining holes were loaded with the separates from the samples. The trays were wrapped in aluminium foil and stacked in an aluminium can. Samples were irradiated in a rotating

facility in the ECN/EU high flux research reactor in Petten (NL) for 150 hours. The irradiation parameter J was determined separately for each tray and was 0.04364, 0.04361 and 0.04363 depending on the tray. The uncertainty of J was 0.3% per tray.

The separates were degassed stepwise, using a defocused laser beam. Details of the extraction and purification have been described in Wijbrans et al. (1995). The isotopes of the purified argon gas were measured using a MAP 215-50 noble gas spectrometer.

Corrections were made for interferences by atmospheric argon and argon isotopes produced from potassium and calcium during irradiation (correction factors for this irradiation: $(^{40}\text{Ar}/^{39}\text{Ar})\text{K} = 0.07361$, $(^{39}\text{Ar}/^{37}\text{Ar})\text{Ca} = 0.000699$ and $(^{36}\text{Ar}/^{37}\text{Ar})\text{Ca} = 0.00027$). The measured amounts of ^{39}Ar and ^{37}Ar were corrected for radioactive decay. The discrimination factor for the mass spectrometer was determined at $1.0030 \pm 0.3\%$ per mass unit for this study, using small aliquots of air argon. System blanks were measured every five steps and were used for a blank correction on the data, based on two blanks for each correction. Over the course of the experiments, the range of observed blanks was: ^{36}Ar $4.3\text{--}22.6 \times 10^{-20}$ mole, ^{37}Ar $2.8\text{--}12.2 \times 10^{-20}$ mole, ^{38}Ar $10.6\text{--}94.1 \times 10^{-20}$ mole, ^{39}Ar $1.5\text{--}3.4 \times 10^{-20}$ mol and ^{40}Ar $12.6\text{--}121.4 \times 10^{-20}$ mole. Within a single experiment (1–2 days) the variation was less than a third of the observed total range.

Most samples were measured once, but duplicates were measured of sample T94/87 and T94/29.

8.2.4 Results of $^{40}\text{Ar}/^{39}\text{Ar}$ dating.

The complete data set of all experiments are given in Appendix 1. The age spectra for all experiments are shown in Figure 8.2. Most age spectra show plateau segments with ages ranging from 3530 to 2785 Ma. All errors in the text and figures are 2σ values. In the following section, the term plateau is used as defined by McDougall & Harrison (1988), i.e. at least 3 subsequent steps within 2σ error. Where plateaus are less well defined, for example where one or two steps are not within 2σ error, the term semi-plateau is used. In all hornblende step-heating experiments the K/Ca ratios are low (< 0.1) except for some of the initial steps with excess argon. The results are summarized in Table 8.1, only samples with irregular or in some way anomalous results are discussed in more detail here.

T93/122 biotites produced so much argon gas in the first two steps of the experiment that it surpassed the measuring capacity of the mass spectrometer. The first two steps (50% of total ^{39}Ar released) are not shown in the age spectrum and the age spectrum is therefore not reliable. However some information can be gained from the last 6 steps. These define a plateau with an age of 2987 ± 10 Ma, which is interpreted to be the cooling age of the biotites.

T94/222 and T94/196 resulted in age spectra with good plateaus, although these contained a number of significantly lower steps. In T94/222 the anomalous step coincides with an increase of K/Ca so it may be caused by exsolution effects in the hornblende or may be due to some fractionation problem in the mass spectrometer. In T94/196 the K/Ca ratio is constant over all the steps (at ca. 0.08) and does not offer an explanation for the two lower steps.

For sample T94/185 age spectra of two different grain size separates were determined ($i = 100\text{--}250 \mu\text{m}$, $ii = 500\text{--}1000 \mu\text{m}$). T94/185i was accidentally heated too fast, causing the release of 83% of the total ^{39}Ar within the first step. The plateau age is 2959 ± 15 Ma whereas the total fusion date is 2993 ± 9 Ma. T94/185ii shows a convex shaped age spectrum with the initial step at ca. 2000 increasing to a well defined plateau at 2993 ± 21 Ma. The total fusion date of the fine-grained hornblende and the

Eastern Coongan Belt and Corunna Downs Batholith

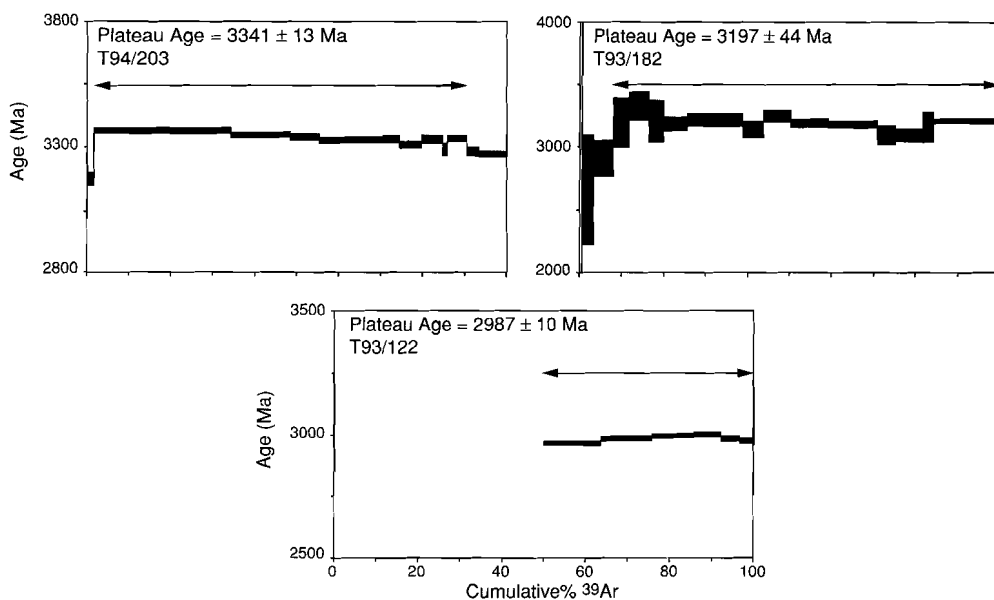


Figure 8.2 $^{40}\text{Ar}/^{39}\text{Ar}$ age spectra for all samples in this study, errors are 2σ , in both figure and plateau age. All analytical data are given in Appendix 1.

plateau age of the coarse-grained hornblende are indistinguishable and are interpreted as the cooling age of both hornblendes types.

T94/50 hornblendes show a distinctly U shaped age spectrum with an anomalously high first step followed by anomalously low steps (ca. 1000 Ma). The last three steps could be used to define a plateau at 3110 ± 60 Ma. In view of the extremely disturbed age spectrum the geologic value of this date remains unclear. The inverse isochron plot shows that the anomalously low steps are due to an increase of ^{39}Ar .

Two step heating experiments were carried out on hornblendes from sample T94/87. The first age spectrum shows irregularities in the first four steps followed by a semi-plateau over 3 steps (88.4% of the total ^{39}Ar released) with an age of 3466 ± 13 Ma. The plateau contains a number of small steps with first lower dates followed by higher dates, then returning to the level of the plateau. It is not clear what caused the variation in these small steps: the K/Ca ratio remained constant. It may be due to a fractionation problem in the mass spectrometer. The second experiment (T94/87duplo) shows a similar variability in the first steps (40% of ^{39}Ar released) and is followed by a well defined plateau over 60% of the ^{39}Ar released at 3522 ± 13 Ma.

The two plateau ages are not within error of each other. The age spectra and the K/Ca plots show different pattern for the two experiments and the total fusion age is different (3439 ± 10 Ma vs. 3599 ± 11 Ma). This may indicate that the two experiments were done on grains with different geological histories, although they are derived from the same sample. Inverse isochron plots show that

Southern Traverse Shaw Batholith/ Coongan Belt

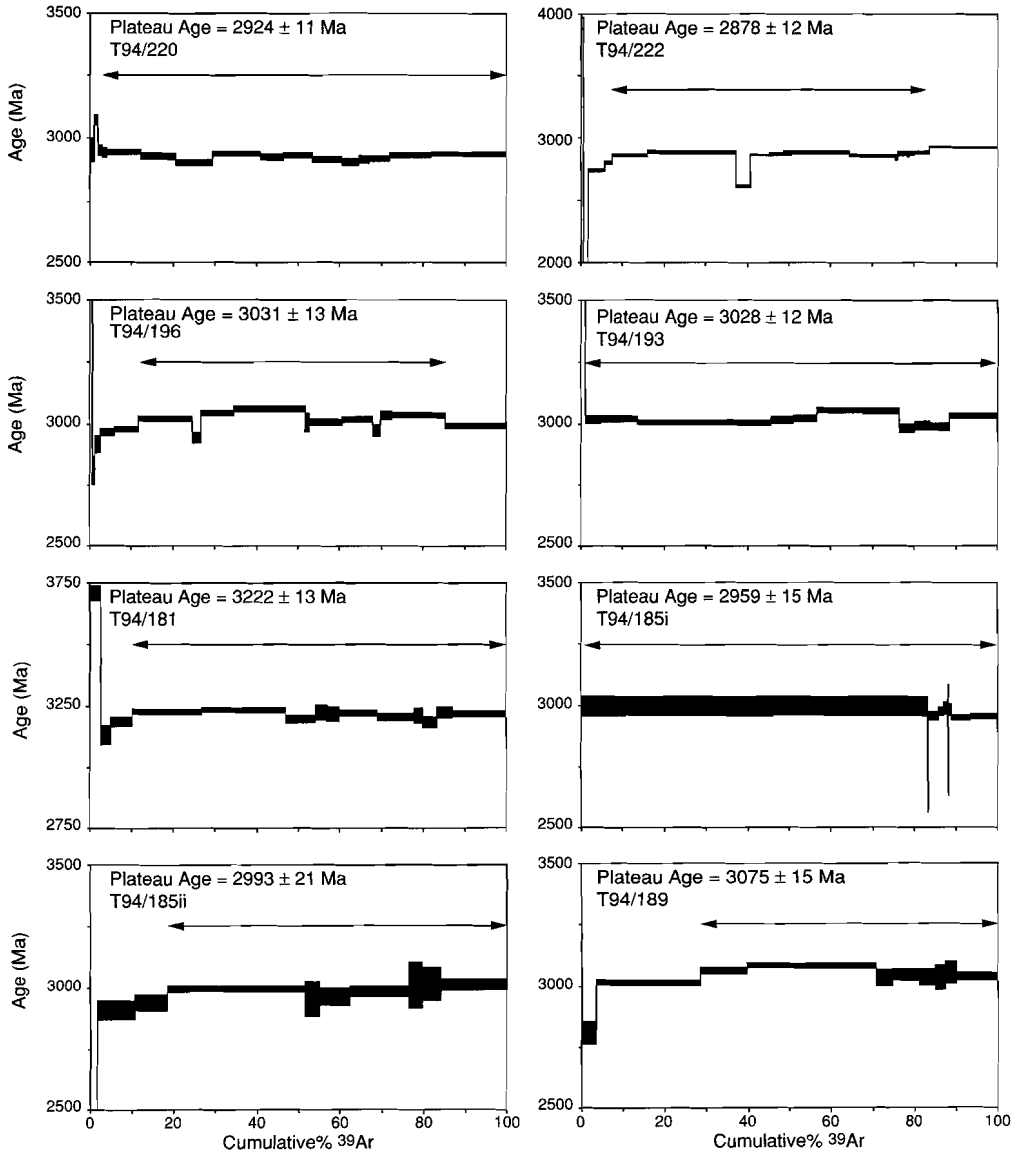


Figure 8.2 Continued.

North of the Cooglegong Adamellite

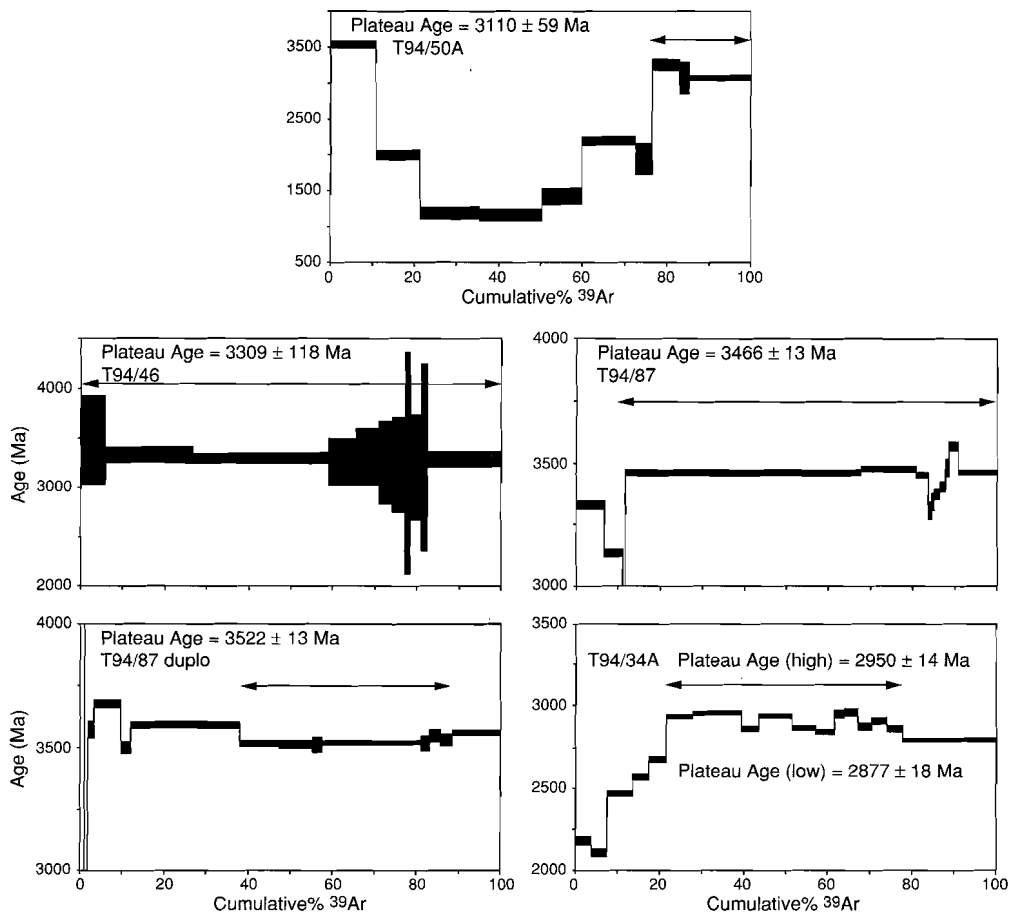
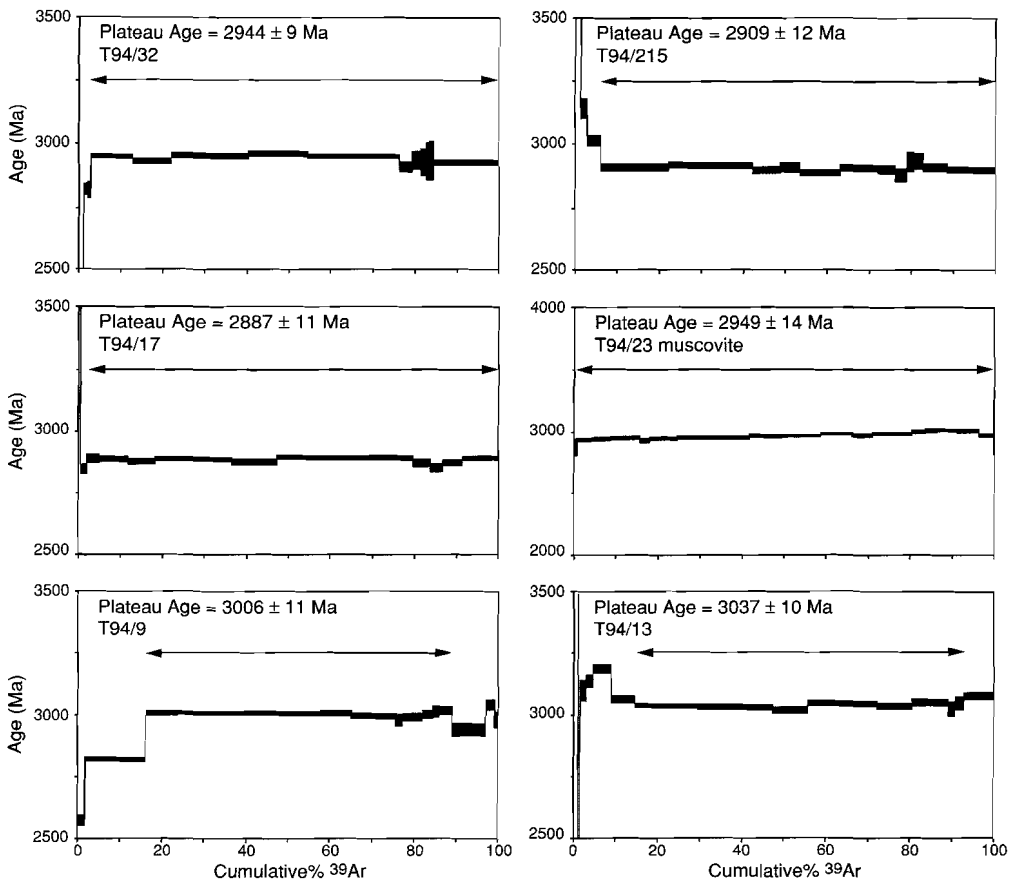


Figure 8.2 Continued.

the anomalous initial age steps in 94/87 are due to mainly ^{39}Ar loss and gain, possibly due to recoil, whereas in 94/87duplo all steps plot close to each other on the $^{39}\text{Ar}/^{40}\text{Ar}$ axis, with some disturbance due to increase of ^{40}Ar (excess argon). This seems to indicate that the grains measured in 94/87duplo are less disturbed than 94/87.

Although the discrepancy in results is not easily explained, it is possible that the first separate contained only the coarse large hornblende grains from the hornblende + quartz zone next to the aplite dyke, whereas the duplo separate also or mainly contained hornblendes from the finer-grained part of the sample. The plateau age of the first experiment (3467 ± 6 Ma) is within error of the U-Pb zircon age of the North Shaw Suite (3466 ± 13 Ma, McNaughton et al., 1988), and is therefore interpreted as the hornblende cooling age of contact metamorphism. The older plateau age of

Mulgandinnah Shear Zone Complex



Black Range Dolerite dyke

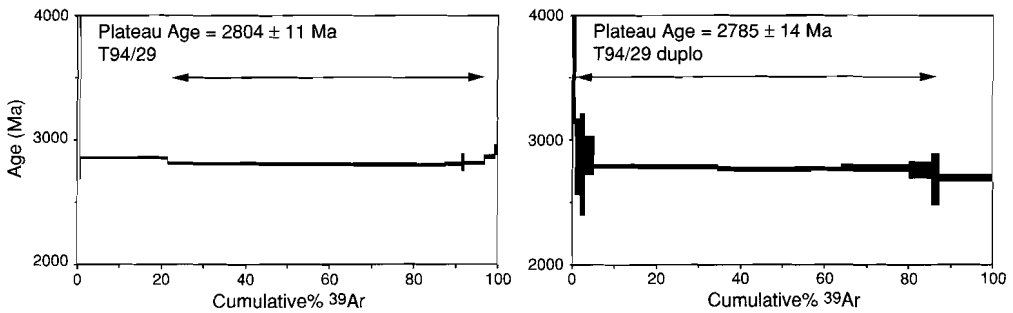


Figure 8.2 Continued.

T₉₄/87duplo can be interpreted in various ways:

- 1 The differences in plateau ages are the result of variable irradiation conditions. This is not likely, because other repeated experiments in this study show consistent results within 2σ error, but it can not be ruled out completely.
- 2 The older plateau age is due to excess argon that was present in the duplo experiment. However, the plateau is defined as the youngest and middle part of the spectrum, for which the inverse isochron plot shows no indication of excess argon.
- 3 The fine-grained part retained the magmatic signature resulting in an older plateau age. As the rock contains a mixture of coarse and fine grains, and is veined with quartz and granitoid, some degree of inhomogeneity is expected.

T₉₄/34 hornblendes from the greenstone enclave in the Shaw batholith show a very irregular age spectrum. The first steps are low (ca. 2100 Ma) increasing in the next four steps to an irregular semi-plateau. This semi-plateau consists of steps alternating between ca. 2950 Ma and ca. 2880 Ma. It is not possible to define a single plateau age for this spectrum. Two separate semi-plateau ages were calculated for the high and low age steps: 2950 ± 14 Ma (32% ³⁹Ar) and 2877 ± 18 Ma (24% ³⁹Ar). Inverse isochron plots indicate that the variation in step ages is mainly due to variations in ³⁹Ar, possibly due to recoil, and may not have a geological significance. The variations in the dates in the semi-plateau can not be explained by fine-grained biotite or exsolution in the hornblendes because the K/Ca ratio remains constantly low (<0.1) over the semi-plateau. The meaning of the two age groups in the semi-plateau remains uncertain.

The two step heating experiments carried out on hornblendes from the Black Range dolerite dyke give similar shaped age spectra, starting with high dates in the first step, followed by a flat part over most of the released ³⁹Ar. T₉₄/29 shows two slightly higher last steps, T₉₄/29duplo shows a slightly lower last step. In both spectra plateaus can be defined with integrated ages of 2804 ± 10 Ma and 2785 ± 14 Ma respectively. The weighted mean of the plateau ages, 2796 ± 9 Ma, is the cooling age of the hornblendes in the dolerite dyke.

8.2.5 Synthesis and structural/metamorphic implications

The step heating experiments generally resulted in age spectra with well defined plateau ages. The spectra typically show disturbances in the first steps, with up to ca. 15% ³⁹Ar released. The first step often gives an unrealistically high age, followed by a very low step with subsequent steps increasing to or slightly above the level of the plateau. In inverse isochron plots the first high step typically falls slightly below the atmospheric argon and radiogenic argon mixing line, indicating an increased ⁴⁰Ar component, i.e. excess argon. The subsequent steps usually plot close to the ³⁹Ar/⁴⁰Ar axis, but vary on a horizontal line, indicating either ³⁹Ar increase or loss. These effects may be due to weathering of the surface of the hornblende grains or may be due to recoil effects in the rims of the hornblendes. In many cases a low initial step can be attributed to ⁴⁰Ar loss, possibly during a later event, if the analysis of the step plots above the mixing line.

The plateau ages determined for the mineral separates are all within the age brackets defined by other dating methods (U–Pb and Pb–Pb) for this part of the Pilbara Craton, i.e. 3.5–2.8 Ga, suggesting that the plateau ages are meaningful in the context of the regional geology. Since the plateau ages of the minerals are all cooling ages, they provide minimum ages for the structures or metamorphism.

Eastern Coongan Belt and Corunna Downs Batholith

Two plateau ages, 3341 ± 13 Ma (T94/203, hornblende) and 2987 ± 10 Ma (T93/122, biotite), provide information on the cooling of the Corunna Downs batholith. They show, in combination with the 3398 ± 12 Ma hornblende cooling age in the southeastern Coongan Belt (Davids et al., in press), that cooling after intrusion of the granitoids occurred at a relatively early stage, in the range between 3341 Ma and 3398 Ma. The younger biotite cooling age indicates that the area was reheated at ca. 2990 Ma to above the biotite closure temperature (300°C), but below the hornblende closure temperature (500°C).

The Warrery Shear Zone was active during granitoid intrusion next to sample T94/203, hence the minimum age of activity on the Warrery Shear Zone is 3341 ± 13 Ma.

The activity on the Central Coongan Shear Zone is constrained by post-kinematic actinolites of sample T94/182 to older than 3197 ± 44 Ma. Since the CCSZ post-dates the 3325 Ma Wyman Formation (McNaughton et al., 1993; Thorpe et al., 1992, Chapter 5), its age is further constrained to between 3325 and 3200 Ma.

The Split Rock Shear Zone, North Shaw Suite and western Coongan Belt

The southern traverse, which was set up to constrain the age and nature (extensional vs. compressional) of the Split Rock Shear Zone, shows the following plateau ages (Figure 8.1), rounded at 10 Ma, from west to east: footwall Shaw Batholith gneisses 2880–2920–3030 Ma, in SRSZ North Shaw Suite 3030–3220 Ma, hanging wall Coongan Belt 2960–2990–3080 Ma. There is no consistent increase or decrease of plateau ages in the traverse. The variation of ages does not appear to be related to their position with respect to the SRSZ. This is particularly obvious for T94/193 and T94/181, which were both sampled in the same structural position, in the SRSZ, but give different plateau ages (3028 ± 12 and 3222 ± 13 Ma respectively). The plateau ages do show a relation to vicinity to younger granites (3.0–2.85 Ga, Bickle et al., 1989), with T94/181 giving the oldest plateau age and further away from late granites.

This shows that this sequence of plateau ages can not provide good constraints on the age and nature of the SRSZ, because they are statically reset by heating due to post-tectonic granite intrusion. The oldest age 3222 ± 13 Ma in the SRSZ provides a minimum age for the shear zone.

In the southwest Coongan Belt two amphibolite samples (T94/185 and T94/189) from the greenstones give interesting results when compared to each other. The two different grain size fractions of the mylonitic amphibolite T94/185 gave plateau ages within error of each other (2993 ± 21 Ma for the coarse grain size and 2959 ± 15 Ma for the fine grain size), indicating post-deformational heating at ca. 2950–3000 Ma, probably due to granite intrusion. The undeformed amphibolite sample T94/189 gave an older plateau age (3075 ± 15 Ma), although the samples were collected very close (20 m.) to each other. This may be an indication that deformed hornblende grains have a lower closure temperature than undeformed grains. Davids et al. (in press) report similar ages for an amphibolite mylonite (3017 ± 14 Ma) from the SRSZ and a greenschist facies shear zone (2941 ± 22 Ma) further to the north. They interpreted these ages as direct evidence for activity of the greenschist facies shear zone at ca. 2950 Ma. This study shows that such an interpretation is not warranted; the cooling age can only provide a minimum age of last activity on the shear zone, but the last activity may have been 500 Ma prior to the cooling age.

North of the Cooglegong Adamellite

The samples north of the Cooglegong Adamellite include three samples taken next to the intrusive North Shaw Suite. Of those T94/50 resulted in a very disturbed spectrum, with a small plateau with a plateau age of 3110 ± 59 Ma. The disturbance may be due to its vicinity to the Cooglegong Adamellite. Of the two other samples next to the North Shaw Suite, the undeformed metadolerite, T94/46, gave a single plateau at 3309 ± 118 Ma, whereas the last sample of the three, T94/87, on which two experiments were done, gave the oldest plateau ages recorded in this study. The younger of the two plateau ages (3466 ± 13 Ma) is interpreted to be the cooling age of intrusion or contact metamorphism of the North Shaw Suite, dated at 3467 ± 6 Ma (U-Pb, single zircon) by McNaughton et al. (1988). The older plateau age of hornblende from the same sample at 3522 ± 13 Ma can be attributed to analytical problems (inhomogeneous radiation of samples), excess argon or as a geological significant age related to magmatic cooling age of this part of the Warrawoona Group, the Talga Talga Subgroup. More experiments on a similar rock would be needed to rule out analytical problems and inhomogeneously distributed excess argon. If the oldest age is a geologically meaningful age this has important implications, because it would indicate that metamorphic resetting can occur on centimetre-scale. Similar ages were obtained from the base of the Warrawoona Group (3560 ± 32 Ma, whole rock Sm-Nd on a suite of mafic to felsic samples) by Hamilton et al. (1981) and for the Coonterunah Succession (3515 ± 3 Ma, U-Pb zircon) by Buick et al. (1995). Davids et al. (in press) report a $^{40}\text{Ar}/^{39}\text{Ar}$ isochron age of 3518 ± 16 Ma for cores of hornblendes in a sample from the SRSZ in the Talga Talga Subgroup in the Coongan Belt (see Figure 8.1). Xenocrystic zircons (this study) from granitoids in the Shaw Batholith are in the same age range, i.e. 3509 ± 15 Ma and 3524 ± 6 Ma.

Sample T94/34 in the western Shaw Batholith gneisses, structurally below the SRSZ, gave a disturbed spectrum, with an estimated cooling age between 2950 and 2880 Ma, i.e. in the range of the late granites and probably reset by contact metamorphic effects.

The Mulgandimah Shear Zone Complex

All samples from the MSZC gave hornblende cooling ages between 2944 and 2887 Ma. This indicates a minimum age for the MSZC of ca. 2900 Ma. To the west of the MSZC two deformed samples from the South Daltons Pluton gave hornblende cooling ages of 3006 ± 11 Ma and 3037 ± 10 Ma, slightly older than the samples from the centre of the MSZC. The muscovite from the sillimanite gneiss sample T94/23 to the east of the MSZC gave a cooling age of 2949 ± 14 Ma, which is similar or older than hornblende cooling ages from the MSZC. The pattern, with slightly older ages outside the MSZC than in the MSZC indicate that the cooling ages within the MSZC, ca. 2900 Ma record the cooling age after amphibolite grade deformation in the MSZC. The argon cooling ages are not enough to provide definite age constraints for the MSZC, but the SHRIMP dating (§8.3) shows that the inferences drawn from the argon cooling ages are correct.

Black Range Dolerite Dyke

The youngest cooling ages in this study at 2796 ± 9 Ma are from the Black Range Dolerite Dyke which intrudes the Shaw Batholith. This cooling age is within the time range for intrusion of the dolerite dyke as constrained by intrusive relations of 2.85–2.77 Ga (Bickle et al., 1989; Arndt et al., 1991) and is interpreted as the cooling age after crystallization of the dolerite dyke.

Of all the age spectra six showed low temperature overprinting ages at ca. 2800, which is likely to

have been caused by the intrusion of the Black Range Dolerite Dyke swarm.

One of the specific aims of this argon dating study, i.e. to provide constraints on the timing and nature (extensional vs. compressional) of the SRSZ, could not be achieved. This is due to the fact that most samples in the Shaw Batholith show cooling ages related to late to post-tectonic granite intrusion (3.08–2.80 Ga). In the resulting plateau ages of this study 4 groups can be distinguished: 2.8 Ga (Black Range Dolerite Dyke), 3080–2880 Ma, 3340–3200 Ma and >3.4 Ga. The significance of the second and third group is further discussed below.

Most cooling ages that were determined are in the range between 3080 and 2880 Ma. This is within the age range of a group of late to post-tectonic granites (3007 ± 48 , 2948 ± 50 and 2847 ± 34 Ma, Pb-Pb, Bickle et al., 1989). These granites occur as a number of large plutons with many smaller satellites in the older gneisses and granitoids. These granites postdate structures in the eastern Shaw Batholith and Coongan Belt (see Chapter 4, 5 and 6). The only area where these late granites show a foliation is in the MSZC in the western Shaw Batholith (Chapter 6). In the rest of the Shaw Batholith they occasionally show brittle deformation. Apparently large parts of the southern Shaw Batholith were statically heated above the hornblende closure temperature during these intrusive events. This thermal resetting effect was particularly strong in the Shaw Batholith, but also occurs in the SW Coongan belt. Wijbrans & McDougall (1987) reported similar ages for post-tectonic olive green hornblendes in the Tambourah Belt. The implication of this regional resetting event is that these late granites are more extensive in the subsurface than apparent from the geological map. The greenstones of the Coongan Belt are not as strongly affected by this late resetting as the Shaw Batholith. This is partly explained by the pattern that late granites preferentially intrude into existing granitoids, but another reason may be that the thermal conductivity of basalts is lower than of granite (1.3–2.9 vs. 2.4–3.8 W/m K, Turcotte & Schubert, 1982), so that the granite-greenstone contact acts as a thermal boundary.

The biotite cooling age of the Corunna Downs Batholith (2987 ± 10 Ma) shows that this late thermal event also occurred in the Corunna Downs Batholith, but the temperatures reached were not high enough to reset hornblendes (Davids et al., in press) from greenstones next to the granitoid.

Of the group with cooling ages between 3340 and 3200 Ma the oldest is the 3341 ± 13 Ma (T94/203) cooling age of the metabasalt next to the Corunna Downs Batholith, clearly related to granite intrusion. Other cooling ages from this group come from an undeformed metadolerite T94/46 (3309 ± 118 Ma), a mylonite in the SRSZ T94/181 (3222 ± 13 Ma) and post-Central Coongan Shear Zone actinolites T93/182 (3197 ± 44 Ma).

This group of ages between 3300 and 3200, recorded in the central and western Coongan Belt, can not be related to any intrusive event in the Shaw Batholith. Davids et al (in press) recorded a similar age in the western Coongan Belt (3240 ± 16 Ma). Wijbrans & McDougall (1987) record ages in the same range (ca. 3200 Ma) for the blue-green pre-tectonic hornblendes, which they interpreted as a regional metamorphic event. The data from this study confirm that interpretation for the Coongan Belt. The post-tectonic actinolites from the CCSZ show that this metamorphic event occurred after a thrusting and folding phase, and may be the regional metamorphic event associated with crustal thickening. England & Thompson (1986) showed that the peak thermal event of regional metamorphism associated with crustal thickening can post date the actual thrusting event 40–60 Ma.

The timing constraints for this group of structures (3.0–3.2 Ga) is long, and may represent several phases of compression and associated metamorphism.

One of the aims of this study: the timing and nature of the Split Rock Shear Zone could not be achieved with the $^{40}\text{Ar}/^{39}\text{Ar}$ dating method and is better constrained with the U–Pb zircon method (§8.3). Although large areas show the 3075–2850 Ma resetting event, it is surprising to see that some local pockets do preserve the oldest signatures, possibly even the cooling age after extrusion of the lower Warrawoona Group (3522 ± 13 Ma). This is only possible if thermal effects occur on a local (<10 km) to very local (<10 cm) scale. This very local effect of resetting is best explained by the activity of fluids which use existing structures, such as major shear zones, as their channel way. The activity of fluids provides a double way to reset the argon systematics:

1. by causing low temperature alteration/metamorphism
2. by acting as a heat transport medium, causing thermal resetting

The effects of resetting should in this case not be seen as a thermal plane moving through a rock volume, but as a network of resetting channels, leaving unaffected pockets in between.

8.3 U–Pb zircon dating

Five granitoid samples from the Shaw Batholith were dated using the U–Pb zircon method. The analyses were done on the SHRIMP-II at Curtin University of Technology in Perth, Western Australia.

The specific aim of this dating study was to place robust temporal constraints on the Split Rock Shear Zone, the Mulgandinnah Shear Zone Complex and the gneisses in the central Shaw Batholith (Chapter 4 and 6).

All five samples were from deformed and metamorphosed rocks. The zircons were therefore expected to show various populations per sample and complex overgrowth/dissolution patterns. Consequently care was taken to characterize the zircon populations, analyzing the morphology (shape, color, internal growth zoning) using an optical microscope and cathodoluminescence imaging on the SEM (XL30 Phillips).

Previous dating (U–Pb and Pb–Pb) in the Shaw Batholith (see Chapter 3 for details) showed that the Shaw Batholith consists of a major granodioritic-tonalitic component (North Shaw Suite and gneisses) dated between 3470 ± 25 Ma (U–Pb, SHRIMP, Williams et al., 1983) and 3431 ± 4 Ma (U–Pb, SHRIMP, McNaughton et al., 1993), with minor anorthositic enclaves dated at 3578 ± 4 Ma (U–Pb, SHRIMP, McNaughton et al., 1993), and late to post tectonic granites dated at 3007 ± 48 Ma, 2948 ± 50 Ma and 2847 ± 34 Ma (Bickle et al., 1989). These dates were collected without recognizing the major structures in the Shaw Batholith described in this thesis. Sample locations and structural relations are not always accurately documented, leaving doubts as to which rocks exactly have been dated.

8.3.1 Structural context and description of samples for U-Pb dating.

Figure 8.1 shows the summarized structures and lithologies of the Shaw Batholith and U-Pb sample locations. Detailed description of structures are given in Chapter 4 and 6.

In Table 8.2 the characteristics and sample locations of the U-Pb samples are summarized.

Table 8.2 U-Pb sample co-ordinates and characteristics of sample and characteristics of zircons per sample, see Figure 8.4 for cathodoluminescence images of zircons showing the variety of textures and shapes of the zircons.

Sample characteristics				
Sample	Co-ordinates		characteristics	structural implication
T94/31	742.0E	7616.0S	biotite granite dike with a mylonitic foliation/lineation	intrudes during deformation in the MSZC
T94/193	768.5E	7583.6S	medium grained biotite granodiorite, weakly foliated	Intrusion partly postdates SRSZ fabric
T94/221	747.9E	7582.5S	fine grained biotite granodiorite gneiss complexly deformed and recrystallized	expected to be older than SRSZ relation to diorite
T94/222	747.9E	7582.5S	coarse grained quartz diorite, weakly foliated and recrystallized	relation to grey gneiss ?
T94/227	767.6E	7621.2S	mylonite in granitic/granodioritic rock	maximum age of SRSZ
Zircon characteristics				
Sample	shape	Length/ width	cores	texture
T94/31	short prismatic slightly rounded	3.7-1.8	featureless and recrystallized cores (20%)	irregular planar zoning
T94/193	short prismatic	3.9-2.4	featureless, truncated zoned and sector zoned cores (50%)	well developed planar zoning around cores
T94/221	short prismatic	3.6-2.4	truncated zoned, featureless and sector zoned cores (50%)	planar zoning around cores
T94/222	oval to short prismatic	2.5-1.7	no cores	homogeneously sector zoned
T94/227	variable, often small long prismatic	variable	zoned truncated cores (10%)	sector zoned and planar zoned

Gneisses in the central Shaw Batholith

Two samples were collected in the central Shaw Batholith, away from the SRSZ and the MSZC. So far no reliable data are available for the migmatic grey gneiss (sample T94/221) and dioritic components (sample T94/222) associated with it. The only dated sample that was assumed to be from the grey gneiss (3470 ± 25 Ma, U-Pb SHRIMP, Williams et al., 1983) is from rocks located in the MSZC and it is uncertain whether or not they are the same rock as the central Shaw Batholith migmatic grey gneiss. The second aim is to resolve the timing relation between the grey gneisses and dioritic components.

T94/221 was collected in the riverbed of the Shaw River where there is a large outcrop of fresh grey gneiss. The gneisses consist of mainly homogeneous fine-grained biotite granodiorite gneiss with nebulitic compositional banding and minor bands (10 cm) of quartz diorite composition. The original relation between the grey gneiss bands and the dioritic bands could not be established. The banding, which is locally folded with a fold axis plunging moderately ($20-40^\circ$) to 330 , is generally NNE trending and $30-40^\circ$ E dipping. The mineral lineation, formed by aligned biotite clots and hornblende grains on the foliation parallel to the banding, is parallel to the fold axis. Sample T94/221 is from the homogeneous biotite granodiorite part.

The microstructure of the grey gneiss is completely recrystallized to a granoblastic texture. The mineralogy consists of plagioclase, minor K-feldspar, quartz, biotite, accessory sphene, epidote and opaques.

The dioritic sample T94/222 was collected in a ca. 50 by 20 m outcrop ca. 1 km west of T94/221. The outcrop consists completely of coarse-grained foliated quartz diorite. The tectonic foliation is WSW trending and steeply west dipping with a weakly developed mineral lineation plunging 40° S. The microstructure is recrystallized to a granoblastic texture. Minerals include plagioclase, clinopyroxene, hornblende, quartz and accessory sphene and zircon.

Hornblende from this sample was used for $^{40}\text{Ar}/^{39}\text{Ar}$ dating.

The Split Rock Shear Zone

Two samples were collected to constrain the timing of the SRSZ: a granodiorite (T94/193) with an intrusive relation to the SRSZ mylonitic foliation in the greenstones and a mylonitic granitoid (T94/227) from the highest strain part of the basal SRSZ. The two samples will provide a minimum (T94/193) and a maximum (T94/227) age of deformation in the SRSZ.

T94/193 is a biotite-hornblende granodiorite collected in an area with good outcrops ca. 300 m from the granitoid-greenstone contact. The contact itself is complicated by contact parallel intrusion of garnet bearing granites and a complex array of pegmatites. The biotite-hornblende granodiorite crops out in a long zone between the basal SRSZ and the greenstones. It is weakly foliated and lineated parallel to the SRSZ close to the contact with the greenstones, with the strain intensity increasing toward the basal SRSZ. At the contact with the greenstones the relation was frequently found to be intrusive, with foliated amphibolite enclaves in the granodiorite close to the contact (see Figure 4.5c). Sample T94/193 shows a weak subvertical foliation and down-dip lineation. It contains plagioclase, K-feldspar, quartz, biotite, green hornblende and accessory sphene and epidote. Quartz grains show undulose extinction and subgrain formation.

Hornblende from this sample was used for $^{40}\text{Ar}/^{39}\text{Ar}$ dating.

Sample T94/227 was collected from a river bed outcrop in the central part of the basal SRSZ. It

shows a strong mylonitic foliation and a strong stretching lineation, with asymmetric clasts indicating an east up sense of shear. The sample shows compositional layering parallel to the foliation of granodiorite and pegmatite bands, all equally deformed. Minerals include K-feldspar, plagioclase, quartz, biotite slightly altered to chlorite, garnet in pegmatite layers, minor epidote and opaques. On microscale the fabric is mylonitic with quartz ribbons and asymmetric clasts in a fine-grained dynamically recrystallized matrix.

The Mulgandinnah Shear Zone Complex

The ultramylonite zones in the MSZC are intruded by granitic dykes during deformation (see Chapter 6). The crystallization age of these dykes provides a direct age of the MSZC. One of these dykes was sampled (T94/31) in a large riverbed outcrop in the Shaw River (see Figure 6.5f). The dyke is approximately 2 m. wide and cuts across the ultramylonitic foliation at a small angle, but shows the same ultramylonitic foliation and lineation.

The granitic dyke contains K-feldspar, plagioclase, quartz, biotite partly altered to chlorite, and epidote. The sample shows a mylonitic microstructure with quartz ribbons, asymmetric clasts and reduced grain size of the matrix.

In Appendix 2 whole rock geochemical analyses of these five samples are given.

8.3.2 Sample preparation and analytical method

Zircon separation and sample preparation

The zircon separation and sample preparation were done in the mineral separation lab at the Free University in Amsterdam. Rock samples with a weight of ca. 10 kg were crushed and ground to a particle size smaller than 500 μm and subsequently sieved in fractions larger and smaller than 250 μm . The zircons were separated from the latter by successively:

- removing particles smaller than 32 μm , by sieving in water
- removing the light quartz-feldspar fraction with a large overflow centrifuge (LOC-500) developed at the Free University (IJst, 1973) using a sodium polytungstate solution ($d = 2.8 \text{ gr/cm}^3$).
- removing magnetic ores with an ore magnet and subsequently separating magnetic fractions with a Carpc magnet separator.
- density separation to remove minerals such as hornblende from the denser fraction, using a laboratory overflow centrifuge (LOC-50, IJst, 1973) with di-iodomethane ($d = 3.28 \text{ gr/cm}^3$).

The heavy fraction was then sieved into size fractions (<30 μm , 30-60 μm , 60-90 μm and 90-120 μm) using anisotropic sieves with oblong holes, whereby crystals are separated based on their width. These fractions were further separated using a Frantz isodynamic magnetic separator.

The final zircon separation was done by hand-picking ca. 50-150 clear, preferably whole grains for each sample.

During the mineral separation procedure particular care was taken to avoid sample cross-contamination.

The selected zircons were mounted in epoxy and sectioned approximately in half. The mount surface was then polished to expose the grain interiors. All zircons were then photographed in trans-

mitted and reflected light under a microscope. Cathodoluminescence images were made on the SEM (XL-30) of the larger grains.

U - Th - Pb measurements were made using the ion microprobe SHRIMP-2 at Curtin University of Technology, employing the operating and data-processing procedures similar to those described by Compston et al. (1984) and Williams et al. (1984). Pb/U ratios were determined relative to that of the standard Sri Lankan zircon CZ-3, which has been assigned a $^{206}\text{Pb}/^{238}\text{U}$ value of 0.0914 corresponding to an age of 564 Ma.

Reproducibility of the Pb/U ratio of the standard was in most cases better than $\pm 3.0\%$. Where this was not the case for part of the session, the standards were grouped separately so that the reproducibility per group was better than 3%. One of the standard measurements was treated as an outlier and was not used in the data reduction procedure. This uncertainty is included in the quoted analytical errors. Errors given on individual analyses are based on counting statistics and are at the 1σ level; those given on pooled analyses are at $t\sigma$ (where t is Fisher's t) or 95% confidence. Error boxes shown in the Figures are at the 1σ level.

The processing of the raw data and plotting on conventional concordia plots was undertaken using computer software written by D.R. Nelson. Experience with the Perth Consortium SHRIMP confirms that the relationship between Pb/U and UO/U is best described by a power law (see Claeue-Long et al., 1995). This relationship has been incorporated into the data reduction procedures. Similar and generally low ^{204}Pb counts were measured on both standards and unknown samples and common-Pb corrections have therefore been applied using the measured ^{204}Pb abundance and assuming the isotopic composition of Broken Hill common-Pb, as this is the composition of ambient lead in the environment. Where this is inapplicable (see Table 8.3), common-Pb compositions have been determined using the model of Cumming and Richards (1975). In general terms, Cumming and Richards (1975) common Pb compositions have been assumed when the measured ^{204}Pb counts (less those measured at the baseline at mass 204.1) on the unknowns are more than six times the average ^{204}Pb counts (less those measured at the baseline at mass 204.1) measured on the standards during the analyses session. Corrections for ^{206}Pb hydride isobaric interference at ^{207}Pb and excess ^{204}Pb counts (commonly observed during measurements on the SHRIMP-1) were not required for any of the samples reported here.

The samples investigated in this study were granitic in nature and the zircon populations recovered from most samples were dominated by a single morphological type. Features such as zircon morphology (size, shape, zonation etc.) and chemistry (U and Th contents, Th/U ratios), degree of discordance of each analyses and evidence of radiogenic Pb loss were taken into account in the assessment of the validity of pooled analyses.

Analyses obtained for the majority of samples were either concordant or defined radiogenic-Pb loss trajectories indicating recent Pb loss. Dates were therefore determined using the mean $^{207}\text{Pb}/^{206}\text{Pb}$ ratios determined from pooled analyses. Individual analyses were weighted according to the inverse square of the individual analytical error (based on counting statistics) of the analyses, for the determination of the mean $^{207}\text{Pb}/^{206}\text{Pb}$ ratio of pooled analyses. Analyses more than $\pm 2\sigma$ from the weighted mean value were treated as outliers and deleted from the pool, and the weighted mean value then

recalculated. This process was repeated until all pooled analyses were all within $\pm 2\sigma$ of the weighted mean value and the remaining pooled data were normally distributed about the mean. A chi-square test was applied to grouped analyses in order to assess the relative effects of analytical sources of error, such as counting statistics and uncertainty in the common Pb composition, and geological sources of error, such as that arising from the inclusion of analyses of slightly older xenocryst zircons or of analyses that may have lost small amounts of radiogenic Pb during ancient disturbances. Chi-square values for grouped analyses of less than or equal to unity indicate that scatter about the weighted mean value determined for the grouped analyses can be accounted for by analytical sources of error alone. A chi-square value significantly greater than unity indicates that analyses are not normally distributed about the weighted mean value and that other (geological) sources of error are present within the grouped population. In these cases, the 95% confidence error is based on the observed scatter about the weighted mean $^{207}\text{Pb}/^{206}\text{Pb}$ ratio of pooled analyses.

8.3.3 Results of U-Pb zircon dating

8.3.3.1 Zircon morphology

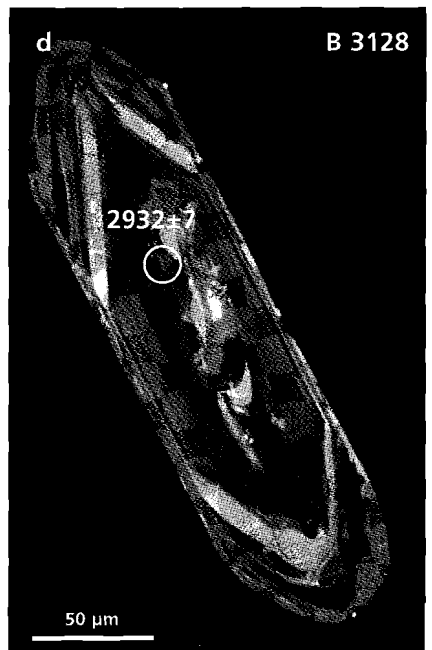
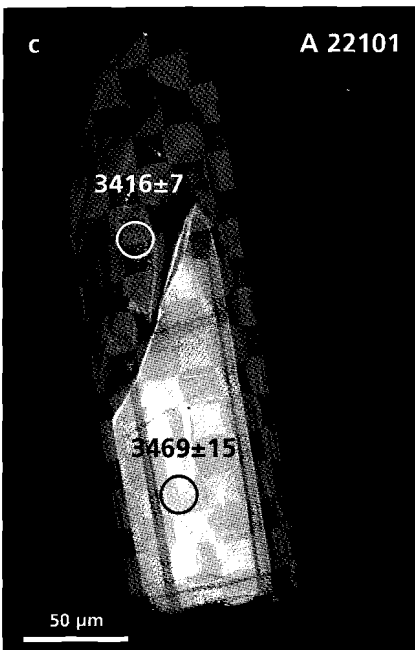
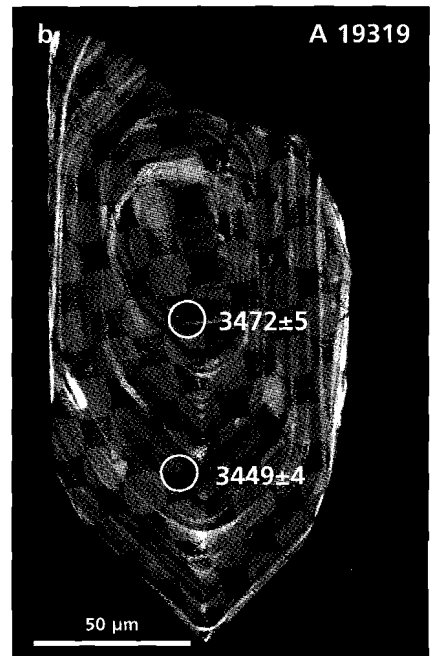
All samples contained enough zircons so that ca. 50 grains larger than 100 μm could be selected. In Table 8.2 the zircon characteristics have been summarized per sample. All zircons have a light to dark brown colour. Figure 8.3 shows cathodoluminescence images of typical textures.

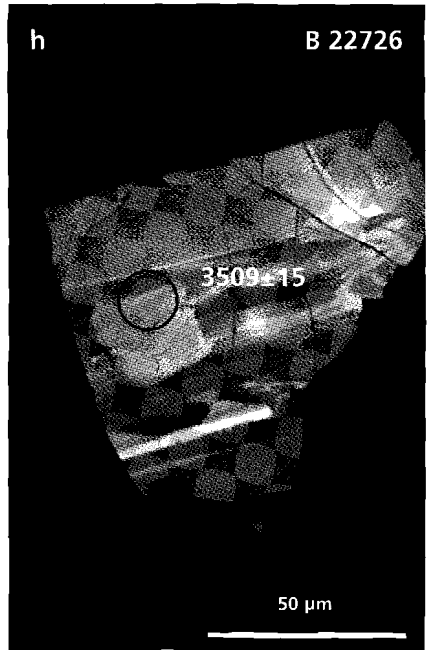
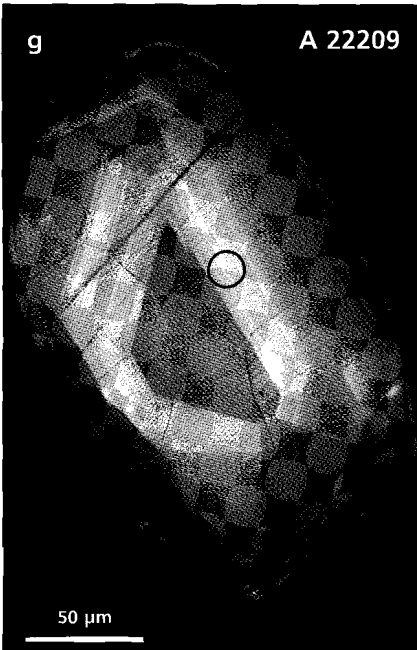
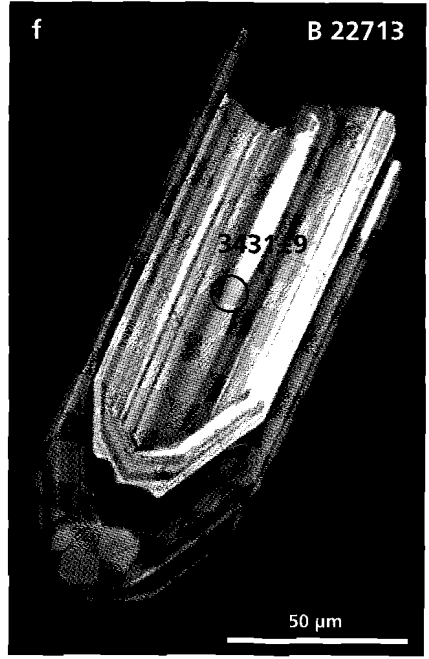
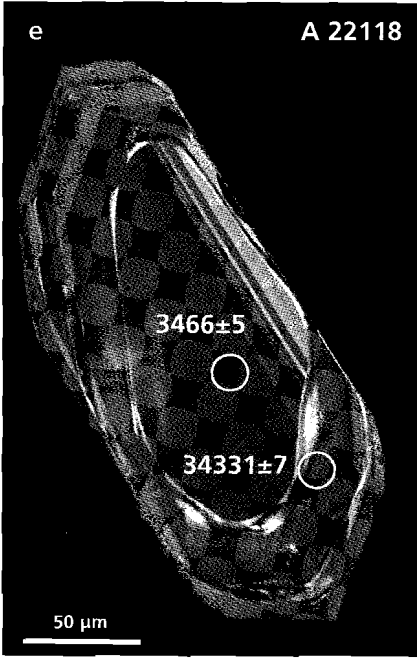
Sample T94/31, T94/193 and T94/221 contain similar zircons: short prismatic, planar zoned with in many cases (rounded) cores. These cores can be either featureless, planar zoned or sector zoned (Figure 8.3). Different types of cores may occur in one sample. An unusual texture found in some domains of various zircons is shown in Figure 8.3a. The growth zonation has almost disappeared in the core and the core region is subdivided in three almost featureless domains. The boundary between the core region and the zoned rim is gradual in parts but well defined in others. This texture is very reminiscent of a recrystallization texture and has previously been described as such by Pidgeon (1992).

The growth zoning can be very sharp and planar as shown in the rim of Figure 8.3a, but is often irregular as illustrated in Figure 8.3b. The zircons from sample T94/222 are distinctly different: they are oval to short prismatic and all show the characteristic sector zoning texture (Figure 8.4g). They show no cores or other textural inhomogeneities.

Figure 8.3 (Next pages). Cathodoluminescence images of zircons.

- a) Sample T94/31 zircon 13, the featureless recrystallized core of the zircon is replacing the planar zoned texture that is still preserved in the rim in an inherited zircon. The spot age is 3251 ± 3 Ma, which is a typical metamorphic age in this study.
- b) Sample T94/193 zircon 19, showing a fine, but in parts irregular zoning. The age of the core is 3472 ± 5 Ma, which corresponds to the earliest magmatic event, the age of the rim is 3449 ± 4 Ma, which is similar to the crystallization age of the grey gneisses
- c) Sample T94/221 zircon 1, showing planar zoning in the core and irregular zoning in the rim
- d) Sample T94/31 zircon 28, planar zoned zircon with irregularly recrystallized patches
- e) Sample T94/221 zircon 18, rounded planar zoned core with a younger rim
- f) Sample T94/227 zircon 13, finely planar zoned zircon
- g) Sample T94/222 zircon 9, sector zoned texture and oval shape typical for zircons from the diorite
- h) Sample T94/227 zircon 26, xenocrystic zircon from the sample in the SRSZ, the spot is partly in a recrystallized area, and may have a mixed xenocrystic and metamorphic age





The zircons in sample T94/227 were less abundant and smaller (frequently $< 30\mu\text{m}$). The smaller zircons have a long prismatic shape. The larger zircons vary in shape from long prismatic with well developed crystal faces (Figure 8.4g) to extremely rounded zircons. The rounded zircons occasionally show pitted surfaces indicating resorption. The textures include all textures found in other samples (planar zoned, sector zoned, irregular zoned) but cores are uncommon.

8.3.3.2 Results of SHRIMP analyses

The analytical data are summarized in Table 8.3. Only groups of ages that have passed the χ^2 -test are quoted as pooled ages. Where analysis had to be left out of a group for this group to pass the χ^2 -test, younger rather than older analysis were left out, because disturbances of the U-Pb systematics generally produce younger ages rather than older ages. All data are shown in concordia plots (Figures 8.4,5,6,7,8).

Sample T94/31- syn-Mulgandinnah Shear Zone Complex granite

Zircons from sample T94/31 were analysed in 26 spots of which 3 zircons were analysed in 2 spots. The majority of analyses give close to concordant $^{207}\text{Pb}/^{206}\text{Pb}$ ages between 2945 and 2909 Ma ($n=15$). Of those 11 analyses give a pooled age of 2934 ± 2 Ma ($\chi^2=1.37$). This age is interpreted as being the crystallization age of the magma. Three analyses give slightly younger pooled age of 2911 ± 4 Ma, but those are all reverse discordant, indicating U loss or excess radiogenic lead.

The rest of the analysed spots give older apparent ages ranging from 3434 to 2981 Ma, those are interpreted as being xenocrystic zircons.

A considerable number of analyses are discordant. This is assumed to be the result of recent Pb loss. A small number of analyses are reverse discordant, due to gain of radiogenic Pb at the analyses site. These spot areas do not have particular textural or chemical characteristic in common.

Of the three zircons that were analysed in two spots one grain (A3102) gave a younger core age (2909 ± 5 Ma) than the rim (2937 ± 7 Ma), possibly indicating recrystallization of the core (Pidgeon, 1992). The second multiple spot zircon (B3123) gave two xenocrystic ages with the core 3434 ± 5 Ma and the rim 3369 ± 3 Ma.

The third multiple spot zircon (A3118) gave a core age within the pooled 2934 ± 2 Ma group and an anomalously young rim age, probably due to radioactive damage as indicated by the very high U content.

One zircon with a recrystallized core (A3113) gave a concordant $^{207}\text{Pb}/^{206}\text{Pb}$ age of 3251 ± 3 Ma.

T94/193 Syn-Split Rock Shear Zone granodiorite

Zircons from sample T94/193 were analysed in 26 spots, of which 5 zircons were analysed in two spots. The analyses show a distinct cluster of concordant ages at ca. 3460 Ma, one distinctly older analyses and a scatter of more discordant analyses with younger $^{207}\text{Pb}/^{206}\text{Pb}$ ages.

Pooling the data of the 13 concordant analyses gives an age of 3462 ± 3 Ma with error in excess of that expected from analytical error alone ($\chi^2=2.66$). Leaving the three youngest points out results in a pooled age of 3468 ± 2 Ma ($\chi^2=0.87$). This age is interpreted as being the age of crystallization of the granodiorite. The older zircon with an $^{207}\text{Pb}/^{206}\text{Pb}$ age of 3524 ± 6 is interpreted as a xenocrystic zircon.

Of the scattered discordant analyses the six youngest, with $^{207}\text{Pb}/^{206}\text{Pb}$ ages between 3150 and 2489

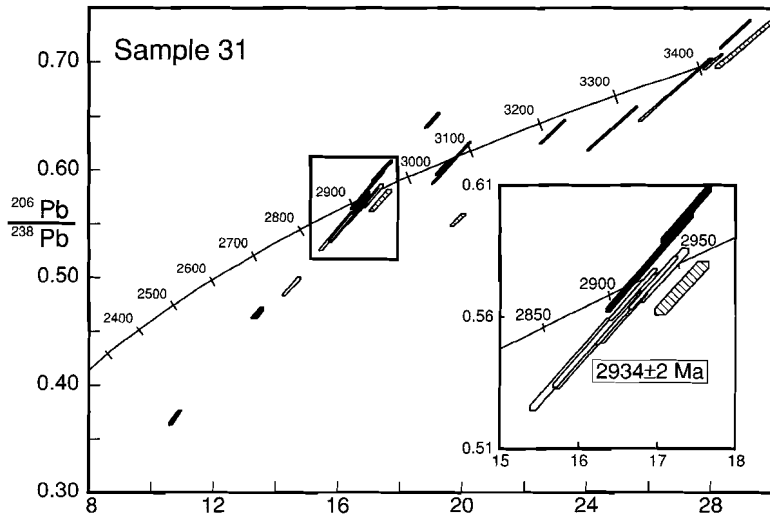


Figure 8.4

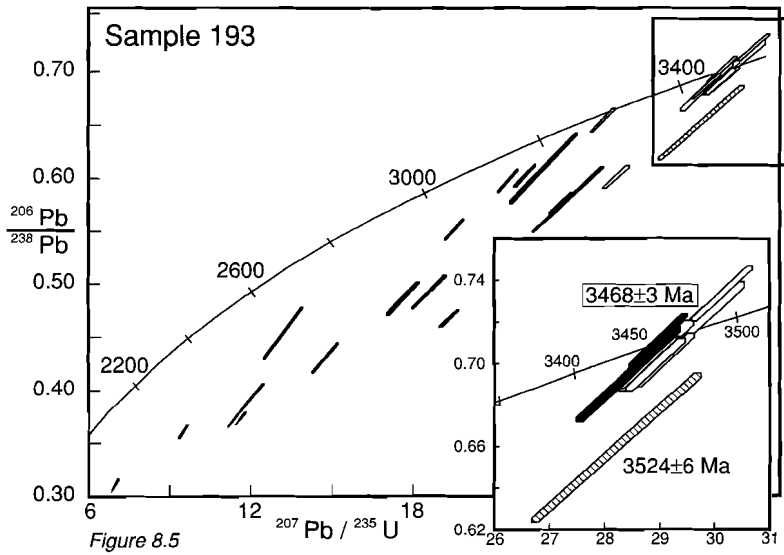


Figure 8.5

-  xenocrystic zircon spot
-  recrystallized or metamorphic rim spot
-  magmatic zircon spot
-  disturbed spot

Figure 8.4 and 8.5 Concordia plots of samples T94/31 and T94/193. All error boxes are 2σ , framed dates are crystallization ages, unframed ages represent other pooled ages. See text for discussion.

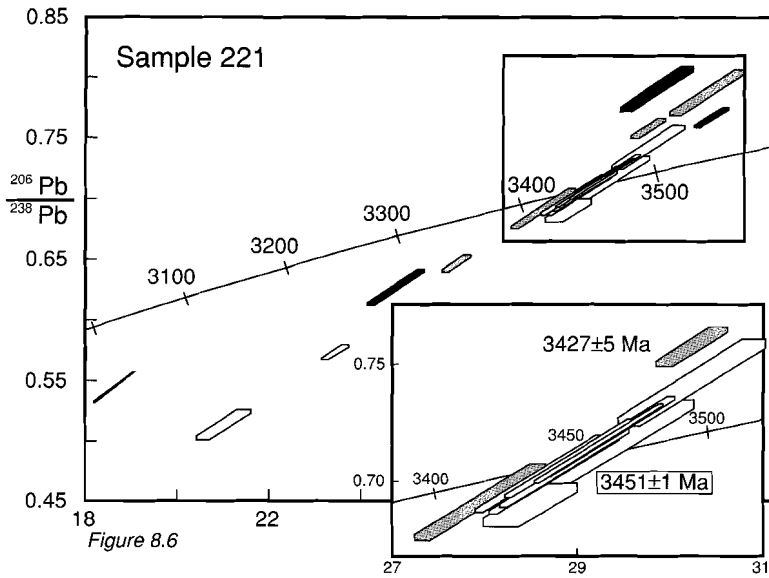


Figure 8.6

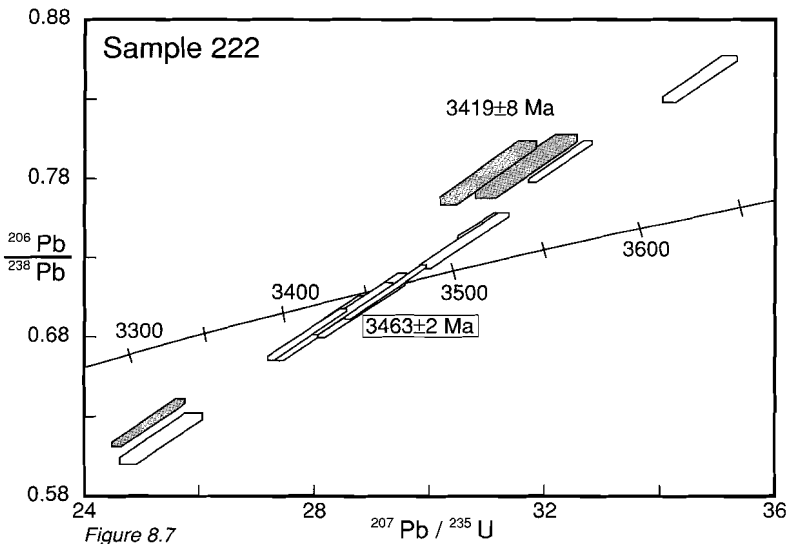


Figure 8.7

- xenocrystic zircon spot
- magmatic zircon spot
- rycrystallized or metamorphic rim spot
- disturbed spot

Figure 8.6 and 8.7 Concordia plots of samples T94/221 and T94/222. All error boxes are 2σ , framed dates are crystallization ages, unframed ages represent other pooled ages. See text for discussion.

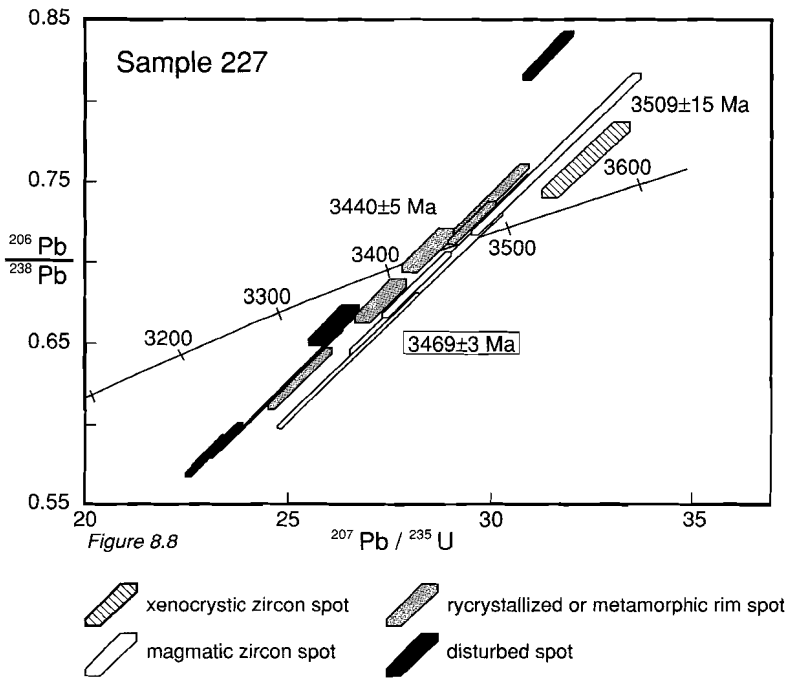


Figure 8.8 Concordia plots of samples T94/227. All error boxes are 2σ , framed dates are crystallization ages, unframed ages represent other pooled ages. See text for discussion.

Ma, are considered to be unreliable because they have either high U contents (>1000 ppm) and /or are very discordant. The relation between high U content, and unreliable ages and discordance is shown in Figure 8.9 for this sample. The $^{207}\text{Pb}/^{206}\text{Pb}$ age for the spots are constant at the crystallization age up to $U = 350$ ppm, then remains constant at ca. 3250 Ma up to $U = 500$ ppm, after which the age decreases with increased U content. The approximately linear relation between the age and the U content in the high U range of the plot is a good indication that those ages are unreliable due to Pb loss as a result of radiation damage. Other samples show similar trends in age versus U plots with the downward bend starting at ca. 500 ppm U, indicating that this is a threshold value above which the resulting $^{207}\text{Pb}/^{206}\text{Pb}$ age is not reliable.

The ca. 3250 Ma group does not show this behaviour and their ages are interpreted as significant geological ages, although they are more discordant than the crystallization age group. They are interpreted as new growth of zircon and recrystallization of zircon during a metamorphic event at ca. 3250 Ma. One analyses in this group is concordant with an $^{207}\text{Pb}/^{206}\text{Pb}$ age of 3308 Ma.

Of the multiple spot zircons one gave unreliable analyses (A19308). Zircon A19303 shows a slightly younger core (3454 ± 4 Ma) than the rim (3476 ± 6 Ma). Zircon A19319 (Figure 8.4c) shows an older core (3472 ± 5 Ma) with a younger rim (3449 ± 6 Ma). Both latter grains give analyses within the concordant group, with the younger ages just out of the pooled age group (3468 ± 2 Ma). The two spots in zircon A19321 give results within error of each other.

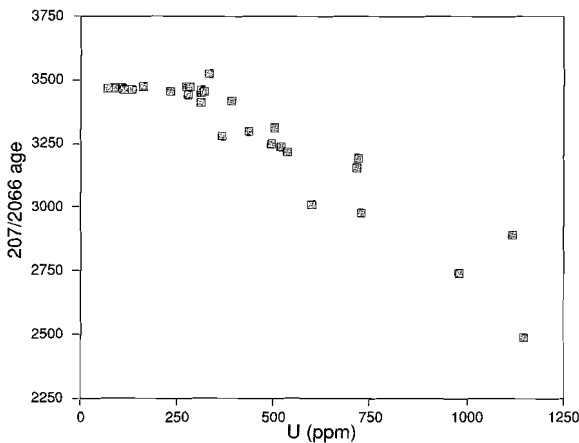


Figure 8.9 Plot of the $^{207}\text{Pb}/^{206}\text{Pb}$ age of spots in sample T94/193 vs. the U content. The crystallization age of the sample is 3468 ± 2 Ma as defined by the spots with low U (0-350 ppm), the spots between 350 ppm and 500 ppm U are recrystallized areas or new grown areas during a metamorphic event at ca. 3250 Ma. For U contents higher than 500 ppm the age decreases linearly with U content, indicating that Pb loss occurred due to radiation damage.

T94/221 Grey Gneiss

Zircons of sample T94/221 were analysed in 21 spots, of which 3 zircons were analysed in two spots. The analyses show one distinct concordant group with a pooled age of 3451 ± 1 Ma ($\chi^2 = 0.62$). This age is interpreted as being the crystallization age of the granodioritic magma. The rest of the analyses are either discordant or reverse discordant and give younger $^{207}\text{Pb}/^{206}\text{Pb}$ ages up to 3359 Ma. In those analyses a group of 4 analyses can be distinguished with a pooled age of 3427 ± 5 Ma ($\chi^2 = 1.35$). Two samples have U contents higher than 1000 ppm and are considered to be unreliable.

Of the three multiple spot zircons the analyses of zircon A22112 are within analytical error. Zircon A22118 (Figure 8.4e) shows an older core (3466 ± 5 Ma) with a younger rim (3433 ± 7 Ma). Zircon B22101 (Figure 8.4d) shows a core of 3416 ± 7 Ma and a rim of 3177 ± 2 Ma. However the rim has a high U content and may not be reliable.

T94/222 Diorite

Zircons of sample T94/222 were analysed in 17 spots in 17 different zircons. The analyses show a single group of 14 analyses which are generally concordant but may be slightly discordant or reverse discordant. The pooled age for this group is 3463 ± 2 Ma ($\chi^2 = 0.96$), which is interpreted as the crystallization age of the magma.

Three analyses give slightly younger ages, those have a pooled age of 3419 ± 8 Ma. There is no difference in morphology or chemical characteristics between the two groups.

T94/227 Mylonite from the SRSZ

Zircons from sample T94/227 were analysed in 19 different spots of which 2 zircons were analysed in two spots. The analyses show a close to concordant cluster between 3.40 and 3.38 Ga and one older than 3.5 Ga zircon and a number of strongly discordant analyses. The oldest zircon has an irregular planar texture with a recrystallized area. The spot is partly situated in the recrystallized part (Figure 8.4h). The $^{207}\text{Pb}/^{206}\text{Pb}$ age of this spot is 3509 ± 15 Ma, but this may be a mixed age between the recrystallized and unrecrystallized part.

The cluster of analyses can be divided in three age groups with pooled ages 3469 ± 3 Ma ($\chi^2 = 0.85$), 3440 ± 5 Ma ($\chi^2 = 0.65$) and 3415 ± 4 Ma ($\chi^2 = 1.28$). However, they do form an almost continuous

Table 8.3a Ion microprobe analytical results for sample T94/31, syn-kinematic granatic dyke in the Mulgandinnah Shear Zone Complex.

labels	graintype	U ppm	Th ppm	Pb ppm	f206 (%)	208/206 a	+/-	208/206 a	+/-	206/238	+/-	207/235	+/-	conc %	Age7/6 Ma	+/-	Pool
A3114.1	pl. zoned	205	78	134	0.010	0.21513	0.00081	0.10555	0.00079	0.5758	0.0103	17.079	0.319	100	2945	6	2934±2
A3103.1	featureless cor	691	200	441	0.035	0.21464	0.00048	0.07831	0.00044	0.5729	0.0101	16.954	0.304	99	2941	4	2934±2
A3119.1	pl.zoned	241	103	155	0.036	0.21449	0.00077	0.11714	0.00091	0.5601	0.0099	16.563	0.306	98	2940	6	2934±2
A3102.2	pl.zoned rim	312	132	177	0.690 *	0.21406	0.00093	0.09642	0.00153	0.4908	0.0087	14.485	0.271	88	2937	7	2934±2
A3117.1	featureless core	375	173	242	0.029	0.21414	0.00064	0.12552	0.00073	0.5592	0.0099	16.510	0.302	97	2937	5	2934±2
B3122.1	pl. zoned rim	374	146	235	0.222	0.21367	0.00087	0.10605	0.00119	0.5506	0.0179	16.220	0.538	96	2934	7	2934±2
B3128.1	irr. zoned core	656	426	433	0.094	0.21344	0.00061	0.17246	0.00083	0.5509	0.0178	16.212	0.532	96	2932	5	2934±2
B3105.1	pl.zoned	338	180	254	0.045	0.21316	0.00076	0.13655	0.00093	0.6457	0.0069	18.976	0.221	110	2930	6	2934±2
B3133.1	irr. zoned	500	215	314	0.353 *	0.21296	0.00079	0.11820	0.00115	0.5420	0.0176	15.916	0.526	95	2928	6	2934±2
A3101.1	irr. zoned	588	317	392	0.019	0.21296	0.00045	0.14613	0.00051	0.5685	0.0100	16.694	0.299	99	2928	3	2934±2
A3118.1	featureless core	234	75	103	1.095 *	0.21167	0.00131	0.12228	0.00237	0.3697	0.0065	10.788	0.210	69	2918	10	2934±2
B3125.1	irr. zoned	862	431	580	0.037	0.21118	0.00058	0.13407	0.00074	0.5807	0.0188	16.908	0.554	101	2915	4	2911±4
A3102.1	featureless core	308	123	210	0.102	0.21046	0.00070	0.10666	0.00086	0.5987	0.0106	17.373	0.320	104	2909	5	2911±4
B3111.1	sector zoned	358	155	191	0.182	0.20892	0.00156	0.11082	0.00231	0.4660	0.0052	13.424	0.190	85	2897	12	2911±4
B3123.1	pl. zoned core	327	212	297	0.265	0.29307	0.00102	0.16919	0.00131	0.7173	0.0233	28.985	0.959	102	3434	5	
B3101.1	dirty core	534	12	419	0.146 *	0.28969	0.00067	0.00628	0.00054	0.6997	0.0073	27.948	0.304	100	3416	4	
B3106.1	irr.zoned	1083	970	939	0.221 *	0.28764	0.00051	0.24590	0.00071	0.6516	0.0067	25.843	0.274	95	3405	3	
B3134.1	pl. zoned	995	260	791	0.029	0.28745	0.00050	0.06808	0.00034	0.6810	0.0220	26.990	0.879	98	3404	3	
A3115.1	featureless core	1053	169	876	0.058	0.28624	0.00039	0.04360	0.00026	0.7255	0.0127	28.635	0.507	104	3397	2	
B3123.2	irr. zoned rim	955	214	701	0.076	0.28110	0.00053	0.05394	0.00039	0.6378	0.0206	24.720	0.805	94	3369	3	
A3113.1	recryst. core	793	23	551	0.070	0.26063	0.00047	0.00811	0.00035	0.6348	0.0111	22.811	0.407	97	3251	3	
B3107.1	irr.zoned	507	110	341	1.234 *	0.25968	0.00099	0.09292	0.00169	0.5527	0.0057	19.791	0.228	87	3245	6	
B3132.1	irr. zoned	871	4	562	0.062	0.23434	0.00054	0.00038	0.00038	0.6062	0.0196	19.586	0.640	99	3082	4	
B3104.1	pl.zoned rim	369	60	250	0.396 *	0.23317	0.00086	0.05724	0.00116	0.6009	0.0063	19.319	0.223	99	3074	6	
A3109.1	irr.zoned	110	22	69	0.057	0.21999	0.00133	0.05777	0.00172	0.5710	0.0103	17.319	0.343	98	2981	10	
A3118.2	pl.zoned rim	2857	119	420	0.398 *	0.10450	0.00036	0.01240	0.00061	0.1509	0.0026	2.174	0.040	53	2705	6	

f206 = 100x (common ²⁰⁶Pb/total ²⁰⁶Pb), * spots for which common Pb correction using Cumming and Richards (1975) correction

a) ratios corrected for common Pb using the measured ²⁰⁴Pb abundance, All errors given are 1sigma

conc = 100x (²⁰⁶Pb/²³⁸U age)/(²⁰⁷Pb/²⁰⁶Pb age)

pool = pooled age group

rim
core
recrystallized
unreliable

Constraints on the timing of deformation and metamorphism

Table 8.3b Ion microprobe analytical results for sample T94/193, North Shaw granodiorite from the eastern Shaw Batholith.

labels	graintype	U ppm	Th ppm	Pb ppm	f206 (%)	208/206 a	+/-	208/206 a	+/-	206/238	+/-	207/235	+/-	conc %	Age7/6 Ma	+/-	Pool
B19322.1	pl. zoned core	333	370	311	0.142	0.31059	0.00114	0.32348	0.00160	0.6590	0.0355	28.223	1.537	93	3524	6	
A19303.2	pl. zoned rim	165	162	156	0.093	0.30117	0.00108	0.26224	0.00143	0.7006	0.0126	29.094	0.547	98	3476	6	3468±2
A19315.1	featureless core	286	269	232	0.450	0.30049	0.00097	0.23224	0.00141	0.6069	0.0108	25.146	0.463	88	3473	5	3468±2
A19319.1	irr. zoned core	276	273	261	0.066	0.30035	0.00104	0.26660	0.00141	0.6985	0.0125	28.929	0.540	98	3472	5	3468±2
A19321.2	pl. zoned core	95	40	84	0.079	0.30001	0.00146	0.11228	0.00141	0.7243	0.0134	29.962	0.589	101	3470	8	3468±2
A19321.1	pl. zoned core	72	60	68	0.048	0.29956	0.00185	0.21868	0.00258	0.7122	0.0136	29.418	0.611	100	3468	10	3468±2
A19322.1	pl. zoned core	110	150	110	0.052	0.29920	0.00133	0.36347	0.00205	0.6989	0.0128	28.831	0.558	99	3466	7	3468±2
A19309.1	pl. zoned	314	229	295	0.031	0.29861	0.00075	0.19393	0.00082	0.7321	0.0130	30.143	0.549	102	3463	4	3468±2
A19318.1	sector zoned core	114	125	110	0.069	0.29827	0.00135	0.28887	0.00192	0.7067	0.0130	29.062	0.565	100	3461	7	3468±2
A19310.1	sector zoned	134	206	138	0.035	0.29803	0.00124	0.40816	0.00206	0.6999	0.0127	28.759	0.549	99	3460	6	3468±2
B19327.1	pl. zoned core	235	352	238	0.074	0.29727	0.00114	0.39496	0.00188	0.6937	0.0226	28.434	0.946	98	3456	6	
A19303.1	dirty core	320	493	326	0.068	0.29692	0.00074	0.40136	0.00120	0.6940	0.0123	28.411	0.516	98	3454	4	
A19319.2	pl. zoned rim	312	338	303	0.051	0.29591	0.00078	0.28587	0.00103	0.7103	0.0126	28.978	0.529	100	3449	4	
A19301.1	pl. zoned core	278	237	183	0.552 *	0.29394	0.00110	0.29927	0.00185	0.4712	0.0083	19.095	0.354	72	3439	6	
B19321.1	irr. zoned	393	136	276	0.126	0.28991	0.00084	0.09692	0.00085	0.5852	0.0315	23.391	1.269	87	3417	5	
A19323.1	dirty core	314	219	242	0.672	0.28846	0.00121	0.21917	0.00194	0.5825	0.0104	23.165	0.436	87	3409	7	
A19324.1	pl. zoned rim	502	240	400	0.053	0.27036	0.00058	0.12581	0.00056	0.6615	0.0116	24.658	0.444	99	3308	3	
B19327.2	pl. zoned rim	439	103	253	0.194	0.26861	0.00090	0.07552	0.00096	0.4959	0.0161	18.366	0.606	79	3298	5	
B19340.1	pl. zoned rim	367	159	269	0.068	0.26521	0.00087	0.11298	0.00091	0.6161	0.0332	22.529	1.225	94	3278	5	
A19329.1	pl. zoned rim	496	333	374	0.095	0.26048	0.00063	0.17709	0.00079	0.6085	0.0107	21.852	0.395	94	3250	4	
B19328.1	irr. zoned	522	78	291	0.335 *	0.25770	0.00089	0.04661	0.00105	0.4903	0.0159	17.420	0.574	80	3233	5	
A19308.1	featureless core	539	211	383	0.122	0.25509	0.00061	0.10840	0.00066	0.6031	0.0106	21.214	0.383	95	3217	4	
A19312.1	pl. zoned	721	395	486	0.073	0.25098	0.00051	0.15149	0.00058	0.5568	0.0098	19.269	0.345	89	3191	3	
B19308.1	pl. zoned	716	825	416	0.503 *	0.24458	0.00083	0.28792	0.00145	0.4329	0.0140	14.598	0.480	74	3150	5	
A19308.2	pl. zoned rim	600	348	267	0.206	0.22383	0.00067	0.15182	0.00096	0.3737	0.0066	11.533	0.209	68	3003	5	
B19336.1	pl. zoned	728	352	331	0.263	0.21932	0.00069	0.13439	0.00099	0.3873	0.0208	11.713	0.635	71	2976	5	
B19337.1	featureless core	1118	621	609	0.388 *	0.20774	0.00056	0.15925	0.00089	0.4566	0.0245	13.077	0.708	84	2668	4	
A19326.1	pl. zoned rim	979	700	431	0.357 *	0.18953	0.00054	0.206049	0.00092	0.3619	0.00633	9.456	0.171	73	2738	5	
A19313.1	pl. zoned	1145	939	424	0.211	0.16316	0.00045	0.21401	0.00080	0.3106	0.0054	6.987	0.126	70	2489	5	

f206 = 100x (common ²⁰⁶Pb/total ²⁰⁶Pb), * spots for which common Pb correction using Cumming and Richards (1975) correctiona) ratios corrected for common Pb using the measured ²⁰⁴Pb abundance, All errors given are 1sigmaconc = 100x (²⁰⁶Pb/²³⁸U age)/(²⁰⁷Pb/²⁰⁶Pb age)

pool = pooled age group

rim
core
recrystallized
unresolvable

Table 8.3c Ion microprobe analytical results for sample T94/221, grey migmatic gneiss from the central Shaw Batholith.

labels	graintype	U ppm	Th ppm	Pb ppm	f206 (%)	208/206 a	+/-	208/206 a	+/-	206/238	+/-	207/235	+/-	conc %	Age7/6 Ma	+/-	Pool
A22101.1	featureless core	54	23	46	0.107	0.29980	0.00285	0.11314	0.00431	0.6893	0.0095	28.495	0.504	97	3469	15	3451±1
B22123.1	sector zoned core	35	16	30	0.064	0.29811	0.00217	0.12081	0.00255	0.7167	0.0179	29.458	0.794	101	3460	11	3451±1
B22121.1	pl. zoned core	39	15	24	0.848	0.29744	0.00302	0.07805	0.00500	0.5128	0.0126	21.029	0.585	77	3457	16	3451±1
B22125.1	irr. zoned	222	135	196	0.053	0.29698	0.00080	0.16225	0.00085	0.7021	0.0167	28.749	0.696	99	3455	4	3451±1
A22112.2	irr. zoned rim	207	29	136	0.012	0.29694	0.00139	0.03617	0.00149	0.5726	0.0064	23.443	0.298	84	3454	7	3451±1
B22142.1	pl. zoned	269	332	266	0.044	0.29691	0.00070	0.32633	0.00103	0.7050	0.0167	28.862	0.695	100	3454	4	3451±1
A22112.1	featureless core	209	68	174	0.042	0.29647	0.00115	0.08442	0.00103	0.6979	0.0077	28.528	0.346	99	3452	6	3451±1
B22132.1	featureless core	291	151	257	0.044	0.29612	0.00068	0.13292	0.00065	0.7188	0.0170	29.346	0.707	101	3450	4	3451±1
B22104.1	zoned core	726	356	638	0.063	0.29620	0.00042	0.12839	0.00040	0.7158	0.0169	29.233	0.696	101	3450	2	3451±1
B22146.1	irr. zoned	282	76	236	0.033	0.29569	0.00066	0.07415	0.00055	0.7093	0.0168	28.917	0.695	100	3448	3	3451±1
B22150.1	pl. zoned core	54	29	50	0.186	0.29560	0.00196	0.14757	0.00272	0.7418	0.0183	30.234	0.798	104	3447	10	3451±1
B22149.1	pl. zoned core	214	233	209	-0.004	0.29513	0.00081	0.31364	0.00115	0.7027	0.0167	28.595	0.693	100	3445	4	3451±1
B22134.1	pl. zoned core	141	76	121	0.122	0.29358	0.00140	0.13991	0.00181	0.6906	0.0166	27.956	0.701	98	3437	7	3427±5
A22118.2	irr. zoned rim	312	141	247	0.290	0.29282	0.00130	0.11804	0.00168	0.6458	0.0070	26.075	0.318	94	3433	7	3427±5
B22110.1	pl. zoned core	219	115	210	-0.104	0.29063	0.00185	0.13252	0.00270	0.7867	0.0191	31.523	0.813	109	3421	10	3427±5
A22101.2	featureless rim	196	42	173	0.159	0.28967	0.00136	0.05367	0.00134	0.7569	0.0085	30.232	0.384	106	3416	7	3427±5
A22118.1	pl. zoned core	374	671	438	0.025	0.29924	0.00091	0.47318	0.00157	0.7662	0.0082	31.612	0.362	106	3466	5	
B22148.1	irr. zoned	263	107	198	0.216	0.28674	0.00129	0.10152	0.00155	0.6266	0.0150	24.774	0.615	92	3400	7	
B22109.1	featureless cor	207	96	196	0.108 *	0.27934	0.00188	0.10512	0.00255	0.7897	0.0191	30.417	0.789	112	3359	11	
B22101.1	featureless cor	1228	580	792	0.082	0.24873	0.00034	0.12461	0.00037	0.5440	0.0128	18.658	0.443	88	3177	2	
B22103.1	zoned core	1991	6605	1063	0.418 *	0.18339	0.00036	0.88562	0.00117	0.2961	0.0070	7.488	0.179	62	2684	3	

206 = 100x (common ²⁰⁶Pb/total ²⁰⁶Pb), * spots for which common Pb correction using Cumming and Richards (1975) correction

a) ratios corrected for common Pb using the measured ²⁰⁴Pb abundance, All errors given are 1sigma

conc = 100x (²⁰⁶Pb/²³⁸U age)/(²⁰⁷Pb/²⁰⁶Pb age)

pool = pooled age group

rim
core
recrystallized
unreliable

Table 8.3d Ion microprobe analytical results for sample T94/222, dioritic gneiss from the central Shaw Batholith.

labels	graintype	U ppm	Th ppm	Pb ppm	f206 (%)	208/206 a	+/-	208/206 a	+/-	206/238	+/-	207/235	+/-	conc %	Age7/6 Ma	+/-	Pool
B22b34.1	sector zoned	135	132	126	0.025	0.30008	0.00102	0.26178	0.00128	0.6954	0.0166	28.772	0.706	98	3471	5	3463±2
B22b30.1	sector zoned	92	99	93	0.063	0.29992	0.00146	0.28483	0.00199	0.7404	0.0180	30.615	0.778	103	3470	8	3463±2
B22b25.1	sector zoned	113	125	109	0.003	0.29963	0.00135	0.29789	0.00173	0.6981	0.0170	28.841	0.729	98	3468	7	3463±2
B22b33.1	sector zoned	176	197	171	0.011	0.29957	0.00090	0.29774	0.00117	0.7080	0.0169	29.244	0.713	100	3468	5	3463±2
A22210.1	sector zoned	121	116	122	0.015	0.29924	0.00163	0.25395	0.00227	0.7494	0.0090	30.920	0.428	104	3466	8	3463±2
B22b15.1	sector zoned	134	175	160	0.192	0.29877	0.00165	0.33636	0.00265	0.8421	0.0143	34.691	0.643	114	3464	9	3463±2
B22b28.1	sector zoned	137	142	130	0.169	0.29887	0.00124	0.27481	0.00170	0.6975	0.0167	28.742	0.714	98	3464	6	3463±2
B22b37.1	sector zoned	135	117	121	0.000	0.29851	0.00132	0.22525	0.00142	0.6811	0.0164	28.035	0.702	97	3463	7	3463±2
B22b21.1	sector zoned	134	151	114	0.020	0.29839	0.00278	0.30921	0.00390	0.6161	0.0158	25.348	0.718	89	3462	14	3463±2
B22b35.1	sector zoned	96	95	91	0.020	0.29804	0.00120	0.26301	0.00158	0.7030	0.0169	28.889	0.718	99	3460	6	3463±2
A22207.1	sector zoned	90	97	86	0.276	0.29782	0.00215	0.28928	0.00344	0.6973	0.0088	28.634	0.436	99	3459	11	3463±2
B22b36.1	sector zoned	115	112	107	0.105	0.29782	0.00116	0.25612	0.00160	0.6976	0.0167	28.648	0.709	99	3459	6	3463±2
B22b27.1	sector zoned	118	110	107	0.100	0.29685	0.00114	0.24684	0.00150	0.6814	0.0163	27.887	0.688	97	3454	6	3463±2
B22b14.1	sector zoned	115	115	121	0.044	0.29613	0.00105	0.24818	0.00134	0.7902	0.0129	32.265	0.553	109	3450	5	3463±2
B22b18.1	sector zoned	104	62	102	0.022	0.29174	0.00257	0.15466	0.00278	0.7874	0.0199	31.674	0.880	109	3427	14	3419±8
B22b20.1	sector zoned	256	333	225	0.212	0.29144	0.00161	0.32635	0.00255	0.6255	0.0150	25.134	0.635	91	3425	9	3419±8
B22b22.1	sector zoned	94	74	95	0.005	0.28718	0.00223	0.19654	0.00230	0.7834	0.0196	31.018	0.841	110	3402	12	3419±8

f206 = 100x (common ^{206}Pb /total ^{206}Pb), * spots for which common Pb correction using Cumming and Richards (1975) correction

a) ratios corrected for common Pb using the measured ^{204}Pb abundance, All errors given are 1sigma

conc = 100x ($^{206}\text{Pb}/^{238}\text{U}$ age)/($^{207}\text{Pb}/^{206}\text{Pb}$ age)

pool = pooled age group

Table 8.3e Ion microprobe analytical results for sample T94/227, Split Rock Shear Zone mylonite from eastern Shaw Batholith.

labels	graintype	U ppm	Th ppm	Pb ppm	f206 (%)	208/206 a	+/-	208/206 a	+/-	206/238	+/-	207/235	+/-	conc %	Age7/6 Ma	+/-	Pool
B22726.1		38	18	36	0.338	0.30756	0.00304	0.11604	0.00441	0.7632	0.0235	32.363	1.084	104	3509	15	
B22706.2	sector zoned rim	435	105	330	0.281 *	0.30096	0.00085	0.06625	0.00094	0.6389	0.0416	26.513	1.736	92	3475	4	3469±3
B22706.1	sector zoned core	113	85	100	0.091	0.29976	0.00154	0.19996	0.00188	0.6877	0.0449	28.424	1.880	97	3469	8	3469±3
B22724.1	sector zoned	141	186	153	0.001	0.29907	0.00142	0.35027	0.00200	0.7666	0.0501	31.613	2.089	106	3465	7	3469±3
A22703.1	sector zoned	105	109	106	0.126	0.29871	0.00143	0.27368	0.00201	0.7403	0.0137	30.490	0.598	103	3464	7	3469±3
B22711.1	sector zoned	234	217	214	0.154	0.29820	0.00126	0.23882	0.00170	0.6858	0.0200	28.197	0.847	97	3461	7	3469±3
A22707.1	sector zoned	127	103	121	0.174	0.29594	0.00145	0.22930	0.00195	0.7241	0.0134	29.544	0.581	102	3449	8	3440±5
B22719.1	sector zoned	101	95	99	0.047	0.29470	0.00176	0.24354	0.00247	0.7387	0.0220	30.017	0.932	104	3443	9	3440±5
A22706.1	sector zoned	93	89	84	0.482	0.29291	0.00297	0.24167	0.00506	0.6757	0.0132	27.288	0.632	97	3433	16	3440±5
B22731.1		115	92	95	0.178	0.29252	0.00166	0.22478	0.00231	0.6279	0.0185	25.324	0.777	92	3431	9	3440±5
A22705.1	sector zoned	119	116	111	0.068	0.29209	0.00292	0.24553	0.00455	0.7071	0.0136	28.477	0.648	101	3429	16	3440±5
B22718.1	pl. zoned	868	560	693	0.269 *	0.29023	0.00058	0.19557	0.00077	0.6183	0.0402	24.743	1.616	91	3419	3	3415±4
B22707.1	pl. zoned core	222	178	164	0.369	0.28821	0.00125	0.16398	0.00174	0.5838	0.0170	23.199	0.696	87	3408	7	3415±4
A22702.1	pl. zoned	133	72	100	0.625	0.28760	0.00156	0.18055	0.00238	0.5829	0.0106	23.114	0.453	87	3405	8	3415±4
A22704.1	sector zoned	138	147	122	0.321 *	0.28699	0.00339	0.25055	0.00581	0.6607	0.0128	26.143	0.624	96	3401	18	3415±4
A22701.1	recryst. core	181	145	212	1.550 *	0.27543	0.00148	0.29667	0.00281	0.8272	0.0150	31.414	0.614	116	3337	8	
B22714.1	pl. zoned	117	50	155	2.683 *	0.26001	0.00205	0.20853	0.00405	0.9578	0.0283	34.339	1.082	133	3247	12	
B22707.2	featureless rim	706	7332	1744	5.367 *	0.23359	0.00089	0.32157	0.00193	1.5643	0.0456	50.381	1.505	197	3077	6	
B22708.1	dirty core	329	5	124	0.043	0.12529	0.00076	0.00457	0.00081	0.3868	0.0112	6.681	0.203	104	2032	11	

206 = 100x (common ²⁰⁶Pb/total ²⁰⁶Pb), * spots for which common Pb correction using Cumming and Richards (1975) correction

a) ratio: corrected for common Pb using the measured ²⁰⁴Pb abundance, All errors given are 1sigma

conc = 100x (²⁰⁶Pb/²³⁸U age)/(²⁰⁷Pb/²⁰⁶Pb age)

pool = pooled age group

rim
core
recrystallized
unresolvable

Constraints on the timing of deformation and metamorphism

group from 3400 to 3480 Ma. The older two groups are mainly spots in sector zoned parts of zircons, whereas the youngest group (3415 ± 4 Ma) come from spots in planar zoned parts. This indicates that there were distinct zircon growth events, although there is no chemical difference between the groups.

The two youngest spots are not reliable because of high U content or an extremely dirty spot location.

8.3.4 Synthesis and structural implications of U-Pb zircon dating

Figure 8.10 shows a series of histogram plots per sample and one for all analyses. The data presented are $^{207}\text{Pb}/^{206}\text{Pb}$ ages of individual spots. The data have been filtered, leaving out highly discordant ages and analyses with high U or Th. The result is a series of peaks which correspond to important age components. The peaks are somewhat broad and skewed toward lower ages, an indication that effects of non-zero age Pb loss are still present.

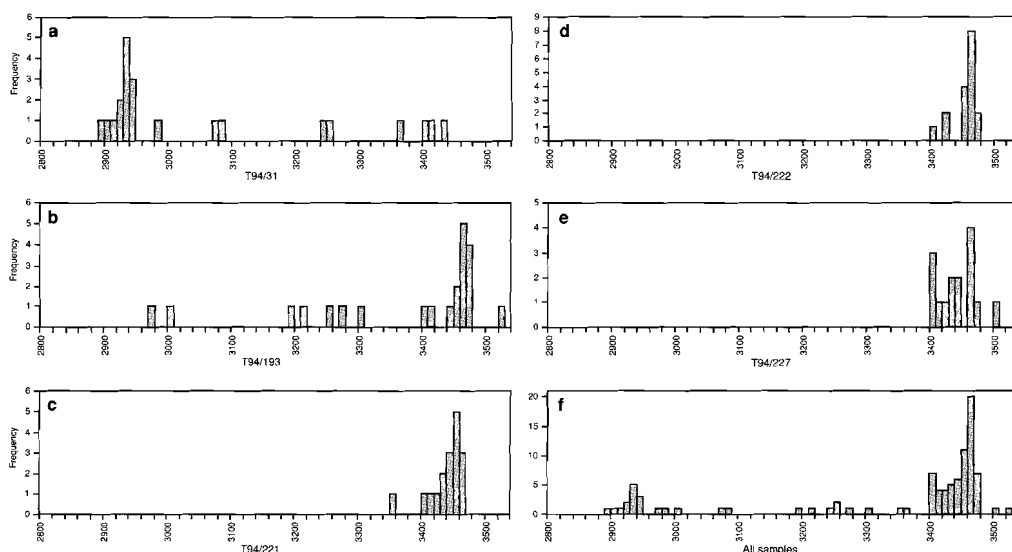


Figure 8.10 $^{207}\text{Pb}/^{206}\text{Pb}$ age histograms compiled from the five samples that were analysed (a-e) and of all spots analysed (f). The age scale is in Ma and the histogram interval is 10 Ma. The data have been filtered using the following criteria: 1) analyses which were more than 15% discordant were omitted, 2) analyses with more than 100 ppm. U were omitted.

The first major age component is the group between 3480 and 3400 Ma (Figure 8.10f). In this range, 3 age groups can be distinguished. This is reflected in the pooled ages of T94/193, T94/222 and T94/227, which belong to the oldest, 3465 Ma, group, and the pooled age of T94/221, which belongs to the second group at ca. 3450 Ma (see Table 8.4 for a summary of data per sample). Several zircons with distinct cores and rims gave core ages in the 3465 Ma range and rim ages around 3450 Ma. This indicates that the 3450 Ma event was an important metamorphic event after the initial crys-

tallization of large volumes of dioritic and granodioritic magma at ca. 3465 Ma. The 3450 Ma age is also the crystallization age of the predecessor of the grey gneiss.

Figure 8.11 shows the chemical characteristics for zircon spots from all samples. In both the Th vs. U plot and the common Pb vs. Th/U plot samples T94/193, T94/227 and T94/222 fall in the same range, although T94/222 shows distinctly lower common Pb (Figure 8.12b). T94/221 and T94/31

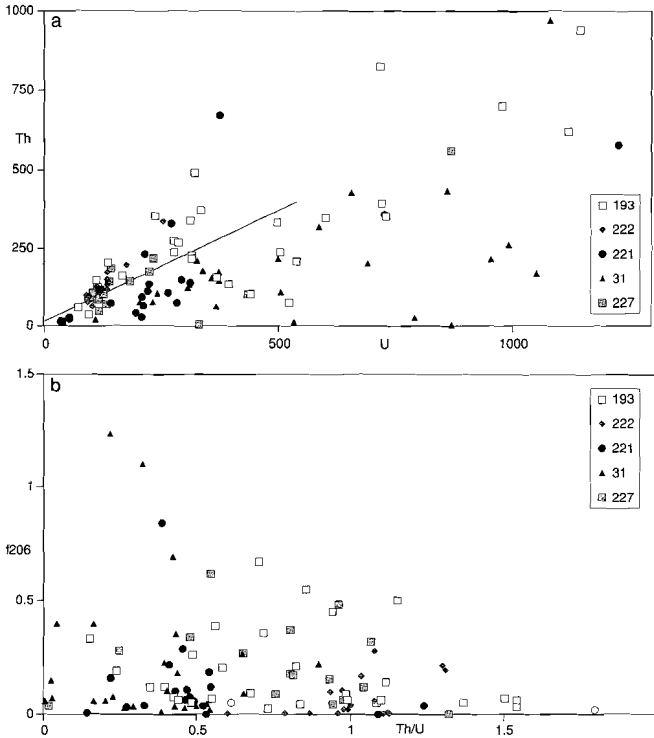


Figure 8.11 Plots of chemistry of spots in different samples
 a) Th vs. U plot, the field below the reference line is mainly occupied by spots from sample T94/31 and T94/221
 b) Ratio of common versus total Pb (f206) vs. Th/U plot, the field closest to the origin is occupied by spots from T94/31 and T94/221, the high Th/U low common Pb area is occupied by T94/222, T94/193 and T94/227 are indistinguishable in those plots.

fall in a different field with generally lower Th/U and low common Pb, with T94/221 having even lower U contents than T94/31. The spots with rim ages at ca. 3450 Ma from T94/193 and T94/227 show the same chemical characteristics as T94/221 and fall in that field.

The chemical characteristics confirm the above inference that the North Shaw Suite (T94/193 and 227) and the diorites (T94/222) crystallized at the same time at ca. 3465 Ma, whereas the gneisses (T94/221) crystallized at ca. 3450 Ma at the same time that new rims grew or recrystallization occurred in older zircon during a metamorphic event. The field observation that diorites occur as xenolithic boudins in the grey gneisses is consistent with this age data, showing that the diorites are older.

The peak in ages at 3400 Ma is mainly due to sample T94/227, the mylonite, which contains zircons from all three age groups. The significance of the 3415 ± 4 Ma pooled age is uncertain, but it may be related to zircon isotopic disturbances due to the intense deformation in this sample. This would sug-

gest that some shear took place at or younger than 3415 ± 4 Ma.

A small and broad peak of $^{207}\text{Pb}/^{206}\text{Pb}$ ages occurs at ca. 3250 Ma (3300 to 3200 Ma). The spots with these ages are usually in featureless to irregularly zoned areas of zircons with textures similar to recrystallization textures; the featureless areas, often in cores, appear to grow at the cost of planar zoned areas (see Figure 8.4a for a good example). The chemical characteristics (U, Th, common Pb) of those spots are not unusual in any respect. They are interpreted as ages due to recrystallization during a metamorphic event. The recrystallization appears to preferentially start in the interior of the zircon. This explains the occasionally observed younger core than rim ages as also noted by Pidgeon (1992). The place where recrystallization starts may be related to the amount of damage to the crystal lattice caused by decay of U and Th.

The third peak in ages occurs at ca. 2930 Ma, which corresponds to the crystallization age of sample T94/31.

Of all the zircons that were analysed, two gave $^{207}\text{Pb}/^{206}\text{Pb}$ ages > 3500 Ma. These are interpreted as xenocrysts of an older volcanic or granitic basement.

Table 8.4 Summarized results of U-Pb SHRIMP dating

Sample	Pooled age-Crystallization age	Other pooled age groups	Xenocrystic zircons	New growth or recrystallization	two spot zircons	
					core	rim
T94/31	2934 \pm 2		3434-2981	3251 \pm 3	3434 \pm 5	3369 \pm 3
T94/193	3468 \pm 2		3524 \pm 6	3308 \pm 3	3456 \pm 6	3298 \pm 5
T94/221	3451 \pm 1	3427 \pm 5		3359 \pm 11	3454 \pm 4	3476 \pm 6
T94/222	3463 \pm 2	3419 \pm 8			3466 \pm 5	3433 \pm 7
T94/227	3469 \pm 3	3440 \pm 5 3415 \pm 4	3509 \pm 15			

Timing of structures

The main objective of this U-Pb dating study is to constrain the age of the SRSZ and the MSZC and to constrain the relation between the grey gneisses and diorites in the core of the Shaw Batholith, as well as their relation with the SRSZ. The crystallization ages of the diorites (T94/222), the little deformed North Shaw Suite (T94/193) and the SRSZ mylonite (T94/227) are all between 3463 and 3469 Ma.

The SRSZ is constrained in time by sample T94/193, T94/221 and T94/227 (see Figure 8.1). The crystallization age of T94/227 (3469 \pm 3 Ma) provides a maximum age of the basal SRSZ forming the contact between the North Shaw Suite and the grey gneisses. The crystallization age of sample T94/193 (3468 \pm 2 Ma) shows that the wedge of granodiorite in the southeastern Shaw Batholith is in fact the continuation of the North Shaw Suite, which was dated by McNaughton et al. (1988) at 3467 \pm 6 Ma (single zircon U-Pb) It provides a minimum age for the mylonitic fabric related to the SRSZ in the amphibolite greenstones, since the granodiorite intrudes this fabric and contains enclaves with this fabric (see Chapter 4). Therefore the main episode of activity of the SRSZ system, both in the Shaw Batholith and the greenstones, is constrained to 3468 Ma.

However, the grey gneisses, with a crystallization age of 3451 ± 1 Ma, were observed (Chapter 4) to be truncated by the base of the SRSZ, indicating that the basal SRSZ must have been active or reactivated during or after 3451 Ma. The brittle extensional structures in the Coongan Belt are constrained by the age of the Duffer Formation at 3452 ± 16 Ma (Pidgeon, 1978a, conventional zircon U-Pb) and more recently using single zircon techniques in other belts of the eastern Pilbara at 3471 ± 3 Ma, 3465 ± 3 Ma and 3470 ± 2 Ma (Thorpe et al., 1992), whereas felsic volcanics of the overlying Salgash Subgroup were dated at 3454 ± 1 Ma, the same age as the crystallization age of the grey gneiss at 3451 ± 1 Ma (this study).

This implies that the basal extensional structure, the SRSZ was formed at 3468 Ma and was active until or reactivated at 3451 Ma, when massive melting occurred below the SRSZ, forming the grey gneisses, and extension occurred in the supracrustals during extrusion of felsic volcanics.

Even younger age groups that occur in T94/227 (3440 ± 5 Ma and 3415 ± 4 Ma) and T94/193 (ca. 3300 Ma) indicate that there were high grade metamorphic events in the SRSZ area postdating its initial activity. These age groups may reflect the moments that the basal SRSZ was re-activated, causing disturbances in the zircon isotopic system. It can not be ruled out with the U-Pb dates that a part of the basal shear zone of the SRSZ was reactivated at an even later stage, for example during the 3.33–3.20 Ga thrusting event in the Coongan Belt. However the structures in the basal SRSZ show no clear indication for such a later reactivation (Chapter 4).

The diorite with a crystallization age of 3463 ± 2 Ma, is older than the gneiss, consistent with the field observation of the diorite as boudins in the grey gneiss.

The ultramylonite in the MSZC is constrained in time by the crystallization age of the synkinematic granitic dyke (sample T94/31) at 2934 ± 2 Ma. This provides a reliable constraint on the age of late movement on the north trending Mulgandinnah Lineament across the eastern Pilbara, of which the MSZC is part.

8.4 Discussion and conclusions

Combined $^{40}\text{Ar}/^{39}\text{Ar}$ dating on hornblende, biotite and muscovite and U-Pb dating on zircons provided a range of new age data on the structural and thermal development of the Shaw Batholith and Coongan Belt. The data from this and previous studies and the relation to structural and metamorphic events in the Shaw area are shown in Figure 8.12.

The first major intrusive event in the Shaw Batholith occurred between 3470 and 3450 Ma. A large volume of granitoids including diorites, North Shaw Suite granodiorites and precursors to the grey gneiss have crystallization ages in this range. Two xenocrysts in this study with ages between 3510 and 3525 indicate that the 3470–3450 Ma granitoids intruded into a slightly older basement. These xenocryst ages coincide with the age of the Coonterunah succession at 3515 ± 3 Ma (U-Pb zircon) as recorded by Buick et al. (1995). An even older basement is indicated by the 3578 ± 4 Ma age of anorthositic enclaves in the South Daltons Pluton (U-Pb zircon, McNaughton et al., 1988).

The main activity on the SRSZ is constrained to 3468 Ma but the basal zone of the SRSZ must have been active at least until 3451 Ma, the crystallization age of the gneiss. The activity in the SRSZ must have started in the greenstones before 3468 Ma, the crystallization age of the granodiorite wedge that intruded the SRSZ mylonitic foliation in the Coongan Belt.

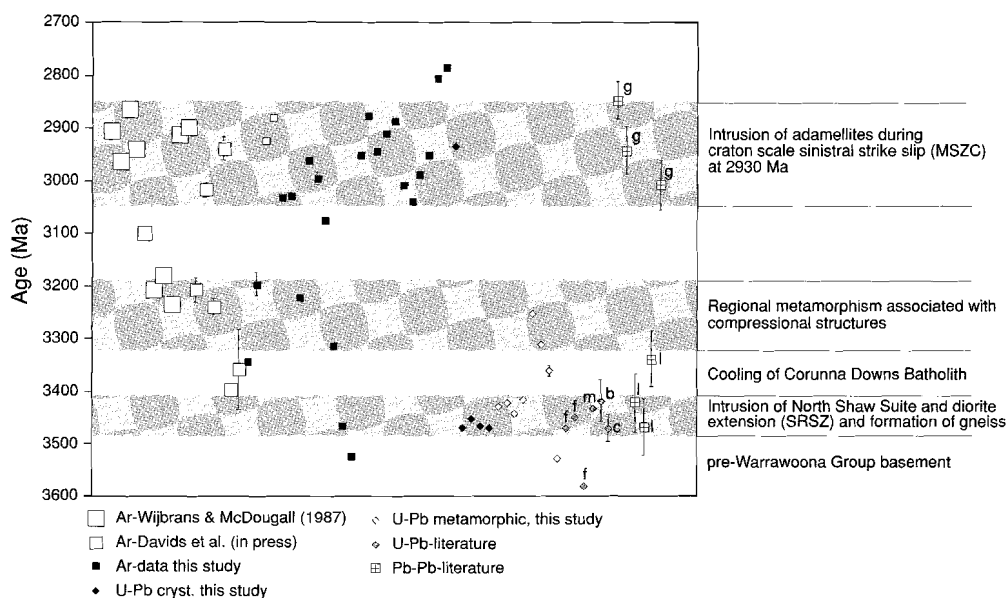


Figure 8.12 $^{40}\text{Ar}/^{39}\text{Ar}$ and U-Pb data from this and previous studies and related structural and metamorphic events in the Shaw area, based on this study and age information from: b= Pidgeon (1978b), c= Williams et al.(1983), f= McNaughton et al.(1988), l=Bickle et al. (1993), m=McNaughton et al. (1993).

Figure 8.10 shows a range of U-Pb zircon ages from this and other studies between 3470 and 3415 Ma. This study shows that most of the zircon ages younger than 3450 Ma come from rim areas and are therefore assumed to be metamorphic ages rather than crystallization ages. The age of the 3415 Ma rims is from the mylonite sample, indicating that the Split Rock Shear Zone may have continued at least until this age.

The oldest $^{40}\text{Ar}/^{39}\text{Ar}$ cooling ages at 3522 ± 11 Ma and 3466 ± 13 Ma (T94/87) coincide with the U-Pb ages of the xenocrysts and first intrusive event. This indicates that at least some areas in the Pilbara have never been heated significantly since this early intrusive event.

The metamorphic aureole of the Corunna Downs Batholith gave hornblende cooling ages between 3400 Ma (Davids et al., in press) and 3340 Ma (this study) indicating that the Corunna Downs Batholith intruded during a relatively early stage in the evolution of the Pilbara Craton. These observations reinforce the observation that extensive parts of the supracrustal rocks have escaped severe overprinting, essentially since the time of first granite emplacement.

A number of U-Pb ages from recrystallized parts of zircons and $^{40}\text{Ar}/^{39}\text{Ar}$ cooling ages fall between 3.3 and 3.2 Ga. The microstructural relations of hornblendes in this age range (actinolite in CCSZ) indicate that this metamorphic event occurred during or directly after the compressional structural event in the greenstones. The main shear zone in the Coongan Belt, the CCSZ is hereby constrained to a minimum age of 3.2 Ga. Since there are no granitoids in the area with crystallization ages in this range it is likely that these metamorphic ages are related to a regional metamorphic event. Bickle et al. (1993) recorded a Pb-Pb whole rock isochron age of 3338 ± 52 Ma in the northwestern Shaw

Batholith. In view of the data presented here this age may well have been a metamorphic rather than a crystallization age.

The large-scale strike-slip deformation in the MSZC is now constrained to 2932 Ma, this is consistent with the $^{40}\text{Ar}/^{39}\text{Ar}$ cooling ages in and close to the MSZC.

In the Shaw Batholith almost all $^{40}\text{Ar}/^{39}\text{Ar}$ ages are reset to ages close to the late to post-tectonic granitoids (3.0–2.85 Ga), whereas older cooling ages occur in the greenstones.

Much of the thermal evolution of the Tambourah Belt - Shaw Batholith - Coongan Belt area can be understood in terms of the effects of granitoid intrusion. This is particularly clear for the large-scale on which the cooling ages are reset at ca. 2950–3000 Ma due to granite intrusion, but some of the oldest cooling ages (3466 ± 13 Ma) can also be directly related to granitoid intrusion of the North Shaw Suite.

Finally, the Black Range dolerite dyke, which indicates the final cratonization of the Pilbara Craton, gave a hornblende cooling age of ca. 2800 Ma.

Discussion and Conclusions

9.1 Introduction

During the studies described in this thesis, new insights have been developed concerning the evolution of the Pilbara granitoid-greenstone terrain. A number of successive structural events were identified during the 800 Ma tectonothermal evolution of the eastern Pilbara. These structural events have been constrained in time by a combination of detailed mapping, structural analysis and isotopic dating (U-Pb SHRIMP and $^{40}\text{Ar}/^{39}\text{Ar}$). In Figure 9.1 the structural episodes and their relation to granitoids, greenstones and metamorphic events, are summarized. A detailed study of one of the main gold deposits in the Pilbara, Bamboo Creek Deposit, provides constraints on the setting and timing of this gold mineralization event.

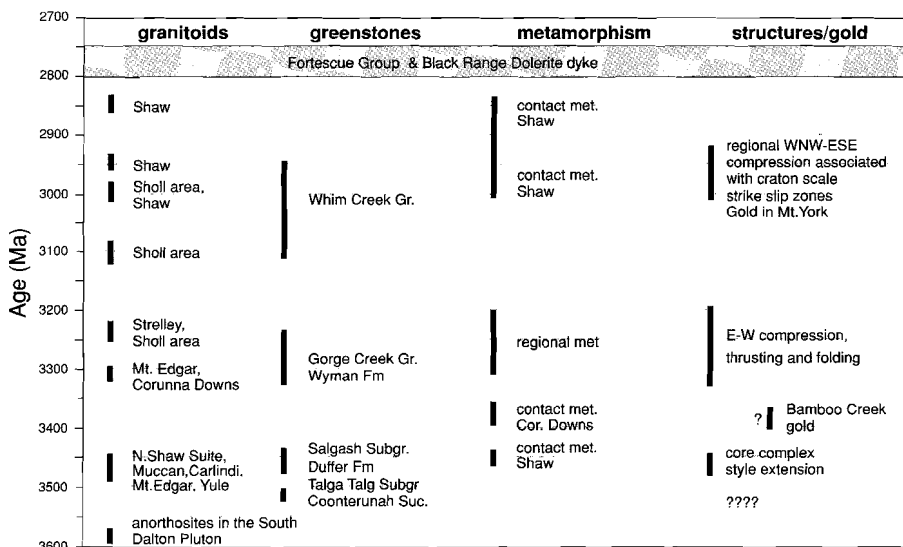


Figure 9.1 Figure showing geochronology of supracrustals, granitoids and metamorphic and structural events. The granitoids and supracrustals are constrained by U-Pb zircon dating (this study and Pidgeon (1978a), Pidgeon (1978b), Williams et al. (1983), Froude et al. (1984), Pidgeon (1984), McNaughton et al. (1988), Bickle et al. (1989), Williams & Collins (1990), Thorpe et al. (1990), Arndt et al. (1991), Thorpe et al. (1992), Bickle et al. (1993), McNaughton et al. (1993), Horwitz & Pidgeon (1993), Buick et al. (1995), Nelson (1996), Smith et al. (in press), upper greenschist to amphibolite metamorphism is constrained by $^{40}\text{Ar}/^{39}\text{Ar}$ cooling ages (this study and Wijbrans & McDougall, 1987; Davids et al., in press), gold mineralization is constrained by Pb-Pb model ages (this study and Neumayr et al., 1993) and structures by cross-cutting relations.

The aim of the first part of this Chapter is to summarize all new information of this study and to present a syntheses with previous work for the (eastern) Pilbara granitoid-greenstone terrain. Where possible parts of the tectonothermal evolution will be compared to elements of modern analogue tectonic settings.

In the second part the evolution of the Pilbara will be compared to that of the contemporaneous Kaapvaal Craton and the late Archean Yilgarn Craton.

Finally the question of plate tectonics in the mid-Archean Pilbara Craton will be addressed.

9.2 Tectonothermal evolution of the Pilbara granitoid-greenstone terrain.

The following description of the tectonothermal evolution of the Pilbara granitoid-greenstone terrain is largely based on the results of this study and is best constrained in the Shaw Batholith and Coongan Belt where the most detailed mapping and structural analysis was done during the course of this study. However, other areas, between the Lionel Lineament and the Mulgandinnah Lineament have been studied, but in less detail by means of traverses and local mapping. In Figures 9.2, 9.3 and 9.4 a three dimensional impression is given of the geometry after the three main structural episodes, in the area between the Lionel Lineament and the Mulgandinnah Lineament.

9.2.1 *The basement to the Duffer Formation*

There is now irrefutable evidence for a continental basement, in at least some areas in the Pilbara, to the upper part of the Warrawoona Group (Buick et al., 1995), consisting of the Coonterunah Succession, dated at 3515 Ma which was folded and foliated, intruded by granodiorites and eroded, prior to deposition of the Upper Warrawoona Group. The exact age of the succession immediately above the unconformity contains no suitable rocks for dating, but Buick et al (1995) interpret the sequence as the lateral equivalent of the Strelley Chert and constrain the unconformity between 3.47 Ga and 3.46 Ga.

Although attempts have been made (McNaughton, 1993), no reliable U-Pb zircon ages of the Talga Talga Subgroup (lower Warrawoona Group) are available, due to the lack of felsic volcanics. McNaughton et al. (1993) used a dolerite sill in the McPhee Formation and a single pillow from the North Star Basalt in the type section of the Talga Talga Subgroup for a U-Pb zircon dating study. Both samples contained very few zircons, approximately 1 per kg sample. The zircons from the dolerite sill gave a pooled U-P age of 3308 ± 4 Ma, which is younger than the overlying Duffer Formation (3466 ± 4 Ma, McNaughton et al., 1993), and a small number of ca. 3450-3470 Ma xenocrysts, indicating that it is a post volcanic sill and does not represent the Talga Talga Subgroup. In the North Star Basalt, all zircons were younger than 3326 Ma, which is the crystallization age of the well documented Wyman Formation (McNaughton et al., 1993; Thorpe et al. 1992). The small number of zircons and the ages typical of the Duffer Formation and Wyman Formation, indicate that these ages do not represent the age of the Talga Talga Subgroup, but are due to intrusives and/or hydrothermal zircon growth (McNaughton et al., 1993). Thorpe et al. (1992) dated a felsic unit in the Mt. Ada Basalt (U-Pb, zircon), which gave two ages: 3449 ± 3 Ma and 3470 ± 3 Ma. Thorpe et al. (1992) concluded that this was a felsic sill of the age of the Salgash Subgroup (3449 ± 3 Ma) with xenocrystic zircon from the Duffer Formation (3470 ± 3 Ma) and not a volcanic sample from the Talga

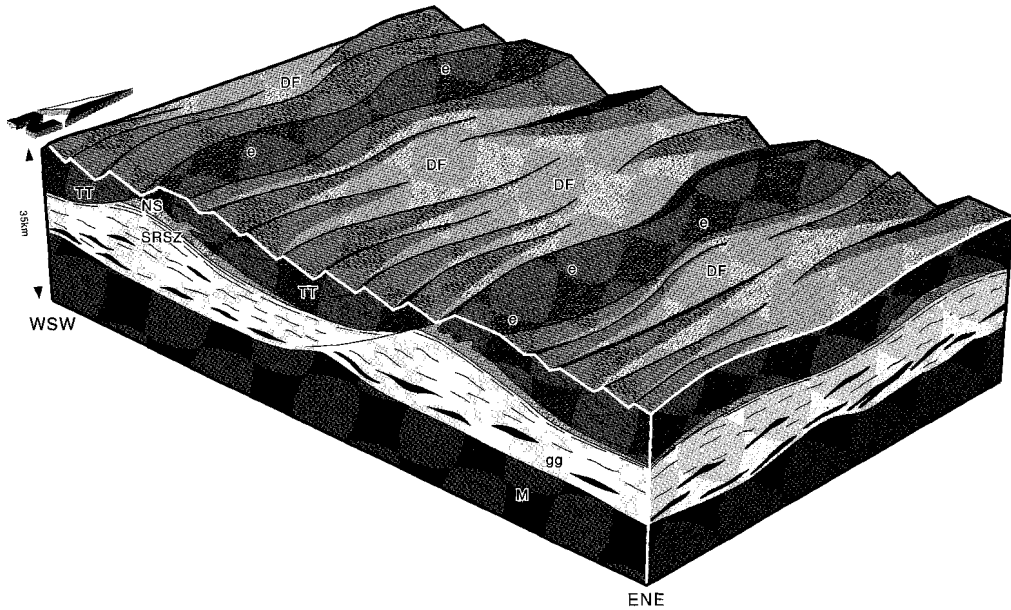


Figure 9.2 Schematic 3-d cartoons showing the structural development of the eastern Pilbara granitoid-greenstone terrain at 3.47-3.45 Ga, largely based on the structures and geochronology of the Coongan Belt and Shaw Batholith.

ENE-WSW extension involving brittle faults and block rotations in the upper crust, and detachment zones (Split Rock Shear Zone, SRSZ) at the mid-crustal level. The lower crust is intruded by mantle (M) derived magmas, causing partial melting of the lower crust forming the grey migmatitic gneisses (gg) with dioritic enclaves in the core of the Shaw Batholith. Granodiorites, the North Shaw Suite (NS) in the Shaw Batholith, intrude during deformation on the detachment zones, forming culminations. Felsic calc-alkaline volcanism (Duffer Formation, DF), the extrusive equivalent of the North Shaw Suite, occurs during the main phase of extension, filling in the relief formed by fault escarpments. The overall geometry consists of domes, in the footwall of the master faults, and basins, although the granites do not surface yet in the domes. The areas where erosion took place in this model are indicated by (e), in the footwall of major extensional faults. The felsic volcanics and clastic sediments of the Duffer Formation are covered by a 20 metre thick dolomite unit, not indicated in this Figure. In parts where the Talga Talga Subgroup (TT) was exposed, an angular unconformity may exist between the dolomite and the Talga Talga Subgroup. The dolomite unit is unconformably covered by pillow basalts and cherts of the Salgash Subgroup. The extension direction is drawn as consistently to the WSW. However, this is not certain and the pattern of transport

Talga Subgroup. Another possibility was raised by van Haaften & White (in press), who showed that the type section of the Warrawoona Group is tectonically disturbed by normal faults and low angle thrusts. They indicate that what is regarded as the Talga Talga Subgroup below the Duffer Formation may have been tectonically emplaced and may be younger than the Duffer Formation (Salgash Subgroup or Gorge Creek Group). However, the stratigraphic sequence of the Talga Talga Subgroup in the type section, basalt with a large component of gabbroic and dolerite sills (Hickman, 1983, Barley, 1993), is sufficiently different from the stratigraphic sequence of the Salgash Subgroup, pillow basalt with distinctive chert units (Hickman, 1983, Barley, 1993), to make this an unlikely option. Hamilton et al. (1981) dated a suite of volcanic samples from the North Star Basalt, in the basal Talga

Talga Subgroup in the type section, with Sm-Nd whole rock at 3560 ± 32 Ma. In this study, a sample from the Talga Talga Subgroup, north of the Shaw Batholith, stratigraphically below the dated Duffer Formation (3458 ± 2 Ma) gave two cooling ages (3466 ± 13 Ma and 3522 ± 13 Ma) of which the higher age could be interpreted as a partially overprinted magmatic argon cooling age. Davids et al. (in press) reported a 3518 ± 16 Ma $^{40}\text{Ar}/^{39}\text{Ar}$ isochron age for cores of hornblendes from the Talga Talga Subgroup in the western Coongan Belt, which may be interpreted as a magmatic cooling age. These ages for the Talga Talga Subgroup are close to the U-Pb zircon age of the Coonterunah Succession, which raises the possibility that, what is now regarded as the Talga Talga Subgroup in the type section and in the Coongan belt, may be the lateral equivalent of the Coonterunah Succession, although the Coonterunah Succession has a slight schistosity (Buick et al., 1995) predating the deposition of the upper Warrawoona Group, whereas in the type section the Talga Talga Subgroup is internally undeformed. The angular unconformity reported in the Carlindi area may be a local, related to extension (e in Figure 9.2) or may be related to pre-Duffer Formation compressional deformation in the Carlindi area. Both successions consist of mainly mafic and ultramafic volcanics, very minor felsic volcanics, minor cherts and a large (50%) component of doleritic/gabbroic sills. The Talga Talga Subgroup is interpreted as a shallow marine marginal setting (Barley, 1979) or an ophiolite complex (Krapez, 1993), whereas the Coonterunah Succession is interpreted as a deep water deposit (Buick et al., 1995).

Other fragments of a pre-Duffer Formation basement consist of 3580 Ma anorthositic enclaves in the Shaw Batholith (McNaughton et al., 1988). In addition, the 3.7 Ga xenocrystic zircon in the Duffer Formation (Thorpe et al., 1992) is an indication of an even older sialic basement.

For a long time the migmatic gneisses in the granitoids were all thought to represent the basement to the Warrawoona Group (Hickman, 1983). This is now clearly shown not to be the case because of the 3451 ± 1 Ma and 3463 ± 2 Ma U-Pb SHRIMP ages of migmatic gneisses and diorites found in this study in the central Shaw Batholith (this study, Chapter 8). The implication is, that although there was a continental basement to the upper Warrawoona Group, little is left now, and judging from the small number of >3.5 Ga xenocrysts found in this and other SHRIMP studies, the felsic component of the basement was not very extensive. The sillimanite-kyanite assemblages described by Bickle et al. (1985) in enclaves in the Shaw Batholith have not been dated, but were interpreted by Bickle et al. (1985) as part of the ca 3200 Ma compressional event. However, it could be argued that these assemblages have been part of the pre-Warrawoona Group basement, as medium to high-pressure assemblages have not definitively been found in other areas of the Pilbara.

9.2.2 Upper Warrawoona Group evolution

The stratigraphy of the upper Warrawoona Group has been the subject of many papers (Lowe, 1983; Barley, 1979, 1993; Buick & Dunlop, 1990; Krapez, 1993) and was recently reviewed in Eriksson et al. (1994). It starts with the Duffer Formation (3460–3470 Ma, Thorpe et al., 1992; McNaughton et al., 1993), which is genetically unrelated to the Talga Talga Subgroup (Krapez, 1993), consists of felsic volcanics and volcanoclastic sediments deposited in and adjacent to volcanic centers (Barley et al., 1984; DiMarco & Lowe, 1989) similar to present day volcanic arcs, but occurring in a large (ca. 130 km²) area with no linear trend.

The overlying Salgash Subgroup (3450 Ma, Thorpe et al., 1992) consists of mainly pillowed and massive tholeiite and high-MgO basalt, with minor chert horizons derived from felsic volcanic sources

(Lowe, 1983). Barley (1993) and Krapez (1993) suggest a shallow marine extensional setting, adjacent to volcanic islands or arcs.

Although some authors (Barley, 1993) mention an extensional setting for the Duffer Formation and Salgash Subgroup, no mention is made of structures during deposition of the upper Warrawoona Group.

In this study (Chapter 4), evidence was found for extensional structures related to deposition of the Duffer Formation in the Coongan Belt and emplacement of the granodioritic North Shaw Suite in Shaw Batholith. It has been argued that the geometry of the extensional structures is similar to that of a metamorphic core-complex (Figure 9.2). A major shear zone, with a transport direction to the WSW, the Split Rock Shear Zone, forms the contact between gneisses and greenstones, with syn-kinematic intrusion of the wedge shaped North Shaw Suite. In combination these produce an initial weak domal geometry. The present pronounced dome shape around parts of the batholiths are not thought to be the result of this extensional phase, but are a later syn- to post Lalla Rookh Sandstone (ca. 2950 Ma) feature. Contemporaneous extensional faults formed in the hanging wall during deposition of the Duffer Formation. These extensional structures are constrained in time to 3470–3450 Ma (Chapter 4) with the main activity during deposition of the Duffer Formation and intrusion of the North Shaw Suite at 3470 Ma, but continued activity on the basal Split Rock Shear Zone in the Shaw Batholith until at least 3450 Ma, during deposition of the Salgash Subgroup. The brittle extensional faults in the Coongan Belt are covered by a silicified dolomite unit, with characteristic stromatoloids. This unit was correlated to the Strelley Pool Chert (base of the Salgash Subgroup) in the North Pole area by DiMarco & Lowe (1989), which is the unit directly overlying the Coonterunah Succession in that area (Buick et al. (1995). In the conceptual model in Figure 9.2a, parts of the Talga Talga Subgroup that are eroded during the extensional phase, in the footwall of main faults, are indicated with e. In these areas an angular unconformity is expected between the Talga Talga Subgroup and the dolomite unit. Brittle faults, active during deposition of the Duffer Formation, have been identified in a large part of the eastern Pilbara (Figure 5.9) between the Kelly and Mulgandinnah Lineaments, but in most cases the directions of transport are not precisely established. Where the directions are well established, they indicate transport to the west (Coppin Gap Belt) and WSW (Coongan - Shaw). Recent U-Pb SHRIMP dating shows that the Carlindi (Buick et al., 1995), the Muccan (Nelson, 1996) and the Yule Batholiths (van Kranendonk, pers.comm.) contain major 3460–3450 Ma components, similar to the Shaw and Mt.Edgar Batholiths (Figure 9.1). No U-Pb SHRIMP data are available of the Corunna Downs Batholith, but the argon dating in this study and by Davids et al. (in press) indicates that at least part of the Corunna Downs Batholith is older than 3.4 Ga (Chapter 8). Therefore, this magmatic event, associated with extension, occurred in at least the area of the Yule, Carlindi, Muccan, Mt.Edgar and Shaw Batholiths and probably the Corunna Down Batholith (150 x 200 km), indicating that this large area may have been subject to extensional deformation between 3460 and 3450 Ma.

In the past ten years the tectonic setting of extensional terrains and the causes of extension have been the subject of much discussion. In Table 9.1 the currently recognized extensional settings in relation to modern day plate tectonic settings have been listed. Many of these are controversial, and recent extensional areas (Basin and Range, Aegean area, East African Rift) are interpreted in different ways. The Basin and Range area has alternatively been interpreted as a back-arc basin (Coney, 1987), late stage extensional collapse after delamination (Dewey, 1988), due to convective thinning of the lithos-

pheric mantle (Hawkesworth et al., 1995) or gravitational collapse (Sonder et al., 1987) and as the result of a mantle plume (Parsons et al., 1994).

For the Pilbara Craton, there is no information on the surrounding tectonic setting, nor on the amount of extension and the thickness of the crust after extension. Therefore it seems unlikely that the unique setting in which the extension at 3450 Ma occurred in the Pilbara can be identified, even if plate tectonic processes are assumed to have operated in the same way as now. However, it is possible to investigate which characteristics of the various extensional models are in agreement with the structural, geochronological and stratigraphic data from the eastern Pilbara. Table 9.1 shows that the main distinguishing criteria are: the basement to the extension, the trend of transport direction and the sequence of magmatic events as related to the onset of extension.

Table 9.1 Characteristics of different extensional tectonic settings

	External forces			Body forces	
	Continental rift	Back-arc basin (Royden, 1993)	Mid oceanic ridge	Mantle plume (Hill, 1991)	Orogenic collapse (Houseman et al., 1981; Dewey, 1988)
Basement	continental crust	(continental crust) oceanic crust	no crustal basement	oceanic or continental crust	orogen
geometrical trend	linear unidirectional transport	linear unidirectional transport	linear unidirectional transport	semi-circular radial transport	semi-circular radial transport
magmatism					
1. pre-extension	no	calc-alkaline in arc		uplift high-Mg basalt komatiite	crustal derived granites
2. extension	crustal melt	alkaline in back-arc	Ophiolite complex	major mafic melt	
3. post-extension	mantle melt	oceanization		crustal melt	

Uniform transport directions over a large area would be a good indication for externally applied boundary forces such as expected in a plate tectonic type extensional setting (back arcs and continental rifts). If however the transport directions show an irregular or radial pattern on the largest scale, it is an indication of extension due to body or gravity forces similar to extensional collapse (Dewey, 1988), or possibly related to extension above a mantle plume (Campbell & Hill, 1988). In the Pilbara, although incomplete, the extensional transport data set seems to be unidirectional which would argue for externally applied forces causing extension.

The sequence of events in the Coongan-Shaw area can be summarized as follows: a basement (Talga Talga subgroup) is covered by thick felsic volcanic and volcano clastics, deposited during extension (3470–3460 Ma) followed by mafic volcanics deposited in shallow water. The complete sequence of events took place between the deposition of the Talga Talga Subgroup, certainly older than 3470 Ma (age of intrusive North Shaw Suite) and possibly as old as 3520 Ma (oldest argon dates in the Coongan Belt, this study and Davids et al, in press), and 3450 Ma (youngest age of Warrawoona Group, Thorpe et al., 1992), i.e. in less than 100 Ma.

The basement to the extension is the Talga Talga Subgroup, which, as argued above, may be equivalent to the Coonterunah Succession. The Talga Talga Subgroup stratigraphy and geochemistry in the type area has been likened to oceanic crust (Krapez, 1993; Barley, 1993). At the type location of the Coonterunah Succession (Buick et al., 1995), the succession is foliated, and intruded by granitoids prior to deposition of the upper Warrawoona Group, i.e. it was continental crust prior to deposition of the upper Warrawoona Group, starting with the deposition of the Strelley Pool Chert. If the correlation between the Coonterunah Succession and the Talga Talga Subgroup is correct, it could be deformed oceanic crust. It seems unlikely that the pre-Duffer Formation basement was part of an orogen, but data is too scarce to rule this out.

An arc type setting is not easily reconciled with the data on the setting of the Warrawoona Group. The main problem with this interpretation is the distinctly non-linear distribution of rocks and structures in the eastern Pilbara. There is no trace of high pressure metamorphism and only very little indication of medium pressure metamorphism, and certainly no indication of paired metamorphic belts, characteristic of a subduction setting (Miyashiro, 1972). Highly deformed melange zones do not occur and neither do turbidites in the Warrawoona Group. The only possible type of setting related to a subduction zone that could be reconciled with the data is a marginal- or back arc basin, because in such tectonic settings extension may occur during (calc-)alkaline magmatic activity. Marginal basins formed by rifting of island-arcs are deposited on oceanic crust. However, at least part of the Warrawoona Group is deposited on a continental basement (Buick et al., 1995) making this an unlikely option.

Rifting in a continental setting could be caused by the arrival of a plume head under the continent as proposed by Hill (1991) and Campbell & Hill (1988) for the Yilgarn Craton. The sequence of events as discussed by Hill (1991) for a hot lithosphere can be summarized as follows: uplift and erosion, komatiitic volcanism, extensive mafic volcanism associated with rapid extension, and at a late stage crustally derived anatectic magmatism due to heating of the crust.

On the other hand, if rifting is the cause of melting, the volcanism, produced by decompression, will start with melts produced high in the lithosphere proceeding to deeper melts (Hawkesworth et al., 1995).

In the Warrawoona Group the main extensional phase, with brittle extensional faults in the supracrustals, occurred during calc-alkaline felsic volcanic and granodioritic magmatism, which seems to be in better agreement with decompression melting than with a plume model. However the widespread alkaline magmas associated with modern continental rifts (Bailey, 1983) do not occur in the Warrawoona Group.

If the extension, during deposition of the Duffer Formation, is related to extensional collapse, remnants of the earlier crustal thickening phase would be expected 20–30 Ma prior to the main extensional phase (Dewey, 1988). The fragments of this age (ca. 3500 Ma, Coonterunah Succession) are small and few and show no clear indication of an earlier crustal thickening event.

Costa & Rey (1995) describe an example of a Variscan metamorphic core-complex in the Massif Central (France) in which intrusion of mantle derived magmas into the base of the crust, granulite grade metamorphism in the lower crust, extraction of granites from the deep crust and deposition of continental basins associated with normal faulting all occur within 40 Ma during the extensional phase. No basement pre-dating this extensional event was found in the footwall. This is consistent

with the data for the upper Warrawoona Group extension: the complexly deformed diorites (3463 Ma) and gneisses (3451 Ma) in the core of the Shaw Batholith are in the same age range as the syn-extension granodioritic North Shaw Suite and the syn-extension felsic volcanics of the Duffer Formation and fragments of pre-extension basement are scarce.

Calc-alkaline major element trends, such as reported for the Duffer Formation (Barley, 1993), are usually interpreted as subduction related magmatism. However, Hawkesworth et al. (1995) show that they can equally well be related to continental extension in the type area of metamorphic core-complexes in the Basin and Range province of the western United States. They attribute the calc-alkaline trend to mixing of mantle derived melts with crustal derived melts. The large amounts of melt in the Warrawoona Group as compared to the Basin and Range could well be the result of the higher geothermal gradient in the Archean lithosphere.

In summary, the structural, kinematic, metamorphic and magmatic patterns for 3450 Ma extension in the Pilbara are most consistent with a continental type extension model, in which extension is either caused by external boundary forces, or by a type of orogenic collapse (delamination or convective thinning of the lithospheric mantle). A back-arc supra-subduction type setting is less likely because there is no strong linear trend of the greenstones and no indication for a nearby subduction zone. A mantle plume setting is not likely because the kinematic data of the extensional phase indicate unidirectional transport to the WSW and the sequence of volcanics is contrary to that expected for a plume model.

Extension may have occurred after stacking of oceanic crust by obduction as proposed by de Wit & Hart (1993). In this model, the calc-alkaline magmatism represents the partial melt of stacked hydrated oceanic crust. This is consistent with models in which TTG suites are best explained as partial melt of garnet-bearing amphibolite or hornblende eclogite (Martin, 1994; Rapp & Watson, 1995)

9.2.3 Gold mineralization

Lode gold deposits occur in greenschist facies shear zones in the Warrawoona Group. The results from this study (Chapter 7) show that the Bamboo Creek Deposit, one of the main gold deposits in the Pilbara which is situated in the Bamboo Creek Shear Zone, is in most respects (alteration, temperature of alteration and stable isotope composition) similar to lode gold deposits in late Archean terrains. However the structural setting is related to, or slightly post-dates the extensional event. Cross cutting relations constrain the gold mineralization event between 3454 Ma and 3300 Ma. Pb-Pb dating of galena associated with the gold gives a 3400 ± 40 Ma model age, which is interpreted as a maximum age. The gold mineralization event is tentatively inferred to be related to the late stages of the extensional event during deposition of the upper Warrawoona Group. The shear zone which contains the deposits is reactivated after gold mineralization, but this happened prior to granitoid intrusion at 3.3 Ga. However, age constraints on the gold mineralization event are not precise enough to establish with certainty whether mineralization occurred during the extensional (3470–3450 Ma) or compressional (3340–3200 Ma) event.

The large, late Archean gold deposits are usually thought to be associated with the final stages of accretion in a subduction setting, related to compressional and strike-slip structures (Kerrick & Cassidy, 1994; Groves et al., 1995) or in some cases to post compressional extension (Wang & White, 1991). This tectonic setting of gold deposits is likened to modern gold deposits associated with volcanic arc of the Pacific Rim (Nesbitt et al., 1986; Barley et al., 1989; Kerrich & Cassidy, 1994).

However, with respect to the structural setting of the Bamboo Creek Deposit, this type of tectonic setting may not be a good analogue for the 3.4 Ga gold mineralization event.

The lode gold deposits in the Warrawoona Group shear zones may be more similar to the relatively few but high grade lode gold deposits in the Basin and Range Province. These have been summarized by Thorman & Christensen (1991). The timing of these lode gold deposits is consistent with their formation in a continental extensional setting (< Eocene) associated with metamorphic core-complexes. A gold district that is particularly similar in setting, alteration style and mineral association to the Bamboo Creek Deposit is the Bullfrog district (Castor & Weiss, 1992) in Nevada. These Miocene lode gold deposits occur in core-complex type extensional settings, in felsic host rocks, and are characterized by low grade alteration with open space infillings of quartz, potassic alteration, mainly visible gold with low to moderate Ag contents. Minerals associated with gold include chalcopyrite, galena, sphalerite and tetrahedrite (Castor & Weiss, 1992), the same assemblage as found in the Bamboo Creek Deposit. The similarity between the Bullfrog district deposits and the Bamboo Creek Deposit is an additional indication that the tectonic setting of the Warrawoona Group was similar to the Basin and Range Province extensional setting.

However, direct comparison with modern settings remains tentative, because only a relatively small area is exposed of the 3.45 Ga Warrawoona Group and a lack of 'far-field data' (Passchier, 1995) such as paleomagnetic plate reconstructions, seismological data, data on spreading and subduction rates of relevant plates. This type of data has proven to be indispensable for the analysis of modern geological terrains.

9.2.4 *Syn- to post Gorge Creek Group evolution*

The stratigraphy of the Gorge Creek Group (3325–3240 Ma, Figure 9.1) has not been as extensively studied as the Warrawoona Group and appears to be more variable than the Warrawoona Group (Horwitz, 1990; Krapez, 1993). In the eastern Pilbara the GCG consists of a felsic basal unit, dated at 3325 Ma and/ or clastic basal units. The GCG is dominated by clastic sediments, clay, sandstones and conglomerates and a thick upper BIF unit. Mafic volcanics are a minor component in the eastern Pilbara but increase toward the west (Horwitz, 1990). Ultramafic intrusives and sills are also thought to be of Gorge Creek Group age (Krapez, 1993). The stratigraphic position of the sandstone, shale and conglomerate Mosquito Creek sequence is uncertain. (Krapez (1993) interpreted this sequence as part of the upper Gorge Creek Group. The age of the upper Gorge Creek Group is unknown but is interpreted by Krapez (1993) to be of similar age as the Strelley Granite (3238±4 Ma, Smith et al., 1997).

Structures formed in an E–W compressional regime are approximately synchronous with deposition of the Gorge Creek Group in the domain between the Mulgandinnah and Lionel Lineaments. Shear zones within the Warrawoona Belt and northern Coppin Gap Belt acted as transfer faults to the compressional structures dividing the domain in a southern subdomain with westward transport, a central domain with eastward transport and a northern subdomain with westward transport (Figure 9.3). These compressional structures appear to have been mostly constrained to the supracrustals, although some of the greenstone intercalation in the western Shaw Batholith may be the result of thrusting, as proposed by Bettenay et al. (1981). The thrusting in the greenstones caused local repetitions of the stratigraphy producing a geometry in which panels of weakly foliated and sometimes folded stratigraphic sequences are separated by greenschist facies shear zones, preferentially developed in carbon-

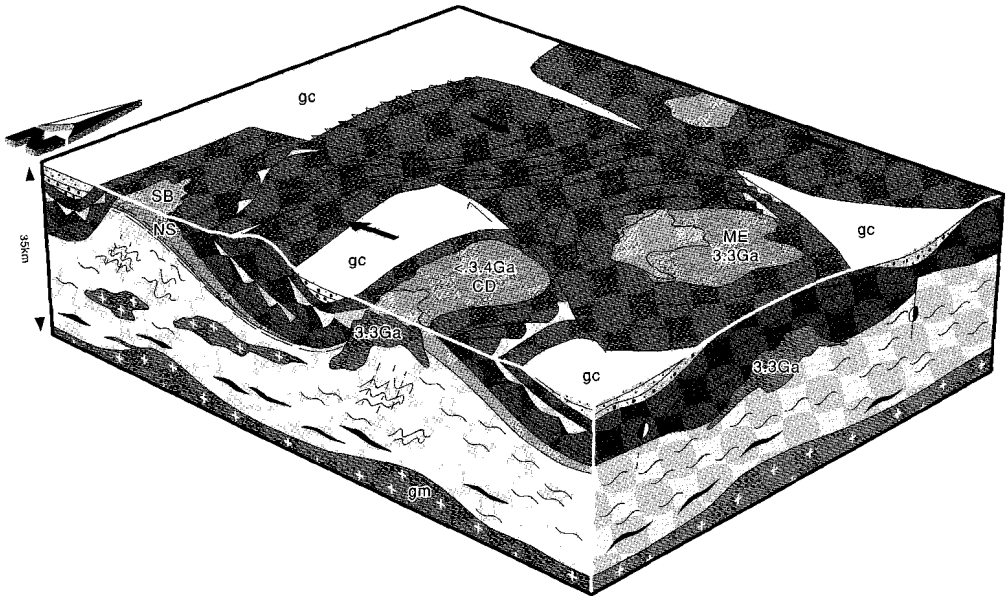


Figure 9.3 Schematic 3-d cartoons showing the structural development of the eastern Pilbara granitoid-greenstone terrain at ca. 3.3, largely based on the structures and geochronology of the Coongan Belt and Shaw Batholith.

E-W compression, involving thrusting and folding, occurs in the greenstone belts, causing repetition of the Warrawoona Group stratigraphy. The relief of the thrust and fold belt is filled in with clastic sediments of the Gorge Creek Group (GC). The domal shape of the granitoids is enhanced by compression and by intrusion of granodiorites (Corunna Downs, CD, 3.3 and <math>< 3.4 \text{ Ga}</math>, Mount Edgar, ME, ca. 3.3 Ga). Parts of the granitoids, such as the Shaw batholith (SB) are surfacing, shedding clastic sediments to the Gorge Creek Group. E-W trending strike slip faults act as transfer faults to domains with opposing transport directions. At the base of the crust a layer of granitic melt (gm) accumulates.

ate altered ultramafic units. These thrusts commonly reactivated the basal shear zones to the brittle extensional faults formed during the 3.45 Ma extensional event. Although the thrusts cause stacking of the stratigraphy they do not appear to significantly alter the geometry of weakly developed granitic domes formed during the 3.45 Ga extensional phase. The dome shape is probably further enhanced by the intrusion of ca. 3300 Ma granitoids in to pre-existing granitoids (Mt. Edgar Batholith, eastern Corunna Downs Batholith). These granitoid intrusions occur during or after thrust events in the greenstones. According to Collins (1993) the geochemistry of the 3.3 Ga granodiorites is consistent with their derivation from partial melting of stacked greenstone sequences.

The precise timing of the E-W compressional deformation phase is not easily established. Wherever the Wyman Formation (the basal felsic volcanic unit of the Gorge Creek Group) is present the E-W compressional structures can be shown to post-date this unit. In one case, one of the thrusts was found to be unconformably covered by a sandstone unit of unknown age, but probably part of the Gorge Creek Group. The upper limit of the Central Coongan Shear Zone is well constrained by the 3200 Ma argon plateau age of post-kinematic actinolites. This constrains the compressional event to 3325–3200 Ma.

A compressional deformation event was described in the western Shaw area by Bickle et al.

(1980,1985) and Boulter et al., (1987). They propose a deformation scheme in which D_1 is a high strain fabric in the western Shaw Batholith, causing intercalation of granites and greenstones, D_2 are isoclinal folds in the Warrawoona and Gorge Creek Group, covered by the Lalla Rookh Sandstone, D_3 are upright N-S trending folds after deposition of the Lalla Rookh Sandstone (Whim Creek Group), and D_4 are N-S trending strike-slip shear zones (Boulter et al., 1987). D_1 and D_2 are thought to be related to a crustal thickening phase (thrusting and folding), with unknown transport direction since no kinematic analysis was done. This crustal thickening phase is constrained by Bickle et al (1985) and Boulter et al. (1987) to between deposition of the Gorge Creek Group and before deposition of the Lalla Rookh Sandstone (Whim Creek Group), i.e. between 3325 and 2950 Ma. The 3200–3300 Ma cooling $^{40}\text{Ar}/^{39}\text{Ar}$ cooling ages of hornblende in that area (Wijbrans & McDougall, 1987) are considered to be an indication of the timing of metamorphism associated with D_1 and D_2 (Bickle et al.,1985; and Boulter et al., 1987). The compressional nature of the deformation and the timing constraints are consistent with the E-W compressional phase found in this study.

Metamorphism associated with, or post-dating the compressional structures never exceeds greenschist facies and no high or medium pressure, low temperature assemblages have been found in this study. The low pressure metamorphism and granitoid intrusion are more reminiscent of Hercynian orogenic belts rather than of Alpine style orogenies. A group of plateau ages (this study, Chapter 8) in the range between 3360 and 3200 Ma can not be related to granitoid intrusions of that age range in the Shaw area. They are interpreted as the result of a regional metamorphic event associated with the compressional structures, confirming the findings of Wijbrans & McDougall (1986). This leaves a long (160 Ma) period in which the compressional structures may have formed. In some cases (Bamboo Creek Shear Zone, Marble bar Belt, van Haaften & White, in press) compressional structures can be further constrained to be older than 3300 Ma. This, combined with the observation that compressional structures postdate the Wyman Formation, provides a much narrower time range (3325–3300 Ma). However, the possibility that there have been several phases of approximately E-W compression in the 3360–3200 Ma range can not be ruled out.

Thick clastic sequences in the Gorge Creek Group occur to the east and west of the central Marble Bar domain. This may indicate that crustal thickening due to E-W compression was largest in the central Marble Bar domain, with the Nullagine and Pilgangoora domains forming foreland basins. The interpretation by Eriksson et al. (1994) that the Gorge Creek Group was deposited in an NW-SE trending back-arc basin with continent to the NE and a volcanic arc to the SW is inconsistent with the observed E-W compression during deposition of the Gorge Creek Group.

9.2.5 Craton Scale Strike Slip Faults and final doming.

Craton scale sinistral NNE trending strike-slip lineaments have been proposed by Krapez (1993, Figure 3.1) as zones dividing the Pilbara into 5 domains. They were thought to have been active during deposition of clastic sediments in the Lalla Rookh and Whim Creek Basins at ca. 2950 Ma. In this study a detailed structural analysis was carried out of part of the Mulgandinnah Lineament (see Figure 6.2 and 9.4) in the Shaw Batholith. This part of the lineament, the MSZC, consists of a complex system of amphibolite to greenschist facies shear zones, showing sinistral and subsidiary vertical, mainly east up, displacement. A granitic dike, which intrudes during the final stages of the MSZC was dated in this study at 2934 ± 2 Ma (U-Pb SHRIMP) placing a precise age constraint on the final stages of movement on this lineament.

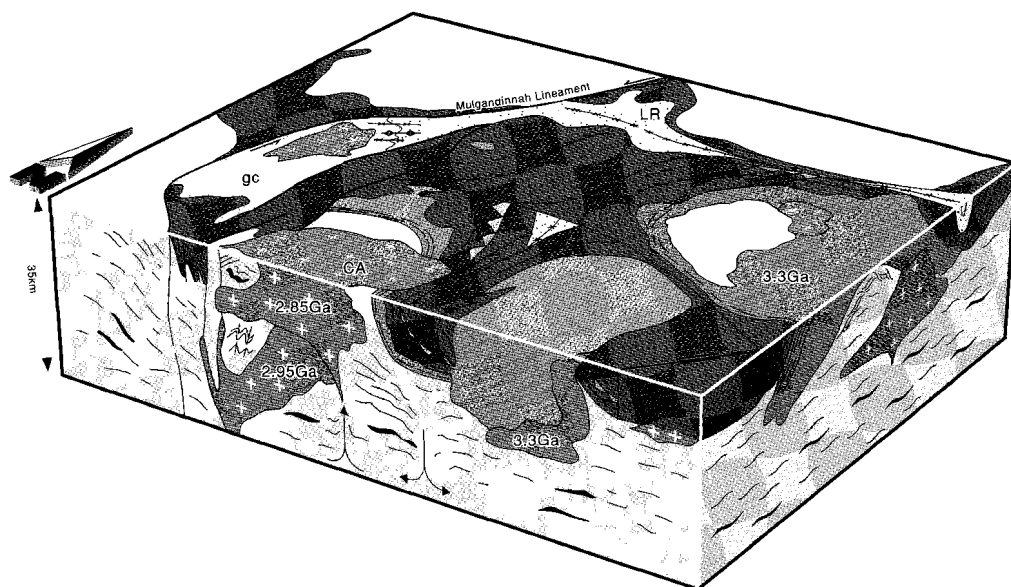


Figure 9.4 Situation at ca. 2.8 Ga, after north trending sinistral strike slip deformation (Mulgandinnah Lineament), contemporaneous intrusion of granites in the upper crust and deposition of the Lalla Rookh Basin (LR). At 2.85 post-tectonic granites intrude the Shaw Batholith (Cooglegong Adamellite, CA). In areas where extensive late (3.0-2.85 Ga) granite intrusion occurred, the upper greenstone sequences (Whim Creek Group) are steepened and folded into synclinal structures (Coongan Belt and SE Kelly Belt).

The Lionel lineament in the east consists of a brittle dextral fault called the Lionel Fault (Chapter 5). Its age is not well constrained but certainly postdates the Wyman Formation (3325 Ma) and the upper Gorge Creek sediments of the Nullagine Block. The straight outcrop pattern of the Lionel Fault indicates that it was active in the late stages of deformation in the eastern Pilbara, but it is covered by the Fortescue Group. Thus, its age is constrained between 3.24 and 2.77 Ga.

Spot checks along the Mallina Lineament in the west showed east up senses of displacement in an E-W compressional setting. The Sholl Lineament was shown to be an east west trending dextral ductile shear zone, which is lost toward the east as it approaches the Mallina Lineament. Smith et al. (in press) constrained the timing of the movement along this lineament to ca. 2960 Ma.

The kinematics and positions of major strike-slip shear zones in the Pilbara are not consistent with previous interpretations (Krapez, 1993; Eriksson et al., 1994), that show NNE trending sinistral shear lineaments associated with west-ward terrane accretion.

In the Superior Province (Card, 1990) and the Yilgarn Craton (Myers, 1995) a parallel set of lineaments with important strike-slip components divide the craton in tectonostratigraphic terranes. The lineaments are the boundary zones formed at different moments, along which terranes of subsequently younger ages have been accreted (Myers, 1995). This pattern is not so clear for the Pilbara Craton. This study shows that the lineaments vary from NE-SW trending (Kelly and Mallina) to N-S trending (Mulgandinnah) to E-W trending (Sholl), and are not all sinistral shear zones, but also dextral and reverse shear zones. Only the Mallina Lineament can be interpreted as a terrane boundary with the data now available, because it is the boundary between an older terrane to the east

(Warrawoona Group, Gorge Creek Group and minor Whim Creek Group) and a younger terrane with substantial 3.2 Ga volcanism to the west (Krapez, 1993). A more reliable interpretation can not be made until more geochronological data are available. However, at this stage the data do not support a general terrane accretion model along NNE trending lineaments. The pattern of lineaments and the kinematics, with the exception of the Lionel Lineament, are more consistent with conjugate sets of shear zones in a WNW-ESE compressional setting. The upright NE to N trending folds (Figure 9.4) in the area between the two main strands of the Mulgandinnah Lineament (1:250,000 geological map, Hickman, 1983) are considered to be another result of this compressional event, consistent with the interpretation by van Kranendonk & Collins (in press), who attribute these folds and the sinistral strike-slip faults to one progressive event. The NE trending folds post-date or are synchronous with the Lalla Rookh Sandstone, and can be correlated to D_3 (Boulter et al., 1987)

In a craton scale NW-SE compressional model, the lineaments would be expected to all have a similar age. This is more consistent with the 2930 Ma and 2960 Ma age constraints of the MSZC and the Sholl Shear Zone (Figure 6.6). In the studied area there is no indication for considerable crustal thickening during the 2950 Ma deformation. Deformation appears to have been localized in major shear zone systems, leaving major unaffected blocks in between.

Sleep (1992) showed that large-scale strike-slip zones can only form if lithospheric plates have obtained a similar rigidity as present day plates. Therefore the system of strike-slip shear zones in the Pilbara at ca. 2950 Ma is a good indication that the rheological properties of the lithospheric plates were no barrier for plate tectonic processes to take place.

In many areas in the eastern Pilbara the youngest clastic sequences, thought to belong to the Whim Creek Group, have moderate to steep dips and show only a small angular unconformity with the underlying sequences, indicating that a large component of the steepening of greenstone sequences in the belts into synclinal structures, occurred relatively late in the overall evolution, after deposition of the Lalla Rookh sandstone, i.e. after movement on the MSZC if the interpretation of the Lalla Rookh Basin as a pull apart basin related to the MSZC is correct (Krapez & Barley, 1987).

This steepening of older structures and stratigraphic sequences may be related to the intrusion of 2.85 Ga granites. Ridley (1992) proposed a model for late stage granites, in which partial melt of the crust accumulates at the base of the crust as granitic melt until the density of the melt is low enough to allow intrusion of granites into the upper crust. The late granites follow and intrude older granites domes. The extraction of melt in the lower crust from under greenstone belts will cause sinking of the greenstone belts in a diapiric pattern. The steep dips of late greenstone sequences around the Shaw Batholith with a large late granite component and the shallow dips of greenstones surrounding the North Pole granite with no known late granite component provide support for this model. However, the late granites must have caused no or very little pervasive deformation during their intrusion.

9.2.6 Dolerite dykes

Finally the granitoid-greenstone terrain was intruded by NNE trending dolerite dikes, dated at 2.8 Ga (this study). This emplacement age is consistent with the suggestion that they have been feeder dikes to the basal sequences of the Fortescue Group, dated as older than 2775 Ma (U-Pb, single zircon, Arndt et al., 1991). These dolerite dykes mark the final cratonization of the Pilbara Craton.

9.2.7 *The role of solid state diapirism*

In the past, and in some cases even today, the Pilbara granitoid-greenstone terrain is described as the best example of terrains formed by solid state diapirism (Hickman, 1983; Choukroune et al., 1995). This model is based on the assumption that there was a felsic-gneissic basement prior to deposition of the greenstone sequences. The difference in density between the basement and the supracrustals is assumed to lead to gravitational sinking of the greenstones in troughs surrounding rising gneissic domes in solid state, i.e. not by intrusion of granite magmas.

A number of papers (Dixon, 1975; Schwerdtner et al., 1978; Schwerdtner and Troëng, 1977) describe the strain pattern in the diapirs and adjacent synclines as resulting from centrifuge models with silicone putty. In more recent numerical models (Weinberg & Schmeling, 1992; Weinberg & Podladchikov, 1994, 1995) polydiapirs and the effects of power law rheology of the deforming rocks are studied. Although models show increasingly complex geometries depending on the rheology and interaction between various diapirs there are a number of basic characteristics of deformation as a result of solid state diapirism that can be compared to field data (van den Eeckhout et al., 1986; Weinberg & Podladchikov, 1995) and which need to be present before solid state diapirism can be assumed to have taken place. They are:

- 1 Diapirs are circular to ovoid in plan and have a domal geometry;
- 2 Foliations are parallel to the contact in the granitoid and increase toward the contact where a shear zone is likely to develop;
- 3 Stretching lineations form radial, down-dip patterns;
- 4 The sense of shear at the contact is consistently greenstones down;
- 5 The greenstones between two diapiric domes have a symmetrical synclinal geometry.

Of these criteria only the first is valid for the Pilbara granitoid-greenstone terrain. When studied in detail structures and kinematics are in disagreement with a diapiric model. Foliations in granitoids are not always parallel to the granitoid-greenstone contacts, many of the actual contacts are intrusive, shear zones do not necessarily develop at the contacts, lineations do not form radial patterns and kinematic analysis often shows greenstone up movements. This means that the structures observed in the Pilbara granitoid-greenstone terrain can not have resulted solely from solid state diapirism.

Collins (1989) interpreted the structures in and around the Mt. Edgar Batholith as the result of a combination of solid state diapirism and intrusion of granitoids. However, the structural and kinematic data are limited to a small area (one side of the batholith) and can be interpreted in more ways than solid state diapirism alone (van Haaften & White, in press).

The whole stratigraphic sequence, from the Talga Talga Subgroup until the Lalla Rookh Sandstone, must have been relatively flat lying until after deposition of the Lalla Rookh Sandstone, although initial weak doming developed during the extensional phase. The strong doming, developed in some areas, is related to the intrusion of late granites, which are themselves undeformed, precluding solid state diapirism as an important process during this doming event.

It can not be ruled out that solid state diapirism had some influence, either together with other deformation processes or at some stage of the evolution, but most of the structures that have been mapped and analysed must have resulted from different processes.

9.3 Comparison to other Archean terrains

The similarities between the Pilbara Craton and the Kaapvaal Craton in age and structural style has been noted by many workers in the past.

The crustal evolution of the Barberton Greenstone Belt is summarized in an overview paper by de Ronde & de Wit (1994). In Table 9.2 these data are compared to the data from the Pilbara.

Table 9.2 Comparison between the Pilbara and Kaapvaal Craton.

Pilbara		Barberton	
>3.47 Ga	mafic ultramafic Coonterunah-Talga Talga succession. Oceanic ?	<3.5 Ga	mafic ultramafic oceanic sequence extension, BIF, chert
3.47-3.45 Ga	calc-alkaline granitoids/ felsic volcanics minor cherts-BIF core-complex extension	3.47-3.43 Ga	calc-alkaline magmatism turbidites, BIF, chert, felsic magmatism thrusting
3.33-3.20 Ga	gold mineralization at Bamboo Creek felsic and mafic granitoids/ volcanics clastic sequences thrusting and folding	3.26-3.13 Ga	thrusting, turbidites and foreland sedimentation
3.1 Ga	volcanic and plutonic event in the western Pilbara	3.25 Ga	felsic volcanism/granitoids
2.95 Ga	crustal scale strike-slip granite intrusion	3.13-3.08 Ga	transpressional strike-slip gold mineralization
2.85 Ga	gold mineralization at Mt. York granite intrusion and tilting of greenstones to present geometry	3.11-3.08 Ga	transtensional strike-slip strike-slip and extension granite intrusion
2.8 Ga	Black Range dolerite dike		

Table 9.2 shows that although both Archean Cratons developed during a polyphase tectonothermal evolution between 3.5 and 2.8 Ga, their evolution is different in many respects. The timing of events and the sequence of events are different. Speculations that the Pilbara and Kaapvaal Craton were once part of one major craton are therefore more difficult to justify.

The Yilgarn Craton is a typical example of a late Archean craton and is in many respects similar to the Superior Province (Myers, 1995). These cratons are characterized by a number of elongated terranes, with diverse early (3.7-3.0 Ga) basement histories, that have been amalgamated.

The following summary of Yilgarn tectonics is deduced from Myers (1995). In the Yilgarn, the main magmatic (island arc and back arc) events in the three subterranes from west to east occurred at 3.0 Ga, 2.8-2.7 Ga and 2.73-2.6 Ga. These terranes were assembled between 2.64 and 2.6 Ga with accretion proceeding from east to west, involving intense compressional deformation causing the linear trend of the craton. Gold mineralization occurred during this compressional event. These compressional events are directly followed by strike-slip and late extensional deformation.

A very similar evolution of accretion is proposed for the Superior Province with final amalgamation proceeding from north to south between 2725 and 2695 Ma (Card 1990).

As noted by Myers (1995), the sequence of crustal growth and amalgamation of crustal fragments occurred in a shorter timespan than in the Mid-Archean granite-greenstone terrains (3.5–2.8 Ga), but the general sequence of events in each terrane (extension + deposition of greenstones, compression +/- clastic sediments, strike-slip +/- extension) is very similar. However, the typical linear arrangement, caused by compressional deformation, of most terranes and structures in Late Archean cratons does not occur in the Pilbara Craton. The compressional event in the Pilbara may have been less intense than in the Late Archean terranes or alternatively the linear arrangement in Late Archean terranes originated from different tectonic processes.

9.4 Plate tectonics in the Pilbara

Although elements of the tectonothermal evolution of the Pilbara can certainly be compared to modern day type tectonic setting, it is not yet clear whether plate tectonic processes, such as operative at present, can be directly extrapolated to the Mid Archean of the Pilbara Craton. In recent years a number of papers on the Pilbara Craton have drawn direct parallels with present day tectonic settings. Bickle et al (1993) show that the 3470 Ma North Shaw Suite in the Shaw batholith is geochemically very similar to modern subduction related calc-alkaline rocks. Barley (1993) comes to a similar conclusion based on the geochemical patterns of the 3470 Ma Duffer Formation and similarities between mineral associations in the Pilbara Craton and alteration patterns with Phanerozoic marginal-basin assemblages. Krapez (1993) and Eriksson et al. (1994) take this a step further and use a sequence stratigraphic model, based on present day plate tectonic processes to correlate the lithostratigraphic evolution of the Pilbara Craton to Wilson Cycles, including opening of oceanic basins, subduction of oceanic crust and closure of oceanic basins. In this interpretation the implicit assumption is made that subduction of oceanic lithosphere did occur in the Mid Archean. The most crucial element of the present day plate tectonic model is that subduction occurs. Other geologic settings are not exclusive to the present day plate tectonic model. For example, extensional settings can be related to plumes, compressional structures can be related to obduction instead of subduction. The interpretations in terms of subduction related models are incompatible with numerical models for plate tectonic processes in a hotter Earth (Davies, 1992; Vlaar et al., 1994), which invariably indicate that subduction does not occur because the oceanic crust would not reach an unstable state. If subduction does not take place, the main driving force for plate movement, slab pull (Wortel & Spakman, 1992; Lithgow-Bertelloni & Richards, 1995) is not present. The often used inference (e.g. Nisbet, 1987, Krapez, 1993) that plate tectonic processes were more rapid in a hotter Earth is in that case not correct. Therefore, before interpretations based on subduction setting (volcanic arcs, Wilson cycles etc.) can be made, it has to be shown independently that subduction did take place. Presently, the following elements are characteristic for subduction zone settings:

- 1 A linear trend of structures, rock associations, metamorphism and sedimentation;
- 2 Paired metamorphic belts, in which the high or medium pressure, low temperature facies is most characteristic;
- 3 Intense compressional deformation shortly after deposition of deep marine sequences (turbidites) on oceanic crust;
- 4 Melange zones in which structures young downward;

5 Volcanic arcs with tholeiite series, calc-alkaline series and alkaline series during or after compressional deformation (Baker, 1982);

In Late Archean granite-greenstone terrains, most of these criteria are satisfied (1,3,5). However, in the Pilbara Craton this is not the case. There is not a well defined linear trend and calc-alkaline magmatism predates the compressional phase by least 100 Ma, while paired metamorphic belts, and melange zones do not occur in the Pilbara. The implication is that subduction can not a priori be assumed to have taken place in the Mid Archean Pilbara granite greenstone terrain and that present day plate tectonic models still have to be used with caution and that interpretations should not be limited to present day style models. In this respect the Pilbara appears to be different from the Kaapvaal Craton, where de Wit et al. (1992) argued strongly for arc related processes starting from ca. 3.2 Ga.

The second crucial element of the present day plate tectonic model is the oceanic crust. Although there is general agreement that oceanic crust must have existed in the Archean, no convincing Archean ophiolites have yet been identified according to Bickle et al. (1994). Bickle et al. (1994) discussed different claims of Archean ophiolite complexes and concluded that they lack sheeted dike complexes and can therefore not be classified as ophiolite complexes. Abbott (1996) argues that because shallow sheeted dikes are only developed in slow spreading ridges and Archean spreading ridges are expected to be faster than present day ones (Bickle, 1986; Sleep, 1992), Archean oceanic crust should not be expected to contain extensive sheeted gabbroic dike complexes. However, the assumption that spreading was faster may be incorrect if, as argued by Wortel & Spakman (1992), the slab pull and not the ridge push is the most important force acting on the oceanic lithosphere.

The only irrefutable argument against an oceanic setting of a sequence that consists of subaqueous basalts with oceanic affinity, is to prove that the volcanics were deposited on a continental basement. This may be the case if older xenocrystic zircons are found in the mafic volcanics.

The only parts of the stratigraphy in the eastern Pilbara that could possibly be regarded as an ophiolite complex is the Talga Talga Subgroup, which consists of mafic and ultramafic volcanics, minor BIFs and a large component of gabbroic, ultramafic and doleritic sills. No xenocrystic zircons have so far been reported in the Coonterunah Succession (Buick et al., 1995) or in mafic volcanics of the Talga Talga Subgroup (McNaughton et al., 1993), so there is no direct argument against an oceanic setting for the Coonterunah Succession or the Talga Talga Subgroup.

In the mid Archean evolution of the Pilbara granitoid greenstone terrain there is no definitive evidence for subduction processes and therefore, no evidence for present day style plate tectonics, although regional compressional and extensional structures occur, which are in many respects similar to present day tectonic settings. Oceanic crust may have been present as, the oldest stratigraphic sequences in the Pilbara Craton, the Talga Talga Subgroup or the Coonterunah Succession.

Other large-scale models for the downgoing side of the plate tectonic cycle, if subduction could not take place are delamination of the lower oceanic crust and obduction of the upper part of the oceanic crust (Hoffman & Ranalli, 1988), obduction of the complete oceanic crust (de Wit et al., 1992), or drip models in which the lower part of the oceanic lithosphere becomes unstable due to conversion to garnet granulite or eclogite and drops off (Campbell & Griffiths, 1992; Davies, 1992; Vlaar et al., 1994). The last of these models could cause an effect similar to extensional collapse, but without the previous thickening event. However, it does not explain the production of tonalites and trond-

hjemites. This may be an alternative interpretation of the large-scale 3470–3450 Ma extensional event seen in the Pilbara Craton.

With the present data on the Pilbara Craton, it is not possible to determine whether the episodic growth models, as proposed by Stein & Hofmann (1994) and Davies (1995), in which Wilsonian and non-Wilsonian (MOMO) periods alternate, are a good description of geodynamic processes that took place in the Archean. Geochronological data over a larger area are needed to assess the synchronicity of major tectonothermal events.

In the late stages of evolution the ca. 2950 Ma craton scale strike-slip zone is a good indication for rigid lithospheric plates, although this is no proof of present day plate tectonic processes, including subduction.

9.5 Conclusions

The Pilbara granitoid-greenstone terrain developed in a polyphase tectonothermal evolution between 3.6 and 2.8 Ga. The main tectonothermal phases include:

- 1 Earliest greenstone sequence at 3.5 Ga, possibly with an oceanic origin.
- 2 A major magmatic event at ca. 3.46 Ga (upper Warrawoona Group), during extension in a Basin and Range style tectonic setting involving formation of metamorphic core-complexes during calc-alkaline magmatism. The initial domal geometry is produced during this event.
- 3 Gold mineralization at Bamboo Creek occurs in greenschist facies shear zones preferentially situated in ultramafic units at ca. 3400 Ma, possibly related to a late stage of the extensional episode.
- 4 An east-west compressive event, constrained between 3300 and 3200 Ma, during deposition of the Gorge Creek Group, involving thrusting and folding of greenstone sequences and causing disruption of the stratigraphic sequence.
- 5 Craton scale dextral and sinistral strike-slip zone at ca. 2950 Ma, consistent with WNW-ESE compression and escape tectonics.
- 6 Intrusion of K-rich granites and tilting of the youngest Whim Creek Group in areas with widespread late granite intrusion.
- 7 Intrusion of the Black Range Dolerite Dike swarm at 2.8 Ga as feeder dikes to the Fortescue Group.

There are no good indications that subduction processes took place in the mid Archean of the Pilbara Craton. Therefore, interpretations involving direct comparison with present day plate tectonic setting must be approached with caution.

9.6 Future work

This study is the initial part of ongoing research in the Pilbara Craton by the University of Utrecht Research School of Geodynamics. Many questions remain after this study, as well as exciting new possibilities for further work in the Pilbara. The main areas that need further work as arising from this study are listed below.

- 1 The stratigraphy of the Pilbara Supergroup is still a problem. There is no reliable dating of the Talga Talga Subgroup, which is needed to establish its relation to the Coonterunah Succession. The age of the Upper Gorge Creek Group remains largely unknown.
- 2 The Talga Talga Subgroup is the only part of the stratigraphy that may be oceanic crust. The detailed mapping of relations between the mafic volcanics and dolerite and gabbroic dykes as well as a detailed geochemical study of the mafic rocks should be undertaken to show whether or not it is an Archean ophiolite complex. This could be done in the type area, close to Marble Bar.
- 3 The volcanics of the Warrawoona and Gorge Creek Groups are intensely hydrothermally altered, with alteration often occurring at an early stage. A detailed mapping and geochemical study of the various alteration types, related to extrusion or to shear zones and/or gold mineralization, may reveal what the reason is for this widespread alteration.
- 4 The two important Mid-Archean structural phases, 3.46 Ga extension and 3.3–3.2 Ga compression, as they have been described in detail in the Shaw-Coongan area have been recognized in a larger area between the Mulgandinnah Lineament and the Lionel Lineament. However, the details of the kinematics and the precise timing constraints are largely unknown in many cases. Both are extremely important for a reliable large-scale interpretation that will provide constraints on the tectonic process underlying these structural events.
- 5 The domain boundaries of the Pilbara Craton as proposed by Krapez (1993) need further study. The data in Chapter 6 show that their position is not clear in all cases and that they are certainly not all sinistral NNE trending shear zones. The Sholl, Mallina and Lionel Lineament need to be studied in more detail with regard to the kinematics and especially their timing. This is necessary to establish whether they are terrane boundaries of accreted terrains or not.
- 6 The gold mineralization events in the Pilbara Craton are poorly constrained at ca. 2950 Ma (Neumayr et al., 1993) and between 3300 and 3450 Ma (Bamboo Creek, this study). The extent of the Bamboo Creek gold mineralization event is unknown, although there are some major deposits (Warrawoona Belt) and quite a few minor deposits in the Warrawoona Group in the eastern Pilbara that show similarities to the Bamboo Creek Deposit. Structural studies and Pb–Pb systematics of various deposits will show whether they all belong to the same event. Precise dating of gold mineralization events is difficult at present because minerals that can be used for U–Pb dating are often not present. However, techniques are improving and the U–Pb SHRIMP on other minerals than zircon may offer possibilities in the future.

- 7 Metamorphic studies, including pressure and temperature estimates, are largely lacking in the Pilbara. It is especially important for tectonic studies to establish the pressure (differences) during metamorphism in both batholiths and greenstones. Although the mafic volcanic rocks and the commonly low grade of metamorphism are not the most suitable for metamorphic studies it is an area of research in the Pilbara that has received too little attention and would be especially valuable if combined $^{40}\text{Ar}/^{39}\text{Ar}$ dating of metamorphic minerals.
- 8 Paleomagnetic studies, combined with structural studies and precise $^{40}\text{Ar}/^{39}\text{Ar}$ and U-Pb dating of the time-temperature path could provide answers to some of the most important questions in Archean Geology: i.e. whether, and at what rate did lithospheric plates move in the Archean.

References:

- Abbott, D. H. (1996) Plumes and hotspots as sources of greenstone belts. *Lithos*, V.37: p.113-127.
- Abbott, D.; Mooney, W. (1995) The structural and geochemical evolution of the continental crust: Support for the oceanic plateau model of continental growth. *Rev.Geoph., Supplement*: p.231-242.
- Anhaeusser, C. R. (1984) Structural elements of Archean granite-greenstone terranes as exemplified by the Barberton Mountain Land, southern Africa. In: *Precambrian Tectonics Illustrated*. Kröner, A. Greiling, R., IUGS, p. 57-78.
- Anhaeusser, C. R.; Mason, R.; Viljoen, M. J.; Viljoen, R. P. (1969) Reappraisal of some aspects of Precambrian shield geology. *Bull.Geol.Soc.America*, V.80: p.2175-2200.
- Armstrong, R. L. (1981) Radiogenic isotopes: the case for crustal recycling on a near steady state no-continent growth Earth. *Phil.Trans.Royal Soc. London*, V.301: p.443-472.
- Arndt, N. T. (1994) Archean komatiites. In: *Archean crustal evolution. Developments in Precambrian Geology*. V.11. Condie, K. C., Elsevier, p. 11-40.
- Arndt, N. T.; Naldrett, A. J.; Pyke, D. R. (1977) Komatiitic and iron-rich tholeiitic lavas of Muro Township, northeastern Ontario. *J.Petrol.*, V.18: p.319-369.
- Arndt, N. T.; Nisbet, E. G. (1982) Komatiites. Allen & Unwin: London: p.420.
- Arndt, N. T.; Jenner, G. A. (1986) Crustally contaminated komatiites and basalts from Kambalda, Western Australia. *Chem.Geol.*, V.56: p.229-255.
- Arndt, N. T.; Teixeira, N. A.; White, W. M. (1989) Bizarre geochemistry of komatiites from the Crixas greenstone belt, Brazil. *Contrib.Mineral.Petrol.*, V.101: p.187-197.
- Arndt, N. T.; Nelson, D. R.; Compston, W.; Trendall, A. F.; Thorne, A. M. (1991) The age of the Fortescue Group, Hamersley basin, Western Australia, from ion microprobe zircon U-Pb results. *Aust.J.Earth Sci.*, V.38: p.261-281.
- Ashwal, L. D. (1993) Anorthosites. Springer-Verlag: p. 422
- Bailey, D. K. (1983) The chemical and thermal evolution of rifts. *Tectonophysics*, V.94: p.585-597.
- Baker, P. E. (1982) Evolution and classification of orogenic volcanic rocks. In: *Andesites*. Thorpe, R. S., Wiley and Sons, p. 11-23.
- Barley, M. E. (1974) Geology of the Copper Range, Jilimbar, Western Australia. unpublished BSc-thesis, University of Western Australia.
- Barley, M. E. (1980) The evolution of Archean calc-alkaline volcanics: a study of the Kelly Greenstone belt and McPhee Dome, eastern Pilbara Block, Western Australia. Unpublished PhD-thesis, University of Western Australia.
- Barley, M. E. (1984) Volcanism and Hydrothermal alteration, Warrawoona Group, East Pilbara. Univ.W.Aust.Geol.Dep. & University Extension, Publ., V.9: p.23-36.
- Barley, M. E. (1986) Incompatible element enrichment in Archean basalts: a consequence of contamination by older sialic crust rather than mantle heterogeneity. *Geology*, V.14: p.947-950.
- Barley, M. E. (1992) Archean volcanic-hosted massive sulfide and sulfate mineralization in Western Australia. *Econ.Geol.*, V.85: p.855-872.
- Barley, M. E. (1993) Volcanic, sedimentary and tectonostratigraphic environments of the ~3.46 Ga Warrawoona Megasequence: a review. *Precamb.Res.*, V.60: p.47-67.
- Barley, M. E.; Dunlop, J. S. R.; Glover, J. E.; Groves, D. I. (1979) Sedimentary evidence for an Archean shallow-water volcanic-sedimentary facies, Eastern Pilbara Block, Western Australia. *Earth Planet.Sci.Lett.*, V.43: p.74.
- Barley, M. E.; Sylvester, G. C.; Groves, D. I.; Barley, G. D.; Rogers, N. (1984) Archean calc-alkaline volcanism in the Pilbara Block, Australia. *Precamb.Res.*, V.24: p.285-321.
- Barley, M. E.; McNaughton, N. J. (1988) The tectonic evolution of greenstone belts and setting of Archean gold mineralization in Western Australia: geochronological constraints on conceptual models. In: *Advances in Understanding Precambrian gold Deposits, Volume II*. Ho, S.E. Groves, D.I., Univ.W.Aust.Geol.Dep.& University Extension, Publ., V.12. p. 23-40.
- Barley, M. E.; Eisenlohr, B. N.; Groves, D. I.; Perring, C. S.; Vearncombe, J. R. (1989) Late Archean convergent margin tectonics and gold mineralization: a new look at the Norseman-Wiluna Belt, Western Australia. *Geology*, V.17: p.826-829.
- Barley, M. E.; Groves, D. I. (1990) Deciphering the Tectonic Evolution of Archean Greenstone Belts: the importance of contrasting histories to the distribution of mineralization in the Yilgarn Craton, Western Australia. *Precamb.Res.*, V.46: p.3-20.
- Barley, M. E.; Groves, D. I. (1992) Supercontinent cycles and the distribution of metal deposits through time. *Geology*, V.20: p.291-294.
- Beghoul, N.; Meren, R. (1992) Pn and mantle lid thickness of major Archean and Proterozoic provinces on Earth (abstract). *Eos Trans. AGU*, V.73: p.43.
- Bettenay, L. F.; Bickle, M. J.; Boulter, C. A.; Groves, D. I.; Morant, P.; Blake, T. S.; James, B. A. (1981) Evolution of the Shaw Batholith; an Archean granitoid-gneiss dome in the Eastern Pilbara, Western Australia. *Spec.Publ.Geol.Soc.Aust.*, V.7: p.361-372.
- Bickle, M. J. (1978) Heat loss from the earth: a constraint on Archean tectonics from the relation between geothermal gradients and the rate of plate production. *Earth Planet.Sci.Lett.* V.40: p.301-315.
- Bickle, M. J. (1984) Growth of continental crust and lithosphere through early Earth history. *Terra Cognita* V.4: p.80.
- Bickle, M. J. (1986) Global thermal histories. *Nature*, V.319: p.13-14.
- Bickle, M. J.; Bettenay, L. F.; Boulter, C. A.; Groves, D. I.; Morant, P. (1980) Horizontal tectonics interaction of an Archean gneiss belt and greenstones, Pilbara block, Western Australia. *Geology*, V.8: p.525-529.
- Bickle, M. J.; Bettenay, L. F.; Barley, M. E.; Chapman, H. J.; Groves, D. I.; Campbell, I. H.; de Laeter, J. R. (1983) A 3500 Ma Plutonic and volcanic calc-alkaline province in the Archean east Pilbara Block. *Contrib.Mineral.Petrol.*, V.84: p.25-35.
- Bickle, M. J.; Archibald, N. J. (1984) Chloritoid and staurolite stability: implications for metamorphism in the Archean

- Yilgarn Block, Western Australia. *J. Metamorphic Geol.*, V.2: p.179-203.
- Bickle, M. J.; Morant, P.; Bettenay, L. F.; Boulter, C. A.; Blake, T. S.; Groves, D. I. (1985) Archean tectonics of the Shaw Batholith, Pilbara Block, Western Australia: Structural and metamorphic tests of the batholith concept. *Geol. Ass. Can. Spec. Pap. V.28*: p.325-341.
- Bickle, M. J.; Bettenay, L. F.; Chapman, H. J.; Groves, D. I.; McNaughton, N. J.; Campbell, I. H.; de Laeter, J. R. (1989) The age and origin of younger granitic plutons of the Shaw Batholith in the Archean Pilbara block, Western Australia. *Contrib. Mineral. Petrol.*, V.101: p.361-376.
- Bickle, M. J.; Bettenay, L. F.; Chapman, H. J.; Groves, D. I.; McNaughton, N. J.; Campbell, I. H.; de Laeter, J. R. (1993) Origin of the 3500-3300 Ma calc-alkaline rocks in the Pilbara Archean: isotope and geochemical constraints from the Shaw Batholith. *Precamb. Res.*, V.60: p.117-149.
- Bickle, M. J.; Nisbet, E. G.; Martin, A. (1994) Archean greenstones are not oceanic crust. *J. Geol.*, V.102: p.121-138.
- Bouhallier, H.; Choukroune, P.; Balleve, M. (1993) Diapirism, bulk homogeneous shortening and transcurrent shearing in the Archean Dharwar craton: the Holenarsipur area, southern India. *Precamb. Res.*, V.63: p.43-58.
- Boulter, C. A.; Bickle, M. J.; Gibson, B.; Wright, R. K. (1987) Horizontal tectonics pre-dating upper Gorge Creek sedimentation, Pilbara Block, Western Australia. *Precamb. Res.*, V.36: p.241-258.
- Bowring, S. A.; Housh, T. (1995) The Earth's early evolution. *Science*, V.269: p.1535-1540.
- Boyd, F. R.; Gurney, J. J. (1986) Diamonds and the African lithosphere. *Science*, V.232: p.472-477.
- Böhlke, J. K. (1989) Comparison of metasomatic reactions between a common CO₂-rich vein fluid and diverse wall rocks: intensive variables, mass transfers, and Au mineralization at Alleghany, California. *Econ. Geol.*, V.84: p.291-327.
- Browning, P.; Groves, D. I.; Blockley, J. R.; Rosman, K. J. R. (1987) Lead isotope constraints on the age and source of gold mineralization in the Archean Yilgarn Block, Western Australia. *Econ. Geol.*, V.82: p.971-986.
- Brun, J. P.; van den Driessche, J. (1994) Extensional gneiss domes and detachment fault systems: structure and kinematics. *Bull. Soc. Geol. France*, V.165: p.519-530.
- Buck, W. R.; Martinez, F.; Steckler, M. S.; Cochran, J. R. (1988) Thermal consequences of lithospheric extension: pure and simple. *Tectonics*, V.7: p.213-234.
- Buick, R. (1985) Life and conditions in the early Archean: evidence from 3500 M.Y. old shallow water sediments in the Warrawoona Group, North Pole, Western Australia. Unpublished Ph.D.-thesis, University of Western Australia.
- Buick, R.; Dunlop, J. S. R.; Groves, D. I. (1981) Stromatolite recognition in ancient rocks: an appraisal of irregular laminated structures in an early Archean chert-barite unit from the North Pole, Western Australia. *Alcheringa*, V.5: p.161-181.
- Buick, R.; Dunlop, J. S. R. (1990) Evaporitic sediments of early Archean age from the Warrawoona Group, North Pole, W.A. *Sedimentology*, V.37: p.247-277.
- Buick, R.; Thornett, J. R.; McNaughton, N. J.; Smith, J. B.; Barley, M. E.; Savage, M. (1995) Record of emergent continental crust ~3.5 billion years ago in the Pilbara Craton of Australia. *Nature*, V.375: p.574-577.
- Bursnall, J. T. (1989) Mineralization and shear zones. *Geol. Ass. Can. Short Course Notes*, V.6: p.300.
- Calvert, A. J.; Sawyer, E. W.; Davis, W. J.; Ludden, J. N. (1995) Archean subduction inferred from seismic images of a mantle suture in the Superior Province. *Nature*, V.375: p.670-674.
- Campbell, I. H.; Hill, R. I. (1988) A two-stage model for the formation of the granite-greenstone terrains of the Kalgoorlie-Norseman area, Western Australia. *Earth Planet. Sci. Lett.*, V.90: p.11-25.
- Campbell, I. H.; Griffiths, R. W.; Hill, R. I. (1989) Melting in an Archean mantle plume: heads it's basalt, tails it's komatiites. *Nature*, V.339: p.697-699.
- Campbell, I. H.; Griffiths, R. W. (1992) The changing nature of mantle hotspots through time: implications for the chemical evolution of the mantle. *J. Geol.*, V.92: p.497-523.
- Card, K. D. (1990) A review of the Superior Province of the Canadian Shield, a product of Archean accretion. *Precamb. Res.*, V.48: p.99-156.
- Castor, S. B.; Weiss, S. I. (1992) Contrasting styles of epithermal precious-metal mineralization in the southwestern Nevada volcanic field, USA. *Ore Geol. Rev.*, V.7: p.193-223.
- Cathelineau, M.; Nieva, D. (1985) A chlorite solid solution geothermometer, the Los Azufres (Mexico) geothermal system. *Contrib. Mineral. Petrol.*, V.91: p.235-244.
- Cattell, A. C.; Taylor, R. N. (1990) Archean basic magmas. In: *Early Precambrian Basic Magmatism*. Hall, R. P. Hughes, D. J., Blackie, Glasgow: p. 11-39.
- Chopin, C.; Maluski, H. (1980) ⁴⁰Ar/³⁹Ar dating of high pressure metamorphic micas from the Gran Paradiso area (Western Alps): Evidence against the blocking temperature concept. *Contrib. Mineral. Petrol.*, V.74: p.109-122.
- Choukroune, P.; Bouhallier, H.; Arndt, N. T. (1995) Soft lithosphere during periods of Archean crustal growth or crustal reworking. In: *Early Precambrian Processes*. Coward, M. P. Ries, A. C., *Geol. Soc. London. Spec. Publ.*, London., V.95: p. 67-86.
- Chown, E. H.; Daigneault, R.; Mueller, W.; Mortensen, J. K. (1992) Tectonic evolution of the Northern Volcanic Zone, Abitibi belt, Quebec. *Can. J. Earth. Sci.*, V.29: p.2211-2225.
- Claoue-Long, J. C.; Compston, W.; Roberts, J.; Fanning, C. M. (1995) Two carboniferous ages: a comparison of SHRIMP zircon dating with conventional zircon ages and ⁴⁰Ar/³⁹Ar analysis. In: *Geochronology Time Scales and Global Stratigraphy*. SEPM Special publication No.54, p. 3-21.
- Collins, W. J. (1983) Geological evolution of an Archean Batholith. unpublished PhD-thesis, La Trobe University.
- Collins, W. J. (1989) Polydiapirism of the Archean Mount Edgar Batholith, Pilbara Block, Western Australia. *Precamb. Res.*, V.43: p.41-62.
- Collins, W. J.; Gray, C. M. (1990) Sr-Sb isotopic systematics of an Archean granite-gneiss terrain: The Mount Edgar

- Batholith, Pilbara Block, Western Australia. *Aust.J.Earth Sci.*, V.37: p.9-22.
- Collins, W. J. (1993) Melting of Archaean sialic crust under high aH₂O conditions: genesis of 3300 Ma Na-rich granitoids in the Mount Edgar Batholith, Pilbara Block, Western Australia. *Precambr.Res.*, V.60: p.151-174.
- Compston, W.; Williams, I.S.; Meyer, C. (1984) U-Pb geochronology of zircons from lunar breccia 73217 using a sensitive high mass-resolution ion microprobe. *J.Geoph.Res.*, V.89: p.B252-B534.
- Compston, W.; Williams, I. S.; Campbell, I. H.; Gresham, J. J. (1986) Zircon xenocrysts from the Kambalda volcanics: age constraints and direct evidence for older continental crust below the Kambalda-Norseman greenstones. *Earth Planet.Sci.Lett.*, V.76: p.299-311.
- Compston, W.; Kröner, A. (1988) Multiple zircon growth within early Archean tonalite gneiss from the Ancient Gneiss Complex, Swaziland. *Earth Planet.Sci.Lett.*, V.87: p.13-28.
- Condie, K. C. (1976) Trace-element geochemistry of Archean greenstone belts. *Earth Sci.Rev.* V.12: p.12-393.
- Condie, K. C. (1981) *Archean Greenstone Belts*. Elsevier Amsterdam: p.434
- Condie, K. C. (1993) Chemical composition and evolution of the upper continental crust: Contrasting results from surface samples and shales. *Chem.Geol.*, V.104: p.1-37.
- Condie, K. C. (1994) *Archean Crustal evolution. Developments in Precambrian Geology* Condie, K. C., Elsevier Amsterdam, V.11. : p. 528 .
- Coney, P. J. (1987) Crustal extension in the Basin and Range Province, southeastern United States. *Geol.Soc.Spec.Publ.*, V.28: p.177-187.
- Cooper, J. A.; James, P. R.; Rutland, R. W. R. (1982) Isotopic dating and structural relationships of granitoids and greenstones in the East Pilbara, Western Australia. *Precambr.Res.*, V.18: p.199-236.
- Costa, S.; Rey, P. (1995) Lower crustal rejuvenation and growth during post-thickening collapse: Insights from a crustal cross section through a Variscan metamorphic core complex. *Geology*, V.23: p.905-908.
- Cousineau, P.; Dimroth, E. (1982) Interpretation of the relations between massive, pillowed and brecciated facies in an Archean submarine andesite volcano - Amulet andesite, Rouyn-Noranda, Canada. *J.Volcanol.Geotherm.Res.*, V.13: p.83-102.
- Crittenden, M. D.; Coney, P. J.; Davis, G. H. (1980) Cordilleran Metamorphic core complexes. *Geol.Soc.America Memoir* 153.: p.443.
- Cumming, G. L.; Richards, J. R. (1975) Ore lead isotope ratios in a continuously changing earth. *Earth Planet. Sci.Lett.*, V.28: p.155-171.
- Daniels, L. R. M.; Gurney, J. J.; Harte, B. (1996) A crustal mineral in a mantle diamond. *Nature*, V.379: p.153-156.
- Davids, C.; Wijbrans, J. R.; White, S. H. (in press) 40Ar/39Ar laserprobe ages of metamorphic hornblendes from the Coongan Belt, Pilbara, Western Australia. *Precambr.Res.*
- Davies, G. F. (1992) On the emergence of plate tectonics. *Geology*, V.20: p.963-966.
- Davies, G. F. (1995) Punctuated tectonic evolution of the earth. *Earth Planet.Sci.Lett.*, V.136: p.363-379.
- Dawes, P. R.; Smithies, R. H.; Centofanti, J.; Podmore, D. C. (1995) Sunrise Hill unconformity: a newly discovered regional hiatus between Archean granites and greenstones in the north eastern Pilbara Craton. *Aust.J.Earth.Sci.*, V.42: p.635-639.
- de Beer, J. H.; Stettler, E. H. (1988) Geophysical characteristics of the southern African continental crust. *J.Petrol.Spec.Lithosphere Issue*, p.163-184.
- de Ronde, C. E. J.; Spooner, E. T. C.; de Wit, M. J.; Bray, C. J. (1992) Shearzone related, Au quartz vein deposits in the Barberton Greenstone Belt, South Africa: field and petrographic characteristics, fluid properties, and stable isotope geochemistry. *Econ.Geol.*, V.87: .
- de Ronde, C. E. J.; de Wit, M. J. (1994) Tectonic history of the Barberton greenstone belt, South Africa: 490 million years of Archean evolution. *Tectonics*, V.13: p.983-1005.
- de Ronde, C. E. J.; Channer, D. M.; Spooner, E. T. C. (1996) Fluids of Archean greenstone belts. In: *Tectonic evolution of Greenstone Belts*. de Wit, M. J. Ashwal, L. D., Oxford Monograph on Geology and Geophysics Series: p.309-336.
- de Wit, M. J. (1982) Gliding and overthrust nappes in the Barberton Greenstone Belt. *J.Struct. Geol.*, V.4: p.117-136.
- de Wit, M. J.; Armstrong, R.; Hart, R.; Wilson, A. (1987) Felsic igneous rocks within the 3.3-3.5 Ga Barberton Greenstone Belt: high level crustal equivalents of the surrounding tonalite-trondhjemite terrain, emplaced during thrusting. *Tectonics*, V.6: p.529-549.
- de Wit, M. J.; Hart, R. A.; Hart, R. J. (1987) The Jamestown ophiolite complex, Barberton Mountain Belt: a section through 3.5 Ga oceanic crust. *J.Afr.Earth Sci.*, V.6: p.681-730.
- de Wit, M. J.; Roering, C.; Hart, R. J.; Armstrong, R. A.; de Ronde, C. E. J.; Green, R. W. E.; Tredoux, M.; Peberdy, E.; Hart, R. A. (1992) Formation of an Archean continent. *Nature*, V.357: p.553-562.
- de Wit, M. J.; Hart, R. A. (1993) Earth's earliest continental lithosphere, hydrothermal flux and crustal recycling. *Lithos*, V.30: p.309-335.
- de Wit, M. J.; Hynes, A. (1995) The onset of interaction between the hydrosphere and oceanic crust, and the origin of the first continental lithosphere. In: *Early Precambrian Processes*. Coward, M. P. Ries, A. C., *Geol.Soc.Spec.Publ.*, V.95.: p. 1-9.
- de Wit, M. J.; Ashwal, L. D. (1996) *Greenstone Belts*. Oxford Monographs on Geology and Geophysics Charnock, H.; Conway Morris, S.; Dewey, J. F.; Navrotsky, A.; Oxburgh, E. R.; Price, R. A. Skinner, B. J., Clarendon Press: Oxford: V.35:p.803
- Delor, C.; Burg, J. P.; Clarke, G. (1991) Diapirism-Metamorphism relationships in the Pilbara Province (Western Australia): implications for thermal and tectonic regimes in the Archean. *C.R. Acad.Sci.Paris*, V.312: p.257-263.
- Des Marais, D. J. (1994) The Archean atmosphere: Its composition and fate. In: *Archean Crustal evolution. Developments in Precambrian geology*. Condie, K. C.,

- Elsevier, V.11: p. 505-525.
- Dewey, J. F. (1988) Extensional collapse of orogens. *Tectonics*, V.7: p.1123-1139.
- Digel, S.; Ghent, E. D. (1994) Fluid-mineral equilibria in prehnite-pumpellyite to greenschist facies metabasites near Flin Flon, Manitoba, Canada: implications for petrogenetic grids. *J. Metamorphic Geol.*, V.12: p.467-477.
- DiMarco, M. J.; Lowe, D. R. (1989) Stratigraphy and sedimentology of an early Archean felsic volcanic sequence, eastern Pilbara Block, Western Australia, with special reference to the Duffer Formation and implications for crustal evolution. *Precamb. Res.*, V.44: p.147-169.
- Dinter, A.; Royden, L. (1993) Late Cenozoic extension in northeastern Greece: Strymon Valley detachment system and Rhodope metamorphic core complex. *Geology*, V.21: p.45-48.
- Dixon, J. M. (1975) Finite strain and progressive deformation in models of diapiric structures. *Tectonophysics*, V.28: p.89-124.
- Dixon, J. M.; Summers, J. M. (1983) Patterns of total incremental strain in subsiding troughs: experimental centrifuged models of inter-diapir synclines. *Can. J. Earth Sci.*, V.20: p.1843-1861.
- Drummond, B. J. (1988) A review of crust/upper mantle structure in the Precambrian areas of Australia and implications for Precambrian evolution. *Precamb. Res.*, V.40/41: p.101-116.
- Drummond, B. J.; Collins, C. D. N. (1986) Seismic evidence for underplating of the lower continental crust of Australia. *Earth Planet. Sci. Lett.*, V.79: p.361-372.
- Drummond, B. J.; Goleby, B. R.; Swager, C. P.; Williams, P. R. (1993) Constraints on Archean crustal composition and structure provided by deep seismic sounding in the Yilgarn Block. *Ore Geol. Rev.*, V.8: p.117-124.
- Drury, M. R.; Vissers, R. L. M.; van der Wal, D.; Hoogerduijn Strating, E. H. (1991) Shear localization in upper mantle peridotites. *Pure Appl. Geophysics*, V.137: p.439-460.
- Dunlop, J. S. R.; Muir, M. D.; Milne, V. A.; Groves, D. I. (1978) A new microfossil assemblage from the Archean of Western Australia. *Nature*, V.274: p.676-678.
- Dunlop, J. S. R.; Buick, R. (1981) Archean epiclastic sediments derived from mafic volcanics, North Pole, Pilbara Block, Western Australia. *Univ. W. Aust. Geol. Dep. & University Extension, Publ.*, V.7: p.225-233.
- Durrheim, R. J.; Mooney, W. D. (1991) Archean and Proterozoic crustal evolution: Evidence from crustal seismology. *Geology*, V.19: p.606-609.
- Durrheim, R. J.; Mooney, W. D. (1994) Evolution of the Precambrian Lithosphere: seismological and geochemical constraints. *J. Geophys. Res.*, V.99: p.15359-15374.
- Easton, R. M. (1985) The nature and significance of pre-Yellowknife Supergroup rocks in the Point Lake area, Slave structural Province, Canada. In: *Evolution of Archean supracrustal sequences*. Ayres, L. D.; Thurston, P. C.; Card, K. D. Weber, W., Geological Association of Canada Special papers, V.28: p. 153-167.
- Ebel, D. S.; Sack, R. O. (1991) Arsenic-silver incompatibility in fahlore. *Mineral. Mag.*, V.55: p.521-528.
- Echeverria, L. M. (1980) Tertiary and Mesozoic komatiites from the Gorgona Island, Colombia: field relations and geochemistry. *Contrib. Mineral. Petrol.*, V.73: p.253-266.
- Eisenlohr, B. N.; Groves, D. I.; Partington, G. A. (1989) Crustal-scale shear zones and their significance to Archean gold mineralization in Western Australia. *Mineral. Deposita*, V.24: p.1-8.
- England, P.; Bickle, M. (1984) Continental thermal and tectonic regime during the Archean. *J. Geol.*, V.92: p.353-367.
- England, P. C.; Thompson, A. B. (1984) Pressure-temperature-time paths of regional metamorphism I. Heat transfer during the evolution of regions of thickened continental crust. *J. Petrol.*, V.25: p.894-928.
- England, P. C.; Thompson, A. B. (1986) Some thermal and tectonic models for crustal melting in continental collision zones. In: *Collision Tectonics*. Coward, M. P. Ries, A. C., *Geol. Soc. Spec. Publ.*, V.19: p. 83-94.
- Eriksson, K. A. (1981) Archean platform-to-trough sedimentation, East Pilbara Block, Australia. In: *Archean Geology*. Glover, J. E. Groves, D. I., *Geol. Soc. Aust. Special Publication*, V.7: p. 235-244.
- Eriksson, K. A.; Krapez, B.; Fralick, P. W. (1994) Sedimentology of Archean greenstone belts: signatures of tectonic evolution. *Earth Sci. Rev.*, V.37: p.1-88.
- Eriksson, K. A.; Fedo, C. M. (1994) Archean synrift and stable-shelf sedimentary succession. In: *Archean crustal evolution. Developments in Precambrian Geology*. Condie, K. C., Elsevier, V.11
- Fisher, N. H. (1945) The fineness of gold with special reference to the Morobe goldfield, New Guinea. *Econ. Geol.*, V.40: p.449-495; 537-563.
- Foster, R. P.; Piper, D. P. (1993) Archean lode gold deposits in Africa: Crustal setting, metallogenesis and cratonization. *Econ. Geol.*, V.8: p.303-347.
- Frapp, R. E. P. (1976) Stratabound gold deposits in Archean banded iron formation, Rhodesia. *Econ. Geol.*, V.71: p.58-75.
- Froude, D. O.; Ireland, T. R.; Kinny, P. D.; Williams, I. S.; Compston, W.; Williams, I. R.; Myers, J. S. (1983) Ion microprobe identification of 4100-4200 Myr-old zircons. *Nature*, V.304: p.616-618.
- Froude, D. O.; Wijbrans, J. R.; Williams, I. S. (1984) 3400-3430 Ma ages from U-Pb analyses in the Western Shaw belt, Pilbara Block. *Aust. Nation. Univ. Res. School Earth Sci. Ann. Rep.* 1983, p.126-128.
- Fyfe, W. S. (1978) Evolution of earth's crust: modern plate tectonics to ancient hot spot tectonics? *Chem. Geol.*, V.23: p.89-114.
- Fyson, W. K.; Helmstaedt, H. (1988) Structural patterns and tectonic evolution of supracrustal domains in the Archean Slave Province, Canada. *Can. J. Earth Sci.*, V.25: p.301-315.
- Gautier, P.; Brun, J. P. (1994) Crustal-scale geometry and kinematics of late-orogenic extension in the central Aegean (Cyclades and Evvia Island). *Tectonophysics*, V.238: p.399-424.
- Gebre-Mariam, M.; Groves, D. I.; McNaughton, N. J.; Mickucki, E. J.; Vearncombe, J. R. (1993) Archean Au-Ag

- mineralisation at Racetrack, near Kalgoorlie, Western Australia: a high crustal-level expression of the Archean composite lode-gold system. *Mineral. Deposita*, V.28: p.375-387.
- Gee, R. D.; Baxter, J. L.; Wilde, S. A.; Williams, I. R. (1981) Crustal development in the Yilgarn Block. 2nd International Archean Symposium. Perth, W.A. Geological Society of Australia, Special Publication, V.7: p.43-56.
- Glikson, A. Y. (1972) Early Precambrian evidence of primitive ocean crust and island nuclei of sodic granite. *Soc.Am.Bull.*, V.83: p.3323-3344.
- Glikson, A. Y.; Hickman, A. H. (1981) Geochemistry of Archean volcanic successions, eastern Pilbara Block, Western Australia., *Bur.Mineral.Res.Geol.Geophys.Aust. Record No.* 1981/36
- Golding, S. D.; McNaughton, N. J.; Barley, M. E.; Groves, D. I.; Ho, S. E.; Rock, N. M. S.; Turner, J. V. (1989) Archean carbon and oxygen reservoirs: their significance for fluid sources and circulation paths for Archean mesothermal gold deposits of the Norseman-Wiluna Belt, Western Australia. In: *The geology of gold deposits: The perspective in 1988*. Keays, R. R.; Ramsay, W. R. H. Groves, D. I., *Economic Geology Monograph*, V.6: p. 376-388.
- Goleby, B. R.; Rattenbury, M. S.; Swager, C. P.; Drummond, B. J.; Williams, P. R.; Sheraton, J. W.; Heinrich, C. A. (1993) Archean Crustal structure from seismic reflection profiling, Eastern Goldfields, Western Australia. *Australian Geological Survey Organisation*. No.1993/15.
- Grambling, J. A. (1981) Pressure and temperature in Precambrian metamorphic rocks. *Earth Planet. Sci.Lett.*, V.53: p.63-68.
- Grieve, R. A. F. (1990) Terrestrial impact: the record in rocks. 53rd meeting of the Meteorological Society. Perth. *Meteorites*, V.25: p.368-369.
- Grove, T. L.; de Wit, M. J. (1995) Wet komatites and Archean mantle conditions. Abstract. *Precambrian '95*. Montreal, Canada. p.29.
- Groves, D. I.; Batt, W. D. (1984) Spatial and temporal variations of Archean metallogenic associations in terms of evolution of granitoid-greenstone terrains with particular emphasis on Western Australian Shield. In: *Archean Geochemistry*. Kröner, A.; Hansen, G. N. Goodwin, A. M., Springer, Berlin: p. 73-98.
- Groves, D. I.; Ho, S. E.; Houston, S. M.; Phillips, G. N. (1986) A review of gold deposits in Archean greenstone belts of Western Australia. 13th Council of Mining and Metallurgical Institutions Congress. Singapore.V.2. p.243-250.
- Groves, D. I.; Barley, M. E. (1988) Gold mineralization in the Norseman-Wiluna Belt, Eastern Goldfields Province, Western Australia. In: *Western Australian Gold deposits, Bicentennial Gold 88, Excursion Guidebook*. Groves, D. I.; Barley, M. E.; Ho, S. E. Hopkins, G. M. F., *Univ.W.Aust. Geol.Dep.& University Extension, Publ.*, V.14: p. 47-66.
- Groves, D. I.; Barley, M. E.; Barnicoat, A. C.; Cassidy, K. F.; Fare, R. J.; Hagemann, S. G.; Ho, S. E.; Hronsky, J. M. A.; Mikucki, E. J.; Mueller, A. G.; McNaughton, N. J.; Perring, C. S.; Ridley, J. R.; Vearncombe, J. R. (1992) Sub-greenschist- to granulite-hosted Archean lode-gold deposits of the Yilgarn Craton: a depositional continuum from deep-sourced hydrothermal fluids in crustal-scale plumbing systems. In: *The Archean: terrains, processes and metallogeny*. Glover, J. E. Ho, S. E., *Univ.W.Aust. Geol.Dep.& University Extension, Publ.*, Perth: V.22: p. 325-338.
- Groves, D. I.; Barley, M. E. (1994) Archean mineralization. In: *Archean crustal evolution. Developments in Precambrian geology*. Condie, K. C., Elsevier, Amsterdam: V.11: p. 461-503.
- Groves, D. I.; Ridley, J. R.; Bloem, E. M. J.; Gebre-Mariam, M.; Hagemann, S. G.; Hronsky, J. M. A.; Knight, J. T.; McNaughton, N. J.; Ojala, J.; Viereicher, R. M.; Mccuaig, T. C.; Holyland, P. W. (1995) Lode-gold deposits of the Yilgarn block; products of Late Archean crustal-scale over-pressured hydrothermal systems. In: *Early Precambrian Processes*. Coward, M. P. Ries, A. C., *Geol Soc.Spec.Publ.*, London: V.95: p. 155-172.
- Gruau, G.; Jahn, B. M.; Glikson, A. Y.; Davy, R.; Hickman, A. H.; Chauvel, C. (1987) Age of the Archean Talga-Talga Subgroup, Pilbara Block, Western Australia, and early evolution of the mantle: new Sm-Nd isotopic evidence. *Earth Planet.Sci.Lett.*, V.85: p.105-116.
- Hall, R. P.; Hughes, D. J. (1990) Early Precambrian basic magmatism. *Blackie*: p.340.
- Hall, R. P.; Hughes, D. J. (1993) Early Precambrian crustal development: changing styles of mafic magmatism. *J.Geol.Soc.London*, V.150: p.625-635.
- Hallberg, J. A. (1974) Whole rock geochemical orientation trip to the Pilbara. *Minerals Res. Labs. Australian Commonwealth Sci. Industrial Research Organization Rept.* FP.3.
- Hallberg, J. A.; Giles, C. W. (1986) Archean felsic volcanism in the northeastern Yilgarn Block, Western Australia. *Austr. J.Earth.Sci.*, V.33: p.413-427.
- Hamilton, P. J.; Evensen, N. M.; O'Nions, R. K.; Glikson, A. Y.; Hickman, A. H. (1981) Sm-Nd dating of the North Star basalt, Warrawoona Group, Pilbara Block, Western Australia. In: *Archean Geology*. Glover, J. E. Groves, D. I., *Geol.Soc.Aust.Spec.Publ.*, V.7: p. 187-192.
- Hammond, E. C.; Nisbet, B. W. (1992) Toward a structural and tectonic framework for the central Norseman-Wiluna greenstone belt, Western Australia. In: *The Archean: Terrains, Processes and Metallogeny*. Glover, J. E. Ho, S. E., *Univ.W.Aust. Geol.Dep.& University Extension, Publ.*, Perth: V.22: p. 39-50.
- Hanchar, J. M.; Rudnick, R. L. (1995) Revealing hidden structures: The application of cathodoluminescence and back-scattered electron imaging to dating zircons from lower crustal xenoliths. *Lithos*, V.36: p.289-303.
- Hanes, J. A. (1991) K-Ar and $^{40}\text{Ar}/^{39}\text{Ar}$ geochronology: methods and applications. In: *Applications of radiogenic isotope systems to problems in geology*. Heaman, L. Ludden, J. N., *Min.Assoc.Can.Short.Course Handbook*, V.19: p. 27-57.
- Hargraves, R. B. (1986) Faster spreading or greater ridge length in the Archean? *Geology*, V.14: p.750-752.

- Hawkesworth, C.; Turner, S.; Gallagher, K.; Hunter, T.; Bradshaw, T.; Rogers, N. (1995) Calc-alkaline magmatism, lithospheric thinning and extension in the Basin and Range. *J.Geoph.Res.*, V.100B: p.10271-86.
- Henderson, J. B. (1981) Archean basin evolution in the Slave Province, Canada. In: *Precambrian Plate Tectonics*. Kröner, A., Elsevier, Amsterdam: p. 213-235.
- Henderson, J. B. (1985) Geology of the Yellowknife - Hearne Lake area, district of MacKenzie: a segment across an Archean basin. *Geological Survey of Canada. Memoir No. 414*.
- Hickman, A. H. (1981) Crustal evolution of the Pilbara Block, Western Australia. *Spec.Publs.Geol.Soc.Aust.*, V.7: p.57-69.
- Hickman, A. H. (1983) Geology of the Pilbara Block and its environs. *Geol.Surv.Austr.Bull.* V.127: p.367.
- Hickman, A. H. (1984) Archean diapirism in the Pilbara. In: *Precambrian Tectonics Illustrated*. Kröner, A. Greiling, R., Nagele und Obermiller, Stuttgart: p. 113-128.
- Hickman, A. H.; Keats, W. (1990) Gold. In: *Geology and Mineral resources of Western Australia. V.Memoir 3*. Geological Survey of Western Australia, p. 645-668.
- Hill, R. I. (1991) Starting plumes and continental break-up. *Earth Planet.Sci.Lett.*, V.104: p.389-416.
- Hill, R. I.; Campbell, G. F.; Davies, G. F.; Griffiths, R. W. (1992) Mantle Plumes and Continental Tectonics. *Science*, V.256: p.186-193.
- Ho, S. E.; McNaughton, N. J.; Groves, D. I. (1994) Criteria for determining initial lead isotopic compositions of pyrite in Archean lode-gold deposits: a case study at Victory, Kambalda, Western Australia. *Chem. Geol.*, V.111: p.57-84.
- Hoffman, P. F. (1991) On accretion of granite-greenstone terranes. In: *Greenstone gold and crustal evolution*. Robert, F., *Geol.Ass.Canada, St.John's, Newfoundland*: p. 32-45.
- Hoffman, P. F.; Ranalli, G. (1988) Archean oceanic flake tectonics. *Geoph.Res.Lett.* V.15: p.1077-1080.
- Horwitz, R. C. (1986) Notes on the legend of the geological map of Western Australia 1966. No.1965, Western Australian Geological Survey.
- Horwitz, R. C. (1990) Paleogeographic and tectonic evolution of the Pilbara Craton, Northwestern Australia. *Precambr.Res.*, V.48: p.327-340.
- Horwitz, R. C.; Pidgeon, R. T. (1993) 3.1 Ga tuff from the Sholl belt in the West Pilbara: further evidence for diachronous volcanism in the Pilbara Craton of Western Australia. *Precambr.Res.*, V.60: p.175-183.
- Houseman, G. A.; McKenzie, D. P.; Molnar, P. (1981) Convective instability of a thickened boundary layer and its relevance for thermal evolution of a convergent mountain belt. *J.Geoph.Res.*, V.91: p.3651-3663.
- Houstoun, S. M. (1988) Competency contrasts and chemical controls as guides to gold mineralization: an example from the Barberton Mountain Land, South Africa. *Univ.W.Aust.Geol.Dep.& University Extension, Publ.*, V.11: p.147-160.
- Hunter, D. R.; Stowe, C. W. (1996) A historical review of the origin, composition, and setting of Archean greenstone belts. In: *Greenstone Belts*. de Wit, M. J. Ashwal, L. D., Clarendon Press, Oxford: p.3-30.
- Hurley, P. M. (1968) Absolute abundance and distribution of Rb,K and Sr in the earth. *Geochim.Cosmochim.Acta*, V.32: p.19-22.
- Hurley, P. M.; Rand, J. R. (1969) Pre-drift continental nuclei. *Science*, V.164: p.1229-1242.
- Hutchinson, R. W. (1993) A multi-process genetic hypothesis for greenstone-hosted gold lodes. *Econ.Geol.*, V.8: p.349-382.
- Ijlst, L. (1973) A laboratory overflow-centrifuge for heavy liquid mineral separation. *Am.Mineral.*, V.58: p.1088-1093.
- Jackson, S. L.; Cruden, A. R. (1995) Formation of the Abitibi greenstone belt by arc-trench migration. *Geology*, V.23: p.471-474.
- Jackson, S. L.; Cruden, A. R.; White, D.; Milkereit, B. (1995) A seismic-reflection-based regional cross section of the southern Abitibi greenstone belt. *Can.J.Earth Sci.*, V.32: p.135-148.
- Jacob, D.; Jagoutz, E.; Lowry, D.; Matthey, D.; Kudrjatzseva, G. (1994) Diamondiferous eclogites from Siberia: remnants of Archean oceanic crust. *Geochim.Cosmochim. Acta*, V.58: p.5191-5207.
- Jacobsen, S. B.; Dymek, R. F. (1988) Nd and Sr isotope systematics of clastic sediments from Isua, West Greenland: Identification of pre-3.8 Ga differentiated crustal components. *J.Geoph.Res.*, V.93: p.338-354.
- James, D. T.; Mortensen, J. K. (1992) An Archean metamorphic core complex in the southern Slave Province: basement-cover structural relationships between the Sleepy Dragon Complex and the Yellowknife Supergroup. *Can.J.Earth Sci.*, V.29: p.2133-2145.
- Jelsma, H. A. (1993) Granite and greenstones in Northern Zimbabwe: Tectono-thermal evolution and source regions. Unpublished PhD-thesis, Vrije Universiteit Amsterdam.
- Jones, D. L.; Howell, D. G.; Coney, P. J.; Monger, J. W. H. (1983) Recognition, character and analysis of tectonostratigraphic terranes in western North America. In: *Accretion tectonics in the Circum Pacific regions*. (eds Hashimoto, M. & Uyeda, S., *Adv.Earth Planet.Sci.*, V.15: p. 21-35.
- Kerrick, R.; Fryer, B. J. (1979) Archean precious metal hydrothermal systems, Dome mine, Abitibi Greenstone Belt. *Can.J.Earth Sci.*, V.16: p.440-458.
- Kerrick, R.; Wyman, D. (1990) Geodynamic setting of mesothermal gold deposits: an association with accretionary tectonic regimes. *Geology*, V.18: p.882-885.
- Kerrick, R.; Kyser, T. K. (1994) 100 Ma timing paradox of Archean gold, Abitibi greenstone belt (Canada): New evidence from U-Pb and Pb-Pb evaporation ages of hydrothermal zircons. *Geology*, V.22: p.1131-1134.
- Kerrick, R.; Cassidy, K. F. (1994) Temporal relationships of lode gold mineralization to accretion, magmatism, metamorphism and deformation- Archean to present: A review. *Ore Geol.Rev.*, V.9: p.263-310.
- Kinny, P. D.; Wijbrans, J. R.; Froude, D. O.; Williams, I. S.; Compston, W. (1990) Age constraints on the geological evolution of the Narryer Gneiss Complex, Western Australia. *Earth Planet.Sci.Lett.*, V.37: p.51-69.
- Kishida, A.; Kerrich, R. (1987) Hydrothermal alteration zoning and gold concentration at the Kerr-Addison Archean

- lode gold deposit, Kirkland Lake, Ontario. *Econ.Geol.*, V.82: p.649-690.
- Kloppenburg, A.; Davids, C.; Knoop, M. I. J.; Zegers, T. E.; White, S. H. (in prep) Structures in the Warrawoona Greenstone Belt, Pilbara, Western Australia. .
- Kranidiotis, P.; MacLean, W. H. (1987) Systematics of Chlorite alteration at the Phelps Dodge Massive Sulfide Deposit, Matagami, Quebec. *Econ.Geol.*, V.82: p.1898-1911.
- Krapez, B. (1989) Depositional styles and geotectonic settings of Archean metasedimentary sequences: evidence from the Lalla rookh Basin, Pilbara Block. Unpublished PhD-thesis, University of Western Australia.
- Krapez, B. (1993) Sequence stratigraphy of the Archean supracrustal belts of the Pilbara Block, Western Australia. *Precambr.Res.*, V.60: p.1-45.
- Krapez, B.; Barley, M. E. (1987) Archean strike-slip faulting and related ensialic basins; evidence from the Pilbara Block, Australia. *Geol.Mag.*, V.124: p.555-567.
- Kröner, A. (1981) *Precambrian Plate Tectonics*. Elsevier, Amsterdam: p.781.
- Kröner, A. (1982) Archean to early Proterozoic tectonics and crustal evolution: a review. *Revista Brasileira de Geociencias* V.12: p.15-31.
- Kröner, A. (1984) Evolution, growth and stabilization of the Precambrian lithosphere. *Phys.Chem.Earth*, V.15: p.69-106.
- Kröner, A. (1991) Tectonic evolution in the Archean and Proterozoic. *Tectonophysics*, V.187: p.393-410.
- Kröner, A.; Layer, P. W. (1992) Crust formation and plate motion in the Early Archean. *Science*, V.256: p.1405-1411.
- Kusky, T. M. (1989) Accretion of the Archean Slave province. *Geology*, V.17: p.63-67.
- Kusky, T. M. (1990) Evidence for Archean ocean opening and closing in the southern Slave Province. *Tectonics*, V.9: p.1533-1563.
- Kusky, T. M. (1993) Collapse of Archean orogens and the generation of late to post-kinematic granitoids. *Geology*, V.21: p.925-928.
- Kuznir, N. J.; Karner, G. D.; Egan, S. (1987) Geometry, thermal and isostatic consequences of detachments in the continental lithosphere extensional basin formation. *Can.Soc.Petrol.Geol.Mem.* V.12: p.185-203.
- Lambert, I. B.; Donnelly, T. H.; Dunlop, J. S. R.; Groves, D. I. (1978) Stable isotopic composition of early Archean sulphate deposits of probable evaporitic and volcanogenic origins. *Nature*, V.276: p.808-811.
- Lister, G. S.; Davis, G. A. (1989) The origin of metamorphic core complexes and detachment faults formed during Tertiary continental extension in the northern Colorado River region, U.S.A. *J.Struct.Geol.*, V.11: p.65-94.
- Lister, G. S.; Baldwin, S. L. (1993) Plutonism and the origin of metamorphic core complexes. *Geology*, V.21: p.607-610.
- Lister, G. S.; Baldwin, S. L. (1996) Modelling the effect of arbitrary P-T-t histories on argon diffusion in minerals using the MacArgon program for the Apple Macintosh. *Tectonophysics*, V.253: p.83-109.
- Lowe, D. R. (1980) Stromatolites 3400 Myr old from the Archean of Western Australia. *Nature*, V.284: p.441-443.
- Lowe, D. R. (1983) Restricted shallow-water sedimentation of early Archean stromatolitic and evaporitic strata of the Strelley Pool Chert, Pilbara block, Western Australia. *Precambr. Res.*, V.19: p.239-283.
- Lowe, D. R. (1994) Abiological origin of described stromatolites older than 3.2 ga. *Geology*, V.22: p.387-390.
- Lowe, D. R. (1994b) Accretionary history of the Archean Barberton Greenstone Belt (3.55-3.22 Ga) southern Africa. *Geology*, V.22: p.1099-1102.
- Ludden, J. (1989) Geochemical constraints on the origin of Archean Magmas: examples from the Superior Province of Canada. *Geol.Ass.Canada/Mineral Ass. Canada, Prog. Abstr.*, V.A8: p.14.
- MacGeehan, P. J.; MacLean, W. H. (1980) An Archean sub-seafloor geothermal system, 'calc-alkali' trends, and massive sulphide genesis. *Nature*, V.286: p.767-771.
- MacGregor, A. M. (1951) Some milestones in the Precambrian of southern Rhodesia. *Proc.Geol.Congr.S.Afr.*, V.54: p.27-71.
- Marcelis, A. H. M. (1986) Geology of the Bamboo Creek Greenstone Belt, Pilbara Block, Western Australia. unpublished MSc-thesis, University of Utrecht.
- Marston, R. J.; Groves, D. I. (1981) The metallogenesis of Archean base-metal deposits in Western Australia. *Spec.Publ.Geol.Soc.Aust.*, V.7: p.409-456.
- Martin, H. (1994) Archean grey gneisses and the genesis of continental crust. In: *Archean Crustal evolution. Developments in Precambrian geology*. Condie, K. C., Elsevier, V.11: p.505-525.
- Martinez, M. L.; York, D.; Hall, C. M.; Hanes, J. A. (1984) Oldest reliable $^{40}\text{Ar}/^{39}\text{Ar}$ ages for terrestrial rocks, Barberton Mountain komatiites. *Nature*, V.307: p.352-354.
- McCall, G. J. H. (1981) Progress in research into the Early history of the Earth; a review, 1970-1980. *Spec.Publ.Geol.Soc.Aust.*, V.7: p.3-15.
- McDougall, I.; Harrison, T. M. (1988) *Geochronology and thermochronology by the $^{40}\text{Ar}/^{39}\text{Ar}$ method*. Oxford Monograph on geology and geophysics Clarendon Press: Oxford, V.9.
- McKenzie, D. P. (1984) The generation and compaction of partially molten rock. *J.Petrol.*, V.25: p.713-765.
- McKenzie, D.; Bickle, M. J. (1988) The volume and composition of melt generated by extension of the lithosphere. *J.Petrol.*, V.29: p.625-679.
- McKenzie, D.; O'Nions, R. K. (1995) The source regions of Ocean Island Basalts. *J.Petrol.*, V.36: p.133-159.
- McKibben, M. (1995) Ore deposits. *Rev.Geoph.*, V.Supplement: p.53-62.
- McLennan, S. M.; Taylor, S. R. (1982) Geochemical constraints on the growth of the continental crust. *J.Geol.*, V.90: p.347-361.
- McNaughton, N. J.; Green, M. D.; Compston, W.; Williams, I. S. (1988) Are anorthositic rocks basement to the Pilbara Craton? *Geol.Soc.Austr.Abstr.*, V.21: p.272-273.
- McNaughton, N. J.; Cassidy, K. F.; Dahl, N.; Groves, D. I.; Perring, C. S.; Sang, J. H. (1990) Source of ore fluids and ore components. *Umv.W.Aust. Geol.Dep.& University Extension, Publ.* V.20: p.226-268.

- McNaughton, N. J.; Cassidy, K. F.; Dahl, N.; de Laeter, J. R.; Golding, S. D.; Groves, D. I.; Ho, S. E.; Mueller, A. G.; Perring, C. S.; Sang, J. H.; Turner, J. V. (1992) The source of ore components in lode-gold deposits of the Yilgarn Block, Western Australia. *Univ. W. Aust. Geol. Dep. & University Extension, Publ.*, V.22: p.351-363.
- McNaughton, N. J.; Compston, W.; Barley, M. E. (1993) Constraints on the age of the Warrawoona Group, eastern Pilbara Block, Western Australia. *Precamb. Res.*, V.60: p.69-98.
- Mikucki, E. J.; Groves, D. I.; Cassidy, K. F. (1990) Wallrock alteration in sub-amphibolite facies gold-deposits. *Univ. W. Aust. Geol. Dep. & University Extension, Publ.*, V.20: p.60-78.
- Moorbath, S. (1978) Age and isotope evidence for the evolution of the continental crust. *Phil. Trans. R. Soc. London*, V. A 288: p.401-413.
- Morant, P. (1984) Metamorphism of an Archean granitoid-greenstone terrain, East Pilbara Block: the western Shaw Batholith and adjacent greenstones. Unpublished PhD-thesis, University of Western Australia.
- Morgan, P. (1984) The thermal structure and thermal evolution of the continental lithosphere. *Phys. Chem. Earth*, V.15: p.107-193.
- Morrison, G. W.; Rose, W. J.; Jaireth, S. (1991) Geological and geochemical controls on the silver content (fineness) of gold in gold-silver deposits. *Ore Geol. Rev.*, V.6: p.333-364.
- Myers, J. S. (1980) The Fiskenaeset Anorthosite Complex - a stratigraphic key to the tectonic evolution of the West Greenland Gneiss Complex 3000-2800 m.y. ago. Second International Symposium Archean Geology. Perth. *Geol. Soc. Aust. Spec. Publ.*, V.7: p.351-360.
- Myers, J. S. (1995) The generation and assembly of an Archean supercontinent: evidence from the Yilgarn Craton, Western Australia. In: *Early Precambrian Processes*. Coward, M. P., Ries, A. C., *Geol. Soc. Spec. Publ.*, V.95: p. 143-154.
- Nelson, D. R. (1996) Compilation of SHRIMP U-Pb zircon geochronology data, 1995., Geological Survey of Western Australia No. 1996/5.
- Nesbitt, B. E.; Muehlenbachs, K. (1989) Geology, geochemistry and genesis of mesothermal lode gold deposits of the Canadian Cordillera: evidence for ore formation from evolved meteoric water. In: *Geology of gold deposits: The perspective in 1988*. *Econ. Geol. Monograph*. V.6. Keays, R. R.; Ramsay, W. R. H. Groves, D. I., p. 553-563.
- Neumayr, P.; Groves, D. I.; Ridley, J. R.; Koning, C. D. (1993) Syn-amphibolite facies Archean lode gold mineralization in the Mt. York District, Pilbara Block, Western Australia. *Mineral. Deposita*, V.28: p.457-468.
- Neumayr, P.; Cabri, L. J.; Groves, D. I.; Mikucki, E. J.; Jackman, J. A. (1993b) The mineralogical distribution of gold and relative timing of gold mineralization in two Archean settings of high metamorphic grade in Australia. *Can. Mineral.*, V.31: p.711-725.
- Nijman, W.; de Bruijne, K. H.; Valkering, M. E. (in press) Cherty sediments, barite mounds, chert-barite veins, and pre-doming deformation above an early Archean Batholith, North Pole, East Pilbara, W. Australia. *Precamb. Res.*
- Nijman, W.; Willigers, B. J. A.; Krikke, A. (in press) Tensile and compressive growth structures: the relation between sedimentation, deformation and granite intrusion in the Archean Coppin Gap Greenstone Belt, East Pilbara, W. Australia. *Precamb. Res.*
- Nisbet, E. G.; Walker, D. (1982a) Komatiites and the structure of the Archean mantle. *Earth Planet. Sci. Lett.*, V.60: p.105-113.
- Nisbet, E. G. (1982b) Definition of Archean - comment and a proposal on the recommendations of the international sub-commission on Precambrian stratigraphy. *Precamb. Res.*, V.19: p.111-118.
- Nisbet, E. G. (1987) *The Young Earth*. Allen and Unwin: London: p. 402.
- Nisbet, E. G.; Fowler, C. M. R. (1983) Model for Archean plate tectonics. *Geology*, V.11: p.376-379.
- Nisbet, E. G.; Arndt, N. T.; Bickle, M. J.; Cameron, W. E.; Chauvel, C.; Cheadle, M.; Henger, E.; Kyser, T. K.; Martin, A.; Renner, R.; Roeder, E. (1987) Uniquely fresh 2.7 Ga komatiites from the Belingwe greenstone belt, Zimbabwe. *Geology*, V.15: p.1147-1150.
- Nutman, A. P.; Kinny, P. D.; Compston, W.; Williams, I. S. (1991) SHRIMP U-PB zircon geochronology of the Narryer Gneiss Complex, Western Australia. *Precamb. Res.*, V.52: p.275-300.
- Nutman, A. P.; McGregor, V. R.; Friend, C. R. L.; Bennett, V. C.; Kinny, P. D. (1996) The Isaq Gneiss Complex of southern West Greenland; the world's most extensive record of early crustal evolution (3900-3600 Ma). *Precamb. Res.*, V.78: p.1-39.
- Nyblade, A. A.; Pollack, H. N. (1993) A global analysis of heat flow from Precambrian terrains: implications for the thermal structure of Archean and Proterozoic lithosphere. *J. Geophys. Res.*, V.98: p.12207-12218.
- O'Nions, R. K.; Evensen, N. M.; Hamilton, P. J.; Carter, S. R. (1978) Melting of the mantle past and present: isotopic and trace element evidence. *Philos. Trans. Soc. Lond.*, V.A258: p.547-559.
- Ohta, H.; Maruyama, S.; Takahashi, E.; Watanabe, Y.; Kato, Y. (1996) Field occurrence, geochemistry and petrogenesis of the Archean Mid-Oceanic ridge basalts (AMORBs) of the Cleaverville area, Pilbara Craton, Western Australia. *Lithos*, V.37: p.199-221.
- Park, R. G. (1981) Origin of horizontal structure in high-grade Archean terrains. In: *Archean Geology*. Glover, J. E. Groves, D. I., *Geol. Soc. Austr. Spec. Publ.*, Perth: V.7: p. 351-360.
- Park, R. G. (1982) Archean Tectonics. *Geol. Rundschau*, V.71: p.22-37.
- Parsons, T.; Thompson, G. A.; Sleep, N. H. (1994) Mantle plume influence on the Neogene uplift and extension of the U.S. western Cordillera? *Geology*, V.22: p.83-86.
- Passchier, C. W. (1995) Precambrian orogenesis: was it really different? *Geol. Mijnbouw*, V.74: p.141-150.
- Passchier, C. W.; ten Brink, C. E.; Bons, P. D.; Sokoutis, D. (1993) d-objects as a gauge for sensitivity of strain rate in mylonites. *Earth Planet. Sci. Lett.*, V.120: p.239-245.
- Passchier, C. W.; Trouw, R. A. J. (1996) *Micro-tectonics*.

- Springer Verlag: p.289.
- Pavlis, T. L. (1996) Fabric development in syn-tectonic intrusive sheets as a consequence of melt-dominated flow and thermal softening of the crust. *Tectonophysics*, V.253: p.1-31.
- Percival, J. A. (1994) Archean high-grade metamorphism. In: *Archean Crustal evolution. Developments in Precambrian geology*. Condie, K. C., Elsevier, V.11: p. 357-396.
- Perring, C. S.; Groves, D. I.; Shellbear, J. N. (1991) The geochemistry of Archean gold ores from the Yilgarn Block of Western Australia: implication for gold metallogeny., Minerals and Energy Research Institute of Western Australia Report No. 82.
- Phillips, G. N.; Powell, R. (1993) Link between gold Provinces. *Econ.Geol.*, V.88: p.1084-1098.
- Pidgeon, R. T. (1978a) 3450 Ma old volcanics in the Archean layered greenstone succession in the Pilbara Block, Western Australia. *Earth Planet.Sci.Lett.*, V.37: p.421-428.
- Pidgeon, R. T. (1978b) Geochronological investigation of granite batholiths of the Archean granite-greenstone terrain of the Pilbara Block, Western Australia. *Archean Geochemistry Conference*. Toronto. p.360-362.
- Pidgeon, R. T. (1984) Geochronological constraints on early volcanic evolution of the Pilbara Block, Western Australia. *J.Geol.Soc.Aust.*, V.31: p.237-242.
- Pidgeon, R. T. (1992) Recrystallization of oscillatory zoned zircon: some geochronological and petrological implications. *Contrib.Mineral.Petrol.*, V.110: p.463-472.
- Rapp, R. P. (1996) Heterogeneous source regions for Archean granitoids: experimental and geochemical evidence. In: *Greenstone Belts*. de Wit, M. J. Ashwal, L. D., Clarendon Press, Oxford: p.267-280.
- Rapp, R. P.; Watson, E. B. (1995) Dehydration melting of metabasalt at 8-32 kbar: implications for continental growth and crust-mantle recycling. *J.Petrol.*, V.36: p.891-931.
- Raymer, A.; Schubert, G. (1984) Phanerozoic addition rates to the continental crust and crustal growth. *Tectonics*, V.3: p.63-78.
- Richardson, S. H. (1989) Radiogenic isotope studies of diamond inclusions. *Workshop on Diamonds*, extended abstracts. Washington DC. p.87-90.
- Richardson, S. H.; Gurney, J. J.; Erlank, A. J.; Harris, J. W. (1984) Origin of diamonds in old enriched mantle. *Nature*, V.310: p.198-202.
- Ridley, J. R. (1992) The thermal causes and effects of voluminous, late Archean monzogranite plutonism. *Univ.W.Aust.Geol.Dep.& University Extension*, Publ., V.22: p.275-285.
- Robert, F. (1990) Structural setting and control of gold-quartz veins of the Val d'Or area, southeastern Abitibi Subprovince. In: *Gold and base-metal mineralization in the Abitibi Subprovince, Canada, with emphasis on the Quebec segment; short course notes*. Ho, S. E.; Robert, F. Groves, D. I., *Univ.W.Aust.Geol.Dep.& University Extension*, Publ., V.24: p. 167-210.
- Royden, L. H. (1993) The tectonic expression of slab pull at continental convergent boundaries. *Tectonics*, V.12: p.303-325.
- Rutter, E. H.; Maddock, R. H.; Hall, S. H.; White, S. H. (1986) Comparative microstructures of natural and experimentally produced clay-bearing fault gouges. *Pure Appl.Geophys.*, V.124: p.3-30.
- Schwerdtner, W. M.; Troëng, B. (1978) Strain distribution within arcuate diapiric ridges of silicone putty. *Tectonophysics*, V.50: p.13-28.
- Schwerdtner, W. M.; Sutcliffe, R. H.; Troëng, G. (1978) Patterns of total strain in the crestal region of immature diapirs. *Can.J.Earth Sci.*, V.15: p.1437-1447.
- Shirley, D. N. (1983) A partially molten magma ocean model. *J.Geophys. Res.*, V.88: p.A519-A527.
- Sibson, R. H. (1977) Fault rocks and fault mechanisms. *J.Geol.Soc.London*, V.133: p.171-191.
- Skinner, B. J. (1979) The many origins of hydrothermal mineral deposits. In: *Geochemistry of hydrothermal ore deposits*. Barnes, H. L., Wiley and Sons, p.1-21.
- Skwarnecki, M. S. (1988) Alteration and deformation in shear zone hosting gold mineralization at Harbour Lights, Leonora, Western Australia. In: *Advances in understanding Precambrian gold deposits II*. Ho, S. E. Groves, D. I., *Univ.W.Aust. Geol.Dep.& University Extension*, Publ., V.12: p. 111-129.
- Sleep, N. H. (1979) Thermal history and degassing of the Earth: some simple calculations. *J.Geol.*, V.87: p.671-686.
- Sleep, N. H. (1992) Archean plate tectonics: what can be learned from continental geology? *Can.J.Earth Sci.*, V.29: p.2066-2071.
- Sleep, N. H.; Windley, B. F. (1982) Archean plate tectonics: constraints and inferences. *J.Geol.*, V.90: p.363-379.
- Smith, H. S.; Erlank, A. J.; Duncan, A. R. (1980) Geochemistry of some ultramafic komatiite lava flows from the Barberton Mountain Land, South Africa. *Precambr.Res.*, V.11: p.399-415.
- Smith, J. B.; Barley, M. E.; Groves, D. I.; Krapez, B.; McNaughton, N. J. (in press) The Sholl Shear Zone, Western Pilbara: Evidence for a Domain Boundary Structure from integrated tectonic analyses, SHRIMP U-Pb dating and isotopic and geochemical data of granitoids. *Precambr.Res.*
- Snowden, P. A. (1984) Non-diapiric batholiths in the north of the Zimbabwe Shield. In: *Precambrian Tectonics Illustrated*. Kröner, A. Greiling, R., Nagele und Obermiller, Stuttgart: p. 135-145.
- Sonder, L. J.; England, P. C.; Wernicke, B. P.; Christiansen, R. L. (1987) A physical model for Cenozoic extension of western North America. In: *Continental extensional tectonics*. Coward, M. P.; Dewey, J. F. Hancock, P. L., *Geol.Soc.London Spec.Publ.*, V.28: p. 187-201.
- Song, B.; Nutman, A. P.; Liu, D.; Wu, J. (1996) 3800 to 2500 Ma crustal evolution in the Anshan area of Liaoning Province, northeastern China. *Precambr.Res.*, V.78: p.79-94.
- Spencer, J. (1984) Role of tectonic denudation in warping and uplift of low-angle normal faults. *Geology*, V.12: p.95-98.
- Steiger, R. H.; Jaeger, E. (1977) Subcommission on geochronology: convention on the use of decay constants in geo- and cosmo-chronology. *Earth Planet.Sci.Lett.*, V.36: p.359-362.

- Stein, M.; Hofmann, A. W. (1994) Mantle plumes and episodic crustal growth. *Nature*, V.372: p.63-68.
- Stettler, E. H.; Plessis, J. G.; de Beer, J. H. (1988) The structure of the Pietersburg greenstone belt, South Africa, as derived from geophysics. *S.Afr.J.Geol.*, V.91: p.292-303.
- Streckeisen, A. (1976) To each plutonic rock its proper name. *Earth Sci.Rev.*, V.12: p.1-33.
- Streckeisen, A.; LeMaitre, R. W. (1979) A chemical classification to the modal QAPF classification of igneous rocks. *Neue Jahrbuch Mineral.Abh.*, V.136: p.169-206.
- Swager, C.; Griffin, T. J. (1990) An early thrust duplex in the Kalgoorlie-Kambalda greenstone belt; Eastern Goldfields Province, Western Australia. *Precambr.Res.*, V.48: p.63-73.
- Sylvester, P. J. (1994) Archean granite plutons. In: *Archean Crustal Evolution. Developments in Precambrian Geology*. Condie, K. C., Elsevier, Amsterdam: V.11: p. 261-314.
- Sylvester, P. J.; Attoh, K. (1992) Lithostratigraphy and composition of 2.1 Ga greenstone belts of the West African Craton and their bearing on crustal evolution and the Archean-Proterozoic boundary. *Geology*, V.100: p.377-393.
- Sylvester, P. J.; Harper, G. D.; Byerly, G. R.; Thurston, P. C. (1996) Volcanic aspects. In: *Greenstone Belts*. de Wit, M. J. Ashwal, L. D., Clarendon Press, Oxford: p.55-90.
- Tatsumoto, M.; Knight, R. J.; Allegre, C. J. (1973) Time differences in the formation of meteorites as determined from the ratio of lead-207 and lead-206. *Science*, V.180: p.1279-1283.
- Taylor, P. N.; Kramers, J. D.; Moorbath, S.; Wilson, J. F.; Orpen, J. L.; Martin, A. (1991) Pb/Pb, Sm-Nd and Rb-Sr geochronology in the Archean Craton of Zimbabwe. *Chem.Geol.*, V.87: p.175-196.
- Taylor, S. R. (1989) Growth of planetary crusts. *Tectonophysics*, V.161: p.147-156.
- Taylor, S. R.; McLennan, S. M. (1985) The continental crust: Its composition and evolution. Blackwell, Oxford.
- Taylor, S. R.; McLennan, S. M. (1995) The geochemical evolution of the continental crust. *Rev. Geophysics*, V.33: p.241-265.
- Thorman, C. H.; Christensen, O. D. (1991) Geologic settings of gold deposits in the Great Basin, western United States. In: *Brazil gold '91*. Ladeira, E. A., Balkema, Rotterdam: p. 65-75.
- Thorpe, R. I.; Hickman, A. H.; Davis, D. W.; Mortensen, J. K.; Trendall, A. F. (1990) Constraints to models for Archean lead evolution from precise zircon U-Pb geochronology for the Marble Bar region, Pilbara Craton Western Australia. *Univ.W.Aust. Geol.Dep.& University Extension, Publ.V.22: p.395-407*.
- Thorpe, R. I.; Hickman, A. H.; Davis, D. W.; Mortensen, J. K.; Trendall, A. F. (1992) U-Pb zircon geochronology of Archean felsic units in the Marble Bar region, Pilbara Craton, Western Australia. *Precambr.Res.*, V.56: p.169-189.
- Thurston, P. C. (1994) Archean volcanic patterns. In: *Archean crustal evolution. Developments in Precambrian Geology*. Condie, K. C., Elsevier, V.11: p. 45-75.
- Todt, W.; Chauvel, C.; Arndt, N. T.; Hofmann, A. W. (1984) Pb isotopic composition and age of Proterozoic komatiites and related rocks from Canada. *EOS*, V.65: p.1129.
- van den Eeckhout, B.; Grocott, J.; Vissers, R. (1986) On the role of diapirism in the segregation, ascent and final emplacement of granitoid magmas - discussion. *Tectonophysics*, V.127: p.161-169.
- van Kranendonk, M. J.; Collins, W. J. (in press) Timing and regional significance of Late Archean, sinistral strike-slip deformation of the Central Pilbara corridor, Pilbara Craton, Western Australia. *Precambr.Res.*
- Vavra, G.; Gebauer, D.; Schmid, R.; Compston, W. (1996) Multiple zircon growth and recrystallization during polyphase Late Carboniferous to Triassic metamorphism in granulites of the Ivrea Zone (Southern Alps): an ion microprobe (SHRIMP) study. *Contrib.Mineral.Petrol.*, V.122: p.337-358.
- Vearncombe, J. R.; Barley, M. E.; Eisenlohr, B.; Grigson, M. W.; Groves, D. I.; Houston, M. S.; Partington, G. A.; Swarnecki, M. S. (1988) Structural controls on gold mineralization- examples from Archean terrains of Western Australia and southern Africa. *Bicentennial Gold '88.Geol.Soc.Austr.Abstr.*, V.22: p.19-23.
- Vearncombe, S.; Barley, M. E.; Groves, D. I.; McNaughton, N. J.; Mickucki, E. J.; Vearncombe, J. R. (1995) 3.26 Ga black smoker-type mineralization in the Strelley Belt, Pilbara, Western Australia. *J.Geol.Soc.London*, V.152: p.587-590.
- Veizer, J.; Jansen, S. L. (1979) Basement and sedimentary recycling and continental evolution. *J.Geol.*, V.87: p.341-370.
- Vervoort, J. D.; Patchett, P. J.; Gehrels, G. E.; Nutman, A. P. (1996) Constraints on early earth differentiation from hafnium and neodymium isotopes. *Nature*, V.379: p.624-627.
- Viljoen, M. J.; Viljoen, R. P. (1969) Evidence for the existence of mobile extrusive peridotitic magma from the Komati formation of the Onverwacht Group. *Spec.Publ.Geol. Soc.S.Afr.*, V.2: p.87-112.
- Vlaar, N. J. (1986) Archean global dynamics. *Geol.Mijnb.*, V.65: p.91-101.
- Vlaar, N. J.; van Keken, P. E.; van den Berg, A. P. (1994) Cooling of the Earth in the Archean: consequences of pressure-release melting in a hotter mantle. *Earth Planet.Sci.Lett.*, V.121: p.1-18.
- Walker, D. (1983) Lunar and terrestrial crust formation. *Proceedings of the 14th Lunar and Planetary Science Conference. J.Geoph.Res.*, V.1: p.B17-26.
- Wang, G. M.; White, S. H. (1993) Gold mineralization in shear zones within a turbidite terrane, examples from Central Victoria, S.E. Australia. *Ore Geol. Rev.*, V.8: p.163-188.
- Weinberg, R. F.; Schmelling, H. (1992) Polydiapirs: multi-wavelength gravity structures. *J.Struct.Geol.*, V.14: p.425-436.
- Weinberg, R. F.; Podladchikov, Y. (1994) Diapiric ascent of magmas through power-law crust and mantle. *J.Geophys.Res.*, V.99: p.9543-9559.
- Weinberg, R. F.; Podladchikov, Y. Y. (1995) The rise of solid-state diapirs. *J.Struct.Geol.*, V.17: p.1183-1195.
- Wernicke, B.; Axen, G. J. (1988) On the role of isostasy in the evolution of normal fault systems. *Geology*, V.16: p.848-851.

- Wheeler, J.; Butler, R. W. H. (1994) Criteria for identifying structures related to true extension in orogens. *J.Struct.Geol.*, V.16: p.1023-1027.
- White, S. H.; Bretan, P. G.; Rutter, E. H. (1986) Fault-zone reactivation: kinematics and mechanisms. *Phil.Trans.R. Soc.Lond.*, V.A317: p.81-97.
- Wijbrans, J. R.; McDougall, I. (1987) On the metamorphic history of an Archean granitoid greenstone terrane, East Pilbara, Western Australia, using the $^{40}\text{Ar}/^{39}\text{Ar}$ age spectrum technique. *Earth Planet. Sci. Lett.*, V.84: p.226-242.
- Wijbrans, J. R.; Pringle, M. S.; Koppers, A. A. P.; Scheveers, R. (1995) Argon geochronology of small samples using the Vulkana laserprobe. *Proc.Kon.Ned.Akad. v. Wetensch.*, V.98: p.185-218.
- Williams, I. S.; Page, R. W.; Froude, D.; Foster, J. J.; Compston, W. (1983) Early crustal components in the Western Australian Archean: zircon U-Pb ages by ion microprobe analysis from the Shaw Batholith and Narryer metamorphic belt. Sixth Australian Geological Convention- Lithosphere dynamics and evolution of continental crust. *Abst.Vol.Geol.Soc.Aust.*, V.9: p.169.
- Williams, I. S.; Compston, W.; Black, L. P.; Ireland, T. R.; Foster, J. J. (1984) Unsupported radiogenic Pb in zircon: a cause of anomalously high Pb-Pb, U-Pb and Th-Pb ages. *Contrib. Mineral.Petrol.*, V.88: p.322-327.
- Williams, I. S.; Collins, W. J. (1990) Granite-greenstone terranes in the Pilbara Block, Australia, as coeval volcano-plutonic complexes; evidence from U-Pb zircon dating of the Mount Edgar Batholith. *Earth Planet. Sci. Lett.*, V.97: p.41-53.
- Williams, P. R.; Whitaker, A. J. (1993) Gneiss domes and extensional deformation in the highly mineralised Archean Eastern Goldfields Province, Western Australia. *Ore Geol.Rev.*V.8: p.141-162.
- Wilson, J. T. (1966) Did the Atlantic close and then re-open? *Nature*. V.211: p.676-681.
- Winther, K. T. (1996) An experimentally based model for the origin of tonalitic and trondhjemitic melts. *Chem.Geol.*, V.127: p.43-59.
- Wong, T. (1986) Metamorphic patterns in the Kambalda area and their significance to Archean greenstone belts of the Kambalda-Widgiemooltha area.unpublished B.Sc-(Honours) thesis, University of Western Australia, p.152.
- Woodall (1988) Distribution of Gold in time. Gold in 1988, extended abstracts Bicentennial Gold '88, Melbourne, *Geol.Soc.Aust.*, 1-12.
- Wortel, M. J. R.; Spakman, W. (1992) Structure and dynamics of subducted lithosphere in the Mediterranean region. *Proc.Kon.Ned.Akad.Wetensch.*, V.95: p.325-347.
- Wyllie, P. J.; Wolf, M. B.; van der Laan, S. R. (1996) Conditions for formation of tonalites and trondhjemitites: magmatic sources and products. In: *Greenstone Belts*. de Wit, M. J. Ashwal, L. D.. Clarendon Press, Oxford: p.256-266.
- Zegers, T. E.; White, S. H.; de Keijzer, M.; Dirks, P. (1996) Extensional structures during deposition of the 3460 ma Warrawoona Group in the eastern Pilbara Craton, western Australia. *Precamb. Res.* (In press).

Appendix I Data set of $^{40}\text{Ar}/^{39}\text{Ar}$ step heating experiments

Sample Number T93/182b
Material actinolite
Irradiation Number VU11

File and step	$^{39}\text{Ar}(a)$	^{39}Ar	^{39}Ar	$^{39}\text{Ar}(K)$	$^{39}\text{Ar}(a+r)$	Age	$\pm 2\sigma$	$^{40}\text{Ar}(r)$	^{39}Ar	$^{39}\text{Ar}(\text{cum})$	K/Ca
95M0253B.DAT	0.01044	0.000	0.0094	0.010	4.437	3528.6	± 3407.1	30.5	0.5	0.5	1042.091
95M0253C.DAT	0.01726	0.362	0.0228	0.048	8.848	2663.2	± 438.1	42.3	2.6	3.1	0.066
95M0253D.DAT	0.01183	3.789	0.0498	0.088	11.586	2913.2	± 140.5	69.8	4.7	7.9	0.011
95M0253E.DAT	0.01590	4.628	0.0553	0.068	12.366	3203.4	± 198.1	62.0	3.7	11.6	0.007
95M0253F.DAT	0.00974	9.983	0.0690	0.088	13.660	3332.6	± 114.8	78.9	4.8	16.3	0.004
95M0253G.DAT	0.00974	7.879	0.0432	0.065	10.274	3211.2	± 167.8	72.0	3.5	19.9	0.004
95M0253I.DAT	0.00702	12.739	0.0665	0.105	13.782	3189.9	± 58.7	84.9	5.7	25.5	0.004
95M0253J.DAT	0.00689	16.430	0.0799	0.117	15.394	3223.3	± 54.1	86.7	6.3	31.9	0.003
95M0253K.DAT	0.00452	18.017	0.0866	0.129	15.928	3218.0	± 50.1	91.6	6.9	38.8	0.003
95M0253L.DAT	0.00296	11.738	0.0527	0.088	10.348	3145.4	± 67.9	91.5	4.7	43.6	0.004
95M0253M.DAT	0.00514	16.714	0.0870	0.121	15.618	3252.5	± 48.5	90.2	6.6	50.1	0.004
95M0253N.DAT	0.00459	24.198	0.0459	0.165	19.909	3200.0	± 36.9	93.1	8.9	59.1	0.003
95M0253P.DAT	0.00568	30.540	0.1413	0.217	25.776	3187.7	± 27.8	93.4	11.7	70.8	0.003
95M0253Q.DAT	0.00263	12.111	0.0468	0.081	9.242	3099.9	± 72.3	91.5	4.4	75.1	0.003
95M0253R.DAT	0.00291	17.570	0.0672	0.118	13.277	3101.9	± 49.6	93.5	6.4	81.5	0.003
95M0253S.DAT	0.00110	7.442	0.0368	0.047	5.428	3166.4	± 119.1	94.0	2.5	84.1	0.003
95M0253T.DAT	0.00779	46.739	0.1939	0.295	35.680	3213.0	± 21.5	93.5	15.9	100.0	0.003

Correction	Factors	Results	$^{40}\text{Ar}/^{39}\text{K} \pm 2\sigma$	Age	$\pm 2\sigma$
K/Ca	= 0.49	Weighted Mean of Plateau	111.945 \pm 3.253	3197.1	\pm 44.4
J	= 0.043625				
sd-J (1s)	= 0.000131				
$1/\lambda$	= 1804.077	Total Fusion		3176.7	\pm 9.0

Sample Number T94/203
Material hornblende
Irradiation Number VU11

File and step	$^{39}\text{Ar}(a)$	^{39}Ar	^{39}Ar	$^{39}\text{Ar}(K)$	$^{39}\text{Ar}(a+r)$	Age	$\pm 2\sigma$	$^{40}\text{Ar}(r)$	^{39}Ar	$^{39}\text{Ar}(\text{cum})$	K/Ca
95M0248A.DAT	0.02946	1.794	0.3472	0.369	49.405	3176.0	± 24.69	82.3	1.3	1.3	0.101
95M0248B.DAT	0.01372	56.622	12.8732	9.108	1144.357	3366.2	± 11.39	99.6	32.7	34.1	0.079
95M0248C.DAT	0.00428	24.731	5.5375	3.980	494.547	3350.9	± 11.10	99.7	14.3	48.4	0.079
95M0248D.DAT	0.00257	12.195	2.6344	1.920	237.242	3341.6	± 12.87	99.6	6.9	55.3	0.077
95M0248E.DAT	0.00216	12.434	2.7779	2.020	247.406	3328.7	± 13.21	99.7	7.3	62.5	0.080
95M0248F.DAT	0.00257	14.402	3.1789	2.254	276.491	3330.6	± 11.99	99.7	8.1	70.7	0.077
95M0248H.DAT	0.00131	6.930	1.6437	1.097	134.793	3333.5	± 14.58	99.7	3.9	74.6	0.078
95M0248I.DAT	0.00243	8.978	1.9117	1.449	175.744	3312.2	± 13.63	99.5	5.2	79.8	0.079
95M0248J.DAT	0.00089	8.894	1.9702	1.392	170.763	3332.9	± 16.06	99.8	5.0	84.8	0.077
95M0248K.DAT	0.00078	2.192	0.4256	0.336	40.382	3294.3	± 24.34	99.4	1.2	86.0	0.075
95M0248L.DAT	0.00187	8.399	1.7221	1.270	156.570	3337.7	± 12.34	99.6	4.6	90.6	0.074
95M0248N.DAT	0.00081	5.596	1.1444	0.855	101.581	3283.4	± 17.81	99.7	3.1	93.7	0.075
95M0248O.DAT	0.00324	15.975	2.2119	1.763	208.894	3275.3	± 12.37	99.5	6.3	100.0	0.054

Correction	Factors	Results	$^{40}\text{Ar}/^{39}\text{K} \pm 2\sigma$	Age	$\pm 2\sigma$
K/Ca	= 0.49	Weighted Mean of Plateau	111.945 \pm 3.253	3197.1	\pm 44.4
J	= 0.043625				
sd-J (1s)	= 0.000131				
$1/\lambda$	= 1804.077	Total Fusion		3176.7	\pm 9.0

Sample Number T93/122
 Material biotite
 Irradiation Number VU11

File and step	³⁶ Ar(a)	³⁷ Ar	³⁸ Ar	³⁹ Ar(K)	⁴⁰ Ar(a+r)	Age	± 2σ	⁴⁰ Ar(r)	³⁹ Ar	³⁹ Ar(cum)/K/Ca	
95M0252A.DAT	7.41734	2.139	1.5745	18.031	1429.357	0.0	± 50.9	-53.3	19.0	19.0	4.131
95M0252B.DAT	2.46833	1.789	2.8925	28.936	1428.623	1298.7	± 7.4	48.9	30.5	49.6	7.924
95M0252C.DAT	0.39694	0.795	1.3104	12.964	1360.293	2968.3	± 9.6	91.3	13.7	63.2	7.987
95M0252D.DAT	0.16789	0.634	1.1892	11.613	1179.177	2989.2	± 10.0	95.7	12.3	75.5	8.969
95M0252G.DAT	0.06323	0.466	1.0074	9.442	943.500	2999.5	± 10.1	97.9	10.0	85.4	9.919
95M0252H.DAT	0.04158	0.417	0.6392	6.203	622.809	3006.4	± 10.2	98.0	6.5	92.0	7.283
95M0252I.DAT	0.02897	0.324	0.4452	4.192	416.359	2989.3	± 10.0	97.9	4.4	96.4	6.333
95M0252J.DAT	0.02286	0.259	0.3567	3.398	335.263	2980.2	± 10.5	97.9	3.6	100.0	6.418

Correction	Factors	Results	⁴⁰ */ ³⁹ K ± 2σ	Age	± 2σ
K/Ca	= 0.49				
J	= 0.043625	Weighted Mean	97.096 ± 0.321	2986.7	± 10.0
sd-J (1s)	= 0.000131	of Plateau			
1 / λ	= 1804.077	Total Fusion		2046.1	± 7.3

Sample Number T94/220
 Material hornblende
 Irradiation Number VU11

File and step	³⁶ Ar(a)	³⁷ Ar	³⁸ Ar	³⁹ Ar(K)	⁴⁰ Ar(a+r)	Age	± 2σ	⁴⁰ Ar(r)	³⁹ Ar	³⁹ Ar(cum)/K/Ca	
95M0250A.DAT	0.02365	0.386	0.1894	0.060	36.863	5635.9	± 79.7	81.0	0.2	0.2	0.08
95M0250C.DAT	0.00190	0.066	0.0034	0.013	1.357	2344.5	± 704.8	58.5	0.0	0.2	0.10
95M0250D.DAT	0.00270	0.335	0.0088	0.052	4.733	2634.9	± 145.3	83.1	0.2	0.4	0.08
95M0250E.DAT	0.00133	1.024	0.0238	0.135	13.184	2946.0	± 49.1	97.0	0.4	0.8	0.06
95M0250H.DAT	0.00023	0.435	0.0096	0.053	5.269	2998.9	± 105.9	98.7	0.2	0.9	0.06
95M0250I.DAT	0.00330	2.513	0.0790	0.326	34.378	3067.3	± 20.1	97.1	0.9	1.9	0.06
95M0250J.DAT	0.00149	2.294	0.0682	0.349	33.348	2945.9	± 20.7	98.6	1.0	2.9	0.07
95M0250K.DAT	0.00086	2.169	0.0661	0.377	35.528	2934.6	± 18.3	99.2	1.1	4.0	0.09
95M0250L.DAT	0.00359	13.651	0.4468	2.823	266.127	2938.1	± 10.1	99.5	8.2	12.1	0.10
95M0250N.DAT	0.00277	14.274	0.4670	2.937	273.368	2921.1	± 13.3	99.6	8.5	20.7	0.10
95M0250O.DAT	0.00306	14.420	0.4725	3.017	275.864	2894.7	± 11.1	99.6	8.7	29.4	0.10
95M0250P.DAT	0.00364	18.853	0.6260	3.928	367.966	2930.5	± 9.4	99.6	11.4	40.8	0.10
95M0250Q.DAT	0.00237	9.519	0.3186	1.952	181.410	2917.6	± 12.8	99.5	5.7	46.5	0.10
95M0250S.DAT	0.00236	11.443	0.3901	2.429	224.130	2908.3	± 12.8	99.6	7.0	60.4	0.10
95M0250U.DAT	0.00094	6.871	0.2327	1.440	131.645	2895.8	± 12.5	99.7	4.2	64.6	0.10
95M0250V.DAT	0.00144	4.245	0.1356	0.842	77.838	2908.3	± 16.7	99.4	2.4	67.0	0.10
95M0250W.DAT	0.00119	8.556	0.2622	1.712	158.242	2911.7	± 11.7	99.7	5.0	72.0	0.10
95M0250X.DAT	0.00151	16.922	0.5348	3.437	320.607	2926.3	± 10.1	99.8	10.0	82.0	0.10
95M0250Y.DAT	0.00328	30.487	0.9957	6.224	582.335	2930.3	± 9.7	99.8	18.0	100.0	0.10

Correction Factors	Results	⁴⁰ */ ³⁹ K ± 2σ	Age	± 2σ
K/Ca	= 0.49			
J	= 0.043625	Weighted Mean	92.996 ± 0.429	2924.0
sd-J (1s)	= 0.000131	of Plateau		± 11.0
1 / λ	= 1804.077	Total Fusion		2933.1
				± 8.7

Sample Number 94/222
 Material hornblende
 Irradiation Number VU11

File and step	³⁹ Ar(a)	³⁹ Ar	³⁹ Ar	³⁹ Ar(K)	⁴⁰ Ar(a+r)	Age	± 2σ	⁴⁰ Ar(r)	³⁹ Ar	³⁹ Ar(cum)	K/Ca
95M0163B	0.03489	0.138	0.0424	0.087	26.000	3933.7	± 47.0	60.3	0.4	0.4	0.31
95M0163C	0.02684	0.527	0.0175	0.256	10.715	701.2	± 142.5	25.9	1.2	1.6	0.24
95M0163D	0.00680	4.376	0.1357	0.807	68.262	2746.8	± 10.6	97.0	3.8	5.5	0.09
95M0163E	0.00242	2.262	0.0683	0.396	34.764	2812.2	± 11.5	97.9	1.9	7.3	0.09
95M0163F	0.00147	4.672	0.1496	0.827	74.116	2862.8	± 11.3	99.3	3.9	11.3	0.09
95M0163G	0.00104	5.424	0.1712	0.961	86.418	2870.2	± 10.8	99.6	4.6	15.8	0.09
95M0163H	0.00248	25.066	0.8029	4.468	407.047	2892.3	± 9.7	99.7	21.2	37.0	0.09
95M0163J	0.00243	3.556	0.1183	0.746	56.787	2623.2	± 10.5	98.6	3.5	40.6	0.10
95M0163K	0.00053	5.329	0.1670	0.935	83.959	2871.7	± 11.3	99.7	4.4	45.0	0.09
95M0163L	0.00045	4.095	0.1260	0.719	65.024	2880.9	± 11.9	99.7	3.4	48.4	0.09
95M0163M	0.00054	2.187	0.0669	0.383	34.807	2884.7	± 14.8	99.5	1.8	50.2	0.09
95M0163P	0.00000	16.726	0.5098	2.973	268.885	2884.5	± 10.5	99.9	14.1	64.4	0.09
95M0163Q	0.00084	6.077	0.1898	1.083	96.597	2860.1	± 12.1	99.7	5.1	69.5	0.09
95M0163R	0.00062	2.666	0.0818	0.469	41.986	2864.2	± 11.9	99.5	2.2	71.7	0.09
95M0163S	0.00035	2.055	0.0631	0.360	32.196	2865.1	± 12.8	99.6	1.7	73.4	0.09
95M0163T	0.00054	2.275	0.0685	0.391	35.003	2863.0	± 11.6	99.5	1.9	75.3	0.08
95M0163V	0.00028	0.962	0.0294	0.167	14.876	2850.7	± 22.2	99.4	0.8	76.1	0.09
95M0163W	0.00027	1.244	0.0372	0.213	19.278	2878.3	± 16.8	99.5	1.0	77.1	0.08
95M0163X	0.00014	1.355	0.0418	0.235	21.370	2888.5	± 17.4	99.7	1.1	78.2	0.09
95M0163Y	0.00025	0.702	0.0215	0.123	11.113	2872.3	± 23.5	99.2	0.6	78.8	0.09
95M0163Z	0.00019	1.311	0.0401	0.225	20.384	2879.8	± 15.3	99.6	1.1	79.9	0.08
95M0163@	0.00127	4.734	0.1323	0.760	69.477	2892.2	± 10.7	99.4	3.6	83.5	0.08
95M0163#	0.00265	22.931	0.6233	3.481	325.450	2928.5	± 9.7	99.7	16.5	100.0	0.07

Correction Factors	Results	⁴⁰ */ ³⁹ K ± 2σ	Age	± 2σ
K/Ca = 0.49	Weighted Mean of Plateau	90.019 ± 0.503	2877.5	± 11.8
J = 0.043625				
sd-J (1s) = 0.000131				
1 / λ = 1804.077				
	Total Fusion		2864.2	± 9.2

Sample Number T94/196
 Material hornblende
 Irradiation Number VU11

File and step	³⁹ Ar(a)	³⁹ Ar	³⁹ Ar	³⁹ Ar(K)	⁴⁰ Ar(a+r)	Age	± 2σ	⁴⁰ Ar(r)	³⁹ Ar	³⁹ Ar(cum)	K/Ca
95M0244A.DAT	0.01252	0.368	0.1650	0.056	53.789	6648.9	± 102.6	93.1	0.3	0.3	0.075
95M0244B.DAT	0.00250	0.705	0.0510	0.133	12.149	2808.2	± 58.6	93.9	0.7	1.0	0.092
95M0244C.DAT	0.00011	1.435	0.0916	0.226	20.982	2915.9	± 34.2	99.8	1.2	2.2	0.077
95M0244D.DAT	0.00049	3.938	0.2448	0.620	59.494	2965.7	± 15.0	99.7	3.3	5.5	0.077
95M0244E.DAT	0.00022	6.873	0.4242	1.111	107.259	2977.4	± 12.2	99.9	5.9	11.5	0.079
95M0244F.DAT	0.00121	14.871	0.9223	2.452	244.135	3020.6	± 10.0	99.8	13.1	24.6	0.081
95M0244H.DAT	0.00002	2.285	0.1407	0.377	35.519	2943.4	± 22.0	99.9	2.0	26.6	0.081
95M0244I.DAT	0.00081	9.381	0.5211	1.466	148.107	3042.3	± 12.1	99.8	7.8	34.5	0.077
95M0244J.DAT	0.00159	20.777	1.1251	3.223	329.580	3060.2	± 12.7	99.8	17.2	51.7	0.076
95M0244M.DAT	0.00000	1.163	0.0661	0.184	18.102	3006.8	± 37.0	99.9	1.0	52.7	0.077
95M0244N.DAT	0.00096	9.225	0.5206	1.490	146.926	3005.9	± 12.1	99.7	8.0	60.7	0.079
95M0244O.DAT	0.00043	8.624	0.4885	1.363	135.476	3019.3	± 12.2	99.8	7.3	68.0	0.077
95M0244P.DAT	0.00026	2.308	0.1313	0.361	34.813	2972.1	± 22.7	99.7	1.9	69.9	0.077
95M0244Q.DAT	0.00012	3.282	0.1879	0.515	51.726	3033.4	± 17.4	99.9	2.8	72.6	0.077
95M0244R.DAT	0.00087	15.240	0.8439	2.395	241.010	3036.8	± 10.4	99.8	12.8	85.5	0.077
95M0244S.DAT	0.00173	16.844	0.9846	2.717	265.495	2992.4	± 10.4	99.7	14.5	100.0	0.079

Correction Factors	Results	⁴⁰ */ ³⁹ K ± 2σ	Age	± 2σ
K/Ca = 0.49	Weighted Mean of Plateau	100.086 ± 0.698	3030.6	13.5
J = 0.043610				
sd-J (1s) = 0.000131				
1 / λ = 1804.077				
	Total Fusion		3051.6	8.8

Sample Number T94/181
 Material hornblende
 Irradiation Number VU11

File and step	³⁶ Ar(a)	³⁷ Ar	³⁸ Ar	³⁹ Ar(K)	⁴⁰ Ar(a+r)	Age	± 2σ	⁴⁰ Ar(r)	³⁹ Ar	³⁸ Ar(cum)	K/Ca
95M0236A.DAT	0.01726	1.086	0.1815	0.231	41.180	3709.6	± 29.7	87.6	2.4	2.4	0.104
95M0236C.DAT	0.00114	1.397	0.1100	0.209	22.834	3136.2	± 38.5	98.5	2.2	4.6	0.073
95M0236D.DAT	0.00134	3.514	0.2807	0.501	56.096	3187.5	± 18.7	99.2	5.2	9.8	0.070
95M0236E.DAT	0.00202	11.507	0.9146	1.612	184.636	3225.8	± 11.3	99.6	16.9	26.7	0.069
95M0236F.DAT	0.00177	12.830	1.0875	1.914	220.312	3234.8	± 10.7	99.7	20.0	46.7	0.073
95M0236G.DAT	0.00115	4.973	0.3922	0.708	79.647	3198.1	± 14.2	99.5	7.4	54.1	0.070
95M0236I.DAT	0.00028	1.950	0.1563	0.271	30.947	3224.5	± 30.8	99.7	2.8	57.0	0.068
95M0236J.DAT	0.00074	2.006	0.1628	0.279	31.950	3218.0	± 29.6	99.2	2.9	59.9	0.068
95M0236K.DAT	0.00125	6.225	0.5070	0.888	101.486	3222.5	± 13.7	99.6	9.3	69.2	0.070
95M0236L.DAT	0.00063	5.738	0.4621	0.827	93.302	3205.8	± 15.0	99.7	8.6	77.8	0.071
95M0236N.DAT	0.00044	1.582	0.1159	0.205	23.295	3212.1	± 30.7	99.4	2.1	80.0	0.063
95M0236O.DAT	0.00058	2.957	0.1817	0.319	35.638	3184.7	± 21.1	99.5	3.3	83.3	0.053
95M0236P.DAT	0.00058	3.095	0.2055	0.358	41.004	3226.5	± 22.1	99.5	3.7	87.0	0.057
95M0236Q.DAT	0.00164	9.644	0.6851	1.238	141.141	3218.8	± 11.9	99.6	13.0	100.0	0.063

Correction Factors	Results	40*/39K ± 2σ	Age	± 2σ
K/Ca = 0.49	Weighted Mean of Plateau	113.851 ± 0.788	3221.9	± 13.760
J = 0.043610				
sd-J (1s) = 0.000131				
1 / λ = 1804.077				
	Total Fusion		3230.2	± 9.018

Sample Number T94/193
 Material hornblende
 Irradiation Number VU11

File and step	³⁶ Ar(a)	³⁷ Ar	³⁸ Ar	³⁹ Ar(K)	⁴⁰ Ar(a+r)	Age	± 2σ	⁴⁰ Ar(r)	³⁹ Ar	³⁸ Ar(cum)	K/Ca
95M0243A.DAT	0.00795	0.417	0.0466	0.107	25.059	4200.4	± 48.7	90.6	0.9	0.9	0.126
95M0243B.DAT	0.00147	1.991	0.0781	0.469	46.940	3017.0	± 16.1	99.0	3.7	4.6	0.115
95M0243E.DAT	0.00062	4.605	0.1688	1.114	110.977	3021.8	± 12.9	99.8	8.9	13.4	0.118
95M0243F.DAT	0.00211	16.238	0.6006	4.021	396.230	3005.4	± 10.7	99.8	32.0	45.5	0.121
95M0243G.DAT	0.00055	2.963	0.1074	0.682	67.733	3016.6	± 13.8	99.7	5.4	50.9	0.113
95M0243H.DAT	0.00064	3.106	0.1076	0.703	70.103	3020.4	± 12.5	99.7	5.6	56.5	0.111
95M0243I.DAT	0.00043	6.198	0.2279	1.389	141.508	3055.6	± 10.4	99.8	11.1	67.5	0.110
95M0243K.DAT	0.00022	5.060	0.1789	1.094	111.127	3051.9	± 11.3	99.9	8.7	76.2	0.106
95M0243L.DAT	0.00000	1.850	0.0684	0.459	44.400	2979.5	± 17.9	99.9	3.7	79.9	0.122
95M0243M.DAT	0.00005	1.869	0.0698	0.476	46.456	2993.6	± 18.1	99.9	3.8	83.7	0.125
95M0243N.DAT	0.00018	2.352	0.0865	0.592	57.670	2989.4	± 15.6	99.8	4.7	88.4	0.123
95M0243O.DAT	0.00073	7.061	0.2248	1.458	146.368	3033.0	± 11.3	99.8	11.6	100.0	0.101

Correction Factors	Results	40*/39K ± 2σ	Age	± 2σ
K/Ca = 0.49	Weighted Mean of Plateau	99.894 ± 0.579	3027.8	± 12.241
J = 0.043610				
sd-J (1s) = 0.000131				
1 / λ = 1804.077				
	Total Fusion		3033.8	± 8.810

Sample Number 94/185i
 Material hornblende
 Irradiation Number VU11

File and step	³⁹ Ar(a)	³⁹ Ar	³⁹ Ar	³⁹ Ar(K)	⁴⁰ Ar(a+r)	Age	± 2σ	⁴⁰ Ar(r)	³⁹ Ar	³⁹ Ar(cum)	K/Ca
95M0165B.DAT	0.07077	145.641	3.9909	8.041	808.875	3000.6	± 39.0	97.3	83.2	83.2	0.027
95M0165C.DAT	0.00032	0.310	0.0088	0.018	1.483	2693.4	± 125.6	93.5	0.2	83.4	0.028
95M0165D.DAT	0.00067	4.142	0.1130	0.230	22.136	2960.3	± 15.8	99.0	2.4	85.8	0.027
95M0165E.DAT	0.00020	2.464	0.0637	0.126	12.189	2978.0	± 19.1	99.4	1.3	87.1	0.025
95M0165F.DAT	0.00006	1.684	0.0447	0.089	8.690	2992.8	± 25.9	99.7	0.9	88.0	0.026
95M0165H.DAT	0.00004	0.341	0.0084	0.017	1.675	2991.7	± 95.1	99.3	0.2	88.2	0.025
95M0165I.DAT	0.00017	0.150	0.0031	0.007	0.707	2859.8	± 229.9	93.0	0.1	88.3	0.024
95M0165J.DAT	0.00017	1.411	0.0367	0.074	7.205	2984.3	± 25.1	99.2	0.8	89.0	0.026
95M0165K.DAT	0.00103	8.068	0.2113	0.428	40.865	2952.0	± 11.1	99.2	4.4	93.5	0.026
95M0165L.DAT	0.00143	11.891	0.3016	0.632	60.552	2958.6	± 10.5	99.2	6.5	100.0	0.026

Correction Factors	Results	⁴⁰ * ³⁹ K ± 2σ	Age	± 2σ
K/Ca = 0.49				
J = 0.043640	Weighted Mean	95.250 ± 0.813	2959.2	± 15.176
sd-J (1s) = 0.000131	of Plateau			
1 / λ = 1804.077	Total Fusion		2993.7	± 8.765

Sample Number T94/185ii
 Material hornblende
 Irradiation Number VU11

File and step	³⁹ Ar(a)	³⁹ Ar	³⁹ Ar	³⁹ Ar(K)	⁴⁰ Ar(a+r)	Age	± 2σ	⁴⁰ Ar(r)	³⁹ Ar	³⁹ Ar(cum)	K/Ca
95M0241A.DAT	0.00586	0.349	0.0114	0.032	3.246	2031.2	± 190.8	46.6	1.5	1.5	0.044
95M0241B.DAT	0.00108	3.014	0.0910	0.187	17.504	2907.4	± 19.1	98.1	8.9	10.4	0.030
95M0241E.DAT	0.00029	3.069	0.0839	0.169	15.944	2938.9	± 17.1	99.4	8.0	18.4	0.027
95M0241F.DAT	0.00015	13.228	0.3490	0.694	67.759	2993.9	± 6.2	99.9	33.0	51.5	0.026
95M0241G.DAT	0.00002	1.478	0.0379	0.077	7.328	2953.7	± 36.5	99.8	3.7	55.1	0.026
95M0241H.DAT	0.00034	2.862	0.0758	0.154	14.754	2961.2	± 18.5	99.2	7.3	62.4	0.026
95M0241I.DAT	0.00049	5.350	0.1457	0.298	28.970	2982.3	± 10.6	99.4	14.2	76.6	0.027
95M0241K.DAT	0.00000	1.283	0.0325	0.067	6.585	3008.0	± 48.1	99.9	3.2	79.8	0.026
95M0241L.DAT	0.00000	1.691	0.0472	0.093	9.207	3014.2	± 34.8	99.9	4.4	84.2	0.027
95M0241M.DAT	0.00000	6.142	0.1647	0.332	32.779	3011.2	± 11.0	99.9	15.8	100.0	0.026

Correction Factors	Results	⁴⁰ * ³⁹ K ± 2σ	Age	± 2σ
K/Ca = 0.49				
J = 0.043610	Weighted Mean	97.548 ± 1.262	2993.0	± 20.8
sd-J (1s) = 0.000131	of Plateau			
1 / λ = 1804.077	Total Fusion		2969.2	± 8.7

Sample Number T94/189
 Material hornblende
 Irradiation Number VU11

File and step	³⁶ Ar(a)	³⁷ Ar	³⁸ Ar	³⁹ Ar(K)	⁴⁰ Ar(a+r)	Age	± 2σ	³⁶ Ar(r)	³⁷ Ar	³⁹ Ar(cum)	K/Ca
95M0242A.DAT	0.00842	8.403	0.1297	0.164	16.564	2807.4	± 44.8	84.9	3.1	3.1	0.010
95M0242B.DAT	0.00157	16.667	1.5395	1.313	130.448	3014.0	± 11.2	99.6	25.1	28.3	0.039
95M0242D.DAT	0.00014	8.153	0.6944	0.585	59.874	3063.5	± 16.0	99.9	11.2	39.4	0.035
95M0242E.DAT	0.00099	22.700	2.0000	1.633	169.705	3083.4	± 10.8	99.8	31.2	70.7	0.035
95M0242F.DAT	0.00000	2.817	0.2369	0.206	20.650	3033.3	± 33.6	99.9	3.9	74.6	0.036
95M0242G.DAT	0.00031	4.585	0.3887	0.338	34.271	3045.9	± 22.6	99.7	6.5	81.1	0.036
95M0242H.DAT	0.00000	2.867	0.2393	0.199	19.955	3036.5	± 35.1	99.9	3.8	84.8	0.034
95M0242J.DAT	0.00045	1.887	0.1574	0.124	12.531	3033.5	± 51.3	98.9	2.4	87.2	0.032
95M0242K.DAT	0.00007	2.039	0.1741	0.137	13.950	3055.4	± 44.8	99.8	2.6	89.8	0.033
95M0242L.DAT	0.00036	7.922	0.6394	0.532	53.651	3038.8	± 16.5	99.7	10.2	100.0	0.033

Correction Factors	Results	⁴⁰ Ar/ ³⁹ K ± 2σ	Age	± 2σ
K/Ca = 0.49	Weighted Mean of Plateau	101.484 ± 0.829	3075.0	± 14.9
J = 0.043610				
sd-J (1s) = 0.000131				
1/λ = 1804.077				
	Total Fusion		3043.1	± 8.8

Sample Number T94/50
 Material hornblende
 Irradiation Number VU11

File and step	³⁶ Ar(a)	³⁷ Ar	³⁸ Ar	³⁹ Ar(K)	⁴⁰ Ar(a+r)	Age	± 2σ	³⁶ Ar(r)	³⁷ Ar	³⁹ Ar(cum)	K/Ca
95M0235B	0.03624	37.145	0.3429	0.133	29.353	3543.9	± 50.9	63.5	10.6	10.6	0.00
95M0235C	0.00236	24.872	0.1195	0.132	6.861	1999.8	± 69.9	89.7	10.6	21.1	0.00
95M0235D	0.00084	6.846	0.0401	0.180	4.130	1198.1	± 82.3	93.7	14.3	35.5	0.01
95M0235E	0.00090	2.087	0.0184	0.185	4.129	1168.0	± 82.1	93.3	14.8	50.2	0.04
95M0235F	0.00061	1.770	0.0229	0.120	3.489	1424.7	± 109.8	94.6	9.6	59.8	0.03
95M0235G	0.00111	3.481	0.0677	0.158	8.965	2199.1	± 57.9	96.2	12.6	72.4	0.02
95M0235I	0.00017	0.781	0.0093	0.050	2.303	1951.4	± 212.7	97.6	4.0	76.4	0.03
95M0235J	0.00112	4.033	0.0610	0.081	9.818	3259.3	± 78.2	96.6	6.5	82.9	0.01
95M0235K	0.00011	1.744	0.0123	0.030	3.104	3079.8	± 218.5	98.9	2.4	85.2	0.01
95M0235L	0.00182	6.397	0.0640	0.185	19.656	3080.5	± 38.9	97.2	14.7	100.0	0.01

Correction Factors	Results	⁴⁰ Ar/ ³⁹ K ± 2σ	Age	± 2σ
K/Ca = 0.49	Weighted Mean	105.636 ± 4.159	3110.2	± 59.0
J = 0.043610				
sd-J (1s) = 0.000131				
	Total Fusion		2374.1	± 36.4

Sample Number T94/46
 Material hornblende
 Irradiation Number VU11

File and step	³⁹ Ar(a)	³⁹ Ar	³⁹ Ar	³⁹ Ar(K)	⁴⁰ Ar(a+r)	Age	± 2σ	⁴⁰ Ar(r)	³⁹ Ar	³⁹ Ar(cum)	K/Ca
95M0234A.DAT	0.00979	0.814	0.0341	0.027	6.524	3480.3	± 901.0	55.6	5.7	5.7	0.016
95M0234B.DAT	0.00110	6.673	0.1977	0.098	12.365	3336.3	± 156.2	97.3	20.8	26.4	0.007
95M0234C.DAT	0.00061	11.713	0.3938	0.153	18.552	3307.2	± 100.3	99.0	32.3	58.7	0.006
95M0234D.DAT	0.00027	3.006	0.0718	0.032	3.770	3263.0	± 478.4	97.8	6.7	65.4	0.005
95M0234E.DAT	0.00028	2.362	0.0633	0.026	3.189	3314.8	± 580.0	97.4	5.4	70.8	0.005
95M0234G.DAT	0.00000	1.953	0.0397	0.015	1.775	3253.5	± 839.9	99.9	3.2	74.1	0.004
95M0234H.DAT	0.00018	1.010	0.0417	0.014	1.658	3232.0	± 969.0	96.8	3.0	77.0	0.007
95M0234I.DAT	0.00001	0.723	0.0156	0.006	0.679	3243.5	± 2230.5	99.5	1.2	78.3	0.004
95M0234J.DAT	0.00025	1.478	0.0314	0.013	1.482	3204.7	± 1077.9	95.0	2.6	80.9	0.004
95M0234K.DAT	0.00000	0.583	0.0169	0.007	0.825	3305.0	± 1888.1	99.9	1.5	82.4	0.006
95M0234L.DAT	0.00000	10.773	0.1967	0.083	9.960	3294.8	± 154.4	99.9	17.6	100.0	0.004

Correction Factors	Results	⁴⁰ Ar/ ³⁹ K ± 2σ	Age	± 2σ
K/Ca = 0.49				
J = 0.043610	Weighted Mean	120.620 ± 9.346	3309.1	± 117.8
sd-J (1s) = 0.000131	of Plateau			
1/λ = 1804.077	Total Fusion		3311.6	± 9.1

Sample Number 94/87
 Material hornblende
 Irradiation Number VU11

File and step	³⁹ Ar(a)	³⁹ Ar	³⁹ Ar	³⁹ Ar(K)	⁴⁰ Ar(a+r)	Age	± 2σ	⁴⁰ Ar(r)	³⁹ Ar	³⁹ Ar(cum)	K/Ca
95M0164C	0.14654	1.279	0.5385	0.757	136.006	3332.9	± 18.0	68.1	6.5	6.5	0.29
95M0164D	0.03100	1.910	0.6637	0.532	66.370	3138.0	± 13.7	86.1	4.5	11.0	0.14
95M0164E	0.00327	0.130	0.0259	0.071	7.070	2809.4	± 23.2	86.3	0.6	11.6	0.27
95M0164F	0.05343	73.634	43.5638	6.543	888.159	3463.1	± 11.3	98.2	55.9	67.5	0.04
95M0164H	0.00596	28.569	19.5125	1.548	210.357	3479.4	± 10.7	99.1	13.2	80.7	0.03
95M0164I	0.00163	5.212	3.5734	0.344	46.022	3452.9	± 12.7	98.9	2.9	83.7	0.03
95M0164J	0.00034	0.958	0.5438	0.080	9.750	3310.2	± 35.9	98.9	0.7	84.4	0.04
95M0164K	0.00035	0.951	0.5115	0.071	8.910	3343.0	± 37.2	98.8	0.6	85.0	0.04
95M0164L	0.00055	2.571	1.2482	0.156	19.829	3372.5	± 21.2	99.1	1.3	86.3	0.03
95M0164M	0.00036	2.551	1.3988	0.158	20.420	3405.8	± 21.9	99.4	1.4	87.7	0.03
95M0164O	0.00053	1.666	0.9782	0.099	13.572	3482.8	± 38.9	98.8	0.8	88.5	0.03
95M0164P	0.00184	5.103	3.1497	0.263	38.115	3570.5	± 17.0	98.5	2.2	90.7	0.03
95M0164Q	0.00580	16.257	9.6362	1.084	146.579	3467.4	± 11.0	98.8	9.3	100.0	0.03

Correction Factors	Results	⁴⁰ Ar/ ³⁹ K ± 2σ	Age	± 2σ
K/Ca = 0.49				
J = 0.043640	Weighted Mean	133.603 ± 0.823	3466.3	± 13.2
sd-J (1s) = 0.000131	of Plateau			
1/λ = 1804.077	Total Fusion		3439.2	± 10.0

Sample Number T94/87 duplo
 Material hornblende
 Irradiation Number VU11

File and step	³⁶ Ar(a)	³⁷ Ar	³⁸ Ar	³⁹ Ar(K)	⁴⁰ Ar(a+r)	Age	± 2σ	⁴⁰ Ar(r)	³⁹ Ar	³⁹ Ar(cum)	K/Ca
95M0238B	0.23333	1.124	0.7410	0.129	136.111	5714.8	± 105.2	49.3	1.1	1.1	0.06
95M0238C	0.00958	0.439	0.1002	0.063	6.672	2337.2	± 148.4	57.5	0.6	1.7	0.07
95M0238D	0.00819	3.269	1.2997	0.177	27.810	3574.5	± 33.8	91.3	1.6	3.3	0.03
95M0238E	0.00978	15.195	7.2778	0.707	111.169	3678.2	± 17.0	97.4	6.3	9.5	0.02
95M0238F	0.00243	7.254	4.0614	0.286	39.862	3504.6	± 23.2	98.1	2.5	12.1	0.02
95M0238G	0.01826	49.992	31.2886	2.912	428.285	3594.7	± 14.1	98.7	25.8	37.9	0.03
95M0238I	0.00426	16.371	10.5771	1.055	147.191	3519.3	± 13.2	99.1	9.4	47.3	0.03
95M0238J	0.00436	13.670	8.8635	0.899	125.497	3517.1	± 16.1	98.9	8.0	55.2	0.03
95M0238K	0.00158	3.768	2.4488	0.261	36.541	3514.8	± 29.8	98.7	2.3	57.5	0.03
95M0238L	0.01049	38.809	25.4407	2.652	370.785	3522.3	± 10.3	99.1	23.5	81.1	0.03
95M0238M	0.00141	4.168	2.2586	0.244	34.127	3518.7	± 30.2	98.7	2.2	83.2	0.03
95M0238O	0.00187	5.128	2.8891	0.290	41.539	3549.7	± 25.5	98.6	2.6	85.8	0.03
95M0238P	0.00138	5.010	2.6841	0.315	44.389	3535.2	± 23.4	99.0	2.8	88.6	0.03
95M0238Q	0.00676	23.061	13.0245	1.285	185.002	3563.7	± 11.7	98.9	11.4	100.0	0.03

Correction Factors	Results	⁴⁰ Ar/ ³⁹ K ± 2σ	Age	± 2σ
K/Ca = 0.49				
J = 0.043610	Weighted Mean	138.627 ± 0.864	3522.3	± 13.4
sd-J (1s) = 0.000131	of Plateau			
1 / λ = 1804.077	Total Fusion		3599.2	± 11.1

Sample Number T94/34
 Material hornblende
 Irradiation Number VU11

File and step	³⁶ Ar(a)	³⁷ Ar	³⁸ Ar	³⁹ Ar(K)	⁴⁰ Ar(a+r)	Age	± 2σ	⁴⁰ Ar(r)	³⁹ Ar	³⁹ Ar(cum)	K/Ca
95M0233A	0.02304	0.991	0.0792	0.580	38.076	2182.1	± 26.2	82.0	3.6	3.6	0.29
95M0233B	0.00261	1.751	0.1353	0.604	31.622	2113.4	± 23.3	97.4	3.7	7.3	0.17
95M0233C	0.00148	3.953	0.3439	0.967	65.698	2475.1	± 14.9	99.2	6.0	13.3	0.12
95M0233D	0.00076	3.286	0.2604	0.643	46.790	2571.2	± 19.7	99.4	4.0	17.3	0.10
95M0233E	0.00080	4.081	0.3191	0.646	50.846	2680.6	± 19.2	99.4	4.0	21.3	0.08
95M0233F	0.00104	7.696	0.6113	1.045	98.430	2937.8	± 13.2	99.6	6.5	27.8	0.07
95M0233I	0.00098	12.554	0.8500	1.879	179.572	2960.8	± 12.2	99.8	11.6	39.4	0.07
95M0233J	0.00056	4.144	0.3617	0.642	57.528	2865.4	± 15.9	99.6	4.0	43.4	0.08
95M0233K	0.00109	7.913	0.6571	1.268	119.992	2944.4	± 13.0	99.7	7.9	51.2	0.08
95M0233L	0.00067	5.318	0.3612	0.912	81.907	2869.8	± 16.1	99.7	5.6	56.9	0.08
95M0233M	0.00073	4.208	0.2982	0.735	65.096	2848.2	± 15.5	99.6	4.6	61.4	0.09
95M0233O	0.00084	2.487	0.3028	0.385	36.837	2954.1	± 23.1	99.2	2.4	63.8	0.08
95M0233P	0.00038	3.621	0.4195	0.524	50.271	2966.1	± 23.8	99.7	3.2	67.1	0.07
95M0233Q	0.00104	4.535	0.2776	0.545	49.498	2880.8	± 21.7	99.3	3.4	70.4	0.06
95M0233R	0.00116	4.801	0.2754	0.561	52.227	2916.6	± 20.3	99.3	3.5	73.9	0.06
95M0233S	0.00074	4.236	0.1916	0.612	54.869	2864.7	± 19.2	99.5	3.8	77.7	0.07
95M0233T	0.00305	24.419	1.8158	3.602	307.992	2798.7	± 11.2	99.6	22.3	100.0	0.07

Correction Factors	Results	⁴⁰ Ar/ ³⁹ K ± 2σ	Age	± 2σ
K/Ca = 0.49				
J = 0.043610	Weighted Mean	90.071 ± 0.979	2877.4	± 17.8
sd-J (1s) = 0.000131	of Plateau	94.720 ± 0.369	2950.1	± 14.3
1 / λ = 1804.077	Total Fusion		2797.1	± 10.5

Sample Number T94/32
 Material hornblende
 Irradiation Number VU11

File and step	³⁶ Ar(a)	³⁷ Ar	³⁸ Ar	³⁹ Ar(K)	⁴⁰ Ar(a+r)	Age	± 2σ	⁴⁰ Ar(r)	³⁹ Ar	³⁹ Ar(cum)	K/Ca
95M0228A.DAT	0.00728	0.227	0.0229	0.076	20.767	4430.0	± 37.5	89.6	0.5	0.5	0.164
95M0228B.DAT	0.00065	0.244	0.0091	0.073	5.132	2478.9	± 30.6	96.1	0.5	1.1	0.147
95M0228D.DAT	0.00017	0.655	0.0222	0.140	12.123	2819.8	± 22.1	99.5	1.0	2.0	0.104
95M0228E.DAT	0.00002	0.477	0.0144	0.096	8.258	2814.6	± 31.8	99.9	0.7	2.7	0.098
95M0228F.DAT	0.00021	6.555	0.2331	1.408	133.223	2947.8	± 9.7	99.9	10.0	12.7	0.105
95M0232B.DAT	0.00057	5.273	0.1969	1.288	120.401	2928.9	± 10.9	99.8	9.1	21.9	0.120
95M0232C.DAT	0.00088	9.801	0.3473	2.591	245.726	2950.1	± 9.6	99.8	18.4	40.3	0.130
95M0232D.DAT	0.00047	7.478	0.2210	1.980	188.732	2958.3	± 10.6	99.8	14.1	54.3	0.130
95M0232E.DAT	0.00199	12.202	0.3989	3.091	292.938	2947.8	± 9.7	99.7	21.9	76.3	0.124
95M0232F.DAT	0.00098	1.627	0.0514	0.420	38.937	2907.0	± 21.6	99.2	3.0	79.3	0.127
95M0232H.DAT	0.00000	1.070	0.0350	0.277	25.947	2932.7	± 35.6	99.9	2.0	81.2	0.127
95M0232I.DAT	0.00014	0.726	0.0219	0.182	17.007	2926.5	± 51.6	99.7	1.3	82.5	0.123
95M0232J.DAT	0.00000	0.502	0.0154	0.127	11.831	2928.1	± 73.0	99.9	0.9	83.4	0.124
95M0232K.DAT	0.00003	0.505	0.0159	0.123	11.542	2932.6	± 75.2	99.8	0.9	84.3	0.119
95M0232L.DAT	0.00105	9.335	0.2885	2.212	205.976	2923.4	± 10.4	99.8	15.7	100.0	0.116

Correction Factors	Results	⁴⁰ Ar/ ³⁹ K ± 2σ	Age	± 2σ
K/Ca = 0.49				
J = 0.043610	Weighted Mean	94.338 ± 0.427	2944.3	± 10.9
sd-J (1s) = 0.000131	of Plateau			
1/λ = 1804.077	Total Fusion		2950.3	± 8.7

Sample Number T94/215
 Material hornblende
 Irradiation Number VU11

File and step	³⁶ Ar(a)	³⁷ Ar	³⁸ Ar	³⁹ Ar(K)	⁴⁰ Ar(a+r)	Age	± 2σ	⁴⁰ Ar(r)	³⁹ Ar	³⁹ Ar(cum)K/Ca	
95M0249B.DAT	0.01331	0.407	0.1511	0.097	55.310	5747.6	± 40.3	92.9	1.0	1.0	0.116
95M0249C.DAT	0.00116	0.812	0.0340	0.139	15.344	3143.0	± 39.7	97.7	1.4	2.4	0.084
95M0249D.DAT	0.00078	2.014	0.0679	0.314	31.264	3013.5	± 20.0	99.2	3.2	5.6	0.076
95M0249E.DAT	0.00141	10.154	0.3013	1.601	147.711	2908.1	± 12.1	99.6	16.3	21.9	0.077
95M0249F.DAT	0.00078	10.476	0.3725	1.972	182.436	2915.0	± 11.0	99.8	20.1	41.9	0.092
95M0249H.DAT	0.00022	3.514	0.1286	0.673	61.439	2896.0	± 13.3	99.8	6.8	48.8	0.094
95M0249I.DAT	0.00022	2.260	0.0862	0.455	41.948	2908.0	± 18.2	99.8	4.6	53.4	0.099
95M0249J.DAT	0.00055	4.602	0.1716	0.930	84.373	2885.0	± 12.3	99.7	9.5	62.9	0.099
95M0249K.DAT	0.00048	4.428	0.1606	0.893	82.009	2903.8	± 12.5	99.7	9.1	71.9	0.099
95M0249L.DAT	0.00035	2.035	0.0714	0.397	36.434	2899.6	± 18.2	99.6	4.0	76.0	0.096
95M0249M.DAT	0.00040	1.452	0.0499	0.277	25.088	2878.6	± 24.7	99.4	2.8	78.8	0.093
95M0249O.DAT	0.00009	0.943	0.0306	0.166	15.563	2930.8	± 38.8	99.8	1.7	80.5	0.086
95M0249P.DAT	0.00035	1.214	0.0432	0.216	20.313	2931.3	± 30.5	99.4	2.2	82.7	0.087
95M0249Q.DAT	0.00034	2.897	0.1030	0.572	52.651	2906.9	± 15.1	99.7	5.8	88.5	0.097
95M0249R.DAT	0.00061	6.016	0.2086	1.129	103.323	2898.2	± 11.2	99.7	11.5	100.0	0.092

Correction Factors	Results	⁴⁰ Ar/ ³⁹ K ± 2σ	Age	± 2σ
K/Ca = 0.49				
J = 0.043625	Weighted Mean	92.007 ± 0.734	2908.5	± 14.4
sd-J (1s) = 0.000131	of Plateau			
1/λ = 1804.077	Total Fusion		2978.1	± 8.7

Sample Number T94/17
 Material hornblende
 Irradiation Number VU11

File and step	³⁶ Ar(a)	³⁷ Ar	³⁸ Ar	³⁹ Ar(K)	⁴⁰ Ar(a+r)	Age	± 2σ	⁴⁰ Ar(r)	³⁹ Ar	³⁹ Ar(cum)	K/Ca
95M0227B.DAT	0.00768	0.515	0.0196	0.028	6.510	3640.7	± 80.6	65.1	0.4	0.4	0.545
95M0227C.DAT	0.00015	0.001	0.0000	0.000	0.092	6138.0	± 36242.2	52.3	0.0	0.4	0.542
95M0227D.DAT	0.00140	0.439	0.0183	0.094	8.710	2848.6	± 20.7	95.2	1.4	1.9	0.704
95M0227E.DAT	0.00047	1.084	0.0418	0.197	18.085	2891.6	± 17.8	99.2	3.0	4.9	0.672
95M0227F.DAT	0.00026	2.289	0.0956	0.446	40.599	2889.7	± 11.8	99.7	6.8	11.6	0.685
95M0227H.DAT	0.00005	2.162	0.0889	0.425	38.412	2880.7	± 11.9	99.9	6.5	18.1	0.687
95M0227I.DAT	0.00023	6.014	0.2610	1.203	109.322	2888.7	± 9.4	99.9	18.3	36.4	0.690
95M0227J.DAT	0.00025	4.026	0.1532	0.694	62.554	2876.6	± 11.1	99.8	10.6	47.0	0.662
95M0227K.DAT	0.00076	13.682	0.4680	2.130	194.419	2894.9	± 10.0	99.8	32.4	79.4	0.646
95M0227L.DAT	0.00015	1.779	0.0623	0.276	24.868	2875.1	± 14.8	99.7	4.2	83.6	0.645
95M0227N.DAT	0.00027	1.116	0.0414	0.193	17.219	2855.1	± 17.3	99.5	2.9	86.5	0.663
95M0227O.DAT	0.00000	1.545	0.0657	0.307	27.604	2875.0	± 12.2	99.9	4.7	91.2	0.689
95M0227P.DAT	0.00023	3.430	0.1272	0.581	52.908	2891.7	± 10.1	99.8	8.8	100.0	0.659

Correction Factors	Results	⁴⁰ Ar/ ³⁹ K ± 2σ	Age	± 2σ
K/Ca = 0.49	Weighted Mean of Plateau	90.666 ± 0.415	2886.9	± 10.9
J = 0.043610				
sd-J (1s) = 0.000131				
1/λ = 1804.077				
	Total Fusion		2890.7	± 8.6

Sample Number 94/23
 Material muscovite
 Irradiation Number VU11

File and step	³⁶ Ar(a)	³⁷ Ar	³⁸ Ar	³⁹ Ar(K)	⁴⁰ Ar(a+r)	Age	± 2σ	⁴⁰ Ar(r)	³⁹ Ar	³⁹ Ar(cum)	K/Ca
95M0294A	0.07180	0.000	0.0016	0.018	23.201	3143.8	± 2058.9	8.5	0.1	0.1	946.236
95M0294B	0.02911	0.000	0.0090	0.100	17.607	2878.7	± 70.2	51.1	0.5	0.6	5147.305
95M0294C	0.05071	0.037	0.0681	0.719	82.603	2940.1	± 14.7	81.8	3.6	4.1	9.432
95M0294D	0.04902	0.050	0.0841	0.890	98.763	2950.1	± 13.3	85.3	4.4	8.5	8.649
95M0294E	0.06926	0.255	0.1340	1.431	156.688	2957.9	± 13.6	86.9	7.1	15.6	2.750
95M0294H	0.03454	0.026	0.0442	0.474	54.592	2933.9	± 16.2	81.3	2.3	18.0	8.945
95M0294I	0.05520	0.155	0.1237	1.315	140.647	2948.2	± 13.6	88.3	6.5	24.5	4.156
95M0294J	0.05735	0.149	0.1175	1.249	135.704	2956.7	± 12.8	87.5	6.2	30.6	4.096
95M0294K	0.09903	0.175	0.2036	2.187	237.409	2958.0	± 12.8	87.6	10.8	41.4	6.107
95M0294L	0.04090	0.132	0.1526	1.643	169.719	2969.3	± 13.5	92.8	8.1	49.6	6.100
95M0294N	0.03362	0.075	0.1702	1.822	185.244	2973.9	± 12.6	94.6	9.0	58.6	11.957
95M0294O	0.02116	0.145	0.1401	1.485	150.790	2990.1	± 13.3	95.8	7.3	65.9	5.011
95M0294P	0.01210	0.138	0.0929	0.992	99.402	2980.1	± 13.8	96.3	4.9	70.8	3.514
95M0294Q	0.01242	0.157	0.0922	0.971	98.438	2993.8	± 13.7	96.2	4.8	75.6	3.037
95M0294R	0.01351	0.119	0.0880	0.921	93.710	2991.3	± 13.8	95.7	4.6	80.2	3.786
95M0294T	0.01207	0.082	0.0670	0.680	70.589	3008.1	± 15.4	94.9	3.4	83.5	4.069
95M0294U	0.01265	0.141	0.0555	0.567	59.991	3017.5	± 16.7	93.7	2.8	86.3	1.976
95M0294V	0.02670	0.507	0.0915	0.941	101.384	3019.9	± 15.2	92.2	4.7	91.0	0.910
95M0294W	0.02640	1.464	0.1042	1.072	113.640	3011.4	± 14.0	93.1	5.3	96.3	0.359
95M0294X	0.02354	0.365	0.0719	0.748	79.355	2981.7	± 14.6	91.2	3.7	100.0	1.005

Correction Factors	Results	⁴⁰ Ar/ ³⁹ K ± 2σ	Age	± 2σ
K/Ca = 0.49	Weighted Mean of Plateau	96.230 ± 0.461	2949.0	± 14.0
J = 0.043630				
sd-J (1s) = 0.000131				
1/λ = 1804.077				
	Total Fusion		2974.6	± 11.7

Sample Number T94/9
 Material hornblende
 Irradiation Number VU11

File and step	³⁹ Ar(a)	³⁷ Ar	³⁶ Ar	³⁹ Ar(K)	⁴⁰ Ar(a+r)	Age	± 2σ	⁴⁰ Ar(r)	³⁹ Ar	³⁹ Ar(cum)	K/Ca
95M0224B.DAT	0.00421	0.361	0.0148	0.115	9.631	2574.9	± 22.7	87.0	1.8	1.8	0.157
95M0224C.DAT	0.00258	2.142	0.1773	0.938	82.158	2823.9	± 9.2	99.0	14.4	16.2	0.215
95M0224D.DAT	0.00119	9.804	1.0837	2.711	267.385	3007.3	± 9.4	99.8	41.6	57.7	0.135
95M0224F.DAT	0.00000	1.900	0.2006	0.490	48.366	3010.9	± 11.7	99.9	7.5	65.3	0.126
95M0224G.DAT	0.00030	2.614	0.2657	0.675	66.173	2998.0	± 10.5	99.8	10.4	75.6	0.127
95M0224H.DAT	0.00000	0.487	0.0426	0.107	10.407	2982.1	± 23.3	99.9	1.6	77.3	0.108
95M0224I.DAT	0.00010	1.596	0.1279	0.315	30.727	2993.1	± 14.9	99.8	4.8	82.1	0.097
95M0224J.DAT	0.00000	1.042	0.0669	0.159	15.666	3003.8	± 17.4	99.9	2.4	84.5	0.075
95M0224L.DAT	0.00000	0.581	0.0396	0.094	9.326	3014.5	± 21.0	99.9	1.4	86.0	0.079
95M0224M.DAT	0.00000	1.110	0.0839	0.205	20.337	3017.3	± 14.0	99.9	3.1	89.1	0.091
95M0224N.DAT	0.00568	4.722	0.2171	0.522	50.886	2942.1	± 24.6	96.6	8.0	97.1	0.054
95M0224O.DAT	0.00031	2.733	0.0685	0.135	13.709	3041.1	± 20.9	99.3	2.1	99.2	0.024
95M0224N.DAT	0.00018	0.397	0.0217	0.052	5.074	2982.0	± 32.1	98.9	0.8	100.0	0.064

Correction Factors	Results	40*/39K ± 2σ	Age	± 2σ
K/Ca = 0.49				
J = 0.043610				
sd-J (1s) = 0.000131	Weighted Mean of Plateau	98.397 ± 0.466	3005.6	± 11.2
1/λ = 1804.077	Total Fusion		2968.9	± 8.7

Sample Number T95/13
 Material hornblende
 Irradiation Number VU11

File and step	³⁹ Ar(a)	³⁷ Ar	³⁶ Ar	³⁹ Ar(K)	⁴⁰ Ar(a+r)	Age	± 2σ	⁴⁰ Ar(r)	³⁹ Ar	³⁹ Ar(cum)	K/Ca
95M0226B.DAT	0.01087	1.076	0.1172	0.040	34.241	6417.6	± 47.8	90.6	1.2	1.2	0.018
95M0226C.DAT	0.00038	0.110	0.0043	0.013	1.130	2630.5	± 136.2	90.1	0.4	1.5	0.060
95M0226D.DAT	0.00117	0.622	0.0341	0.042	4.734	3100.4	± 42.6	92.7	1.2	2.8	0.033
95M0226E.DAT	0.00089	1.015	0.0583	0.060	6.715	3138.7	± 25.3	96.0	1.7	4.5	0.029
95M0226F.DAT	0.00073	2.717	0.1705	0.149	16.794	3187.8	± 14.9	98.7	4.3	8.8	0.027
95M0226G.DAT	0.00061	3.546	0.2192	0.192	19.877	3066.1	± 14.1	99.0	5.6	14.4	0.027
95M0226H.DAT	0.00055	9.813	0.6053	0.517	52.180	3037.4	± 10.1	99.6	15.0	29.5	0.026
95M0226I.DAT	0.00065	11.518	0.7181	0.612	61.515	3032.2	± 10.2	99.6	17.8	47.2	0.026
95M0226K.DAT	0.00071	5.443	0.3385	0.290	29.081	3020.5	± 12.5	99.2	8.4	55.7	0.026
95M0226L.DAT	0.00060	10.829	0.6702	0.568	57.670	3047.8	± 10.4	99.6	16.5	72.2	0.026
95M0226M.DAT	0.00031	5.215	0.3240	0.278	28.062	3037.2	± 11.8	99.6	8.1	80.3	0.026
95M0226N.DAT	0.00061	5.638	0.3604	0.301	30.761	3052.3	± 13.8	99.3	8.7	89.0	0.026
95M0226O.DAT	0.00043	1.052	0.0651	0.056	5.756	3024.5	± 29.4	97.7	1.6	90.7	0.026
95M0226Q.DAT	0.00029	1.223	0.0762	0.067	6.883	3048.2	± 26.3	98.7	2.0	92.6	0.027
95M0226R.DAT	0.00059	4.792	0.2870	0.254	26.437	3075.9	± 15.5	99.3	7.4	100.0	0.026

Correction Factors	Results	40*/39K ± 2σ	Age	± 2σ
K/Ca = 0.49				
J = 0.043610				
sd-J (1s) = 0.000131	Weighted Mean of Plateau	100.581 ± 0.492	3037.8	± 11.4
1/λ = 1804.077	Total Fusion		3161.0	± 10.2

Sample Number T94/29
 Material hornblende
 Irradiation Number VU11

File and step	³⁹ Ar(a)	³⁹ Ar	³⁹ Ar	³⁹ Ar(K)	⁴⁰ Ar(a+r)	Age	± 2σ	⁴⁰ Ar(r)	³⁹ Ar	³⁹ Ar(cum)	K/Ca
95M0225B	0.01634	0.599	0.1030	0.030	12.171	4441.6	± 57.9	60.3	0.5	0.5	0.02
95M0225C	0.00514	9.512	4.0255	1.203	108.101	2853.4	± 9.3	98.5	20.8	21.4	0.06
95M0225D	0.00396	15.659	8.0530	2.322	200.591	2809.2	± 9.4	99.3	40.2	61.6	0.07
95M0225E	0.00165	7.240	3.1100	1.097	94.175	2800.7	± 9.9	99.4	19.0	80.6	0.07
95M0225F	0.00081	2.656	0.9027	0.394	33.698	2792.7	± 10.7	99.2	6.8	87.4	0.07
95M0225H	0.00051	1.860	0.6680	0.235	20.312	2804.8	± 14.1	99.2	4.1	91.5	0.06
95M0225J	0.00020	0.200	0.0808	0.023	2.081	2819.1	± 69.1	97.1	0.4	91.9	0.06
95M0225J	0.00063	2.457	0.9266	0.286	24.805	2812.4	± 12.3	99.2	5.0	96.8	0.06
95M0225K	0.00053	1.280	0.4841	0.145	13.113	2862.3	± 17.1	98.7	2.5	99.3	0.06
95M0225L	0.00039	0.333	0.1231	0.038	3.673	2918.0	± 40.1	96.8	0.7	100.0	0.06

Correction Factors	Results	⁴⁰ Ar/ ³⁹ K ± 2σ	Age	± 2σ
K/Ca = 0.49				
J = 0.043610	Weighted Mean	85.586 ± 0.383	2804.3	± 10.6
sd-J (1s) = 0.000131	of Plateau			
1 / λ = 1804.077	Total Fusion		2831.5	± 9.0

Sample Number 94/29 duplo
 Material hornblende
 Irradiation Number VU11

File and step	³⁹ Ar(a)	³⁹ Ar	³⁹ Ar	³⁹ Ar(K)	⁴⁰ Ar(a+r)	Age	± 2σ	⁴⁰ Ar(r)	³⁹ Ar	³⁹ Ar(cum)	K/Ca
95M0293A.DAT	0.00191	0.091	0.0107	0.006	1.561	3720.7	± 286.6	63.9	0.6	0.6	0.034
95M0293B.DAT	0.00025	0.319	0.0095	0.012	1.113	2872.5	± 153.3	93.4	1.2	1.8	0.018
95M0293C.DAT	0.00026	0.144	0.0189	0.009	0.855	2813.1	± 205.1	91.0	0.9	2.7	0.031
95M0293D.DAT	0.00036	0.259	0.0777	0.024	2.242	2883.5	± 76.9	95.2	2.4	5.1	0.045
95M0293E.DAT	0.00069	2.114	1.1692	0.293	25.122	2795.5	± 8.7	99.1	29.3	34.3	0.068
95M0293H.DAT	0.00049	1.960	1.1733	0.295	24.839	2774.0	± 9.1	99.3	29.4	63.8	0.074
95M0293I.DAT	0.00023	1.163	0.6618	0.162	13.757	2782.7	± 13.2	99.4	16.2	80.0	0.068
95M0293J.DAT	0.00014	0.641	0.1574	0.053	4.464	2765.8	± 34.7	99.0	5.3	85.3	0.041
95M0293K.DAT	0.00000	0.175	0.0602	0.018	1.398	2695.1	± 105.5	99.9	1.8	87.0	0.050
95M0293L.DAT	0.00005	1.183	0.4354	0.130	10.344	2702.0	± 16.0	99.8	13.0	100.0	0.054

Correction Factors	Results	⁴⁰ Ar/ ³⁹ K ± 2σ	Age	± 2σ
K/Ca = 0.49				
J = 0.043630	Weighted Mean	84.388 ± 0.749	2784.9	± 13.8
sd-J (1s) = 0.000131	of Plateau			
1 / λ = 1804.077	Total Fusion		2782.9	± 5.7

Appendix 2 Whole rock XRF analyses of SHRIMP samples

	T94/31	T94/193	T94/221	T94/222	T94/227
	wt%				
SiO₂	69.81	66.09	71.85	60.89	74.10
TiO₂	0.33	0.41	0.34	0.51	0.06
Al₂O₃	14.84	15.49	15.74	15.01	13.08
Fe₂O₃	2.43	3.31	2.34	5.81	1.15
MnO	0.04	0.06	0.04	0.11	0.03
MgO	0.47	1.25	0.65	3.03	<0.30
CaO	1.92	3.16	2.63	6.39	1.13
Na₂O	4.42	5.17	5.93	4.93	4.30
K₂O	3.43	2.05	0.92	2.44	3.95
P₂O₅	0.06	0.09	0.07	0.39	<0.04
LOI	0.73	0.81	0.44	0.81	0.42
total	98.47	97.90	100.94	100.31	98.22
	ppm				
Ni	<10	20	<10	34	<10
Rb	139	92	62	62	191
Sr	381	374	308	953	100
Y	11	25	14	21	15
Zr	190	202	191	85	113
Pb	24	16	16	17	37
Cu	10	14	<10	18	<10
Zn	57	70	58	76	31
Co	6	6	6	18	<3
Nb	8	12	12	9	6
Ga	18	22	21	17	16
Th	12	9	7	7	23
U	<7	<7	<7	<7	9.2

Curriculum Vitae

- 12-1-1967 Geboren te Varese (*Italië*)
- 1979-1985 Atheneum-B, Spinoza Lyceum *Amsterdam*
- Juni 1992 **Doctoraal examen Geologie**, *Universiteit Utrecht*
- Hoofdvak Structurele Geologie van Kristallijne Gesteenten
- 1992-1996 **Assistent in opleiding**, Vakgroep Geologie, *Universiteit Utrecht*

Acknowledgements (Dankbetuiging)

This Ph.D. thesis was completed with the help of many people. In the first place I want to thank my promotor, Prof. dr. Stan White, for the never ending time and effort that he has spent with me in all aspects of my research and writing. I am particularly grateful for the way in which he taught me the details of scientific argumentation. I am equally grateful for the support that my co-promotor, dr. Jan Wijbrans, gave me in all matters, but especially for his expertise in geochronology. It was always a pleasure to work with Jan during the fieldtrips to the Pilbara.

I am very grateful to Prof.dr. David Groves, dr. Mark Barley and dr. Neil McNaughton for their support and co-operation during my study of the Bamboo Creek deposit and for the opportunity to spend a few months at the Key Centre For Teaching and Research in Strategic Mineral Deposits in Perth. I thank dr. Dave Nelson for his very efficient and expert help in the SHRIMP-lab, without which the zircon dating would not have been possible.

I want to thank all the people in the Department who have managed to create a stimulating and warm home base at the University of Utrecht. In particular I want to thank Rachel Walcott for the stimulating discussions on all topics, the fun and support she gave me during the almost four years that we shared a room, and Armelle Kloppenburg for the good times in the field and the discussions on Pilbara geology. Andrew Curtis, Julie Newman, Sieger van der Laan and Armelle Kloppenburg read and corrected early versions of chapters in this thesis. Martyn Drury and Timon Fliervoet helped with SEM work on the zircons used for dating. Johan ten Veen and Michiel van der Meulen were excellent colleagues during the supervision of the first year students' fieldwork in Spain. Prof.dr. Maarten de Wit, who was on sabbatical at the University of Utrecht during the last year of my Ph.D., made Archean geology even more exciting with his short course and discussions with him helped me sharpen my views on Archean geology.

The following people went along on fieldtrips to the Pilbara: Corinne Davids, Maaïke Knoop, Albert Krikke, Mariëtte Valkering, Karen de Bruijne, Yvette Kuiper, Yvonne Smit, Willem Maarten van Haften, Willem Flierman, Cees Passchier, Wout Nijman, I want to thank them all for their part in the Pilbara fieldwork. I especially want to thank Bart Willigers, Martin de Keijzer and Paul Dirks for making the Pilbara fieldworks memorable in all respects, and for their part in developing some of the ideas in this thesis.

The Pilbara is a special place and is made so by the (part time) Pilbarians. I want to particularly thank Dennis and Myrna O'Meara for giving us a home at what must be the nicest part of Marble Bar (the old hospital), Alec, of the Marble Bar Garage, for keeping our cars running and always being in for a party, Charles Robinson for teaching me how to change and repair punctured car tires, Gary and Monica Mullens for their support in the Warrawoona Belt, and all barkeepers of the Iron Clad Hotel for the endless supply of cold beer.

I thank Joshua Pitt and Gary Strong of Great Southern Mining for the tracks they had made in the Coongan Belt, without which the study of the Coongan Belt would have been impossible, and for the use of some of their maps and aerial photographs of the Coongan Belt. I am greatly indebted to John Martin, who first showed me Dolomite Creek and then prepared the best bush barbecue ever. Kitchener Mining gave me the opportunity to study the Bamboo Creek Deposit. I could not have done the Bamboo Creek study without the help of Jeremy Peters, the mine geologist at the time.

Acknowledgements

Apart from the help during the sampling and analysis of the mining area, he is also a great friend and we shared many good times.

During my longer stays in Perth a number of people made life particularly enjoyable, these were Lisa, Richard, Trudy, Marit, Willem, Wouter, Erik, Hilco and Mylene. Julie and Rob lent me their house during my second visit to Perth. I am also grateful to all Ph.D. students at the Key Centre for welcoming me during my stay there.

Dank ben ik verschuldigd aan alle medewerkers van de Audio-Visuele Dienst, met name Fred Trappenburg voor zijn zeer efficiënte en vakkundige tekenwerk. Ik bedank de medewerkers van de slijpkamer in Utrecht voor de vele slijpplaten die ze voor mij gemaakt hebben en de medewerkers van de slijpkamer van de Vrije Universiteit voor het ingieten en polijsten van de zirkonen. Lodewijk IJlst bedank ik voor zijn zeer vakkundige leiding van het mineraalscheidingslab van de Vrije Universiteit.

Financial support for the fieldwork in the Pilbara was granted by the Dr. Schürmannfonds (grants No. 1992/03, 1993/05, 1994/09, 1995/14). Financial support for other travels came from the Dutch Science Foundation (N.W.O.), the Molengraaf Fonds and the VSB-Fonds.

Buiten de Universiteit hebben een aantal goede vrienden en vriendinnen, burens, wijn fanaten en familie gezorgd voor afleiding en plezier in de afgelopen jaren. Lotte Jaspers heeft mij in het begin van mijn promotie met veel inzet geholpen om de aanvraag voor de VSB-beurs in begrijpelijk Nederlands te vatten.

Ragnhild Andersson, Piet Zegers en Mara Reijntjes hebben vanaf mijn vroegste herinneringen gezorgd voor een liefhebbende, stimulerende en ondersteunende omgeving. Ragnhild reisde bovendien helemaal naar de Pilbara en zag de Pilbara op z'n mooist.

Jan Kees heeft in mij in vrijwel alle onderdelen van mijn promotie geholpen. Hij ging mee naar de Pilbara, waardoor ik onafhankelijk kon werken, las en corrigeerde de meeste hoofdstukken in een vroeg stadium, en diende in het algemeen als klankbord. Bovendien heeft hij, meer dan enig ander, de moeilijker momenten meegemaakt en mij in de afgelopen jaren gesteund en plezier gegeven.